

**Characterisation of the Unfolded Protein Response in Prostate  
Cancer, and Investigation of the ATF6 Interactome Using a  
Modified Mammalian Expression System.**

Ana Maria Isac

**A thesis submitted for the degree of Doctor of Philosophy in Cell  
and Molecular Biology**

SCHOOL OF LIFE SCIENCES

UNIVERSITY OF ESSEX

**Date of submission October 2021**

## **Statement of Originality**

Unless otherwise stated in the text, this thesis is the result of my own work.

*Ana Maria Isac*

*2021*

## Abstract

Prostate cancer (PCa) cells grow in an environment which is known to cause endoplasmic reticulum (ER) stress. This activates a process called the unfolded protein response (UPR) which PCa utilises in order to survive and adapt to the adverse environmental conditions. Using interdisciplinary approaches and tissue culture models representing different stages of PCa, this project investigated the link between the UPR and the key oncogenic driver of PCa, the androgen receptor. It has been observed that hormone responsive PCa utilises all three UPR arms in order to promote ER homeostasis and cell survival. The importance of the UPR during the progression of PCa to the castrate resistant stage was also assessed. Interestingly, UPR signalling was inactivated in castrate-resistant models of PCa, and the cells were instead dependent on the ER-associated degradation (ERAD) pathway in order to resolve the stress and survive. These findings have identified potential UPR vulnerabilities that can be targeted to prevent disease progression.

Little is known about the structure and interaction partners of the UPR sensor ATF6, as protein expression has been shown to be problematic. To resolve this issue a stable tetracycline-inducible HEK293S GnTI(-) cell line for the expression of ATF6 was generated and mass spectrometry performed to characterise the ATF6 interactome. Sixty novel interaction partners of ATF6 were identified, most of which are associated with the cytoskeleton, such as Spectrin  $\beta$ -II and p195, which were validated by immunoblotting. It is hoped that the use of this modified expression system will provide an advantage in the process of expression, solubilisation and structure determination of ATF6 and of other membrane proteins.

## **Acknowledgements**

I would like to express my sincere gratitude to my supervisors, Dr Greg Brooke, Dr Filippo Prischi and Dr Philip Reeves for their expertise and continuous support throughout my PhD studies and related research. I would like to extend a very special thank you to Dr Greg Brooke, his timely advice with kindness, patience and motivation have helped me to a very great extent to accomplish this task.

I would also like to thank Dr Ralf Zwacka, my supervisory board member, for his guidance and advice throughout my PhD, Dr Andrea Mohr for her technical support with the flow cytometric assays, and Dr Metodi Metodiev for his valuable advice and assistance with the mass spectroscopy analysis. I am also grateful to my fellow lab mates, past and present members of the Molecular Oncology Lab: Dr Angela Whipple, Dr Emine Cil, Ms Eleanor Rees, Dr Amna Allafi, Dr Mila Pavlova and Dr Mohammad Alkheilewi for their support and friendship throughout my PhD studies.

Next, my sincere gratitude goes to the University of Essex and School of Life Sciences for awarding me the Doctoral Scholarship to carry out this research. I am also extremely thankful to my parents, my sister, and my grandparents for their kindness, support, and constant encouragement throughout my research period.

*Ana Maria Isac*

*2021*

## **COVID-19 Statement**

My research has been significantly impacted by the COVID-19 pandemic due to closure of research facilities and restricted laboratory access.

## **Abbreviations**

AF-1: Activation Function 1

AF-2: Activation Function 2

AR: Androgen receptor

ARE: Androgen Response Element

ATF4: Activating Transcription Factor 4

ATF6: Activating Transcription Factor 6

BIC: Bicalutamide

BiP: Binding Immunoglobulin protein

BPH: Benign Prostatic Hyperplasia

BSA: Bovine serum albumin

CaCl<sub>2</sub>: Calcium chloride

cDNA: Complementary DNA

CHOP: CCAAT/enhancer binding proteins Homologous Protein

CRPC: Castrate Resistant Prostate Cancer

C-Terminal: Carboxyl-Terminal

DBD: DNA Binding Domain

ddH<sub>2</sub>O: Double distilled water

DDM: n-Dodecyl-beta-D-Maltoside

DHT: Dihydrotestosterone

DMSO: Dimethyl Sulphoxide

DNA: Deoxyribonucleic acid

E. coli: Escherichia coli

EDTA: Ethylenediaminetetraacetic acid

ENZA: Enzalutamide

ER: Endoplasmic Reticulum

ERAD: Endoplasmic Reticulum-Associated Degradation

EtOH: Ethanol

FBS: Foetal bovine serum

Ferr-1: Ferrostatin-1

HCl: Hydrochloric acid

HERPUD1: Homocysteine-responsive endoplasmic reticulum-resistant ubiquitin-like domain member 1 protein

HRP: Horseradish peroxidase

HSP: Heat Shock Protein

IRE1 $\alpha$ : Inositol-requiring enzyme 1 alpha

kDa: Kilodaltons

LB: Luria Broth

LBD: Ligand Binding Domain

LH: Luteinizing Hormone

L19: RPL19 ribosomal protein

MIB: Mibolerone

Min/s: Minute/s

mL: Millilitre

mRNA: messenger RNA

NaB: Sodium Butyrate

NaCl: Sodium Chloride

nm: Nanometre

N-Terminal: Amino-Terminal

Nec-1: Necrostatin-1

PBS: Phosphate Buffered Saline

PCa: Prostate Cancer

PCR: Polymerase Chain Reaction

PERK: Protein kinase RNA-like ER kinase

PFA: Paraformaldehyde

PSA: Prostate Specific Antigen

PVDF: Polyvinylidene difluoride

RIDD: IRE1-Dependent Decay of mRNA

RIPA: Radioimmunoprecipitation assay

RNA: Ribonucleic acid

Rpm: Revolutions per minute

RPMI: Roswell Park Memorial Institute

RT: Room temperature

RT-PCR: Real Time PCR

SDS: Sodium Dodecyl Sulphate

SDS-PAGE: Sodium Dodecyl Sulphate Polyacrylamide gel electrophoresis

TAE: Tris/Acetic acid/EDTA

TE: Tris/EDTA

TET: Tetracycline

TNM: Tumour, Nodes & Metastasis

Tris-HCl: Tris-Hydrochloric Acid

TUN: Tunicamycin

UPR: Unfolded Protein Response

UV: Ultra violet

XBP1: X-Box Binding Protein 1

XBP1s: X-Box Binding Protein 1 spliced

$\mu\text{L}$ : micro litre

$\mu\text{g}$ : micro gram

## Table of Contents

<b>STATEMENT OF ORIGINALITY</b>	<b>2</b>
<b>ABSTRACT</b>	<b>3</b>
<b>ACKNOWLEDGEMENTS</b>	<b>4</b>
<b>COVID-19 STATEMENT</b>	<b>5</b>
<b>ABBREVIATIONS</b>	<b>6</b>
<b>TABLE OF CONTENTS</b>	<b>10</b>
<b>LIST OF TABLES AND FIGURES</b>	<b>13</b>
<b>CHAPTER 1: INTRODUCTION</b>	<b>16</b>
1.1 THE PROSTATE	16
1.1.1 ENDOCRINE CONTROL OF THE PROSTATE	18
1.1.2 DISEASES OF THE PROSTATE	18
1.2 PROSTATE CANCER (PCA)	19
1.2.1 PCA SCREENING	20
1.2.2 TYPES OF PCA. GLEASON SCORE.	21
1.3 ANDROGEN RECEPTOR (AR) AS THE KEY ONCOGENIC DRIVER OF PCA	22
1.3.1 STRUCTURE OF THE ANDROGEN RECEPTOR	22
1.3.2 ANDROGEN RECEPTOR SIGNALLING	26
1.4 TREATMENT OF PCA	28
1.5 MECHANISMS OF THERAPY RESISTANCE AND CASTRATE RESISTANT PROSTATE CANCER	29
1.6 THE UNFOLDED PROTEIN RESPONSE IN PROSTATE CANCER	31
1.6.1 THE ENDOPLASMIC RETICULUM (ER)	32
1.6.2 PROTEIN SYNTHESIS AND FOLDING	33
1.6.2.1 Binding immunoglobulinprotein (BiP)	35
1.6.3 THE UNFOLDED PROTEIN RESPONSE	37
1.6.3.1 Inositol requiring-enzyme 1 alpha (IRE1 $\alpha$ )	40
1.6.3.2 Protein kinase RNA-like ER kinase (PERK)	40
1.6.3.3 Activating transcription factor 6 (ATF6)	41
1.6.4 THE ADAPTIVE UPR	44
1.6.5 THE PRO-APOPTOTIC UPR	47
1.6.6 THE UNFOLDED PROTEIN RESPONSE IN CANCER	50
1.6.7 THE ROLE OF UPR SIGNALLING IN PROSTATE CANCER	54
1.7 RESEARCH AIMS	57
<b>CHAPTER 2: MATERIALS AND METHODS</b>	<b>59</b>
2.1 REAGENTS, BUFFERS AND SOLUTIONS	59
2.1.1 REAGENTS AND KITS	59
2.1.2 SOLUTIONS AND BUFFERS	61
2.2 CELL CULTURE	66
2.2.1 PASSAGE OF CELLS	68
2.2.2 CELL COUNTING AND PLATING	68
2.2.3 DEFROSTING/FREEZING CELLS	68

<b>2.3 CRYSTAL VIOLET PROLIFERATION ASSAY</b>	<b>69</b>
<b>2.4 FLOW CYTOMETRIC ASSAYS</b>	<b>70</b>
<b>2.4.1 CELL CYCLE ANALYSIS</b>	70
<b>2.4.2 PI INCLUSION AND DNA HYPODIPLOIDY ASSAY</b>	71
<b>2.5 QUANTITATIVE PCR (QPCR)</b>	<b>71</b>
<b>2.5.1 RNA EXTRACTION</b>	71
<b>2.5.2 NANO DROP® ND-1000 UV/VIS SPECTROPHOTOMETER</b>	72
<b>2.5.3 REVERSE TRANSCRIPTASE PCR</b>	72
<b>2.5.4 REAL-TIME QPCR</b>	72
<b>2.6 CLONING ATF6 INTO PACMVTET-O VECTOR</b>	<b>74</b>
<b>2.6.1 DESIGN OF CLONING PRIMERS</b>	74
<b>2.6.2 PCR AMPLIFICATION OF ATF6 DNA</b>	75
<b>2.6.3 AGAROSE GEL ELECTROPHORESIS</b>	75
<b>2.6.4 LIGATION OF ATF6 INTO PGEM®-T EASY VECTOR</b>	75
<b>2.6.5 TRANSFORMATION OF COMPETENT CELLS</b>	76
<b>2.6.6 RE-CLONING INTO PACMVTET-O VECTOR</b>	76
<b>2.7 STABLE TRANSFECTION OF HEK293S GNTI(-) CELLS</b>	<b>77</b>
<b>2.7.1 EXPANDING CLONES AND CELL INDUCTION</b>	77
<b>2.8 PROTEIN IMMUNOBLOTTING/WESTERN BLOTTING</b>	<b>78</b>
<b>2.8.1 PREPARING CELL LYSATE AND PROTEIN QUANTIFICATION</b>	78
<b>2.8.2 SDS POLYACRYLAMIDE GEL ELECTROPHORESIS</b>	78
<b>2.8.3 IMMUNOBLOTTING</b>	79
<b>2.9 DOT BLOT</b>	<b>79</b>
<b>2.9.1 PREPARING CELL LYSATES AND SAMPLES</b>	79
<b>2.9.2 BLOTTING</b>	80
<b>2.10 COOMASSIE BLUE STAIN</b>	<b>80</b>
<b>2.11 PROTEIN PURIFICATION</b>	<b>80</b>
<b>2.11.1 CELL LYSIS</b>	80
<b>2.11.2 COLUMN PREPARATION</b>	81
<b>2.11.3 ELUTION OF THE PURIFIED PROTEIN</b>	81

**CHAPTER 3: INVESTIGATING THE EFFECTS OF ENDOPLASMIC RETICULUM STRESS UPON PROSTATE CANCER PROLIFERATION, CELL CYCLE AND CELL DEATH** **82**

<b>3.1 EXPRESSION LEVELS OF IRE1A, PERK AND ATF6 IN PCA CELL LINES</b>	<b>86</b>
<b>3.2 EFFECTS OF ER STRESS UPON PCA CELL PROLIFERATION AND CELL CYCLE</b>	<b>86</b>
<b>3.3 EFFECTS OF ER STRESS UPON PCA CELL DEATH</b>	<b>90</b>
<b>3.4 MECHANISMS OF CELL DEATH INDUCED BY UPR</b>	<b>98</b>
<b>3.5 UPR ACTIVATION IN RESPONSE TO ER STRESS</b>	<b>101</b>
<b>3.6 EFFECTS OF TARGETING UPR SIGNALLING UPON PROSTATE CANCER PROLIFERATION AND TARGET GENE EXPRESSION</b>	<b>103</b>
<b>3.7 DISCUSSION</b>	<b>112</b>
<b>3.7.1 UPR SENSOR PROTEINS HAVE HIGH LEVELS OF EXPRESSION IN HORMONE SENSITIVE MODELS OF PROSTATE CANCER</b>	112
<b>3.7.2 ANDROGEN RESPONSIVE CELLS ATTEMPT TO DELAY CELL DEATH BY ENTERING INTO G1-PHASE ARREST</b>	114
<b>3.7.3 UPR-INDUCED APOPTOSIS IS DEPENDENT ON CASPASE 8 AND ITS ACTIVATING COMPLEX</b>	117
<b>3.7.4 DEFICIENT UPR SIGNALLING IN CASTRATE-RESISTANT MODELS OF PROSTATE CANCER</b>	118
<b>3.7.5 METASTATIC MODELS OF PROSTATE CANCER RELY ON ER-ASSOCIATED DEGRADATION (ERAD) PATHWAY IN ORDER TO SURVIVE</b>	120
<b>3.7.6 IRE1A SIGNALLING PROMOTES SURVIVAL OF ANDROGEN RESPONSIVE CELLS</b>	122
<b>3.7.7 CONCLUSIONS</b>	123

<b><u>CHAPTER 4: CHARACTERISING THE EFFECTS OF ANDROGENS AND ANTIANDROGENS UPON UPR SIGNALLING IN PROSTATE CANCER</u></b>	<b>124</b>
4.1 EFFECTS OF ANDROGEN AND ANTI-ANDROGENS UPON EXPRESSION OF UPR COMPONENTS	125
4.2 EFFECTS OF UPR INHIBITORS UPON AR SIGNALLING	130
4.2.1 TARGETING BIP	130
4.2.2 TARGETING IRE1A, PERK, AND ATF6	132
4.3 DISCUSSION	138
<b><u>CHAPTER 5: INVESTIGATION OF THE ATF6 INTERACTOME USING A MODIFIED MAMMALIAN EXPRESSION SYSTEM</u></b>	<b>143</b>
5.1 GENERATION OF STABLE HEK293S GNTI(-) CELL LINES FOR THE TETRACYCLINE-INDUCED ATF6 GENE EXPRESSION	146
5.2 OPTIMISATION OF THE INDUCTION CONDITIONS AND CONFIRMATION OF ATF6 EXPRESSION	146
5.3 PROTEIN PURIFICATION	149
5.3.1 AFFINITY PURIFICATION	149
5.3.2 CLEAVAGE OF ATF6 IN RESPONSE TO ENDOPLASMIC RETICULUM STRESS	151
5.4 CHARACTERISATION OF THE ATF6 INTERACTOME	156
5.5 DISCUSSION	165
<b><u>CHAPTER 6: GENERAL DISCUSSION AND CONCLUDING REMARKS</u></b>	<b>169</b>
6.1 CHARACTERISING THE UPR IN PROSTATE CANCER	169
6.1.1 BENIGN PROSTATE CELLS (BPH-1)	170
6.1.2 HORMONE RESPONSIVE PROSTATE CANCER (LNCAP)	171
6.1.3 PROGRESSION OF PROSTATE CANCER FROM ANDROGEN DEPENDENCE TO ANDROGEN INDEPENDENCE (C42, C42B, 22Rv1)	172
6.1.4 CASTRATE RESISTANT PROSTATE CANCER (DU145, PC3)	173
6.2 INVESTIGATION OF THE ATF6 INTERACTOME USING A MODIFIED MAMMALIAN EXPRESSION SYSTEM	173
6.3 CONCLUDING REMARKS	175
6.4 FUTURE WORK	177
<b><u>BIBLIOGRAPHY</u></b>	<b>179</b>

## List of Tables and Figures

FIGURE 1.1 GROSS AND MICROSCOPIC ANATOMY OF THE PROSTATE.	17
FIGURE 1.2. GLEASON PATTERNS.	23
FIGURE 1.3. THE STRUCTURE OF THE ANDROGEN RECEPTOR.	25
FIGURE 1.4. ANDROGEN RECEPTOR SIGNALLING IN THE PROSTATE.	27
FIGURE 1.5 MECHANISMS THAT PROMOTE THE PROGRESSION OF CASTRATE RESISTANT PROSTATE CANCER.	30
FIGURE 1.6. ER STRESS SENSORS AND THE UPR SIGNALLING PATHWAYS.	39
FIGURE 1.7. APOPTOSIS PATHWAYS INDUCED BY ER STRESS.	48
FIGURE 1.8 UPR AND THE HALLMARKS OF CANCER.	51
TABLE 2.1.1 REAGENTS AND KITS USED IN THIS STUDY.	59
TABLE 2.1.2.1 BUFFERS AND SOLUTIONS USED FOR WESTERN BLOTTING.	61
TABLE 2.1.2.2 BUFFERS AND SOLUTIONS USED FOR CLONING.	63
TABLE 2.1.2.3 BUFFERS AND SOLUTIONS USED FOR FLOW CYTOMETRY.	64
TABLE 2.1.2.4 DRUGS USED IN THIS STUDY	64
TABLE 2.2.1 PROSTATE CANCER CELL LINES USED IN THIS STUDY.	67
TABLE 2.5.3 CYCLE DETAILS FOR THE SYNTHESIS OF CDNA USING THE LUNASCRIPT RT <sup>®</sup> SUPERMIX.	73
TABLE 2.5.4.1 THERMOCYCLING PROTOCOL FOR REAL-TIME QPCR USING LUNA SYBR GREEN MASTER MIX.	73
TABLE 2.5.4.2 PRIMERS USED FOR REAL-TIME QPCR.	73
TABLE 2.6.1 ATF6 CLONING AND SEQUENCING PRIMERS.	75
FIGURE 3.1 EXPRESSION OF UPR COMPONENTS ACROSS A PANEL OF PCA CELL LINES.	87
FIGURE 3.2 ER STRESS REDUCES PROLIFERATION OF PCA CELL ONES AND CAUSES G1 ARREST IN LNCAP CELLS.	89
FIGURE 3.3.1 APOPTOTIC LEVELS OF PCA CELL LINES IN RESPONSE TO A DOSE RANGE OF TUNICAMYCIN.	91
FIGURE 3.3.2 PI INCLUSION LEVELS OF PCA CELL LINES IN RESPONSE TO A DOSE RANGE OF TUNICAMYCIN.	92
FIGURE 3.3.3 Z-VAD-FMK INHIBITS TUNICAMYCIN-INDUCED APOPTOSIS IN BPH-1 CELLS.	94

FIGURE 3.3.4 APOPTOTIC AND PI INCLUSION LEVELS OF LNCAP CELLS IN RESPONSE TO TUNICAMYCIN AND CELL DEATH INHIBITORS.	95
FIGURE 3.3.5 Z-VAD-FMK INHIBITS TUNICAMYCIN INDUCED APOPTOSIS IN DU145 CELLS.	96
FIGURE 3.3.6 Z-VAD-FMK INHIBITS TUNICAMYCIN INDUCED APOPTOSIS IN PC3 CELLS.	97
FIGURE 3.4 APOPTOTIC AND PI INCLUSION LEVELS OF DU145 KO CELL LINES IN RESPONSE TO TUNICAMYCIN.	100
FIGURE 3.5 UPR ACTIVATION IN RESPONSE TO ER STRESS.	102
FIGURE 3.6.1 DOSE RESPONSE CURVES, AND IC <sub>50</sub> VALUES, FOR THE UPR INHIBITORS.	104
FIGURE 3.6.2 INHIBITION OF UPR SIGNALLING FURTHER REDUCES PROLIFERATION DURING ER STRESS.	105
FIGURE 3.6.3 EFFECTS OF UPR INHIBITORS UPON UPR TARGET GENE EXPRESSION IN LNCAP CELLS.	107
FIGURE 3.6.4 EFFECTS OF UPR INHIBITORS UPON UPR TARGET GENE EXPRESSION IN C42 CELLS.	108
FIGURE 3.6.5 EFFECTS OF UPR INHIBITORS UPON UPR TARGET GENE EXPRESSION IN 22RV1 CELLS.	109
FIGURE 3.6.6 EFFECTS OF UPR INHIBITORS UPON UPR TARGET GENE EXPRESSION IN DU145 CELLS.	110
FIGURE 3.6.7 EFFECTS OF UPR INHIBITORS UPON UPR TARGET GENE EXPRESSION IN PC3 CELLS.	111
FIGURE 4.1.1 EXPRESSION OF UPR COMPONENTS IN RESPONSE TO ANDROGEN.	126
FIGURE 4.1.2 UPR ACTIVATION IN RESPONSE TO ANDROGEN AND ANTIANDROGENS.	128
FIGURE 4.1.3 UPR ACTIVATION IN RESPONSE TO ANDROGEN AND ANTIANDROGENS.	129
FIGURE 4.2.1 THE BIP INHIBITOR HA15 REDUCES PCA PROLIFERATION AND THE EXPRESSION OF THE AR TARGET GENE <i>TMPRSS2</i> .	131
FIGURE 4.2.2.1 ANDROGEN RECEPTOR ACTIVITY IN RESPONSE TO ANDROGEN AND UPR INHIBITORS.	133
FIGURE 4.2.2.2 IRE1A ACTIVATION IN RESPONSE TO ANDROGEN AND UPR INHIBITORS.	134
FIGURE 4.2.2.3 PERK ACTIVATION IN RESPONSE TO ANDROGEN AND UPR INHIBITORS.	135
FIGURE 4.2.2.4 ATF6 ACTIVATION IN RESPONSE TO ANDROGEN AND UPR INHIBITORS.	136
FIGURE 4.2.2.5 PERK/ATF6 ACTIVATION IN RESPONSE TO ANDROGEN AND UPR INHIBITORS.	137
FIGURE 5.1 EXPRESSION OF THE 1D4-TAGGED PROTEIN ACROSS A PANEL OF STABLY TRANSFECTED COLONIES.	147
FIGURE 5.2.1 EXPRESSION OF THE 1D4-TAGGED PROTEIN UNDER DIFFERENT CONDITIONS.	148

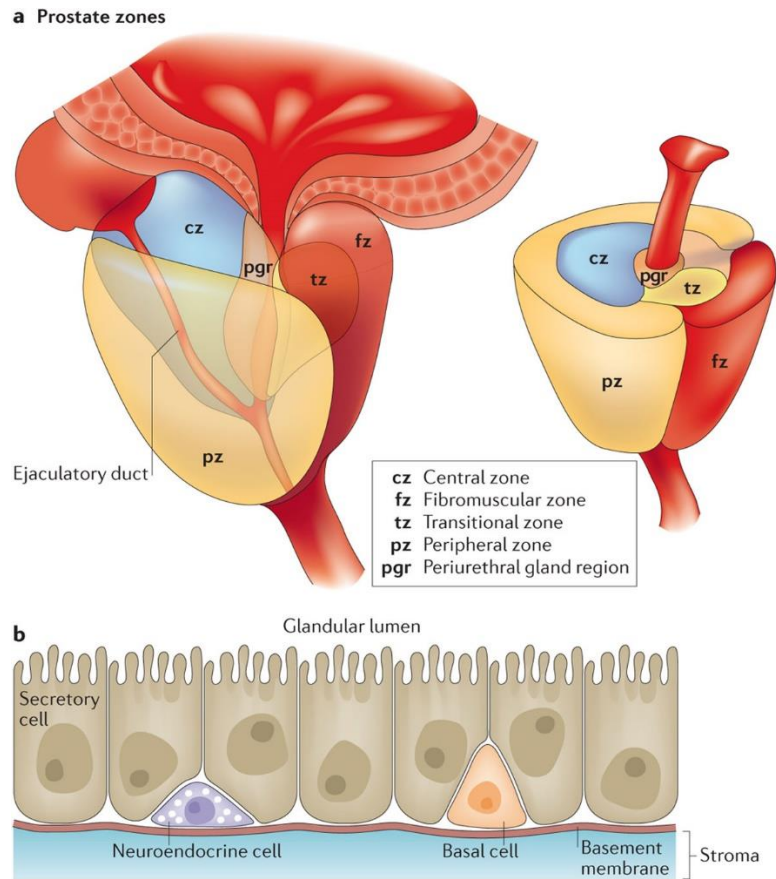
<b>FIGURE 5.2.2 THE EFFECT OF NOT BOILING THE SAMPLES UPON PROTEIN MIGRATION.</b>	<b><u>150</u></b>
<b>FIGURE 5.3.1.1 VISUALISATION OF THE PURIFIED PROTEINS BY WESTERN BLOTTING AND COOMASSIE BLUE STAINING.</b>	<b><u>152</u></b>
<b>FIGURE 5.3.1.2 MASS SPECTROMETRY DATA FOR ATF6.</b>	<b><u>153</u></b>
<b>FIGURE 5.3.1.3 MASS SPECTROMETRY DATA FOR BIP.</b>	<b><u>154</u></b>
<b>FIGURE 5.3.2.1 CLEAVAGE OF ATF6 IN RESPONSE TO ER STRESS.</b>	<b><u>155</u></b>
<b>FIGURE 5.4.1 ATF6 PULL-DOWN.</b>	<b><u>158</u></b>
<b>FIGURE 5.4.2 MASS SPECTROMETRY ANALYSIS OF THE PULL-DOWN SAMPLES.</b>	<b><u>159</u></b>
<b>FIGURE 5.4.3 VALIDATION OF MASS SPECTROMETRY DATA VIA WESTERN BLOT.</b>	<b><u>160</u></b>
<b>TABLE 5.4.1 TABLE SUMMARISING ALL THE INTERACTION PARTNERS OF ATF6 THAT WERE IDENTIFIED IN THE INDUCED SAMPLES AND IN THE PRESENCE OF ER STRESS.</b>	<b><u>161</u></b>

## Chapter 1: Introduction

### 1.1 The prostate

The prostate is a walnut-sized secretory gland in the male reproductive system which helps in the production of semen (Moore et al., 2011). It is localised at the base of the bladder and it is anatomically divided into four regions: the peripheral zone (comprises 70% of glandular tissue and most carcinomas arise from this area), the central zone (surrounds the ejaculatory ducts and comprises 25% of the glandular tissue), the transition zone (surrounds the urethra and comprises 5-10% of the glandular tissue; it is also the site of origin of benign prostatic hyperplasia) and finally, the anterior fibromuscular stroma – which is a non-glandular tissue that surrounds the anterior surface of the three glandular regions (Figure 1.1a) (McNeal, 1981, Verze et al., 2016).

Structurally, the prostate is formed of glandular elements embedded in a fibromuscular stroma. The glandular elements consist of a secretory layer – which is responsible for the production of several factors found in the seminal fluid, such as prostate specific antigen (PSA), prostatic acid phosphatase and human kallikrein-2; and a basal layer – which is made of cuboidal epithelial and neuroendocrine cells that support the secretory layer. The basal layer is then lined by a basement layer which separates the basal cells from the stroma (Figure 1.1b) (Verze et al., 2016). The stroma that encapsulates the prostate consists of collagen, elastin and smooth muscles - which upon ejaculation, contract and force the prostatic fluid into the urethra (Aumuller and Seitz, 1990). The prostatic fluid plays a major role in male fertility as it triggers the molecular pathways involved in ejaculation and regulates proteins that activate sperm maturation and capacitation (Verze et al., 2016).



Nature Reviews | Urology

**Figure 1.1** Gross and microscopic anatomy of the prostate.

A. The prostate has three main zones: the central zone, transition zone and the peripheral zone. B. Microscopic structure of the prostate. The glandular epithelium, composed of the secretory layer and the basal layer, is embedded in the fibromuscular stroma. From (Verze et al., 2016).

### **1.1.1 Endocrine control of the prostate**

In order to maintain endocrine homeostasis, the prostate is regulated by the central nervous system through the hypothalamus and pituitary glands (de Lecea et al., 1998, Sandberg, 1980). Hormones secreted by the pituitary gland, such as luteinizing hormone (LH), follicle stimulating hormone (FSH) and prolactin, control prostatic physiology and anatomy. For example, prolactin plays a role in prostatic growth, function and integrity and the LH regulates testosterone synthesis in the testes (Sandberg, 1980).

Androgens, such as testosterone, are the male sex hormones that are part of the steroid hormone family. They are produced in the testes and adrenal glands and play a crucial role in prostate biology (Evans, 1988). The prenatal development of the prostate is dependent on androgens, and in adults, they promote the survival of secreting epithelia and maintain the functional state of the gland (Heinlein and Chang, 2004, Wilding, 1995). Androgens are also responsible for the development of internal and external genitalia and, during puberty, for the development of secondary sexual characteristics, such as increased skeletal muscle bulk, voice deepening and axillary and pubic hair growth. Reduced levels of androgens have been associated with infertility, whilst increased levels of androgens were found to increase the risk of developing prostate cancer (PCa) (Dart et al., 2013).

### **1.1.2 Diseases of the prostate**

The prostate can be affected by a number of diseases, both benign and malign. Examples of such diseases include prostatitis, benign prostatic hyperplasia (BPH) and PCa (Verze et al., 2016). Prostatitis is an inflammation of the prostate that affects 11-13% of adult men, with 5- 10% of the cases being caused by bacterial strains (Wagenlehner et al., 2013, Roberts et al., 1997). It can be classified into four

categories: acute bacterial prostatitis, chronic bacterial prostatitis, inflammatory or non-inflammatory chronic pelvic pain syndrome and asymptomatic inflammatory prostatitis (Nickel, 2003). Regardless of its cause or type, prostatic inflammation can affect male fertility and remains a possible predisposing factor for the development of BPH and PCa (Verze et al., 2016).

Benign prostatic hyperplasia (BPH) is an enlargement of the prostate that is more common in older men, affecting 8% of men in their forties, more than 50% aged over 60 and 90% of men over 80 years. When the benign enlargement compresses the prostatic urethra, it obstructs the urine flow, leading to the development of lower urinary tract symptoms (LUTS) which are characterised by bothersome voiding. BPH can lead to acute or chronic urinary retention that could cause serious medical complications, such as renal failure, recurrent urinary tract infection, bladder calculi and haematuria. Patients are therefore carefully examined in order to receive the correct treatment, with the standard treatment being the surgical removal of the obstructing tissue (Thorpe and Neal, 2003).

## **1.2 Prostate cancer (PCa)**

In 1853, a surgeon from The London Hospital discovered “a very rare disease” during a histological examination. The condition he discovered became the first recorded case of PCa (Denmeade and Isaacs, 2002). Over a century and a half later, PCa has become a major health problem, being the most common malignancy in men and the second most common form of cancer in the UK. It accounts for 13% of all new cases of cancer, with 1 in 8 men being diagnosed with the disease during their lifetime (Attard et al., 2016).

Although PCa has not been linked to any preventable risk factors (CRUK, 2014), the risk of developing the disease depends on factors such as age, ethnicity,

a previous cancer, family history and genetics. PCa is more common in older men, being rarely diagnosed in men under 50 (CRUK, 2015). It has also been shown that the incidence of PCa is at least 50% higher in black-African men than in other racial and ethnic groups (Greenlee et al., 2001). On the other hand, Asian populations have a significantly lower incidence of PCa compared with the Western populations. Interestingly, men who have emigrated to the Western nations have an increased risk of developing the disease, which suggests a possible environmental or dietary effect (Denmeade and Isaacs, 2002). Furthermore, patients who have had a previous cancer, such as kidney, bladder, lung, thyroid or melanoma skin cancer, have a slightly increased risk of developing PCa (CRUK, 2015).

Another established risk factor for PCa is a family history of the disease. Studies have shown that first-degree relatives of men with PCa have double the risk of developing the disease than the general population. Moreover, the risk is four times higher for the first-degree relatives of men that have been diagnosed with the disease younger than 60 years. Other genetic factors that influence the risk of getting the disease include the PCa predisposition gene HOXB13 and the rare germline BRCA2 mutations from families with increased rates of breast and ovarian cancer; these mutations can increase the risk of developing PCa up to seven times (reviewed in (Attard et al., 2016)).

### **1.2.1 PCa screening**

The prostate-specific antigen (PSA) test measures the amount of PSA present in the blood stream and has been used to aid disease diagnosis since 1994 (Greenlee et al., 2001). PSA is a 33-kDa serine protease, part of the glandular kallikreins family, that is synthesized in the epithelial cells of the prostate. It is secreted into the glandular ducts where it prevents the coagulation of semen by

digesting the seminal vesicle protein, seminogelin (Lilja, 1985, Henttu and Vihko, 1994). The androgen receptor (AR) regulates *PSA* gene expression through three androgen response elements, located in the *PSA* promoter (Heinlein and Chang, 2004) and increases its expression, whilst epidermal growth factor and activation of protein kinase C decreases *PSA* expression (Henttu and Vihko, 1994).

Under normal conditions, *PSA* does not escape from the prostate capsule and therefore *PSA* levels in the blood are undetectable. However, under certain circumstances, *PSA* can leak from the ducts into the prostatic extracellular fluid and enter the blood stream. As *PCa* progresses, the malignant cells affect the normal structure of the ducts and *PSA* is able to enter the circulation. Higher levels of *PSA* can therefore be detected in the blood. *PSA* testing is able to distinguish between cancer-free controls, localised disease and the metastatic stages of the disease (Heinlein and Chang, 2004, Lilja et al., 2008). However, increased serum concentrations of *PSA* are not specific to *PCa*, as they are also found in patients with *BPH*; this has led to over-diagnosis and the treatment of insignificant *PCa* cases (Lilja et al., 2008, Henttu and Vihko, 1994). There is therefore no national screening programme for *PCa* running in the UK (CRUK, 2016a).

### **1.2.2 Types of *PCa*. Gleason score.**

Depending on the type of cell where the cancer originated, *PCa* can be classified into different types: acinar adenocarcinoma –the most common type of *PCa* and develops in the gland cells that line the prostate gland; ductal adenocarcinoma – develops in the cells that line the ducts of prostate gland; transitional cell cancer – develops in the cells that line the urethra and normally starts in the bladder and then spreads into the prostate; squamous cell cancer - originates in the cells that cover the prostate and tends to spread quickly; and finally, the small cell *PCa* which is a

type of neuroendocrine cancer (CRUK, 2016b).

Upon histological examination of prostatic tissue, which was obtained from a biopsy or radical prostatectomy, the diagnosis of PCa can be confirmed only if the basal cell layer is lost. Gleason histologic grading system is based on the glandular differentiation and pattern of tumour growth in the prostatic stroma. The patterns of tumour are classified from the most differentiated (Gleason 1) to the least differentiated (Gleason 5) (Figure 1.2). The scores of the two most abundant patterns of tumour are then added to obtain the Gleason score (H Lee et al., 2011) (H Lee et al., 2011).

### **1.3 Androgen Receptor (AR) as the key oncogenic driver of PCa**

The normal development of the prostate and the maintenance of the male phenotype is regulated by androgens, which act through the androgen receptor (AR) (Heinlein and Chang, 2004). Huggins and Hodges first demonstrated that PCa is also dependent on androgens, and hence that the AR plays a crucial role in the development and progression of the disease (Chen et al., 2009). AR expression is maintained throughout all stages of the disease and promotes cancer progression by continuously conferring growth signals to PCa cells (Germann, 2002, Heinlein and Chang, 2004).

#### **1.3.1 Structure of the androgen receptor**

The androgen receptor (AR) is a ligand-dependent transcription factor that belongs to the Nuclear Receptor Family (Robinson-Rechavi et al., 2003). It is encoded by a gene located on the X-chromosome (locus Xq11-Xq12) (Brown et al., 1989) and consists of 2757-nucleotide long protein coding region. This region spans eight exons, with introns of different sizes (ranging from 0.7 to 2.6 kb) and codes for a 110-kDa protein (919 amino acids) (Germann, 2002).

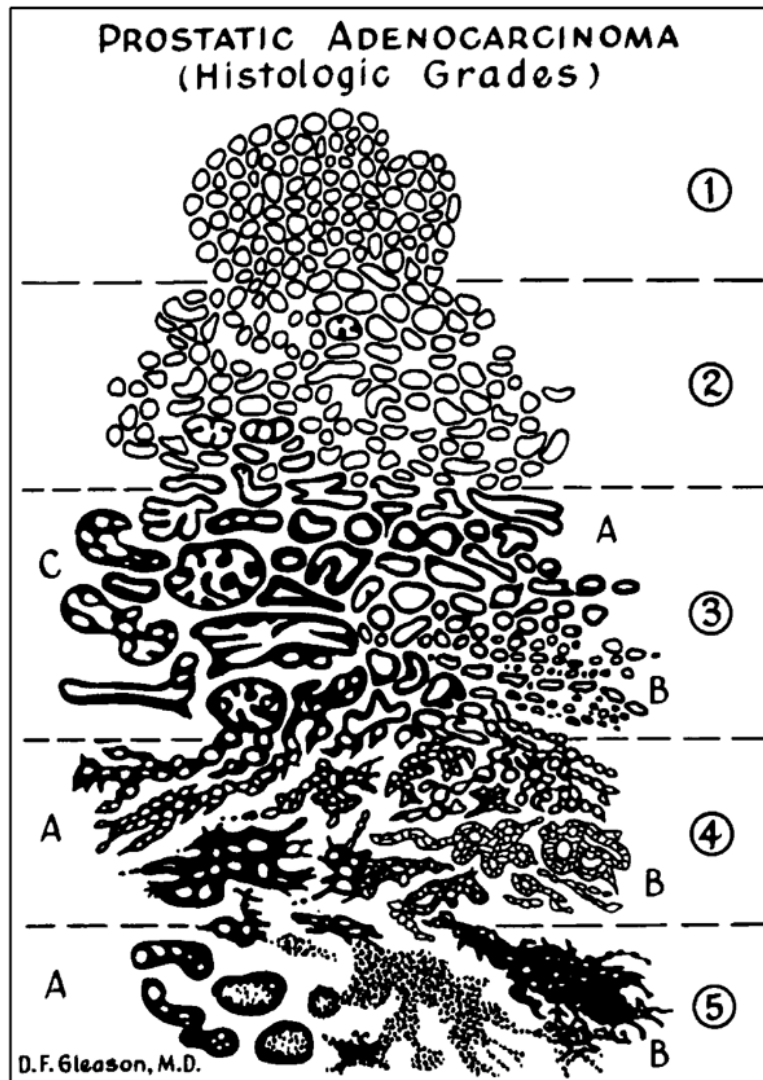


Figure 1.2. Gleason patterns.

Grade 1 and 2 are considered normal prostate cells. Grade 3 is considered as prostate cancer – the glands are single, rounded, vary in shape, size and spacing of the acini and they tend to infiltrate among normal acini. Grade 4 prostate cancer – infiltrating cords that form an anatomically sponge-like epithelium and some cells have an abundant clear cytoplasm (hypernephroid). Grade 5 is the least differentiated prostate cancer – cells do not form glands and are tightly packed together. From (Humphrey, 2004)

AR, like other nuclear receptors, has a modular structure consisting of an N-terminal domain (NTD), followed by a DNA-binding domain (DBD) that is connected to the C-terminal ligand-binding domain (LBD) by a flexible hinge region (Figure 1.3) (Claessens et al., 2008, Robinson-Rechavi et al., 2003). The AR also has two activation functions, AF-1 in the N-terminus (residues 142-485, constitutively active) and the ligand dependent AF-2 in the LBD (Jenster et al., 1992, He et al., 1999).

The NTD is encoded by exon 1 and is the first and largest domain of the AR (residues 1-555). The poly-Q repeat region is highly variable in the human population and its length affects the folding and structure of the NTD. Removal of the poly-Q repeats leads to a decrease in the  $\alpha$ -helical structure of the NTD, whilst an increase in the length of the poly-Q repeats leads to a slight increase in the  $\alpha$ -helical structure (Davies et al., 2008, Tan et al., 2015). These changes in the NTD also affect the AR transcriptional activity, the shorter repeats imposing a higher AR transactivation activity and longer repeats reducing activity.

It has been demonstrated that the structural plasticity of the NTD allows the interaction of the AR with structurally diverse binding partners, such as co-activators, basal transcription factors and intramolecular interactions with the LBD. All these interactions are important for AR activity and the NTD is required for full transcriptional activity (Tan et al., 2015).

The DNA-binding domain (DBD) is the second domain of the AR (residues 556-623) and each DBD is organised into two zinc finger-like modules. The AR functions as a dimer and binds to DNA response elements, such as androgen response elements (ARE) in the regulatory region of target genes. A nuclear localisation signal (NLS), responsible for the nuclear import of the receptor, is found between the DBD and the hinge region (residues 617-633) (Tan et al., 2015).

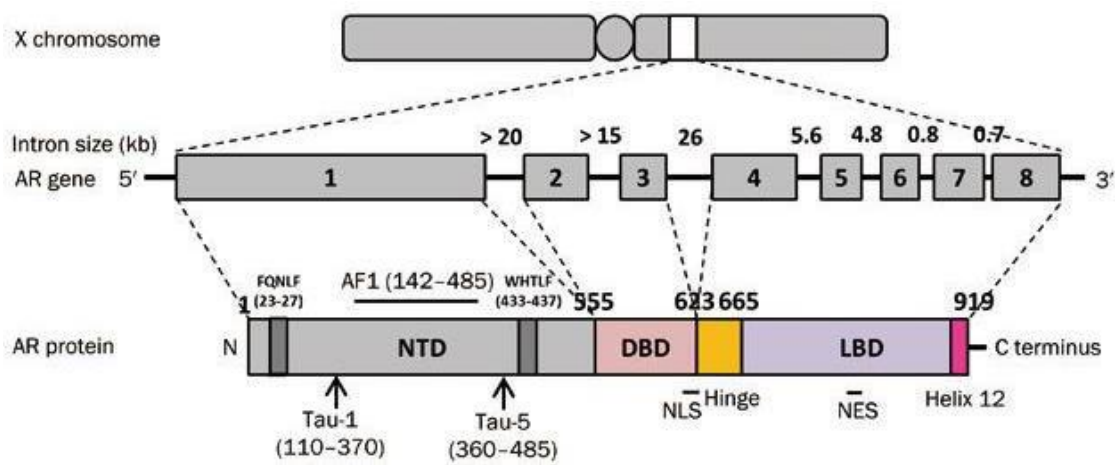


Figure 1.3. The structure of the Androgen Receptor.

AR gene is located on the X- chromosome (Xq11-q12) and codes a 919 amino acids protein. The protein has a N-terminal domain (NTD) encoded by exon 1, a DNA-binding domain (DBD) encoded by exons 2 and 3, a hinge and a ligand-binding domain (LBD) encoded by exons 4-8 (adapted from (Tan et al., 2015)).

The flexible hinge region (residues 624-665) separates the DBD and LBD and consists of the last  $\alpha$ -helix of the DBD and the first  $\alpha$ -helix of the LBD. The NLS is found in this region (Evans, 1988) and mutations within the NLS have been associated with PCa and androgen- insensitivity syndrome (Cutress et al., 2008, Claessens et al., 2008).

The LBD (residues 666-919) is organised in a three-layer, anti-parallel  $\alpha$ -helical sandwich, with eleven  $\alpha$ -helices (H) and two anti-parallel  $\beta$ -sheets. The first layer comprises H1 and H3 helices, the second layer is formed by H4, H5, first  $\beta$ -sheet and H8, H9 and the final layer is completed by H10 and H11. Instead of an H2, the AR has a long flexible linker. The ligand- binding pocket (LBP) is central to the LBD and is surrounded by H3, H5 and H11 that directly contact the bound ligand. H12 acts as a lid to the LBD, closing following ligand binding, resulting in additional cofactor binding sites (Claessens et al., 2008, Tan et al., 2015).

### **1.3.2 Androgen receptor signalling**

The AR is a ligand-dependent transcription factor that is responsible for mediating the physiological effects of androgens. It binds to androgen-responsive genes, such as PSA and transmembrane protease serine 2 (TMPRSS2) and promotes growth and survival of the cells (Gelman, 2002, Heinlein and Chang, 2004). The AR signalling pathway is summarised in Figure 1.4. The pituitary gland secretes the luteinizing hormone (LH) that initiates the production of testosterone by the Leydig cells in the testes. After the testicular synthesis, testosterone is transported to the target tissues, such as the prostate, and is converted to the more potent testosterone metabolite dihydrotestosterone (DHT) by 5- $\alpha$ -reductase. DHT binds to the LBP and promotes the dissociation of the heat-shock protein (HSP) complex from the AR. The AR translocates into the nucleus, dimerizes and binds to

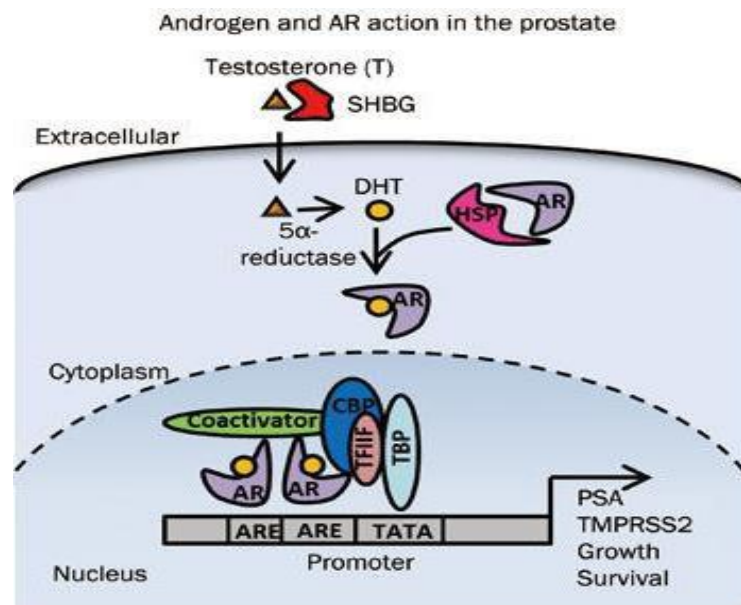


Figure 1.4. Androgen Receptor signalling in the prostate.

First, testosterone is converted to DHT by 5- $\alpha$ -reductase, then it binds the LBP of the AR. AR then translocates into the nucleus, binds to the promoter region of the target genes and initiates transcription.

Target genes of the AR promote growth and survival of the cells. SHBG – Sex Hormone Binding Globulin.

Adapted from (Tan et al., 2015).

AREs in the regulatory regions of target genes. At these response elements, the AR is able to recruit co-activators that facilitate transcription (Tan et al., 2015).

#### **1.4 Treatment of PCa**

Depending on different factors, such as the clinical stage of the tumour, age, serum PSA, Gleason score and number of positive prostate biopsies, patients have different treatment options. For the localised disease and low-grade tumours, therapy options include active surveillance (in order to avoid unnecessary treatment), radical prostatectomy, radiation therapy or cytotoxic chemotherapy. Other options such as cryotherapy, high-intensity focal ultra-sound and photodynamic therapy may also be used (Attard et al., 2016, Denmeade and Isaacs, 2002).

Tumours that have spread from the prostate are usually treated with hormone therapy that blocks the AR signalling pathway and inhibits tumour growth. Androgen deprivation therapy aims to induce chemical castration by either blocking the production or the action of androgens (Brooke and Bevan, 2009). Androgen deprivation therapy can be divided into two categories: androgen depletion therapy and anti-androgens. Androgen depletion therapy prevents the production of androgens by using gonadotropin-releasing hormone (GnRH) agonists and corticosteroids to inhibit the pituitary stimulation of the testes and the adrenals. Furthermore, the conversion of circulating testosterone into DHT by 5 $\alpha$ - reductase can also be inhibited (Chen et al., 2009).

Anti-androgens target the AR signalling pathway by preventing the binding of androgen to the AR. Anti-androgens can be steroidal (such as progesterone analogues) or non-steroidal (such as bicalutamide and enzalutamide) (Chen et al., 2009). Steroidal anti-androgens have a partial agonist activity; therefore, they cannot be used as a first-line therapy (Labrie et al., 1987). Non-steroidal anti-androgens do

not activate AR-dependent reporters or genes and are considered “pure antagonists” (Chen et al., 2009).

In most cases, anti-androgens and androgen depletion therapy are combined in order to achieve a maximal androgen blockade (Labrie et al., 1987, Labrie et al., 1983). However, despite their initial success, these therapies cannot completely inhibit AR activity and invariably fail. The tumours develop resistance and progress to the aggressive and difficult to treat castrate resistant stage (Katsogiannou et al., 2015).

### **1.5 Mechanisms of Therapy Resistance and Castrate Resistant Prostate Cancer**

There are many mechanisms that cause the progression of PCa to a castrate resistant stage (CRPC), and most of them are related to the AR and its reactivation (Figure 1.5). These mechanisms include *AR* gene amplification and over-expression, AR mutations that lead to promiscuous ligand interaction, changes in the balance of AR cofactors and activation via the outlaw pathway (Saraon et al., 2011, Montgomery et al., 2008).

The overexpression of the AR hyper-sensitises the pathway to low androgens environments and is found in 40% of all CRPC cases (Feldman and Feldman, 2001). The AR can also be activated in a ligand independent manner or by other molecules, such as growth factors or kinases (Taplin and Balk, 2004). Mutations of the AR often allow the receptor to be activated by alternative steroids or anti- androgens (such as amino acid substitutions H874Y, T877A and T877S) (Brooke et al., 2008). Increased levels of AR co-activators and decreased levels of co-repressors can also enhance receptor signalling (Brooke et al., 2011).

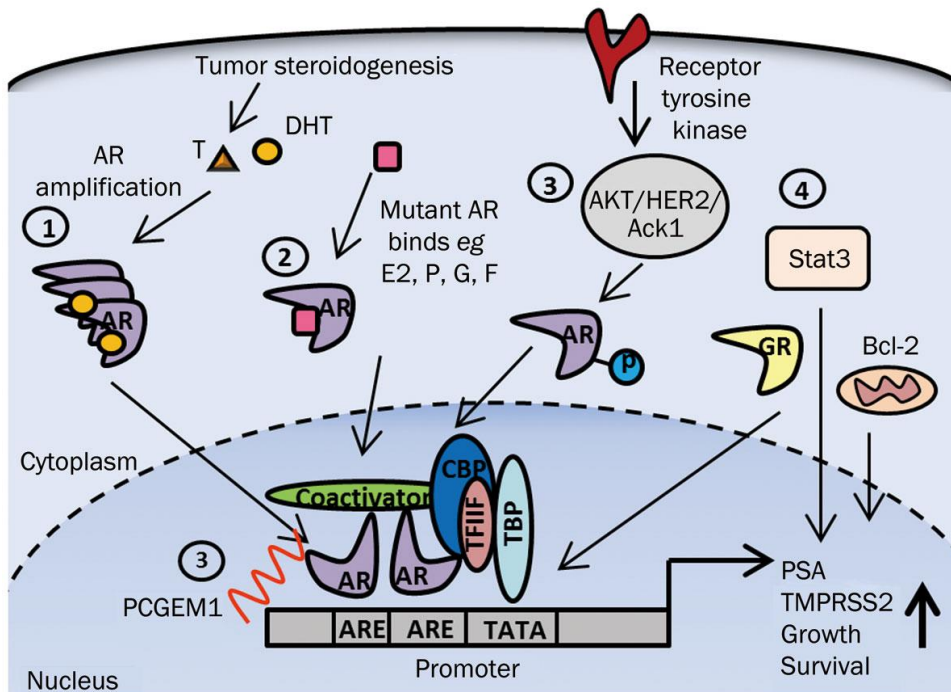


Figure 1.5 Mechanisms that promote the progression of castrate resistant prostate cancer.

AR dependent mechanisms include: (1) Amplification of the AR gene and overexpression of AR protein. (2) Promiscuous pathway – mutations in the AR allow its activation by alternative steroids or anti-androgens. (3) Ligand-free activation of the AR via its crosstalk with AKT, HER2, or Ack1. (4) Androgen-independent mechanisms. E2 – oestrogen receptor, P – progesterone receptor; C – glucocorticoids; F – flutamide; GR – glucocorticoid receptor. Figure from (Tan et al., 2015).

Mechanisms that do not involve the AR pathway, but have been associated with the development of CRPC have also been identified, and they include the over-expression of anti-apoptotic proteins (such as BCL2, and Hsp27), loss of expression of tumour suppressor genes, activation of oncogenes, post-transcriptional modifications using miRNA, epigenetic alterations, alternative splicing and gene fusion (Katsogiannou et al., 2015, Feldman and Feldman, 2001).

### **1.6 The Unfolded Protein Response in Prostate Cancer**

Castrate-Resistant Prostate Cancer is a highly aggressive and difficult to treat terminal stage of the disease that has a major impact on patient's quality of life. Studies have been conducted in order to improve our understanding of the biology of the disease and several mechanisms have already been identified (Katsogiannou et al., 2015, Feldman and Feldman, 2001). However, there is still a great need to characterise the mechanisms of therapy resistance in PCa and develop new approaches to treat this often-terminal stage of the disease.

PCa, like many other solid tumours, is characterised by uncontrolled proliferation of transformed cells, which grow in an environment characterised by lack of oxygen and nutrients and often experience oxidative stress and lactic acidosis; these conditions are known to cause stress in a part of the cell called the endoplasmic reticulum (Storm et al., 2016). This stress impairs protein folding, which is detected by three sensor proteins, IRE1 $\alpha$ , PERK and ATF6 that initiate the unfolded protein response (UPR). If the stress cannot be resolved, the UPR switches from being pro-survival to activating programmed cell death (Corazzari et al., 2017). PCa cells take advantage of the pro-survival UPR pathway - that enables them to survive, adapt to adverse environmental conditions, and promotes therapy resistance. Importantly, the UPR has also been shown to be regulated by the AR, linking the UPR to the key

oncogenic driver of PCa (Sheng et al., 2015).

### **1.6.1 The endoplasmic reticulum (ER)**

Prostate, like all the major secretory organs and cells, has the potential to secrete high protein loads. However, in order to do so, it is reliant on the proper functioning of the endoplasmic reticulum (ER) (Hetz, 2012).

The ER is a large organelle involved in the regulation of protein synthesis, folding and secretion; it also plays an important role in several key cellular functions, such as lipogenesis, gluconeogenesis, calcium storage and organelle biogenesis (Hetz, 2012, Storm et al., 2016). It has a complex architecture and is composed of a dynamic, continuous membrane bilayer that can be divided into three main functional domains – the nuclear envelope (NE), and the peripheral ER cisternae and tubular network. The NE surrounds the nucleus and is formed of two large and flat lipid bilayers – the inner nuclear membrane (INM) and the outer nuclear membrane (OCM) which are separated by the internuclear membrane space. The two membranes connect with each other at nuclear pores, facilitating and regulating the transport of molecules, such as RNAs and proteins, into and out of the nucleus. The NE then extends into cisternae and tubules that are part of the peripheral ER. These structures have different morphologies and so they each have different roles in the cellular processes that are regulated by the ER. The sheets, or cisternae, have ribosomes on their cytosolic surface and they are the main site for protein synthesis, folding, and post-translational modifications, whilst the tubules are mainly involved in lipid synthesis, calcium signalling and contacts with other organelles (Schwarz and Blower, 2016, Friedman and Voeltz, 2011, English and Voeltz, 2013).

The architecture of the ER depends on the type and function of the cell. For example, the ER of secretory cells, such as the one of prostate and pancreatic cells,

have a high density of sheets, whilst liver or adrenal cells tend to have a mainly tubular network (Schwarz and Blower, 2016).

The ER is connected with the plasma membrane (PM) and a number of organelles, including the Golgi apparatus, mitochondria, endosomes, lipid droplets and peroxisomes (English and Voeltz, 2013). The ER membrane frequently comes into contact with the plasma membrane and forms structures called the ER-PM junctions – which have been proved to have important roles in regulating  $Ca^{2+}$  levels and lipid transfer (Carrasco and Meyer, 2011). The ER membrane also interacts with the membrane of the Golgi apparatus in order to regulate the protein and lipid transfer between the two organelles, and this interaction between the membranes is particularly important for the non-vesicular lipid transport. The vesicular transfer of proteins from the ER to Golgi (anterograde transport) is COPII mediated whilst the transfer from Golgi back to the ER (retrograde transport) is COPI mediated. Furthermore, the connection between the ER and mitochondrial membrane is needed in order to regulate  $Ca^{2+}$  signalling, lipid biosynthesis, mitochondrial division and organelle inheritance (English and Voeltz, 2013). Therefore, the ER plays a central role in the proper functioning of a cell and in retaining organismal homeostasis (Rutkowski and Hegde, 2010).

### **1.6.2 Protein synthesis and folding**

However, the main function of the ER is the regulation of synthesis and folding of secretory and transmembrane proteins, being responsible for ~30% of the cellular proteome (Rutkowski and Hegde, 2010). Protein synthesis is initiated on the cytosol side of the ER, where a mRNA-ribosome complex is formed. The nascent polypeptide contains a signal sequence at its N-terminus that is recognised by the signal recognition particle (SRP) and allows the recruitment of the mRNA-ribosome-nascent

polypeptide-SRP complex to the ER membrane where it binds the SRP receptor. The polypeptide then enters the ER lumen via the translocon complex (Rapoport, 2007) and translation continues as the protein threads into the ER lumen. Folding of the protein begins co-translationally and, due to the hydrophobic nature of the signal sequence, the N-terminus of the polypeptide remains integral to the ER membrane, allowing the folding process to take place in a controlled manner (Pearse and Hebert, 2010). Once the signal peptide is cleaved and translation is complete, the ribosome is released into the cytosol bulk and the polypeptide undergoes post-translocation modifications and continues its folding process (Schwarz and Blower, 2016, Adams et al., 2019). These are important processes that allow the protein to mature into its functional tertiary or quaternary state and, because it is a highly error-prone process, it needs to be tightly regulated by ER chaperones and their cofactors (Pobre et al., 2019).

Molecular chaperones, such as those from the protein disulfide isomerase (PDI) family, promote the formation of disulphide bonds – modifications which allow the protein to attain and maintain its tertiary and quaternary structure. Another important quality control measure is the addition of N-linked oligosaccharides ( $\text{Glc}_3\text{Man}_9\text{GlcNAc}_2$ ) to the polypeptide; the subsequent trimming of glucoses by glucosidases I and II influences protein solubility, degradative processes, and interactions with ER chaperones (Williams, 2006, Trombetta and Helenius, 1998, Pearse and Hebert, 2010, Pobre et al., 2019). The lectin chaperones, and predominantly the Calnexin and Calreticulin members, are ER chaperones that are associated with the N-linked glycosylation system – they recognise incompletely folded glycoproteins and bind to the terminal glucose residue of the  $\text{Glc}_1\text{Man}_9\text{GlcNAc}_2$  intermediate oligosaccharide in order to support the proper folding

and oligomerisation of the protein (Hebert et al., 1995).

Other molecular chaperones that reside within the ER include members from the Heat shock protein 40 (Hsp40), Hsp70, Hsp90 and Hsp100, with the Hsp70 member BiP (binding-immunoglobulin protein/GRP78) being one of the most abundant protein in the ER (Williams, 2006, Pobre et al., 2019).

#### **1.6.2.1 Binding immunoglobulinprotein (BiP)**

BiP is an ER chaperone that is able to interact with both glycosylated and non-glycosylated proteins. It has various roles in the cell – from supporting the correct folding of the proteins, contributing to ER calcium stores, maintaining the permeability barrier of the ER and targeting misfolded proteins for proteasome degradation, to sensing stress within the ER and activating the unfolded protein response (UPR) in order to restore ER homeostasis (Pobre et al., 2019). Under physiological conditions, BiP is bound to the three stress sensor proteins: IRE1 $\alpha$ , PERK and ATF6 and inhibits their activation (Hetz, 2012). BiP forms a stable complex with the luminal domains of both IRE1 $\alpha$  and PERK, and is able to inhibit their activation by stopping their spontaneous self-dimerization, oligomerization and autophosphorylation (Bertolotti et al., 2000), whilst for ATF6, BiP binding masks the Golgi-localisation signals leading to the retention of ATF6 in the ER membrane (Shen et al., 2002). The build-up and accumulation of misfolded proteins in the ER results in the relocalisation of BiP which dissociates from the three UPR sensor proteins and binds the unfolded proteins instead (Walter and Ron, 2011).

An indirect model and a direct recognition model have been proposed as potential mechanisms through which ER stress is sensed by IRE1 $\alpha$  and PERK (Hetz et al., 2020). One indirect model suggests that in the presence of unfolded proteins, BiP releases the IRE1 $\alpha$  sensor in order to preferentially bind the misfolded peptide

chains. In this model, unfolded proteins compete for BiP and ERdj4, a co-chaperone of BiP which is required to stabilise BiP binding to IRE1 $\alpha$  and prevent the dimerization of IRE1 $\alpha$  (Amin-Wetzel et al., 2017, Amin-Wetzel et al., 2019). Another indirect model states that BiP has the ability to sense the ER stress and that it binds the misfolded peptide chains via its substrate binding domain. This interaction then causes the ATPase domain of BiP to dissociate from IRE1 $\alpha$  and PERK leading to their activation and initiation of UPR (Carrara et al., 2015b, Kopp et al., 2018). Finally, due to the major histocompatibility complex (MHC)-like structure of IRE1 $\alpha$ 's luminal domain, the direct model suggests that unfolded proteins are able to bind directly to IRE1 $\alpha$ . However, this model is not widely supported as the crystal structure of the MHC type I groove suggests that the luminal domain of IRE1 $\alpha$  is not compatible with peptide binding and following further investigations, no misfolded proteins bound to IRE1 $\alpha$  could be detected *in vitro* (Hetz et al., 2020).

Once BiP dissociates from the three sensors, it supports the proper folding pathways of the newly synthesised proteins by binding to the hydrophobic regions that are present in their unfolded regions; this action prevents the aggregation of the nascent polypeptides and is regulated by the binding of ATP and ADP molecules (ATPase cycle). BiP is able to bind the hydrophobic regions of the unfolded proteins when it is bound by ATP and is, therefore, in an open state. Once bound to the protein, members of the DNAJ proteins support the hydrolysis of ATP into ADP, locking BiP onto the misfolded protein. Folding of the protein progresses when the ADP molecule is released from BiP – a process which is supported by ER nucleotide exchange factors and members of the DNAJ family that allows ATP to rebind and leads to the release of the protein from BiP. As the ATPase cycle continues, the folding of the nascent proteins progresses (Ma and Hendershot, 2004a, Pobre et al., 2019).

Finally, when the proteins are correctly folded into their functional conformation, they are released by chaperones and are prepared for their transport to the Golgi apparatus. The exit of secretory proteins from the ER occurs exclusively via the ER exit sites (ERES) – which are smooth ER projections that are coated with COPII coat components that facilitate the generation of COPII vesicles (Barlowe, 2002, Sato and Nakano, 2007). The vesicles carrying the cargo are then transported to the ERGIC (vesicular-tubular clusters) where they are sorted into anterograde carriers that transfer them to the Golgi. After their passage through the Golgi, the proteins are delivered to their final destination within the cell or beyond (Szul and Sztul, 2011).

However, if the newly synthesized proteins fail to mature into their native conformation, they are targeted by the ER-associated degradation (ERAD) pathway - which cause the protein to be retro-translocated into the cytosol, where it is ubiquitylated and degraded by the 26S proteasome (Vembar and Brodsky, 2008, Kumari and Brodsky, 2021). If the misfolded proteins cannot be degraded by the ERAD, then another pathway is activated in order to increase the capacity of the ER, reduce protein translation, control the expression of ERAD genes, autophagy and restore the ER homeostasis (Qi et al., 2017, Hwang and Qi, 2018). This pathway is called the Unfolded Protein Response (UPR).

### **1.6.3 The Unfolded Protein Response**

Stressful conditions, such as hypoxia, nutrient deprivation, increase in secretory demand, or loss of calcium homeostasis lead to an accumulation of unfolded proteins in the ER. This disrupts the ER function and is termed ER stress (Clarke et al., 2014, Hetz and Papa, 2017). When unfolded proteins accumulate above a critical threshold, three sensor proteins - IRE1 $\alpha$  (inositol requiring-enzyme 1

alpha), PERK (protein kinase RNA-like ER kinase) and ATF6 (activating transcription factor 6) initiate several signal transduction pathways, collectively called the unfolded protein response (UPR), in an attempt to restore homeostasis (Figure 1.6) (Corazzari et al., 2017). The signal transduction pathways initiated by the sensors work together to maintain the function of the ER and the accuracy of protein folding by attenuating protein translation, increasing the folding capacity of the ER, controlling protein trafficking, and degrading the misfolded proteins via the ERAD and autophagy pathways. If the cells have been under prolonged ER stress that cannot be resolved, then the UPR switches to a pro-apoptotic response where it regulates several mechanisms that initiate programmed cell death (Hetz et al., 2020).

Although the main function of the UPR is to reduce the stress and restore proteostasis, it has also been associated with the regulation of other cellular processes, such as lipid and cholesterol metabolism, energy homeostasis, inflammation, and cell differentiation (Rutkowski and Hegde, 2010, Hetz, 2012).

Furthermore, the UPR is involved in the pathogenesis of various diseases, involving both secretory cells and diseases that are linked to protein misfolding and aggregation. Abnormal levels of ER stress have been associated with diabetes mellitus, retinitis pigmentosa, immunological disorders, neurodegenerative conditions and cancer (Hetz et al., 2020, Oakes and Papa, 2015).

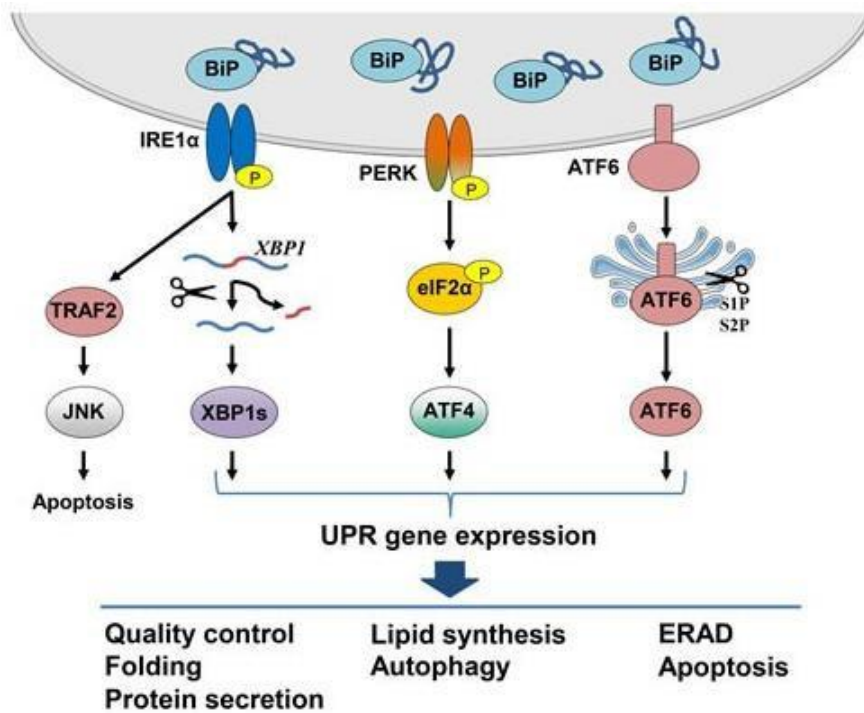


Figure 1.6. ER stress sensors and the UPR signalling pathways.

The dissociation of BiP from the three UPR sensors leads to the phosphorylation of IRE1 $\alpha$  and PERK and the translocation of ATF6 to the Golgi apparatus. The sensor proteins initiate the UPR pathways in order to restore homeostasis. From (Storm et al., 2016).

### **1.6.3.1 Inositol requiring-enzyme 1 alpha (IRE1 $\alpha$ )**

IRE1 $\alpha$  is a 1115 amino acid type I transmembrane protein that is encoded by the ERN1 gene (located on chromosome 17, locus 17q23.3) and has a site-specific endoribonuclease (RNase) and serine/threonine kinase activity (Mori et al., 1993, Hetz and Papa, 2017). The protein has two domains: the ER-luminal N-terminal domain and the cytoplasmic C-terminal domain. The crystal structure of the N-terminal domain has been solved by Zhou *et al.* and is made of 367 amino acids which form a triangular  $\beta$ -sheet cluster. On each side of the triangular plate there are three major  $\beta$ -sheet motifs (N, C, and M motifs) which have several  $\alpha$ -helices inserted between them (Zhou et al., 2006). The N-terminal domain senses the unfolded proteins and upon dissociation of BiP, it dimerises to form an MHC-like groove that is stabilised by hydrogen bonds and hydrophobic interactions. The cytoplasmic domain of IRE1 $\alpha$  has two parts: the kinase domain and the kinase-extension nuclease (KEN)/RNase domain which is located at the C-terminal of the molecule (Siwecka et al., 2021). The kinase domain (amino acids 571-832) has a bilobal structure and contains the ATP-binding site located between the  $\beta$ -sheet N-terminal lobe and the  $\alpha$ -helical C-terminal lobe. The activation segment is located at amino acids 711-741; a possible phosphorylation site is also present at the Ser724 and an APE and DFG motifs at amino acid 746-748 and 711-713, respectively. The RNase domain is located at amino acids 835-963 and has a helical conformation (Lee et al., 2008, Carlesso et al., 2019, Ali et al., 2011, Siwecka et al., 2021).

### **1.6.3.2 Protein kinase RNA-like ER kinase (PERK)**

PERK is a type I transmembrane serine/threonine protein encoded by the EIF2AK3 gene on chromosome 2 (locus 2p11.2) and has a ER-luminal domain and a cytosolic domain – which contains the protein kinase domain (Harding et al., 1999).

The structure of the N-terminal domain has been solved by (Carrara et al., 2015a) and was found to have both a dimeric state as well as a transient ring-type tetramer structure. The four monomers (A, B, C, D) consist of mainly  $\beta$ -sheets and two  $\alpha$ -helices; their structure can be divided into three structural motifs – the dimerization subdomain,  $\beta$ -sandwich subdomain, and the tetramer subdomain. The dimerization subdomain consists of a series of anti-parallel  $\beta$ -sheets that allow the formation of the A-B and C-D dimers. The role of the  $\beta$ -sandwich subdomain is to stabilize the other domains and is made of  $\beta$ -strands arranged into a two-layer  $\beta$ -sandwich fold. Finally, the tetramer subdomain was found to stabilize the interaction between the A-B and C-D dimers and consists of  $\beta$ -strands and one  $\alpha$ -helix. As the  $\alpha$ -helix of the tetramer domain is swapped between the monomers, it indicates that the tetramer interphase of PERK is transient and that it plays an important role in the activation of UPR (Carrara et al., 2015a).

### **1.6.3.3 Activating transcription factor 6 (ATF6)**

The stress sensor ATF6 is a type II ER membrane protein, part of the basic leucine zipper (bZIP) transcription factor family. It is encoded by a gene located on chromosome 1 (locus 1q23.2) and it consists of 670 amino acids (Haze et al., 1999a, NCBI, 2019). The protein has three main domains – the ER-luminal domain (C-terminus), a trans-membrane domain that allows its integral association with the ER membrane, and the cytoplasmic domain (N-terminus). Similarly to other members of the bZIP family, the cytoplasmic segment of ATF6 contains the transcription-activation domain and the well-conserved bZIP domain. The binding site for the ER chaperone BiP, the Golgi localization sequences (GLS) as well as the cleavage sites for the site-1 (S1P) and site-2 proteases (S2P) are found on its luminal domain. These are important sites that allow the detection of unfolded proteins as well as its

translocation from the ER to the Golgi – where it is processed by S1P and S2P (Asada et al., 2011, Jheng et al., 2018).

#### **1.6.3.3.1 Mammalian expression of membrane proteins for structural studies**

The structures of IRE1 $\alpha$  and PERK have already been solved (Ali et al., 2011, Zhou et al., 2006, Carrara et al., 2015a, Lee et al., 2008) however, the study of ATF6 has proved problematic. Many difficulties are encountered during the expression of a membrane protein, as well as during its solubilisation, purification and crystallisation (Carpenter et al., 2008).

In order to solve the structures of IRE1 $\alpha$  and PERK, their luminal domains (and IRE1 $\alpha$ 's cytosolic domain) had to be expressed in bacterial cells (*E. coli* BL21, BL21 (DE3) and Rossetta 2 (DE3) strains). Because bacterial cells are easy to manipulate, are fast growing, and have inexpensive culture costs and high levels of overexpression, they have been widely used for the expression of soluble proteins (Mathieu et al., 2019). However, the expression of functional eukaryotic membrane proteins in bacterial systems has been difficult to achieve. One difficulty consists in the complexity of eukaryotic membrane proteins – they have a partial hydrophobic surface, are flexible, they lack stability, and they require molecular chaperones that facilitate their folding into a functional state. Post-translational modifications, such as N-glycosylation, palmitoylation and disulfide bond formation are often essential for the efficient folding of membrane proteins and bacterial or yeast systems do not have the necessary machinery that allow this process to occur (Andréll and Tate, 2013). Using a mammalian expression system that allows the post-translational modifications to take place is therefore recommended. However, the attachment of large and highly heterogeneous N-glycans to the expressed protein, as is often observed for HEK293 cells, could be a major drawback in the process of crystallisation (Reeves et al., 2002).

Furthermore, the nature of the lipids in which the proteins are embedded may affect their stability and ultimately, the process of crystallisation (Carpenter et al., 2008). This limitation is addressed in Chapter V, where I used a modified mammalian expression system (Reeves et al., 2002) to overcome the difficulties encountered during the expression of ATF6.

Detergents also play an important role in the process of solubilisation, purification, and crystallisation of membrane proteins. The challenge consists in the selection of appropriate detergents that are suitable for these processes. In most cases, the detergent that is used for solubilisation is not adequate for purification and crystallisation. During solubilisation, detergents have to disrupt the phospholipid bilayer and cover the hydrophobic region of the protein to form a water-soluble protein-detergent complex that prevents the aggregation of proteins once they are removed from the cell. Ionic detergents, such as sodium dodecyl sulphate (SDS), disrupt the hydrophobic interaction of the protein core and leads to their denaturation. Milder non-ionic detergents only break the lipid-lipid interactions, not the protein-protein interactions, and are therefore preferred in membrane protein research. N-dodecyl- $\beta$ -D-maltoside (DDM) is an example of such a detergent and has been broadly used in this field (Carpenter et al., 2008, Moraes et al., 2014, Parker and Newstead, 2016).

The next challenge consists in finding the optimal conditions that promote the protein and detergent molecules into crystal formation. There are different types of crystallisation methods available. The most common one is known as *in surfo* crystallisation, where vapour diffusion, microdialysis and microbatch techniques are used for membrane proteins. Then, there is crystallisation *in meso*, where certain lipids are mixed with the protein-detergent complex. This leads to the formation of lipidic cubic phases (LCP) which can then be turned into sponge phases (useful for

large proteins or protein complexes) (Moraes et al., 2014). An advantage of this method is that the membrane proteins are able to diffuse in the lipid, rather than being confined by the detergent (Carpenter et al., 2008). However, regardless of the crystallization method, many parameters must be taken into consideration, such as purity of the protein and its aggregation state, buffers, pH values, temperature, precipitants, salts and additives. Although automation and membrane crystallization screens are available, this remains a tedious process where many difficulties are encountered (Moraes et al., 2014). The detergent covering the hydrophobic regions of the protein reduces the protein-protein interactions and that leads to the formation of fragile crystals with poor diffraction ability. Addition of other detergents or additives in the crystallisation drop can improve their quality; however, for growth of crystals, optimisation still remains difficult to achieve (Carpenter et al., 2008, Moraes et al., 2014).

#### **1.6.4 The adaptive UPR**

The first cellular event initiated by the activated UPR involves a general reduction in protein synthesis and an enhanced degradation of unfolded proteins, whilst the second event involves the transcriptional upregulation of target genes that are involved in the global control of protein homeostasis. In the adaptive activity of the UPR, IRE1 $\alpha$ , PERK and ATF6 work as a complex signalling network that restores ER proteostasis and preserves cellular function (Hetz and Papa, 2017).

##### **1.6.4.1 Adaptive signalling of IRE1 $\alpha$**

The IRE1 $\alpha$  branch initiates pathways that increase the folding capacity of the ER and its ability to deal with ER stress (Storm et al., 2016). Activation of IRE1 $\alpha$  in response to ER stress occurs following the dissociation of BiP from the sensor domain which allows the IRE1 $\alpha$  to dimerise, oligomerise and trans-

autophosphorylate its kinase domains. This leads to the activation of the RNase domain that is involved in the splicing of its substrate (Yoshida et al., 2001, Yoshida et al., 2006). Splicing of XBP1 mRNA is assisted by Sec61, a component of the translocon (Hetz et al., 2020). Spliced XBP1 mRNA encodes a protein (XBP1s) which is a more stable transcription factor that is involved in the regulation of various genes that modulate protein folding, secretion, ER-associated degradation (ERAD), protein translocation into the ER, lipid synthesis and production of proteins that are involved in ER biogenesis (Lee et al., 2005, Acosta-Alvear et al., 2007).

Furthermore, the RNase domain of IRE1 $\alpha$  has been found to regulate the stability of multiple other mRNAs in a process known as “regulated IRE1-dependent decay” (RIDD) which aims to reduce the protein load during stressful conditions by targeting mRNAs that contain the consensus sequence CTGCAG and have a secondary structure similar to that of XBP1. This is a very important process is that is able to either preserve ER homeostasis or induce programmed cell death (Siwecka et al., 2021). It was also found to be involved in the regulation of inflammation, glucose metabolism and liver function (Hollien and Weissman, 2006, Maurel et al., 2014).

#### **1.6.4.2 Adaptive signalling of PERK**

PERK initiates a pathway that reduces the rates of protein translation (Hetz et al., 2020). Upon dissociation of BiP, PERK is activated by oligomerisation and trans-autophosphorylation. Once active, it phosphorylates the eukaryotic translation initiator factor-2 (eIF2 $\alpha$ ) at serine 51 (Harding et al., 1999), an event that leads to an attenuation of protein translation and that reduces the number of proteins entering the ER. The eIF2 $\alpha$  phosphorylation also triggers the selective CAP-independent translation of the ATF4 mRNA – which encodes for a transcription factor that

regulates genes involved in redox balance, amino acid metabolism, protein folding, autophagy and cell survival. The enhancement of ATF4 translation ultimately leads to an increased folding capacity of the ER and an upregulation of macroautophagy (Hetz and Papa, 2017, Clarke et al., 2014). ATF4 is also involved in a feedback loop that restores protein synthesis once the stress has been resolved. ATF4 upregulates the expression of protein phosphatase 1 (PP1), the regulatory subunit of GADD34, which promotes the dephosphorylation of eIF2 $\alpha$  and the resumption of protein synthesis (Hetz et al., 2020).

#### **1.6.4.3 Adaptive role of ATF6**

Upon the dissociation of BiP, the Golgi localization sequences (GLS) of ATF6 are exposed and ATF6 is able to interact with the coat protein complex II (COPII). This leads to the translocation of ATF6 to the Golgi apparatus (Sato and Nakano, 2007, Shen et al., 2002) where S1P and S2P cleave within its luminal and transmembrane domains. The released cytoplasmic domain (ATF6f) is a bZIP transcription factor that translocates to the nucleus and binds to the ER stress response elements in target genes (Haze et al., 1999a). ATF6f activates the transcription of various genes, including ER chaperones (BiP, GRP94 and PDI), ERAD components (protein degradation enzymes), UPR genes such as XBP1, and, together with PERK, activates the transcription of CCAAT/Enhancer-Binding Protein homologous protein (CHOP) (Park et al., 2017, Hayat, 2015). Therefore, activation of ATF6 helps restore ER homeostasis through an increase in the folding capacity of the ER, the activation of ERAD and the induction of autophagy (Bommiasamy and Popko, 2011, Yu et al., 2017).

### 1.6.5 The pro-apoptotic UPR

The ways in which UPR promotes the survival of cells in response to ER stress have been described above. However, in conditions of chronic stress, the UPR switches from being pro-survival to activating programmed cell death (Figure 1.7).

The pro-apoptotic response is mainly mediated by IRE1 $\alpha$  and PERK, however ATF6 is also involved in these processes through the upregulation of CHOP (Storm et al., 2016, Hetz, 2012).

The adaptive IRE1/XBP1 branch is first activated in response to stress with the aim of restoring proteostasis. However, in response to prolonged ER stress, IRE1 $\alpha$  ceases to splice XBP1 and targets RIDD substrates instead. This results in the endonucleolytic decay of many ER-localised mRNAs, including those encoding for chaperones, such as BiP. This reduction in molecular chaperones impairs protein folding even further and causes additional ER stress that ultimately leads to apoptosis (Han et al., 2009).

Hyper-phosphorylated IRE1 $\alpha$  induces apoptosis by reducing (by degradation) the levels of microRNAs that suppress pro-apoptotic targets, such as the anti-Casp2 miRNA, miR-17, miR-96 and miR125b. This leads to the activation of the apoptotic initiator Caspase-2 and an increased expression of thioredoxin-interacting protein (TXNIP) (Chen and Brandizzi, 2013). The activation of Caspase-2 initiates mitochondrial oxidative stress-induced apoptosis (Lopez-Cruzan et al., 2016) whilst increased levels of TXNIP activate the NLRP3 inflammasome and Caspase-1 cleavage leading to sterile inflammation. Sterile inflammation then triggers the production of pro-inflammatory cytokines and chemokines, such as interleukin-1 $\beta$  (IL-1 $\beta$ ) and causes pyroptotic death (Chen and Nunez, 2010, Lerner et al., 2012).

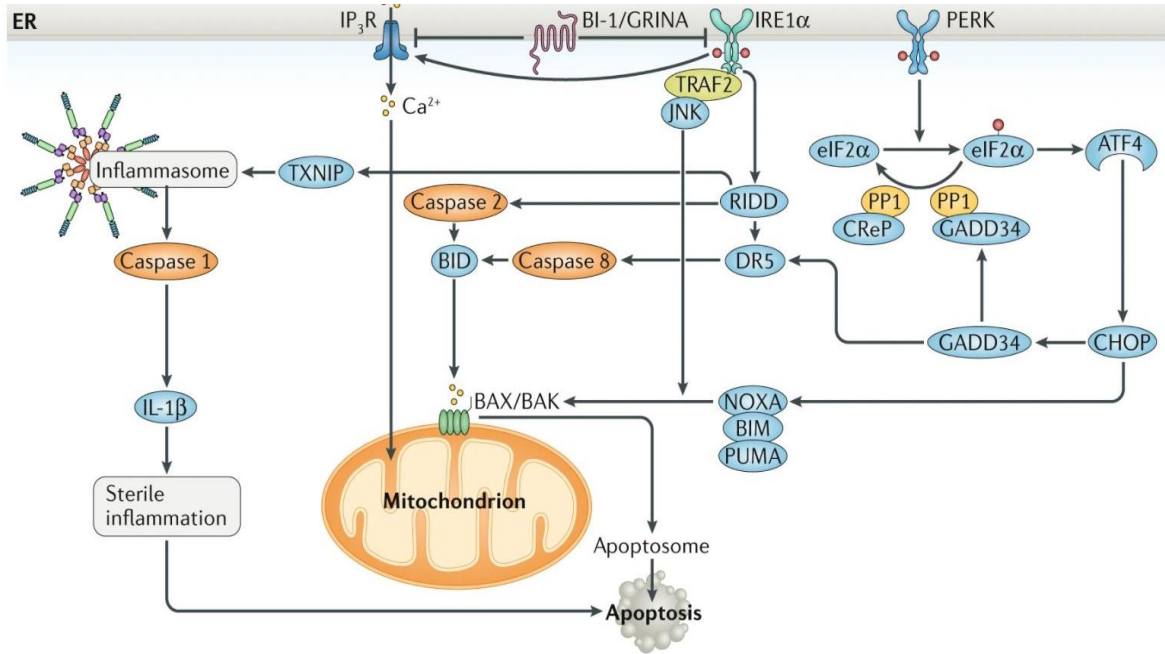


Figure 1.7. Apoptosis pathways induced by ER stress.

In the presence of chronic ER stress, IRE1 $\alpha$  and PERK become hyper-phosphorylated and initiate the pro-apoptotic response. Adapted from (Hetz et al., 2020)

Another mechanism through which IRE1 $\alpha$  can initiate apoptosis is through the recruitment of the adaptor protein tumour necrosis factor receptor (TNFR)-associated factor 2 (TRAF2) and apoptosis signal regulating kinase 1 (ASK1) to the ER membrane. This activates c-Jun N-terminal kinase (JNK) and p38 MAPK and results in the activation of the pro-apoptotic factors BID and BiM and inhibition of the anti-apoptotic factors BCL-2, BCL-XL, and MCL-1 (Adams et al., 2019).

PERK signalling is also an important regulator of the switch between the adaptive response and the pro-apoptotic response (Storm et al., 2016). PERK activation leads to a decreased secretory load; however, its sustained signalling is not compatible with survival (Hetz and Papa, 2017). CHOP, one of the target genes of ATF4 and ATF6, encodes a transcription factor responsible for the regulation of the pro- and anti-apoptotic members of the BCL-2 family. When PERK is hyperphosphorylated, CHOP suppresses the expression of anti-apoptotic BCL-2, whilst up-regulating the pro-apoptotic members, such as BIM, PUMA and NOXA (Urra et al., 2013, Zinszner et al., 1998). Another mechanism through which CHOP promotes apoptosis is through the regulation of the GADD34 gene. GADD34 (growth arrest and DNA damage inducible 34) associates with the phosphatase PP1, promotes the dephosphorylation of eIF2 $\alpha$  and reinitiates protein synthesis. This may in turn trigger proteotoxicity and lead to apoptosis through an increased reactive oxygen species (ROS) production and ATP depletion (Urra et al., 2013). Furthermore, it has been found that CHOP activation induces the transcription of death receptor 5 (DR5). The increase in the protein levels of DR5 leads to a ligand-independent activation of the receptor and of the apoptotic machinery via caspase-8 (Lu et al., 2014).

Furthermore, accumulation of ROS in the ER leads to a release of Ca<sup>2+</sup> from the ER lumen through the inositol 1,4,5-triphosphate receptor (IP<sub>3</sub>R); the subsequent

uptake of  $\text{Ca}^{2+}$  by the mitochondria leads to a release of cytochrome c and formation of the BAX/BAK-dependent apoptosome (Hetz et al., 2020).

In summary, chronic ER stress leads to the activation of the pro-apoptotic response, which through the interaction of many different mechanisms, aims to eliminate the damaged cells from the system.

### **1.6.6 The Unfolded Protein Response in Cancer**

It is known that tumours grow in an environment characterised by hypoxia, nutrient deprivation and lactic acidosis. These conditions, together with intrinsic factors, such as oncogenic activation, alteration in chromosome number, genomic instability, increased mutations and redox imbalance, lead to ER stress (Ma and Hendershot, 2004b, Urra et al., 2016). The UPR was found to be highly active in various cancers including breast, colorectal, liver and glioma (Madden et al., 2019). Therefore, the UPR activation has been studied in different human tumours and cellular models and it was found that individual components of the UPR are associated with cell transformation, dormancy, angiogenesis, immunogenicity, genomic instability, metastasis and resistance to treatment (Figure 1.8) (Urra et al., 2016). Moreover, the ER chaperones BiP and GRP94 were found to be overexpressed in solid tumours and BiP abundance was particularly associated with poor prognosis and increased proliferation rate and invasion of several types of cancer. Hence, the UPR has become an attractive therapeutic target for both solid and blood cancers (Urra et al., 2016). The mechanisms through which the UPR drives tumourigenesis, cancer progression, cell dormancy and therapy resistance will be described below.



Figure 1.8 UPR and the hallmarks of cancer.

The UPR sensors have individual roles in the development of cancer. ATF6 is mainly linked to dormancy and metastasis, whilst IRE1 $\alpha$  is associated with many hallmarks, with the exception of dormancy. PERK is involved in most of the hallmarks involving cancer growth and progression. From (Urrea et al., 2016).

### 1.6.6.1 UPR in tumourigenesis and cancer progression

The UPR promotes tumour progression by regulating mechanisms that enhance cell survival, trigger cell transformation, and change the metabolic status of the cell (Urrea et al., 2016). Neoplastic transformation is the process through which a cell becomes malignant and requires an accumulation of mutations that either activate oncogenes (such as BRAF<sup>V600E</sup>, c-MYC, H-RAS) or cause the loss or inactivation of tumour suppressor genes (such as p53). This transformation then leads to a rapid and uncontrolled cell growth which overloads the ER due to the constant need for high level protein synthesis; these conditions lead to the activation of the UPR, which the cells exploit in order to survive and support cancer progression (Madden et al., 2019). For example, in melanoma cells, the BRAF<sup>V600E</sup> mutation activates IRE1/XBP1 and ATF6 signalling and the knockdown of BiP and XBP1 were found to delay melanoma cell proliferation (Croft et al., 2014).

Loss of the p53 tumour suppressor gene in HCT116 colorectal carcinoma cells was found to increase IRE1 $\alpha$  expression and activate IRE1 $\alpha$ /XBP1s signalling which enhanced the function of the ER and promoted cell proliferation (Namba et al., 2015).

However, the process through which the UPR is able to sustain its pro-survival signalling, and not trigger apoptosis in the rapidly growing tumours, is not entirely understood. It has been proposed that this is achieved through the activation of pro-survival mechanisms, such as autophagy, as well as the inhibition of pro-apoptotic components, such as CHOP (Madden et al., 2019). For example, Hart *et. al.* demonstrated that in both mouse and human lymphoma, c-MYC was able to activate PERK/eIF2/ATF4 signalling which resulted in the activation of autophagy; this was found to promote the c-MYC dependent cell transformation and increase tumour growth (Hart et al., 2012). Moreover, a study conducted by Rong *et. al.* showed that

the suppression of the pro-apoptotic component CHOP by the oncogenic H-RAS<sup>V12</sup> was one of the mechanisms through which H-RAS<sup>V12</sup> was able to promote cellular transformation (Rong et al., 2005). In several cancers, such as glioblastoma and pre-B acute lymphoblastic leukaemia, overexpression of XBP1s has been associated with poor prognosis (Pluquet et al., 2013, Kharabi Masouleh et al., 2014), and in chronic lymphocytic leukaemia and triple-negative breast cancer (TNBC) is involved in tumour progression (Storm et al., 2016). In TNBC, XBP1 promotes tumour progression by interacting with hypoxia-inducible factor 1-alpha (HIF1 $\alpha$ ) and induces the expression of hypoxia signature genes (Chen et al., 2014). Furthermore, the P58IPK protein, which is regulated by XBP1 and ATF6, promotes the survival of tumour cells undergoing ER stress (Huber et al., 2013) and mutations of IRE1 $\alpha$  have been associated with loss of its apoptotic function (Urrea et al., 2016).

PERK is involved in the initiation of cancer and tumour progression, mainly by regulating protein translation in hypoxic tumours, the NRF2 pathway and cellular redox, metabolism, and lipid biosynthesis (Bu and Diehl, 2016, Urrea et al., 2016). It is well known that solid tumours grow in a harsh, hypoxic environments, and so the tumours must tolerate these conditions in order to survive (Muz et al., 2015). The protective role of PERK in response to these conditions is conferred by ATF4 and CHOP – which bind directly to the promoters of MAP1LC3B and ATG5 and induces their expression. The increased expression of MAP1LC3B and ATG5 leads to the expansion of the phagophore and formation of the autophagosome which ultimately induces autophagy (Rouschop et al., 2010, Bu and Diehl, 2016). Furthermore, PERK maintains redox homeostasis in tumours through its interaction with NRF2 – a direct substrate of PERK which regulates the expression of genes involved in the production of glutathione, an important antioxidant which protects cellular

macromolecules from reactive oxygen and nitrogen species (Pizzorno, 2014), and prevents the accumulation of ROS in the ER (Bu and Diehl, 2016).

#### **1.6.6.2 UPR in tumour dormancy and therapy resistance**

The UPR has been linked to tumour dormancy. Dormant cells are inactive, they do not divide and are in a state of cell cycle arrest (G0/G1 phase). When the optimal conditions for cell proliferation and metabolism are restored, these cells may be reactivated and cause cancer recurrence, especially after a course of chemotherapy or radiotherapy (Paez et al., 2012). ATF6 is constitutively active in dormant cells and a study has found that the inhibition of ATF6 in these tumours causes a downregulation of adaptive pathways (such as mTOR) leading to reduced tumour cell survival and proliferation (Schewe and Aguirre-Ghiso, 2008). It is also found overexpressed in recurrent cells (mainly in metastatic lesions) where it has been linked with poor prognosis (Ramaswamy et al., 2001). Furthermore, ATF6 is able to control proteins involved in tumour transformation and increased chemo- and radiotherapy resistance. IRE1 $\alpha$  and PERK also have a role in this process. IRE1 $\alpha$ /XBP1s signalling can control cell cycle progression and proliferation through the regulation of cyclin D1 expression whilst PERK may induce dormancy through the negative regulation of cyclin D1 and promote drug resistance of dormant cells (Urrea et al., 2016). The UPR is therefore involved in many aspects of tumour cell biology, such as angiogenesis, invasion, mitochondrial function, intercellular communication and tumour associated inflammation (Clarke et al., 2014).

#### **1.6.7 The role of UPR signalling in Prostate Cancer**

The activation of the UPR in PCa enables cells to survive, adapt to adverse environmental conditions and promotes therapy resistance (Storm et al., 2016, Corazzari et al., 2017). Importantly, the UPR has also been shown to be directly

regulated by the AR, linking the UPR to the key oncogenic driver of PCa (Sheng et al., 2015). For instance, the AR was able to bind to gene regulatory sites and activate the IRE1 $\alpha$  arm whilst inhibiting PERK signalling. Activation of the IRE1 $\alpha$  restored homeostasis and secured cell survival, whilst inhibiting JNK signalling; this reduced apoptosis and resulted in an increase in proliferation. XBP1s expression, when compared to normal prostate, was also upregulated in PCa samples, suggesting that IRE1 $\alpha$  is important in PCa progression. Furthermore, inhibition of the IRE1 $\alpha$  branch reduced PCa cell growth in both *in vitro* and *in vivo* models (Sheng et al., 2015). Using preclinical mouse models, Sheng *et. al.* further demonstrated that the use of a specific IRE1 $\alpha$  RNase inhibitor (MKC8866) was able to inhibit the growth of PCa tumours and increase the effects of the chemotherapeutic Cabazitaxel. Using global transcriptomic analysis, Sheng *et. al.* also demonstrated that XBP1s directly activates the expression of c-MYC and controls the activation of the c-MYC transcriptional program (Sheng et al., 2019). c-MYC is an oncogenic pathway that is highly active in all stages of PCa (Wu et al., 2021, Hawksworth et al., 2010) and recently, it has been found that there is a significant positive correlation between the levels and activity of c-MYC and AR – where c-MYC regulates the expression of the full-length and splice variants of the AR in CRPC (Bai et al., 2019). Therefore, an important role may emerge for the IRE1 $\alpha$ /XBP1s branch of the UPR, where crosstalk between c-MYC and androgen signalling promotes PCa progression (Zhang et al., 2020).

Recently, PERK signalling has also been found to support the progression of PCa. For example, Nguyen *et. al.* used a mouse model of MYC-hyperactivated PCa and showed that PERK signalling, and most importantly the phosphorylation of eIF2 $\alpha$ , was selectively activated in advanced PCa in order to enhance protein

synthesis to a level that supports tumour development. The use of a small molecule (ISRIB) that reinitiates protein synthesis (despite the phosphorylation of eIF2 $\alpha$ ) in a patient-derived xenograft model was found to impair the progression of metastatic PCa (Nguyen et al., 2018). An additional study highlighted the importance of ATF4 in PCa and identified a novel ATF4 target gene – the *family with sequence similarity 129 member A (FAM129A)*. The expression of ATF4 and FAM129A were found to be increased in PCa samples and inhibition of ATF4-FAM129A branch successfully restricted tumour growth in a preclinical PCa model (Pällmann et al., 2019). Furthermore, Liu et. al. looked at the expression levels of IRE1 $\alpha$ , PERK and ATF6 in a panel of 160 PCa and 30 BPH tissues and found that their expression was correlated with the Gleason grade, PSA level, T stages and M stage of the tissues. They could also associate high expression levels of the UPR sensors with poor prognosis, shorter survival duration and PSA recurrence (Liu et al., 2017).

Radiation therapy is a common and effective treatment for PCa, however the tumours can become resistant to such treatments and the cancer progresses to an inoperable stage (Nørgaard et al., 2010). In order to enhance the effect of radiotherapy upon PCa, Amoroso *et. al.* used ONC21 – a molecule that activates the UPR – to enhance the activation of UPR in response to radiation and promote cell death. Their results showed that ONC21 was able to increase the radiation response by increasing the expression of the UPR components and by suppressing the expression of cell cycle and DNA repair factors (Amoroso et al., 2021).

ER chaperones such as BiP, HSP27 and HSP90 also play an important role in PCa and their overexpression has been associated with aggressive PCa; HSP27 was able to promote metastasis in PCa and inhibit apoptosis in PC3 cells, whilst the inhibition of HSP90, in combination with non-invasive low energy focused ultrasound,

led to a shift between pro- survival UPR signalling to the pro-apoptotic response (Storm et al., 2016). BiP is the most studied ER chaperone in PCa (Storm et al., 2016) and its overexpression is associated with a greater risk of PCa recurrence and a worse survival (Pootrakul et al., 2006). Although it is normally located in the ER lumen, in PCa and several other cancers, BiP is found on the cell membrane (Arap et al., 2004); this translocation has also been linked with the Castrate-Resistant PCa (Zhang et al., 2013). Because BiP is only present on the cell surface of malignant cells and not in healthy cells (Arap et al., 2004), several approaches have already been employed to try and develop a targeted therapy against cancer (Storm et al., 2016). One particular study was able to demonstrate that targeting the surface BiP suppressed castration-resistant osteoblastic bone metastases *in vivo* (Mandelin et al., 2015).

Furthermore, a pro-apoptotic protein (prostate apoptosis response 4 PAR-4) secreted by cancer cells was able to bind to the surface BiP and induce apoptosis (Burikhanov et al., 2009).

Therefore, ER stress and the UPR play an important role in PCa. The AR directly regulates the UPR, and the UPR sensors together with the ER chaperones have a key role in tumour survival and therapy resistance (Storm et al., 2016). However, despite the medical relevance of the pathway, our understanding of the UPR in PCa is limited.

## **1.7 Research Aims**

This study aims to characterise the UPR in PCa, to identify methods to target this pathway to promote tumour death and to generate an expression system to facilitate the characterisation of ATF6:

- 1) *Investigate the effect of targeting UPR signalling upon Prostate Cancer*

### *proliferation*

Proliferation assays (Crystal Violet) and qPCR will be used in order to investigate the effect of UPR inhibitors on PCa cell lines. These inhibitors will block the activity of IRE1 $\alpha$ , PERK, and ATF6 in cell lines representing different stages of the disease, in the presence/absence of ER stress (induced using tunicamycin). Flow cytometry and Caspase 3/7 apoptosis assays will also be performed to determine whether the inhibition of the sensor proteins induces cell cycle arrest and/or apoptosis.

### *2) Investigate the expression of components of the UPR components in Prostate Cancer*

The expression levels of IRE1 $\alpha$ , PERK and ATF6 in the different PCa cell lines will be measured using qPCR and immunoblotting. Protein expression will be correlated with drug sensitivity assessed in Aim 1 to see if expression levels correlate with pathway sensitivity.

### *3) Characterise the effects of androgens and anti-androgens upon UPR signalling in Prostate Cancer*

AR positive prostate cancer cells (e.g. LNCaP) will be treated with androgen and the effect upon the expression of UPR members measured using qPCR and immunoblotting. The effect of anti-androgens and the role of UPR signalling in cellular outcome, will be measured using the experiments described in Aim 1.

### *4) Address the lack of a suitable expression system for the study of membrane proteins, with a particular focus on ATF6.*

Stable tetracycline-inducible HEK2935 GnTI(-) cell lines will be generated in order to express ATF6. Mass spectroscopy, Coomassie blue staining and immunoblotting will be used to investigate whether ATF6 is expressed as a functional protein and to identify novel interaction partners of the protein.

## Chapter 2: Materials and Methods

### 2.1 Reagents, buffers and solutions

#### 2.1.1 Reagents and kits

All the reagents and kits used in this study are shown in the tables below.

**Table 2.1.1 Reagents and kits used in this study.**

Reagent/Kit	Supplier
Acrylamide	Sigma-Aldrich
Agar	Fisher Scientific
Agarose	Fisher Scientific
Amicon® Ultra – 0.5 Centrifugal Filter Devices kit	Millipore, MERK
APS (Ammonium persulfate)	Sigma-Aldrich
Bovine serum albumin (BSA)	Sigma-Aldrich
Crystal Violet (CV) stain	Sigma-Aldrich
Coomassie Blue staining solution	Thermo-Fisher Scientific
DC Assay kit	Bio-Rad
DMEM	LONZA
DMEM/F-12 50/50 1x growth medium	Corning®
Dimethyl sulfoxide (DMSO)	Sigma-Aldrich
Ethidium bromide	Sigma-Aldrich
Foetal bovine serum (FBS)	SLS (Cat No. YPMI-25)
GeneJet Gel Extraction Kit	Thermo-Fisher Scientific
Glycine	Thermo-Fisher Scientific

Glycogen blue	Thermo-Fisher Scientific
Halt phosphate inhibitor cocktail	Thermo-Fisher Scientific
Heat-inactivated foetal bovine serum (HI-FBS)	SLS
HiYield™ Plasmid Kit (Mini)	Real Biotech Corporation
IPTG ((Isopropyl-B-D-thiogalactoside)	Sigma-Aldrich
Luria Broth (LB)	Lennox, Fisher Scientific
Luria Broth (LB) agar	Sigma-Aldrich
Luna® Universal qPCR Master Mix	New England Biolabs
LunaScript RT® SuperMix Kit	New England Biolabs
Luminata™ Forte Western HRP Substrate	Millipore
PageRuler™Plus Prestained Protein Ladder	Thermo-Fisher Scientific
Penicillin-Streptomycin-Glutamine (PSG)	Sigma-Aldrich
Phenol red-free RPMI-1640	SLS
Phosphate-buffered saline (PBS) tablets	Sigma-Aldrich
PMSF (Phenylmethylsulfonyl fluoride)	Sigma-Aldrich
Propidium iodide (PI) 1 mg/ml	Sigma-Aldrich
PureLink™ RNase A (20 mg/ml)	Thermo-Fisher Scientific
Q5® High-Fidelity DNA Polymerase (M0491)	New England Biolabs
QIAEX®II Kit (cat. no. 20021)	QIAGEN
RPMI-1640	SLS
TEMED (Tetramethylethylenediamine)	Sigma-Aldrich
TRIS	Sigma-Aldrich

TRIzol® Reagent	Ambion
Trypsin/EDTA	Sigma-Aldrich
Tween® 20	Sigma-Aldrich
XGal	Sigma-Aldrich
Sodium dodecyl sulphate (SDS)	Fisher Scientific

## 2.1.2 Solutions and buffers

All the solutions and buffers used in this study are shown in the tables below.

**Table 2.1.2.1 Buffers and solutions used for Western Blotting.**

Name	Description	Storage
RIPA (radioimmunoprecipitation) cell lysis buffer	0.5 ml of 1mM Tris-Cl (pH 8.0), 1 mM of EDTA (20 mg), 1% Triton X-100, 0.1% sodium deoxycholate (50 mg), 0.1% SDS, 140 mM NaCl, protease inhibitors (added in time of experiment).	Filter sterilised and stored at 4°C.
10x Running buffer	30.3g of Tris, 144g of Glycine, 100 ml of 10% SDS, ddH <sub>2</sub> O to 1 L.	Autoclaved and stored at room temperature.
Semi-dry Transfer Buffer	11.26 g glycine, 2.44 g Tris, 200 ml methanol, H <sub>2</sub> O up to 1 L	Stored at room temperature

10% acrylamide gel	1.65 ml acrylamide, 1.9 ml 1 M Tris pH 8.9, 1.4 ml ddH <sub>2</sub> O, 50 µl 10% SDS, 50 µl 10% APS, 5 µl TEMED (Tetramethylethylenediamine).	Prepared fresh every time
Stacking gel	425 µl acrylamide, 947 µl 1 M Tris pH 6.8, 1.1 ml H <sub>2</sub> O, 25 µl 10% SDS, 25 µl 10% APS, 2.5 µl TEMED	Prepared fresh every time
10% SDS	50 g of SDS, 500 ml H <sub>2</sub> O	Stored at room temperature

**Table 2.1.2.2 Buffers and solutions used for cloning.**

<b>Name</b>	<b>Description</b>	<b>Storage</b>
Luria Broth (LB)	10 g LB, 500 ml ddH <sub>2</sub> O; Supplemented with antibiotics as needed	Autoclaved and stored at room temperature
LB Agar	35 g LB agar, 1 L ddH <sub>2</sub> O.	Autoclaved and stored at room temperature. Supplemented before use with antibiotics and poured into plates.
SOC medium (super optimal broth with catabolite repression)	2% tryptone, 0.5% yeast extract, 10 mM NaCl, 2.5 mM KCl, 10 mM MgCl <sub>2</sub> , 10 mM MgSO <sub>4</sub> , and 20 mM glucose, made up in 1 L of ddH <sub>2</sub> O.	Autoclaved and stored at room temperature
1% agarose gel	0.75 g agarose, 75 ml 1X TAE, 1-2 µl EtBr	Prepared fresh every time
10X TAE (Tris acetic acid EDTA) buffer	800 ml ddH <sub>2</sub> O, 48.4 g TRIS, 3.7 g EDTA, 11.4 ml acetic acid	Autoclaved and stored at room temperature

**Table 2.1.2.3 Buffers and solutions used for flow cytometry.**

<b>Name</b>	<b>Description</b>	<b>Storage</b>
Nicoletti buffer	10 g Sodium citrate, 10 ml Triton (100x), ddH <sub>2</sub> O up to 1 L; Before use, 1 ml Nicoletti buffer was mixed with 20 µl PI	Stored at 4°C
PI staining solution for cell cycle measurement	1 ml PBS, 10 µl RNase A (20 mg/ml), 10 µl PI (1 mg/ml)	Prepared fresh

**Table 2.1.2.4 Drugs used in this study**

<b>Name / Company</b>	<b>Description</b>	<b>Storage</b>
<b>Mibolerone (MIB)</b> (Sigma-Aldrich)	Synthetic androgen.	Dissolved in EtOH -20°C
<b>Bicalutamide (BIC)</b> (Sigma-Aldrich)	Anti-androgen drug. Blocks activity of androgens by binding to the AR.	Dissolved in EtOH -20°C

<b>Enzalutamide (ENZA)</b> (Sigma-Aldrich)	Anti-androgen drug. Blocks translocation of AR from the cytoplasm to the nucleus.	Dissolved in DMSO -20°C
<b>Tunicamycin (TUN)</b> (Abcam)	ER stress-inducer. Nucleoside antibiotic that inhibits protein glycosylation.	Dissolved in DMSO -20°C
<b>4μ8c</b> (Sigma-Aldrich)	Selective inhibitor of IRE1α. Blocks substrate access to the active site of IRE1α and inhibits splicing of XBP1 and RIDD.	Dissolved in DMSO -20°C
<b>Toyocamycin</b> (Abcam)	Selective IRE1α inhibitor. PI3-kinase inhibitor. Suppresses tunicamycin-induced XBP1 mRNA splicing.	Dissolved in DMSO -20°C
<b>AEBSF</b> (Sigma-Aldrich)	Inhibitor of ATF6. Irreversible serine protease inhibitor.	Dissolved in ddH <sub>2</sub> O -20°C
<b>GSK-2656157 (GSK)</b> (Santa Cruz Biotechnology)	Highly selective inhibitor of PERK. ATP-competitive. Decreases apoptosis and excessive autophagy.	Dissolved in DMSO -20°C
<b>HA15</b> (Sigma-Aldrich)	Specific inhibitor of BiP. Inhibits the ATPase activity of BiP.	Dissolved in DMSO -20°C

<b>Z-VAD-FMK</b> (Selleckchem)	Irreversible inhibitor of pan-caspase; blocks all features of apoptosis.	Dissolved in DMSO -20°C
<b>Necrostatin-1</b> (Sigma-Aldrich)	Inhibitor of necroptosis. Allosteric inhibitor of RIP1 Kinase. Blocks necroptosis, leading to necrosis.	Dissolved in DMSO -20°C
<b>Ferrostatin-1</b> (Sigma-Aldrich)	Inhibitor of ferroptosis. Blocks lipid peroxidation.	Dissolved in DMSO -20°C

## 2.2 Cell culture

A panel of human prostate cancer cell lines that represent the different stages of the disease was utilised in this study (Table 2.2.1). BPH-1, LNCaP, C42, C42B, 22Rv1, DU145 and PC3 cells were purchased from the ATCC and grown in Roswell Park Memorial Institute (RPMI) 1640 growth medium that was supplemented with 10% foetal bovine serum (FBS) and 1% Penicillin Streptomycin-Glutamine (PSG). The HEK293S GnTI (-) cells were kindly supplied by Dr Philip Reeves (University of Essex) and grown in Corning® DMEM/F-12 50/50 1x growth medium that was supplemented with 10% heat-inactivated foetal bovine serum (HI-FBS), 1% L-Glutamine and 1% Penicillin-Streptomycin. All the cells were incubated at 37 °C, in humidified air and at 5% CO<sub>2</sub>.

**Table 2.2.1 Prostate Cancer cell lines used in this study.**

<b>Cell line</b>	<b>Origin / Type</b>	<b>Characteristics</b>	<b>Mutations</b>	<b>Reference</b>
<b>BPH-1</b>	Prostate / Epithelial	Benign prostate hyperplasia  Androgen independent	<b>Express:</b> WT p53, PTEN, Bax, p21  <b>Do not express:</b> AR, PSA, PAP	(Hayward et al., 1995)
<b>LNCAP</b>	Prostate / Epithelial	Metastatic prostate adenocarcinoma  Androgen responsive	<b>Express:</b> AR, PSA, PAP WT p53 PTEN inactivation CK-8, 18, and 20.	(Horoszewicz et al., 1983, Cunningham and You, 2015)
<b>C42</b>	Prostate / Epithelial-like	Derived from LNCAP  Androgen responsive	<b>Express:</b> AR, PSA CK-8	(Wu et al., 1994)
<b>C42B</b>	Prostate / Epithelial-like	Derivative subline of C42  Androgen responsive	<b>Express:</b> AR, PSA CK-8	(Thalmann et al., 1994)
<b>22RV1</b>	Prostate / Epithelial	Castration-induced regression and relapse  AR splice variants	<b>Express:</b> AR, PSA	(Cunningham and You, 2015)
<b>DU145</b>	Prostate / Epithelial	Castrate Resistant PCa  Androgen independent	<b>Express:</b> P223L/V274F p53 PTEN, CK-5, 7, 8, 19  <b>Do not express:</b> AR, PSA	(Stone et al., 1978, Namekawa et al., 2019)
<b>PC3</b>	Prostate / Epithelial	Castrate Resistant PCa  Androgen independent	<b>Express:</b> Mutated p53 TGF- $\alpha$ , EGFR  <b>Do not express:</b> AR, PSA, PTEN	(Kaighn et al., 1979, Namekawa et al., 2019)
<b>HEK293S GnTI-</b>	Embryonic Kidney / Epithelial-like	Lack complex N-glycans	<b>Do not express:</b> GnTI (N-acetylglucosaminyltransferase I)	(Reeves et al., 2002)

### **2.2.1 Passage of cells**

The cells were grown until they reached 70 - 80% confluency and then passaged as follows: the growth medium was aspirated, the cells were washed with warm phosphate buffered saline solution (PBS) and incubated with Trypsin-EDTA for several minutes at 37°C. Once the cells had detached from the flask, 5 or 10 mL of growth medium was added, and the required volume of cell suspension was added to a new cell culture flask (Thermo Fisher Scientific) containing fresh growth medium.

### **2.2.2 Cell counting and plating**

The cell suspension (from Section 2.2.1) was used to seed plates for new experiments. To be able to seed a specific number of cells per well, the number of cells in the suspension was calculated. This was done as follows: 0.5 mL of cell suspension was diluted in 4.5 mL medium, 10 µl of this mixture was added to a haemocytometer and the cells that were present in 10 haemocytometer squares were counted. The counted cells were averaged, and the value converted into number of cells  $\times 10^6$ ; this value was then utilised to determine the number of cells per mL by dividing this value to the number of RPMI mL utilised to resuspend the cells. Finally, this value was used to determine the volume of cell suspension and growth medium needed to seed plates with the desired cell concentration.

### **2.2.3 Defrosting/freezing cells**

The frozen stock was quickly defrosted by placing the cryovial in warm water (37 °C). The cell suspension was transferred to 5 ml of warm growth medium. The cells were collected by centrifugation (500xg, 3 minutes), the supernatant was removed, and the cells were re-suspended in 5 ml of fresh growth medium. The cell suspension was then transferred to an appropriately sized flask (25 cm<sup>2</sup> or 75 cm<sup>2</sup>)

and incubated overnight under the previously described conditions. After 24 h, the growth medium was replaced with fresh medium.

To create a frozen stock, the cells were passaged as previously described in Section 2.2.1. The cells were then collected by centrifugation (500xg, 3 minutes) and resuspended in freezing medium (10% DMSO, 90% FBS). The volume of freezing medium utilised in this step depended on the size of the flask that the cells were grown in – 2 ml freezing medium for a 25 cm<sup>2</sup>, and 4 ml freezing medium for a 75 cm<sup>2</sup>. 1 ml of this cell suspension was then transferred to a cryovial, which was then wrapped in a few layers of insulating material and stored at -80°C. To ensure preservation, the cells were transferred into liquid nitrogen after 24 h.

### **2.3 Crystal Violet Proliferation Assay**

To determine IC<sub>50</sub> values, BPH-1, LNCaP, DU145 and PC3 cells were treated for 72 h with a dose range of Tunicamycin (TUN) and UPR inhibitors (0 µM, 0.01 µM, 0.1 µM, 1 µM, 10 µM). The IC<sub>50</sub> values were subsequently used for combination treatments, in order to inhibit the three UPR arms during ER stress. The cells were seeded in 96-well plates, at a concentration of 4,000 cells per well (100 µl). After 24 h, the cells were treated as previously described and incubated at 37 °C for another 72 h. To fix the cells, 100 µl of 4% PFA-PBS were added to the wells and incubated for 1 h at RT. The plate was then washed three times with H<sub>2</sub>O and left to dry. Next, 40 µl of 0.08% crystal violet stain were added to each well and left for 1 h at RT. The plate was then washed three times with H<sub>2</sub>O and left to dry. Finally, 100 µl of 10% acetic acid was added per well and left on a shaker for 1 h, at RT. The plates were read at 490 nm, using the FLUOstar Omega microplate reader (BMG LABTECH).

## **2.4 Flow cytometric assays**

BPH-1, LNCaP, DU145 and PC3 cells were seeded in 12-well plates at a cell concentration of 30,000 cells per well. To investigate the effect of ER stress upon PCa cell cycle and cell death, the cells were treated with a dose range of Tunicamycin (0  $\mu$ M, 0.01  $\mu$ M, 0.1  $\mu$ M, 1  $\mu$ M, 10  $\mu$ M) for 72 h. Next, to determine what type of cell death was triggered by ER stress, the cells were treated with inhibitors of cell death (Z-VAD-FMK, Necrostatin-1 and Ferrostatin-1) 30 minutes before the treatment with Tunicamycin (1  $\mu$ M). The plates were then incubated at 37°C for 72h before being collected and analysed using the BD Accuri™ C6 flow cytometer. The mechanisms of cell death were investigated using DU145 CASP8, FADD and RIP1 knock-out cell lines treated with 1  $\mu$ M Tunicamycin for 72 h.

### **2.4.1 Cell cycle analysis**

After treatment (described in Section 2.4), the growth medium was transferred to a 2 ml Eppendorf tube. 500  $\mu$ l of PBS were added to each well and then transferred to the corresponding Eppendorf tube. The cells were detached with 100  $\mu$ l trypsin/EDTA, resuspended in 500  $\mu$ l of the collected medium and transferred to the corresponding Eppendorf tubes. The cells were centrifuged for 5 minutes at 5500 RPM (MiniSpin mini centrifuge, Eppendorf) and resuspended in 50  $\mu$ l PBS. 500  $\mu$ l of 70% EtOH was added dropwise, whilst mixing with a vortex, to each tube and stored at 4 °C. Before performing the analysis, the cells were pelleted for 5 minutes, 5500 RPM (MiniSpin mini centrifuge, Eppendorf) and resuspended in 200  $\mu$ l PI staining solution (see Section 2.1.2). The samples were analysed using the BD Accuri™ C6 flow cytometer (BD Biosciences).

### **2.4.2 PI inclusion and DNA Hypodiploidy Assay**

The cells were harvested, as previously described in Section 2.4.1, and kept on ice. For the PI inclusion assay, 20 µg/ml of propidium iodide (PI) were added to the cells, vortexed, and analysed immediately. Next, in order to perform the DNA Hypodiploidy assay, the cells were centrifuged for 2 minutes at 5000 RPM and then resuspended in 200 µl Nicoletti buffer (see Section 2.1.2). Analysis for both assays was performed using the BD Accuri™ C6 flow cytometer (BD Biosciences).

### **2.5 Quantitative PCR (qPCR)**

Quantitative PCR was used to analyse the expression of various UPR target genes. The starting material for this technique is total RNA, extracted from the cells of interest. The RNA was reverse transcribed into complementary DNA (cDNA) used as the template for the qPCR reaction.

#### **2.5.1 RNA extraction**

Cells were seeded in 12-well plates and treated as necessary. After the desired time, growth medium was removed, and the cells were washed once with PBS. 400 µl of TRIzol® Reagent (Ambion) was added to each well, transferred to a 1.5 ml Eppendorf tube and incubated at RT for 10 minutes. 100 µl of chloroform were added to each tube, the tubes were shaken for 15 seconds, and incubated at RT for 3 minutes. The tubes were centrifuged at 12000 x g for 15 minutes, at 4°C. The top phase was transferred to a fresh tube and, to help the precipitation of RNA, 1 µl of Glycogen Blue and 250 µl cold isopropanol were added to each tube; the tubes were mixed by inversion for a few seconds and incubated at RT for 10 minutes. To precipitate the RNA, the tubes were centrifuged for 10 minutes at 12000 x g, 4°C. The pellets were washed 2 times with 400 µl 75% EtOH (5 minutes centrifugation at 7500 x g, 4°C). After the ethanol was removed, the pellets were allowed to dry at RT and

resuspended in 20 µl ddH<sub>2</sub>O. The concentration of RNA was determined by Nanodrop® ND-1000 UV/VIS Spectrophotometer.

### **2.5.2 NanoDrop® ND-1000 UV/VIS Spectrophotometer**

The RNA concentration was measured with the help of NanoDrop® ND-1000 UV/VIS Spectrophotometer (Thermo Scientific) according to manufacturer's guidelines. The ratio of absorbance at 260 nm over the absorbance at 280 nm (260/280) as well as the ratio of absorbance at 260 over the absorbance at 230 (260/230) were used to assess the quality of the RNA - values over 1.8 indicating that the RNA was clean and pure. Nanodrop was also used to determine the concentration of DNA extracted from different sources.

### **2.5.3 Reverse Transcriptase PCR**

cDNA was synthesised using the LunaScript RT® SuperMix Kit (New England Biolabs). 2 µl LunaScript RT SuperMix (5X), 125 ng of RNA and nuclease-free H<sub>2</sub>O up to a total volume of 10 µl were added in a PCR tube and incubated in a thermocycler (T100™, Bio-Rad) according to manufacturer's instructions. The cycle details are shown in Table 2.5.3. Prior to use, each cDNA sample was diluted with 30 µl ddH<sub>2</sub>O and then stored at -20°C.

### **2.5.4 Real-time qPCR**

Real-time qPCR was performed using a Roche LightCycler 96. The reaction mix consisted of 2 µl cDNA, 5 µl Luna® Universal qPCR Master Mix (New England BioLabs), 0.4 µl forward primer (10 µM), 0.4 µl reverse primer (10 µM) and 2.2 µl ddH<sub>2</sub>O. The thermocycling conditions were set according to the manufacturer's guidelines (New England Biolabs) and are shown in Table 2.5.4.1. The primers used for these experiments are shown in Table 2.5.4.2 and were purchased from Sigma. The expression levels of the studied genes were normalised to the expression of the

60S ribosomal protein L19 (RPL19) gene. The delta-delta Ct method was used to calculate changes in gene expression.

**Table 2.5.3 Cycle details for the synthesis of cDNA using the LunaScript RT<sup>®</sup> SuperMix.**

Cycle step	Temperature	Time	Cycles
Primer annealing	25°C	2 min	
cDNA synthesis	55°C	10 min	1
Heat inactivation	95°C	1 min	

**Table 2.5.4.1 Thermocycling protocol for real-time qPCR using Luna Sybr green master mix.**

Cycle step	Temperature	Time	Cycles
Initial denaturation	95°C	60 sec	1
Denaturation	95°C	15 sec	40-45
Extension	60°C	30 sec	
Melt curve	60-95°C	60 sec	1

**Table 2.5.4.2 Primers used for Real-time qPCR.**

Primer name	Primer sequence (5'-3')
XBP1s_F	TGCTGAGTCCGCAGCAGGTG
XBP1s_R	GCTGGCAGGCTCTGGGGAAG
ATF4_F	GGGACAGATTGGATGTTGGAGA

ATF4_R	ACCCAACAGGGCATCCAAGT
HERPUD1_F	TCCTCCTCCTGACGTTGTAAA
HERPUD1_R	TGCTCGCCATCTAGTACATCC
CHOP_F	ACCAAGGGAGAACCAGGAAACG
CHOP_R	TCACCATTTCGGTCAATCAGAGC
IRE1 $\alpha$ _F	GGGTCTGAGGAAGGTGATGC
IRE1 $\alpha$ _R	CAGTGGGGTTTCATGGTGTC
PERK_F	AGATCGCAGAGGCAGTGGAG
PERK_R	CGAGACCTCTGTCTGAGCAC
ATF6_F	CATCCGCAGAAGGGGAGACA
ATF6_R	CAGGGTCCCACGCTCAGTTT
BiP_F	GTATGGTGCTGCTGTCCAGG
BiP_R	GGTGTCAGGCGATTCTGGTC
L19_F	GCGGAAGGGTACAGCC AAT
L19_R	GCAGCCGGCGCAA

## 2.6 Cloning ATF6 into pACMVtet-O vector

### 2.6.1 Design of cloning primers

Cloning primers were designed using the OligoPerfect™ Primer Designer from Thermo Fisher Scientific. Based on the NEB Restriction Enzyme Chart, the optimised restriction sites of *Xba*I (forward) and *Xho*I (reverse) were added to the primer sequences. The Rho-1D4 epitope (TETSQVAPA) was also added to the reverse primer (Table 2.6.1).

**Table 2.6.1 ATF6 Cloning and Sequencing Primers.**

	Primer	Sequence (5'-3')
<b>Cloning</b>	ATF6_forward	GCTCTAGAGCATGGGGGAGCCGGC
	ATF6_reverse	CCGCTCGAGCGGTTAGGCAGGCGCCACTTGGCT GGTCTCTGTTTGTAAATGACTCAGGGATGGTG
	ATF6_F1	AGCAGCACCCAAGACTCAAACAA
<b>Sequencing</b>	ATF6_F2	GGCAGCTGGATGAAGTTGTGTCA
	ATF6_F3	GGCTCAAATTCTCAGCTGATGGC

### 2.6.2 PCR amplification of ATF6 DNA

In order to amplify the DNA of ATF6, the pEGFP-ATF6 plasmid (#32955) was purchased from AddGene. The plasmid was isolated using the Real Genomics HiYield™ Plasmid Kit (Mini), according to the high copy number protocol instructions. The ATF6 DNA was amplified using the Q5® High-Fidelity DNA Polymerase (M0491, New England Biolabs). A 25 µl reaction was performed according to the kit instructions.

### 2.6.3 Agarose Gel Electrophoresis

To assess the size and quality of the ATF6 DNA, the PCR products were run on 1% agarose gel in 1x TAE buffer (Section 2.1.2) for 15 minutes at 120V, 400 mA. The DNA bands were visualised using a UV box. Gel extraction was performed using the QIAEX®II Kit (cat. no. 20021) from QIAGEN.

### 2.6.4 Ligation of ATF6 into PGEM®-T Easy Vector

To improve cloning efficiency, the ATF6 insert was sub-cloned into the PGEM®-T Easy Vector System I (cat. no. A1360) according to manufacturer's instructions. The reaction consisted of 5 µl 2X Rapid Ligation Buffer, 1 µl pGEM®-T Easy Vector (50

ng), 1 µl PCR product (1:3 ratio with vector DNA) and 1 µl T4 DNA ligase and ddH<sub>2</sub>O to a total volume of 10 µl. The reaction was mixed and incubated at RT for 2 h.

### **2.6.5 Transformation of competent cells**

The ATF6-PGEM<sup>®</sup>-T Easy plasmid was transformed into XL-1 Blue Supercompetent cells as follows: 1 µl of ligation reaction was added to 25 µl of bacteria and left on ice for 30 minutes; heat shock was performed for 45 seconds at 42°C and the tubes were immediately placed on ice for 2 minutes; 450 µl of SOC medium was added and incubated for 1h at 37 °C with shaking. The bacteria were pulse span, 450 µl of medium was removed, and the pellet re-suspended in the remaining 50 µl. This cell suspension was spread on a LB agar plate which contained 10% ampicillin and had 40 µl XGAL (20 mg/mL) and 4 µl IPTG (200 mg/mL) spread on the surface. The plate was incubated overnight at 37°C. Blue-white screening was performed to select for the recombinant bacteria – a white colony was picked and grown overnight at 37°C in 5 ml LB broth supplemented with 50 µg/mL ampicillin. 4.5 mL of the bacterial culture was collected by centrifugation and the cell pellet was used to isolate the plasmid (Real Genomics HiYield<sup>™</sup> Plasmid Kit (Mini)).

### **2.6.6 Re-cloning into pACMVtetO vector**

After the ATF6-PGEM<sup>®</sup>-T plasmid was extracted, 3 µg of DNA was digested with *Xho*I and *Xba*I restriction enzymes. The samples were run on 1% low-melt agarose gels, and the insert extracted. 3 µg of the pACMVtetO vector (supplied by Dr Philip Reeves) was also digested with *Xho*I and *Xba*I, then alkaline phosphatase and PCR clean-up (kit from New England Biolabs) were performed. The alkaline phosphatase reaction consisted of 18 µl (912.6 ng) pACMVtetO digest, 3 µl alkaline phosphatase 10x buffer, 2 µl ddH<sub>2</sub>O and 2 µl alkaline phosphatase enzyme. The reaction was incubated for 10 minutes at 37 °C and then for 5 minutes at 75 °C. Finally,

the ATF6 insert was ligated into pACMVtetO as previously described. Sanger sequencing of the construct was performed by Eurofins Scientific.

## **2.7 Stable transfection of HEK293S GnTI(-) cells**

HEK293S GnTI (-) cells were grown as previously described. 24 h before transfection, the cells were split 1:3 in complete DMEM (10% FBS, 1% L-Glu, 1% Penicillin Streptomycin) in order to seed three 150 mm<sup>2</sup> culture dishes.

First, 30 µg of ATF6-PACMVtetO DNA was mixed with 50 µl CaCl<sub>2</sub> (2.5 M) and ddH<sub>2</sub>O to a total volume of 500 µl. Importantly, in order to form a better precipitate, the CaCl<sub>2</sub> was added last, in a dropwise manner whilst vortexing for 60 seconds. Next, 500 µl of 2x BES (pH 7.02) was added to the first solution dropwise with vortex for 60 seconds, followed by another 60s of vortexing. The final solution was then slowly added to the cells, again in a dropwise manner while gently rocking the plate to stop the formation of precipitate. The cells were then incubated at 37°C, 1% CO<sub>2</sub>. After 24h, the medium was changed to DMEM/F12 and the cells were incubated at 37°C, 5% CO<sub>2</sub>. 24h later, the transfected cells were split in DMEM/F12 as follows: 1:5 (2 x 10 ml dishes), 1:10 (3 x 10 ml dishes), 1:50 (2 x 10 ml dishes) and 1:100 (2 x 10 ml dishes). After 24h, the transfected cells were fed with DMEM/F12 containing 30% conditioned medium and Geneticin. The cells were fed every 4 days with this conditioned media until colonies started to form.

### **2.7.1 Expanding clones and cell induction**

Colonies were picked using sterile discs and transferred to the top row (A) of 4 x 24-well plates. From this point, the cells were grown in DMEM/F12 with Geneticin. Once the cells were confluent, they were split into their corresponding 3 wells (rows B, C, D). When the cells were confluent, row B was fed with 500 µl complete DMEM, row C was fed with complete DMEM and induced with 1 µg/ml Tetracycline and

Sodium Butyrate (5mM), whilst row D was frozen (-80°C) for future work. After 72h, the cells from rows B and C were harvested and the pellets stored at -20°C.

## **2.8 Protein immunoblotting/western blotting**

### **2.8.1 Preparing cell lysate and protein quantification**

Cells were seeded in 6-well plates and treated as necessary. The growth medium was removed, and the cells were washed with PBS and placed on ice. The lysis buffer (RIPA buffer supplemented with protease inhibitors, 10 µl/ml Halt phosphatase inhibitor cocktail and 5 µl/ml PMSF) was added onto the cells and the plates left on ice for another 10 minutes. The cells were harvested by cell scraping, transferred into 1.5 ml Eppendorf tubes, and lysed using sonication (3 cycles of 30 seconds on and 30 seconds off; Biorupter® Plus, Diagenode). The lysates were centrifuged at 12000 x g, for 10 minutes, at 4 °C. The supernatant was transferred into a fresh, pre-chilled Eppendorf tube and the protein concentration was determined by performing a Protein Detergent Compatible (DC, BioRad) assay according to manufacturer's instructions. Standard concentrations of bovine serum albumin (BSA) were used as a reference in this assay. A FLUOstar Omega plate reader (BMG LABTECH) was used to detect the concentration of protein in the lysates by reading the absorbance at 750 nm. The lysate was diluted as necessary with lysis buffer so that each sample had a final concentration of 10 µg protein per 10 µl sample. 6X SDS Protein Loading Buffer (containing beta-mercaptoethanol) was added to the samples and the mixes were boiled for 5 minutes at 95 °C and then placed immediately on ice.

### **2.8.2 SDS polyacrylamide gel electrophoresis**

The acrylamide gels were prepared as described in (Section 2.1.2). 5 ml of 10% or 8% acrylamide gel were poured in a glass cassette and allowed to set before adding the stacking buffer. A total of 30 µg of protein were loaded per well. To identify the

estimated molecular weight of the target protein, 4 µl of PageRuler™ Plus Prestained Protein Ladder (Bio-Rad) was also loaded on the gel. The gels were then run in 1x Running Buffer (Section 2.1.2) for 2h at 125V, 40 mA.

### **2.8.3 Immunoblotting**

Before assembling the gel / PVDF membrane sandwich, the gel was soaked for a few minutes in transfer buffer, whilst the membrane was soaked both in methanol and then in transfer buffer. A semi-dry electro-blotting apparatus (Bio-Rad) was used to transfer the proteins onto the membrane; the transfer was performed for 2 h at 15mA and 100 V. The membrane was blocked for at least 30 minutes with 5% Milk PBS-T (0.1% Tween). Incubation with primary antibody was performed at RT, with rocking, for at least 2 h. The membrane was washed 3 times (5 minutes each time) with PBS-T. Incubation with mouse or rabbit secondary antibody (concentration 1:2000, diluted in 5% Milk PBS-T) was performed for 1 h at RT. The protein of interest was detected by the addition of Luminata™ Forte Western HRP Substrate (Millipore) to the membrane and the chemiluminescence imaged using a Fusion FX (VILBER LOURMAT) system.

## **2.9 Dot Blot**

### **2.9.1 Preparing cell lysates and samples**

The pellets (from Section 2.7.1) were re-suspended in 100 µl of 1% (w/v) DDM in PBS, mixed for 1 h at 4 °C and centrifuged for 30 minutes, 12000 x g, at 4°C. The supernatants were transferred to fresh tubes. Samples were serially diluted in a 96-well plate the (1:4, 1:16, 1:64), as follows: 25 µl of sample were added to rows A and E which contained 50 µl 0.1% (w/v) DDM in PBS; the samples were then serially diluted by taking 25 µl from row A / E and adding to rows immediately bellow (rows B, C, D and F, G, H, respectively) which contained 75 µl 0.1% (w/v) DDM in PBS.

## **2.9.2 Blotting**

Using vacuum, 25  $\mu$ l of the diluted samples were transferred to the nitrocellulose membrane, which was previously soaked in water. The membrane was washed 4 times with 150  $\mu$ l 0.1% (w/v) Triton X-100 in PBS, applying vacuum after each wash. The membrane was then blocked overnight at 4 °C with 10% (w/v) milk in PBS. The membrane was incubated for 5 h, RT, with a primary antibody solution containing 100 mM K-PO<sub>4</sub> buffer (pH 7.4), 0.5% (w/v) gelatine, 0.25% (w/v) BSA and 10  $\mu$ g/ml of Rho-1D4 antibody. The membrane was washed 5 x 5 minutes with 50 ml of PBS containing 0.5% (w/v) milk and 0.1% (v/v) Tween-20. Incubation with secondary antibody was for 1h at RT (30 ml wash buffer with goat anti-mouse IgG HRP antibody (Pierce, Lot RH240915) at a dilution of 1:5000). The membrane was once again washed 5 x 5 minutes and then developed using ECL buffer (100 mM Tris-HCl pH 8.5; 250 mM Luminol (Sigma); 10 mM coumaric acid and 30% H<sub>2</sub>O<sub>2</sub>).

## **2.10 Coomassie blue stain**

The protein samples were prepared by mixing 1  $\mu$ g of protein with 6x protein loading dye. The samples were boiled for 5 minutes at 95°C, cooled on ice and then 5  $\mu$ l loaded on a 10% acrylamide gel. The gel was run for 2h at 125 V and 40 mA. The gel was soaked in Coomassie Blue stain and left rocking overnight at RT. ddH<sub>2</sub>O was used to de-stain the gel. Pictures of the gel were taken using a EPSON Perfection 1250 scanner.

## **2.11 Protein Purification**

### **2.11.1 Cell lysis**

Two clones of the stably transfected HEK293S GnTI- cells were plated in a 150 mm culture dish and once they were confluent, the cells were fed with complete DMEM. After 24h, the cells were induced for 48h as previously described. Cells were

harvested and lysed with 2 ml of PBS solution containing 1% (w/v) DDM and 4  $\mu$ l of protease inhibitor PMSF. The samples were mixed at 4°C for 1h, centrifuged at 12000 x g, 4 °C for 30 minutes and the supernatants transferred to fresh tubes.

### **2.11.2 Column preparation**

Rho-1D4 agarose beads (100  $\mu$ l) were added to the supernatants and mixed head-over-end for 1h at 4 °C. Then, at 4 °C, the samples were added to a 2 mL Pierce™ disposable plastic column (Thermo Fisher Scientific) (cap on). The cap was then removed and the flow through saved. Next, the column was washed 5 times with 2 ml wash buffer (0.1% DDM in PBS) and each flow-through was saved in a different tube.

### **2.11.3 Elution of the purified protein**

Elution buffer was prepared by mixing 800  $\mu$ l wash buffer with 8  $\mu$ l competitive Rho-1D4 peptides. At RT, the first elution was performed by adding 100  $\mu$ l elution buffer to the column and saving the flow-through. For the second and third elution, the flow through was collected after 1h. Finally, for the fourth elution, the elution buffer was added to the column, left overnight at 4°C, and the flow though collected the next morning. Samples were kept at 4°C. Amicon® Ultra – 0.5 Centrifugal Filter Devices kit (Millipore, MERK, REF: UFC500324, LOT: R8KA97949) was used to concentrate the eluates from 300  $\mu$ l to 50  $\mu$ l.

### **Chapter 3: Investigating the effects of endoplasmic reticulum stress upon Prostate Cancer proliferation, cell cycle and cell death**

Treatment options for PCa vary depending on the stage of the disease. Androgen deprivation therapy (ADT) is the main treatment option for tumours that have spread from the prostate. However, after 18-24 months of hormone therapy, for most patients the disease progresses to the incurable castrate-resistant stage (castrate resistant prostate cancer, CRPC) (Brooke and Bevan, 2009, Huang et al., 2018). According to the advanced PCa Consensus Conference, CRPC can only be diagnosed if the serum testosterone level of the patient is less than 1.7 nmol/L and if there are signs of biochemical progression, such as a consecutive increase in PSA levels (measured twice in a row over a week, or over 3 measurements that show that the lowest value has increased by at least 50% or  $\geq 2$  g/L). The increase in new lesions is also important during the diagnostic process (Thomas et al., 2016, Huang et al., 2018).

The molecular mechanisms that promote the progression of PCa to CRPC, in response to ADT, can be divided into AR-dependent mechanisms, AR bypass signalling and AR-independent mechanisms. A few examples for the AR-dependent mechanisms include the amplification of the *AR* gene and overexpression of the AR protein, which is present in over 80% of CRPC patients and is associated with the failure of ADT and development of CRPC (Koivisto et al., 1997, Huang et al., 2018). Mutations in the AR are also common in CRPC, and the majority of them occur in the LBD or NTD. Over 100 AR mutations have been identified and these can lead to a more active/constitutively active AR. These can also decrease receptor ligand specificity, allowing activation by other steroids such as glucocorticoids, or result in anti-androgens becoming agonists (Huang et al., 2018). AR splice variants have also

been identified in CRPC and these lack the LBD and are constitutively active; this can be particularly important in CRPC as these splice variants can activate AR target genes without the need of androgen (Haile and Sadar, 2011). Other AR-dependent mechanisms include the altered expression and function of AR co-regulators, aberrant post-translational modifications of the AR (which result in a decrease in apoptosis and increase in the expression of AR target genes), and the synthesis of intra-tumoural androgen (Huang et al., 2018). Additional therapy resistance mechanisms that are AR independent include: alterations in the PI3K-Akt-mTOR pathway that allow it to be constitutively active and promote cell survival and angiogenesis, increased SRC kinase family signalling which promotes angiogenesis and inhibits apoptosis, differential expression of microRNAs (miRNA) defects in the DNA damage repair genes resulting in an increase in genomic instability (Huang et al., 2018).

Treatment options for metastatic CRPC have been recently reviewed by Leung *et. al.* and they include the use of chemotherapy drugs, such as docetaxel and cabazitaxel; hormonal agents, such as abiraterone and enzalutamide; Sipuleucel-T – an oncological vaccine; Radium-223 – which emits alpha-particle radiation to bone metastasis; and Olaparib – a PARP inhibitor (Leung et al., 2021). Although the use of some of these drugs improved the survival of CRPC patients, their effects were limited and patients experienced bothersome side effects. Therefore, more investigations are needed to understand the molecular biology of PCa and to improve the therapeutic options for CRPC (Leung et al., 2021). Modulation of the Unfolded Protein Response (UPR) may be a promising approach for the management of PCa and CRPC.

PCa cells grow in an environment that is known to compromise ER function

and cause ER stress (Storm et al., 2016). The tumour microenvironment has two main components: the cellular components and the extracellular matrix. The tumour cells, tumour stromal cells, endothelial cells, and immune cells (microglia, macrophages, lymphocytes) comprise the cellular components, whilst collagen, fibronectin, hyaluronan, laminin and others form the extracellular matrix. Soluble factors secreted by the tumour cells manipulate these components in order to promote tumourigenesis, angiogenesis, control the response to therapy, promote metastasis and multi-drug resistance (Baghban et al., 2020, Jing et al., 2019). Due to the rapid abnormal proliferation of the tumour cells and an insufficient blood supply, the quantity of nutrients and oxygen is often sparse in the tumour microenvironment. Therefore, most solid tumours grow in a hypoxic microenvironment, where the level of oxygen in the cells drops from 2-9% to less than 2%. These conditions stimulate the growth of new vasculature (angiogenesis) however the distribution of the blood vessels is irregular and characterised by increased distances between the capillaries that do not permit the efficient diffusion of oxygen. Therefore, the tumours always have hypoxic regions – either permanent or transient (Jing et al., 2019, Petrova et al., 2018). Hypoxia and nutrient deprivation impair the redox potential and limits the formation of disulphide bonds which leads to an accumulation of unfolded proteins and a disruption of the ER function (Morreall et al., 2019).

Activation of the UPR in PCa has been shown to support cancer progression (Storm et al., 2016). The IRE1 $\alpha$ /XBP1s branch is the most studied branch of the UPR and was found to be directly activated by the AR in order to increase proliferation of PCa cells (Sheng et al., 2015, Sheng et al., 2019). Moreover, inhibiting the RNase activity of IRE1 $\alpha$  with the MKC8866 inhibitor resulted in a reduction of PCa cell growth *in vitro* and *in vivo*; importantly, when combined with the CRPC drugs abiraterone

acetate and cabazitaxel, it synergistically inhibited tumour growth (Sheng et al., 2019). XBP1s was also found to have common genomic binding sites with the AR (Stelloo et al., 2020) and the ability to directly activate the transcriptional program of the c-MYC oncogene (Sheng et al., 2019). Furthermore, the expression of XBP1s was increased in patients who received AR-targeted therapy and high levels of unspliced XBP1 in primary PCa tumours correlated with a better bio-chemical recurrence outcome (Stelloo et al., 2020). PERK has also been shown to have a pro-survival role in MYC-hyperactivated PCa – where the high demand for protein synthesis is not compatible with cell survival. Through the phosphorylation of eIF2 $\alpha$ , PERK decreases the rate of protein synthesis allowing the cells to survive (Nguyen et al., 2018).

There is a definite link between the UPR and PCa progression and further investigations are needed in order to advance our understanding of the UPR in PCa. In this Chapter, I use tunicamycin – a compound that blocks protein folding and induces the UPR (Guillemette et al., 2011) – to mimic the stressful conditions of the tumour microenvironment and investigate the ways in which PCa cells respond to ER stress. I specifically look into the way ER stress affects the proliferation of PCa cells and continue the investigation by assessing the effects of ER stress upon cell cycle and cell death. I also study the activation of the UPR sensor proteins in response to stress and assess the implications of these findings. Finally, I study the effects of targeting UPR signalling upon the proliferation of PCa and characterise the crosstalk between the UPR arms by looking at the expression of IRE1 $\alpha$ , PERK, and ATF6 target genes. These results will further characterise the activity of UPR in PCa and help us understand how PCa utilises the UPR in order to survive.

### **3.1 Expression levels of IRE1 $\alpha$ , PERK and ATF6 in PCa cell lines**

To better understand UPR signalling in PCa, the expression levels of different sensor proteins was investigated. The expression of IRE1 $\alpha$ , PERK and ATF6 was investigated using immunoblotting in eight PCa cell lines, representing different stages of the disease (Table 3.1; information was collected from ATCC: The Global Bioresource Centre). Low levels of IRE1 $\alpha$  expression were found in the normal and non-cancerous cells (PNT1A, BPH-1) and in the advanced stages of the disease (22Rv1, DU145, PC3), whilst high levels of expression were present in androgen responsive cells (LNCaP, C42, C42B) (Figure 3.1). PERK had a relatively stable expression across the lines, with a lower expression in castrate resistant models (DU145, PC3) and lowest in 22Rv1. The expression of ATF6 varied across the lines. For example, the lowest level of expression was found in BPH-1 and normal prostate cells (PNT1A). Its expression was then higher in androgen responsive (C42B, LNCaP) and highest in castrate resistant cells (PC3, DU145, 22Rv1). Therefore, the UPR components had differential expression across the lines, however a trend could be observed, in which all the three proteins had high levels of expression in the androgen responsive cells, and IRE1 $\alpha$  and PERK had lower expression in castrate resistant models.

### **3.2 Effects of ER stress upon PCa cell proliferation and cell cycle**

In order to mimic the stressful conditions of the tumour microenvironment, Tunicamycin - a natural occurring antibiotic that blocks protein folding by inhibiting the N-linked glycosylation of nascent peptides (Guillemette et al., 2011), was used to induce ER stress in four PCa cell lines (BPH-1, LNCaP, DU145 and PC3). Crystal violet assays, as well as flow cytometry analysis were used to study the effects of ER stress upon PCa cell proliferation, cell cycle and cell death.

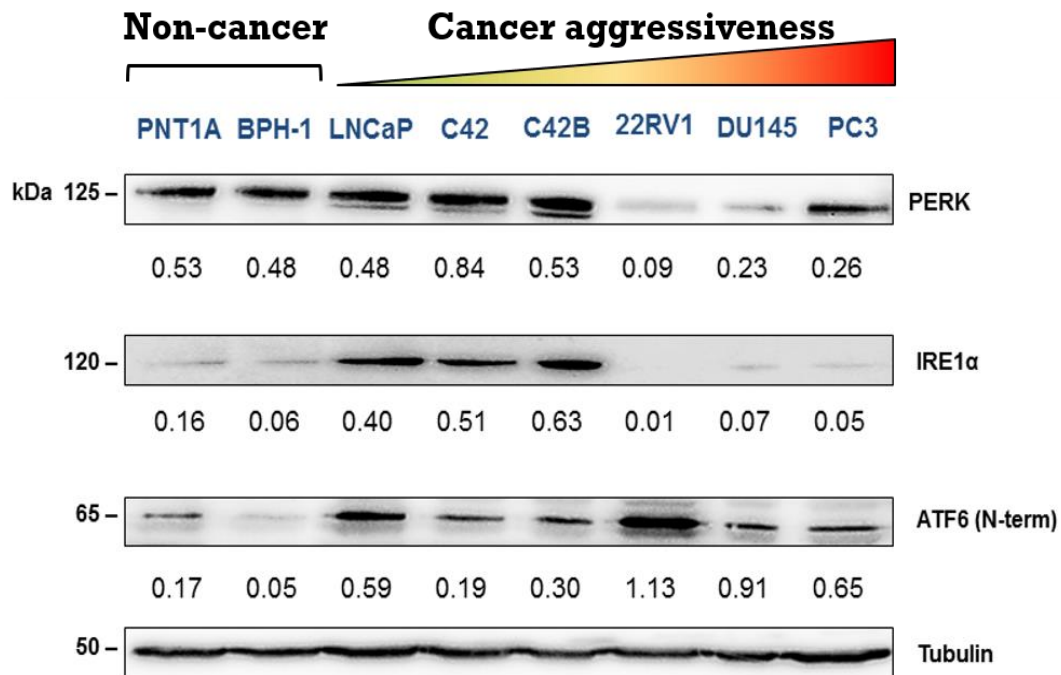


**Figure 3.1** Expression of UPR components across a panel of PCa cell lines.

Cells were grown at 37<sup>o</sup> C in RPMI 1640 containing 10% FBS and 1% PSG. The cells were collected and lysed for western blot analysis. Images are representative of three individual repeats.  $\beta$ -Tubulin was used as a loading control. Densitometry was performed using ImageJ software. The levels of IRE1 $\alpha$ , PERK and ATF6 are the mean of the 3 individual repeats.

Cells were grown to in media supplemented with 10% FBS before being treated with a dose range of Tunicamycin (0-10  $\mu$ M) for 72h. After the treatment, the cells were fixed with 4% PFA and stained with crystal violet; the  $IC_{50}$  values of tunicamycin were calculated using GraphPad Prism software (Figure 3.2.A). It has been observed that tunicamycin reduced the proliferation of all of the cell lines, with DU145 being the most sensitive to stress ( $IC_{50}$  = 33 nM), followed by PC3 cells ( $IC_{50}$  = 73 nM), BPH-1 ( $IC_{50}$  = 85 nM) and finally, LNCaP cells - which were the least affected by stress ( $IC_{50}$  = 697 nM).

In order to assess whether the reduction in proliferation was due to cell cycle arrest or due to cell death, the same four cell lines were treated again for 72 h with the same dose range of tunicamycin. Flow cytometry was performed to study the effects of ER stress upon the cell cycle of PCa (Figure 3.2.B). Although it is known that Tunicamycin is able to cause G1 arrest in cells (Brewer et al., 1999), the flow cytometric analysis revealed that Tunicamycin had no such effect on the cell cycle of BPH-1 cells. LNCaP cells showed a clear increase in G1 phase at the higher concentrations (1-10  $\mu$ M) of tunicamycin, indicating that increased levels of ER stress are able to induce G1 arrest in these androgen responsive cells. However, at the same higher concentrations, the castrate resistant DU145 and PC3 cells only experienced a small increase in G1 phase.

Taken together, these results suggest that the non-cancerous prostate cells (BPH-1) were the most resistant to ER stress – their proliferation was not greatly reduced by tunicamycin nor did it affect their cell cycle progression. When compared to the other cell lines, the proliferation of LNCaP cells had been the least affected by ER stress and upon further analysis, it was also revealed that they were in G1-phase cell cycle arrest. Finally, the proliferation of the castrate resistant models was greatly

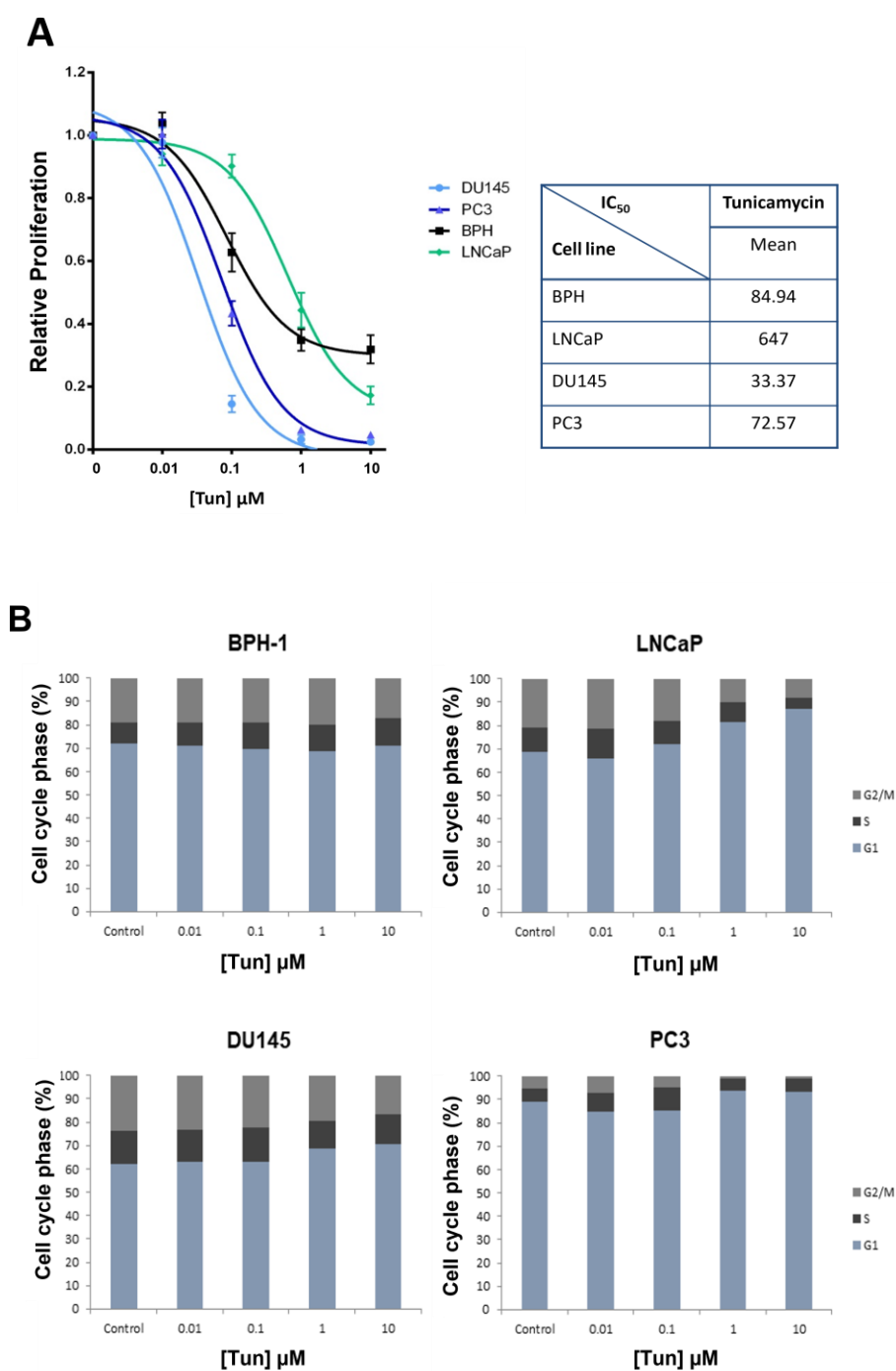


**Figure 3.2 ER stress reduces proliferation of PCa cell ones and causes G1 arrest in LNCaP cells.**

BPH-1, LNCaP, DU145 and PC3 cell lines were incubated at 37 °C in RPMI 1640 containing 10% FBS and 1% PSG and treated with 0-10  $\mu\text{M}$  Tunicamycin for 72h. **A.** Cells were fixed with 4% PFA in PBS and stained with crystal violet. Dose response curves and the IC<sub>50</sub> values were generated using GraphPad Prism 7 software.

**B.** Cell cycle analysis of PCa cells in response to a dose range of Tunicamycin was measured using a BD Accuri™ C6 flow cytometer. Graphs are the mean of 3 individual repeats.

reduced by ER stress; however, this stress had no effect on cell cycle regulation.

### **3.3 Effects of ER stress upon PCa cell death**

To assess the effect of ER stress upon PCa cell death, cells were treated with the same dose range of tunicamycin for 72 h and DNA Hypodiploidy and PI inclusion assays were used to determine whether ER stress was able to induce apoptosis or a different type of cell death in the PCa cells (Figure 3.3.1-2). DNA Hypodiploidy is a flow cytometric assay that is able to measure the percentage of apoptotic (hypodiploid) nuclei from a heterogenous cell population (Nicoletti et al., 1991), whilst PI inclusion method measures the percentage of propidium iodide (PI) intake by the cells. PI is a membrane-impermeable DNA-binding dye and so it can only cross compromised plasma membranes in order to stain the DNA. As ruptured plasma membranes are indicators of a different type of cell death, such as necrosis, the PI inclusion assay is used as an indicator of non-apoptotic cell death (Rosenberg et al., 2019, Galluzzi et al., 2007).

Tunicamycin was able to significantly induce apoptosis in DU145 cells starting from the low concentration of 0.1  $\mu\text{M}$ , ( $p < 0.0001$ ) (Figure 3.3.1A). These results correlate with the previous findings, where it was found that the proliferation of these cells was affected by ER stress and that the reduction in proliferation was not due to a cell cycle arrest. Taken together, these results suggest that ER stress was able to inhibit the proliferation of DU145 cells by inducing apoptosis.

LNCaP and PC3 cells had similar results to those seen for DU145. However, Tunicamycin induced apoptosis only at the highest concentration tested (10  $\mu\text{M}$ ) ( $p < 0.0001$ ). BPH-1 was found to undergo significantly less apoptosis than the other cell lines and so these non-cancerous cells were, again, found to be the most resistant

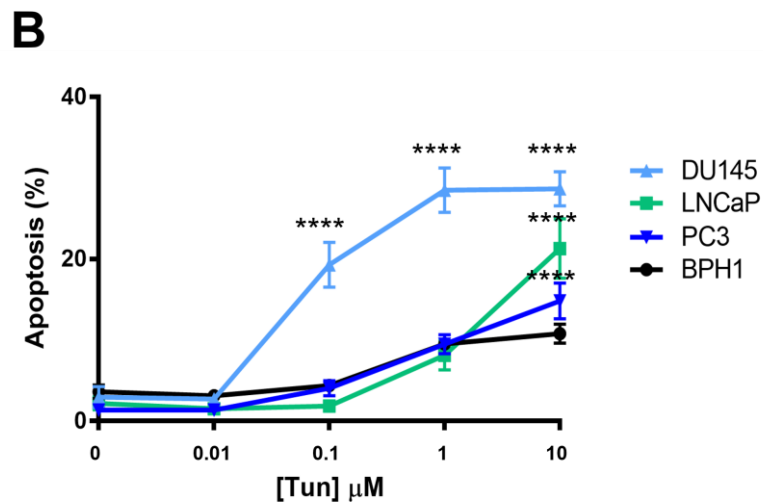
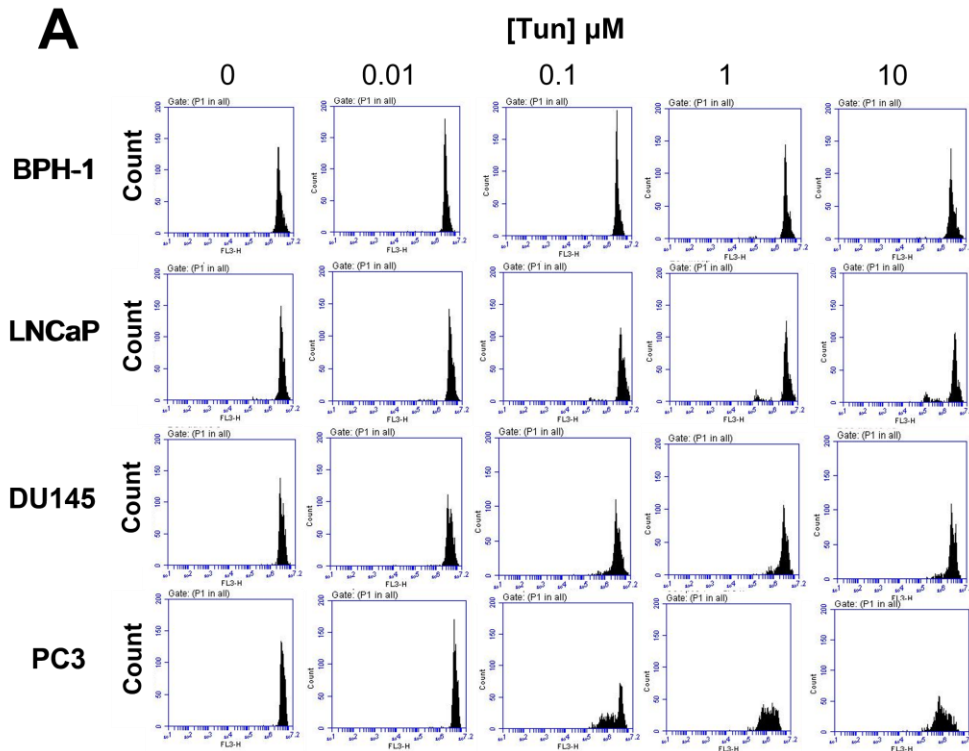


**Figure 3.3.1 Apoptotic levels of PCa cell lines in response to a dose range of Tunicamycin.**

Cells were treated for 72h, then collected and analysed using the BD Accuri™ C6 flow cytometer. **A.** DNA Hypodiploidy assay of PCa cell lines. **B.** Line graphs are the mean of 3 individual repeats. Graphs and statistical analysis (two-way ANOVA) were performed using GraphPAD Prism 7 software. \* $p < 0.05$ , \*\* $p < 0.005$ , \*\*\* $p < 0.0005$ .

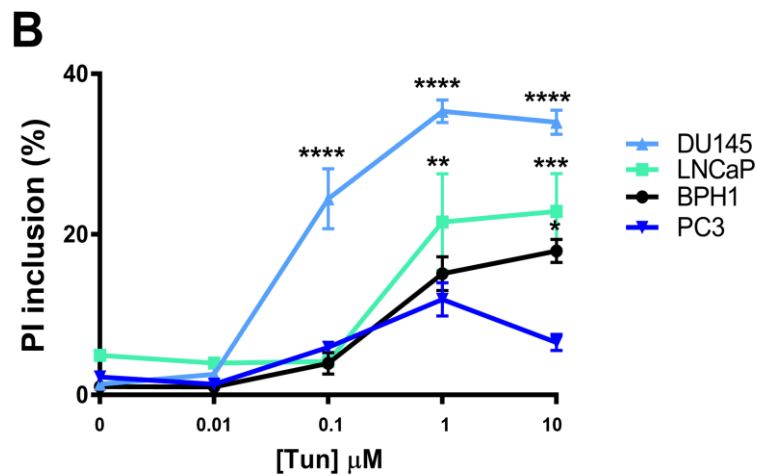
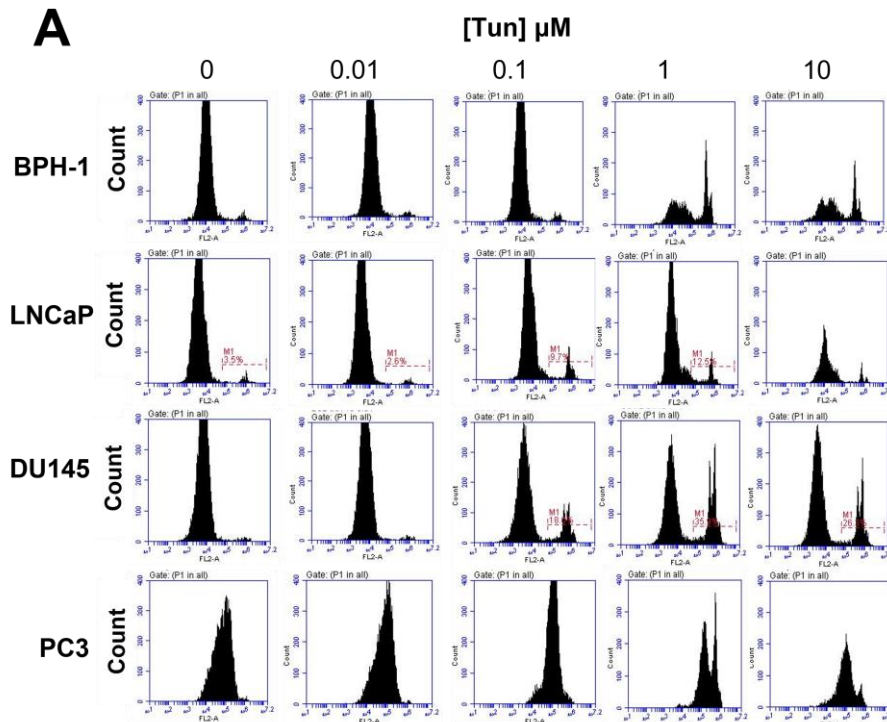


**Figure 3.3.2 PI inclusion levels of PCa cell lines in response to a dose range of Tunicamycin.**

Cells were treated for 72h, then collected and analysed using the BD Accuri™ C6 flow cytometer. **A.** PI inclusion assay of PCa cell lines. **B.** Line graphs are the mean of 3 individual repeats. Graphs and statistical analysis (two-way ANOVA) were performed using GraphPAD Prism 7 software. \* $p < 0.05$ , \*\* $p < 0.005$ , \*\*\* $p < 0.0005$ .

cells to ER stress (Figure 3.3.1). Furthermore, high levels of PI inclusion were found in DU145 cells (at concentrations 0.1- 10 $\mu$ M) and these percentages were significantly higher than in BPH-1. High levels of PI inclusion were also found in LNCaP and BPH-1 cells (at concentration 1-10  $\mu$ M and 10  $\mu$ M, respectively) (Figure 3.3.2).

In order to confirm the type of cell death induced by ER stress, I assessed whether the cellular effects of tunicamycin can be inhibited by the addition of apoptosis (Z-VAD-FMK), necroptosis (Necrostatin-1) and ferroptosis (Ferrostatin-1) inhibitors. The cells were grown in medium supplemented with 10% FBS and treated with the inhibitors 30 minutes prior to the addition of tunicamycin. The cells were treated for 72 h with one concentration of tunicamycin, found to induce both apoptosis and had high levels of PI inclusion in all cell lines (1 $\mu$ M). As before, tunicamycin induced apoptosis and high levels of PI inclusion were recorded in all cell lines (Figures 3.3.3 – 6).

Apoptosis and PI inclusion levels were significantly reduced in BPH-1, DU145 and PC3 in response to the pan caspase inhibitor Z-VAD-FMK, confirming that the ER stress is able to induce PCa cell death by triggering apoptosis. Interestingly, in BPH-1 cells, the ferroptosis inhibitor was also able to significantly reduce the levels of PI inclusion whilst in PC3 cells Ferr-1 increased the percentages of PI inclusion. In LNCaP none of the inhibitors had a significant effect.

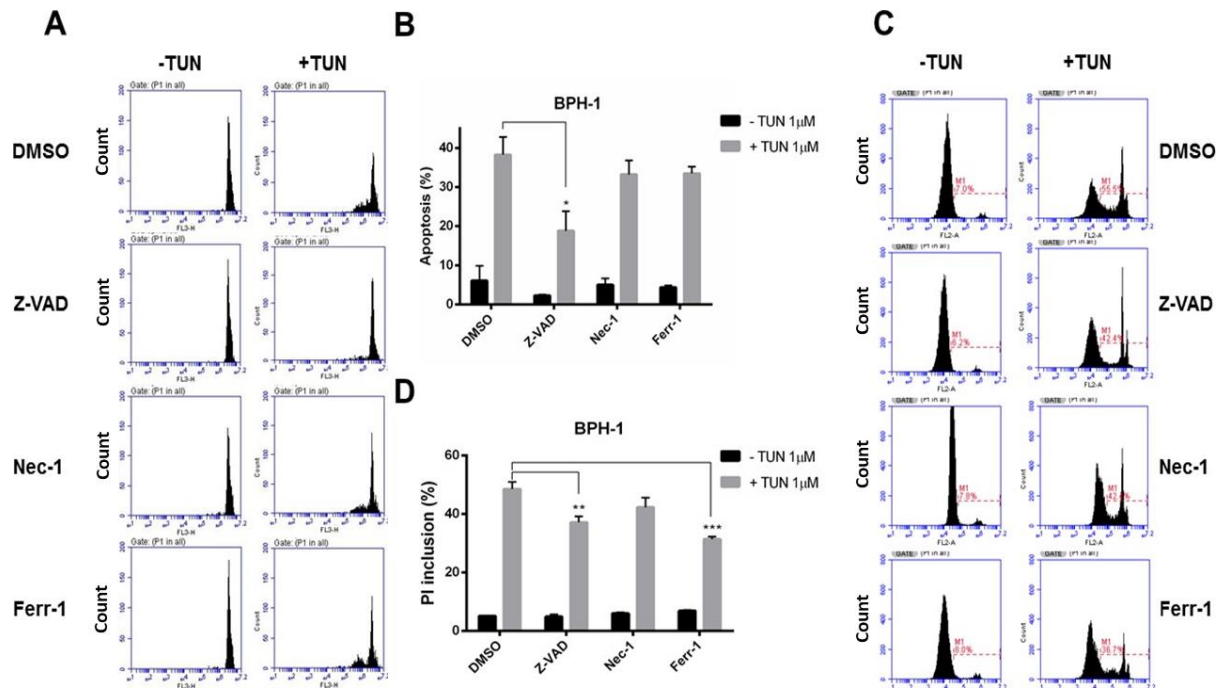


**Figure 3.3.3 Z-VAD-FMK inhibits tunicamycin-induced apoptosis in BPH-1 cells.**

Cells were treated for 72h with DMSO, Z-VAD-FMK, Necrostatin-1 and Ferrostatin-1 in the presence or absence of tunicamycin (1µM). For the combined treatment, inhibitors were added 30 min before tunicamycin. Cells were then collected and analysed using the BD Accuri™ C6 flow cytometer. Graphs are the mean of 3 individual repeats. Two-way ANOVA tests were performed using GraphPAD Prism 7 software. **A-B.** DNA Hypodiploidy assay. **C-D.** PI inclusion assay. \* $p < 0.05$ , \*\* $p < 0.005$ , \*\*\* $p < 0.0005$

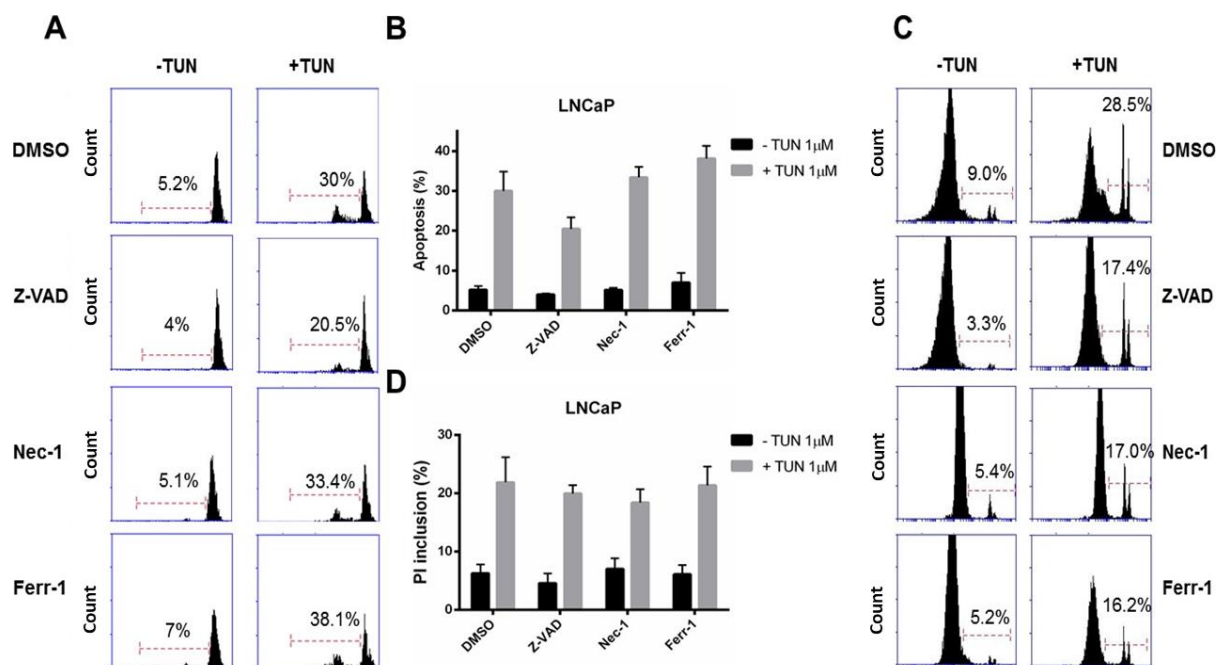


**Figure 3.3.4 Apoptotic and PI inclusion levels of LNCaP cells in response to tunicamycin and cell death inhibitors.**

Cells were treated for 72h with DMSO, Z-VAD-FMK, Necrostatin-1 and Ferrostatin-1 in the presence or absence of tunicamycin (1 $\mu$ M). For the combined treatment, inhibitors were added 30 min before tunicamycin. Cells were then collected and analysed using the BD Accuri™ C6 flow cytometer. Graphs are the mean of 3 individual repeats. Two-way ANOVA tests were performed using GraphPAD Prism 7 software. **A-B.** DNA Hypodiploidy assay. **C-D.** PI inclusion assay. \* $p < 0.05$ , \*\* $p < 0.005$ , \*\*\* $p < 0.0005$

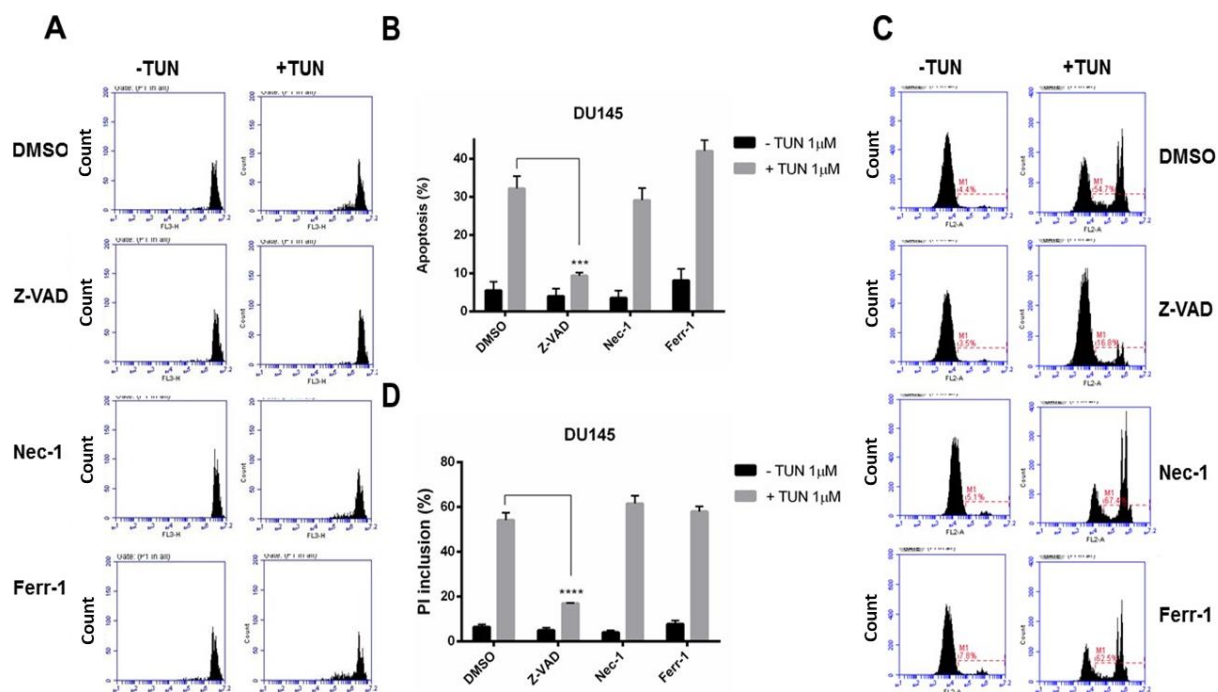


**Figure 3.3.5 Z-VAD-FMK inhibits tunicamycin induced apoptosis in DU145 cells.**

Cells were treated for 72h with DMSO, Z-VAD-FMK, Necrostatin-1 and Ferrostatin-1 in the presence or absence of tunicamycin (1 $\mu$ M). For the combined treatment, inhibitors were added 30 min before tunicamycin. Cells were then collected and analysed using the BD Accuri™ C6 flow cytometer. Graphs are the mean of 3 individual repeats. Two-way ANOVA tests were performed using GraphPAD Prism 7 software. **A-B.** DNA Hypodiploidy assay. **C-D.** PI inclusion assay. \* $p < 0.05$ , \*\* $p < 0.005$ , \*\*\* $p < 0.0005$

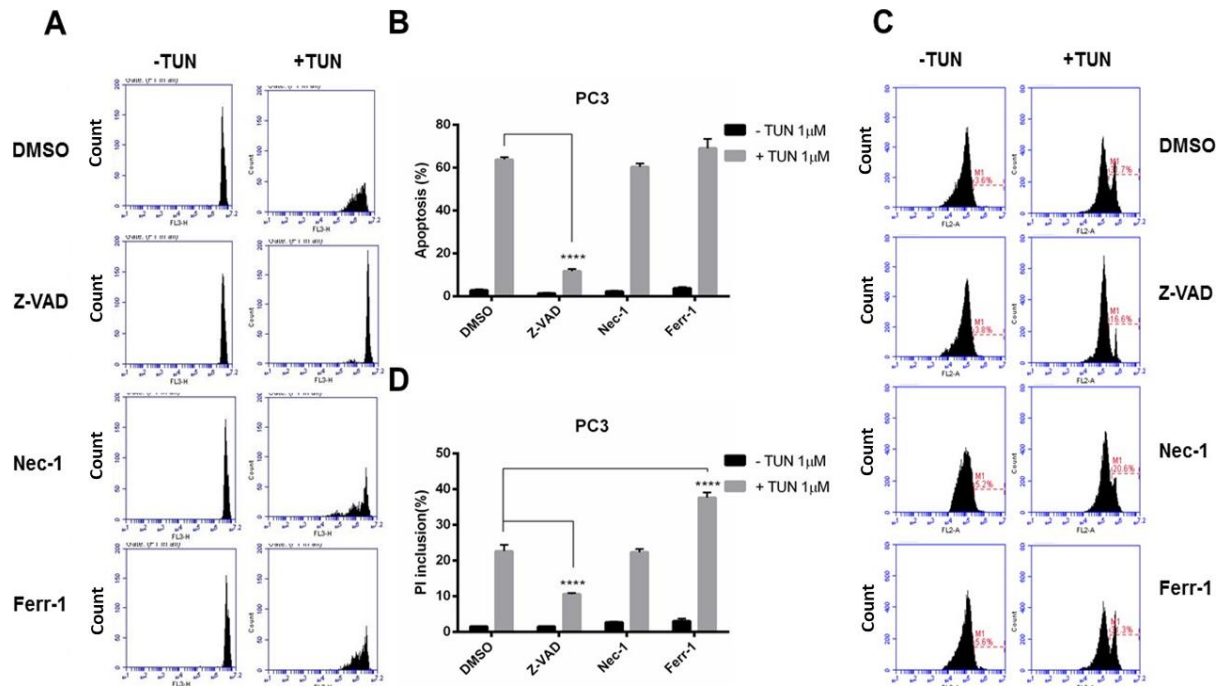


**Figure 3.3.6 Z-VAD-FMK inhibits tunicamycin induced apoptosis in PC3 cells.**

Cells were treated for 72h with DMSO, Z-VAD-FMK, Necrostatin-1 and Ferrostatin-1 in the presence or absence of tunicamycin (1 $\mu$ M). For the combined treatment, inhibitors were added 30 min before tunicamycin. Cells were then collected and analysed using the BD Accuri™ C6 flow cytometer. Graphs are the mean of 3 individual repeats. Two-way ANOVA tests were performed using GraphPAD Prism 7 software. **A-B.** DNA Hypodiploidy assay. **C-D.** PI inclusion assay. \* $p < 0.05$ , \*\* $p < 0.005$ , \*\*\* $p < 0.0005$

To summarise, ER stress had little effect on the proliferation and cell cycle of BPH-1 cells; however, apoptosis was triggered when the cells were under high levels of stress. The results also show that the proliferation of the androgen responsive cells, LNCaP, was reduced in the presence of ER stress because of a G1-phase arrest. Although low levels of apoptosis were also found in these cells, the addition of the apoptosis inhibitor Z-VAD-FMK could not significantly reverse these effects, and so it could not be confirmed whether ER stress was able to induce apoptosis in LNCaP cells. The proliferation of DU145 and PC3 cells was significantly reduced by tunicamycin, and the results suggest that this inhibition of proliferation was caused by ER stress-induced apoptosis.

### **3.4 Mechanisms of cell death induced by UPR**

Activation of the UPR is able to induce apoptosis in PCa cells, however, the signalling event leading to cell death remain unclear. It was proposed that UPR stress can promote apoptosis through the activation of Death Receptor 5 (DR5) and caspase 8 (Lu et al., 2014). In response to ER stress, the transcription factor CHOP, downstream of the PERK - ATF4 axis and of ATF6, induces the expression of DR5 and directly controls its accumulation. As a result, the activation of DR5 occurs intracellularly (ligand-independent) and the caspase 8-activating complex (caspase 8, DR5, FADD) is formed (Lu et al., 2014, Sano and Reed, 2013).

In order to further investigate this mechanism in PCa, several knock-out DU145 cell lines were used: two caspase 8 knock-out clones, two FADD knock-out clones and one RIP1 (part of the necrosis machinery) knock-out cell line. These cell lines were kindly provided by Dr Andrea Mohr and Dr Ralf Zwacka (University of Essex). To induce ER stress, the cells were treated with 1  $\mu$ M Tunicamycin for 72h. DNA Hypodiploidy and PI inclusion assays were performed to assess the levels of cell death

in the knock-out clones (Figure 3.4). It was observed that the levels of apoptosis in caspase 8 and FADD knock-out cell lines were significantly lower compared to the parental DU145 cells. The PI inclusion levels of caspase 8 knock-out (clone 4b) were also significantly lower than the ones present in the normal cells. However, no such difference was recorded for the FADD knock-out lines. However, a western blot to confirm the knock-out of caspase 8 and FADD in these two clones is needed. Interestingly, the RIP1 clone had significantly higher levels of apoptosis and necrosis than the normal DU145 cells.

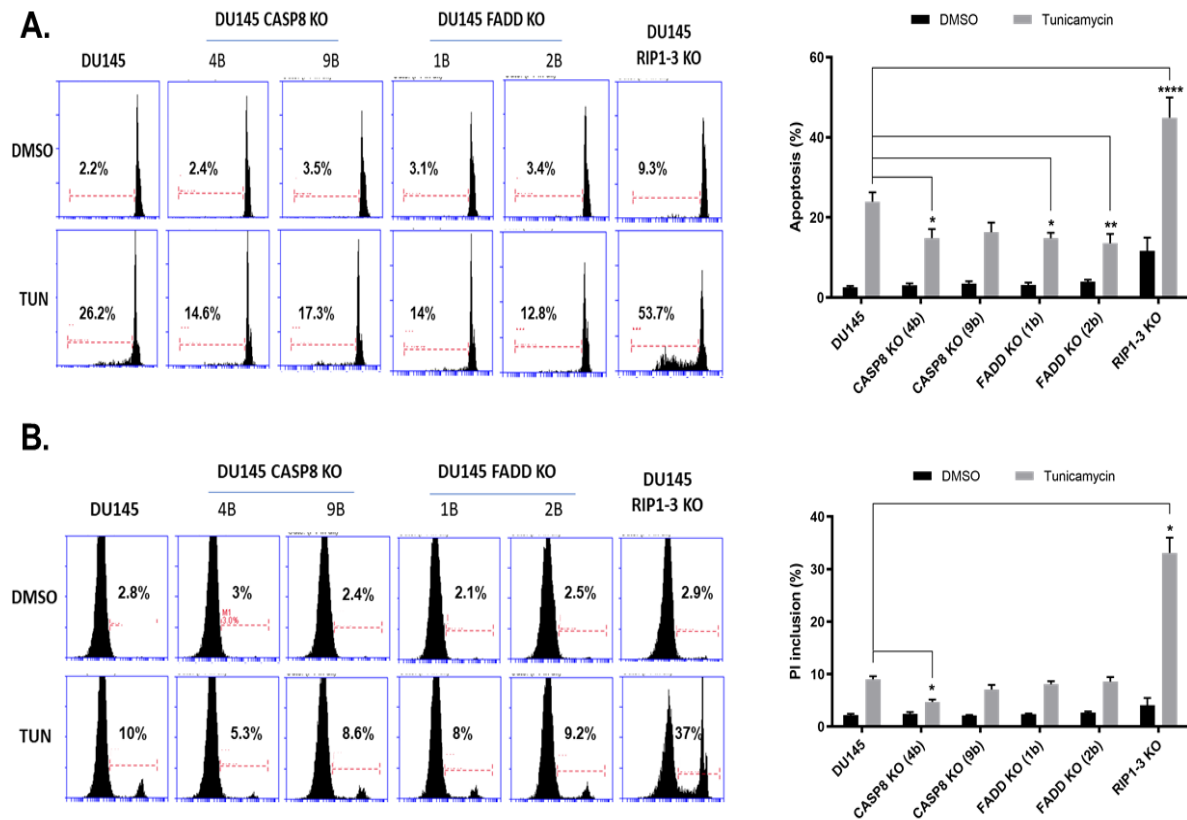


**Figure 3.4 Apoptotic and PI inclusion levels of DU145 KO cell lines in response to tunicamycin.**

Cells were treated 1  $\mu$ M Tunicamycin for 72h, then collected and analysed using the BD Accuri™ C6 flow cytometer. **A.** DNA Hypodiploidy assay of DU145 KO cell lines. **B.** PI Inclusion assay of DU145 KO cell lines. Graphs are the mean of 3 individual repeats. Graphs and statistical analysis (two-way ANOVA) were plotted/performed using GraphPAD Prism 7 software. \* $p < 0.05$ , \*\* $p < 0.005$ , \*\*\* $p < 0.000$

### 3.5 UPR activation in response to ER stress

In order to study UPR activation in PCa, the cells were grown in medium supplemented with 10% FBS and then treated with a dose range of Tunicamycin for 6 and 24 hours. After the RNA was harvested and cDNA synthesised, the expression levels of the UPR target genes *XBP1s* (downstream of IRE1 $\alpha$ ), *ATF4* (downstream of PERK), *HERPUD1* (downstream of ATF6) and *CHOP* (pro-apoptotic gene regulated by both PERK and ATF6) was assessed by q-PCR (Figure 3.5). These results only show the changes in the expression levels of these genes and not the activity of the encoded proteins.

Splicing of XBP1 by IRE1 $\alpha$  was activated after 6h in BPH-1 and LNCaP cells (0.1- 10 $\mu$ M and 10 $\mu$ M, respectively) and after 24h in DU145 cells (1 $\mu$ M). In LNCaP cells, *ATF4* expression was significantly increased after 6 h of tunicamycin (10 $\mu$ M) treatment. However, PERK was not activated in BPH-1, DU145 or PC3 cells, as *ATF4* mRNA levels remained unchanged during the 6 and 24h of stress. Furthermore, the expression of the ATF6 target gene *HERPUD1* was significantly increased in BPH-1 and LNCaP cells after 6 h of tunicamycin (0.1  $\mu$ M and 10  $\mu$ M, respectively) treatment and in BPH-1 after 24 h of treatment. Finally, the expression of *CHOP* (downstream of PERK and ATF6) was found to be induced in LNCaP cells after 6h of ER stress and in LNCaP and PC3 cells after 24h.

To summarise, after 6h of stress, IRE1 $\alpha$  and ATF6 were activated in the non-cancerous cells and in the incipient stage of the disease (BPH-1, LNCaP). PERK was activated in LNCaP cells only. After 24h, IRE1 $\alpha$  was activated in LNCaP and castrate resistant PCa (DU145), ATF6 in BPH-1 and LNCaP cells, whilst CHOP signalling (mediated by PERK/ATF6) was activated in LNCaP and PC3 cells.

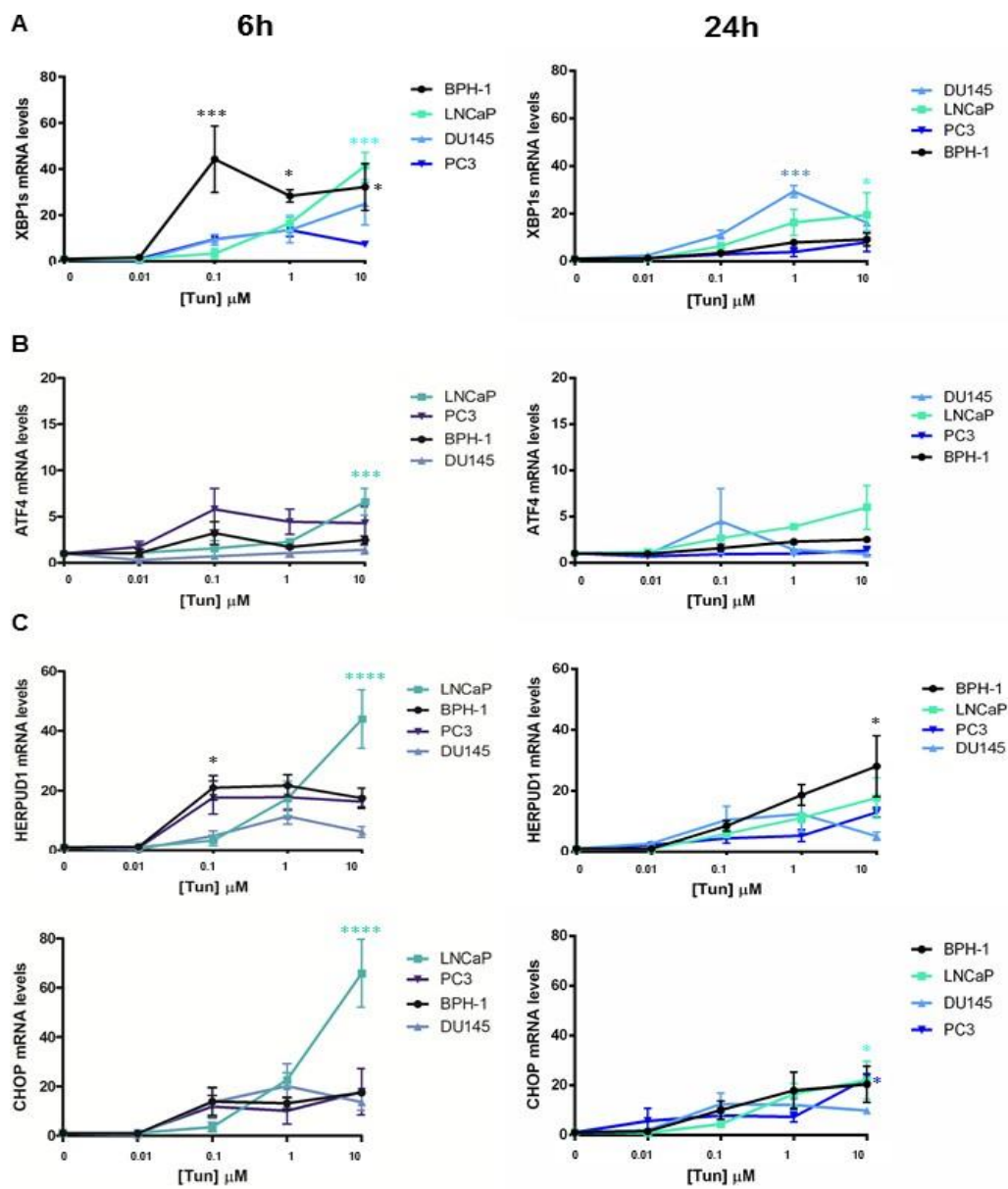


**Figure 3.5 UPR activation in response to ER stress.**

Cells were treated with tunicamycin (dose range) for 6 and 24 hours and the activation of the UPR was assessed using q-PCR. **A.** IRE1 $\alpha$  activation. **B.** PERK activation. **C.** ATF6 activation. **D.** PERK/ATF6 activation. Graphs are the mean of 3 individual repeats, respectively. Two-way ANOVA tests were performed using GraphPAD Prism 7 software. \* $p < 0.05$ , \*\* $p < 0.005$ , \*\*\* $p < 0.0005$ .

### **3.6 Effects of targeting UPR Signalling upon Prostate Cancer proliferation and target gene expression**

The UPR has been proposed to protect cancer cells from cellular stress and to promote proliferation (Storm et al., 2016). To assess the effect of disruption of UPR signalling upon PCa proliferation, crystal violet proliferation assays were performed in order to investigate the effect of UPR inhibitors in four PCa cell lines. The inhibitors used are able to block the activity of IRE1 $\alpha$  (4 $\mu$ 8c), PERK (GSK-2656157) and ATF6 (AEBSF). Cells were grown in medium supplemented with 10% FBS and underwent single-agent treatment for 72 h with a dose range (0-10  $\mu$ M) of the inhibitors. The cells were then fixed with 4% PFA and stained with crystal violet in order to assess the effect of the inhibitors upon the proliferation of PCa and to obtain the IC<sub>50</sub> values of the inhibitors (Figure 3.6.1). Inhibition of PERK reduced the proliferation of all PCa cell lines and GSK-2656157 had an average IC<sub>50</sub> of 5.54  $\mu$ M. The other drugs showed little activity in the cell lines at the concentrations tested.

Next, the inhibitors were used as combined treatments in the presence or absence of ER stress induced using tunicamycin (Figure 3.6.2). It was observed that in the absence of tunicamycin, the proliferation of LNCaP cells was significantly reduced by the inhibition of PERK, and IRE1 $\alpha$ . Furthermore, in UPR stressed cells that had the IRE1 $\alpha$  and PERK, IRE1 $\alpha$  and ATF6, or all UPR arms inhibited, proliferation was significantly reduced compared to cells treated with Tunicamycin only (BPH1, DU145, PC3). However, no such significant difference was observed in LNCaP cells. In summary, combined inhibition of IRE1 $\alpha$  with PERK or ATF6 in the presence of ER-stress caused a further reduction in the proliferation of castrate resistant models and BPH-1 cells.

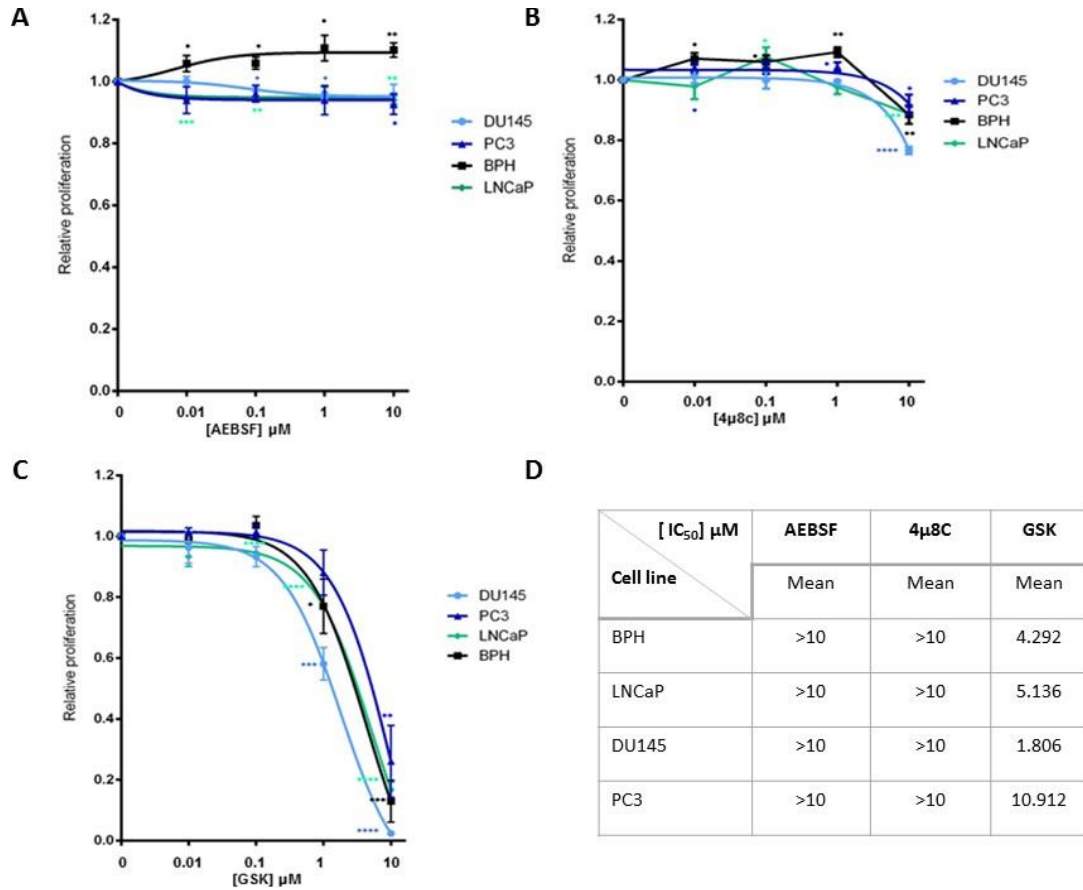


**Figure 3.6.1 Dose response curves, and IC<sub>50</sub> values, for the UPR inhibitors.**

The cells were treated with the inhibitors (0-10  $\mu\text{M}$ ) or with DMSO as the control. Cells were incubated with the treatment for 72h and fixed with 4% PFA in PBS. **A.** Dose response curves for AEBSF, inhibitor of ATF6. **B.** Dose response curves for 4 $\mu$ 8c, inhibitor of IRE1 $\alpha$ . **C.** Dose response curves for GSK-2656157, inhibitor of PERK. **D.** IC<sub>50</sub> values for the inhibitors were generated using GraphPad Prism software. \* $p < 0.05$ , \*\* $p < 0.005$ , \*\*\* $p < 0.0005$ .

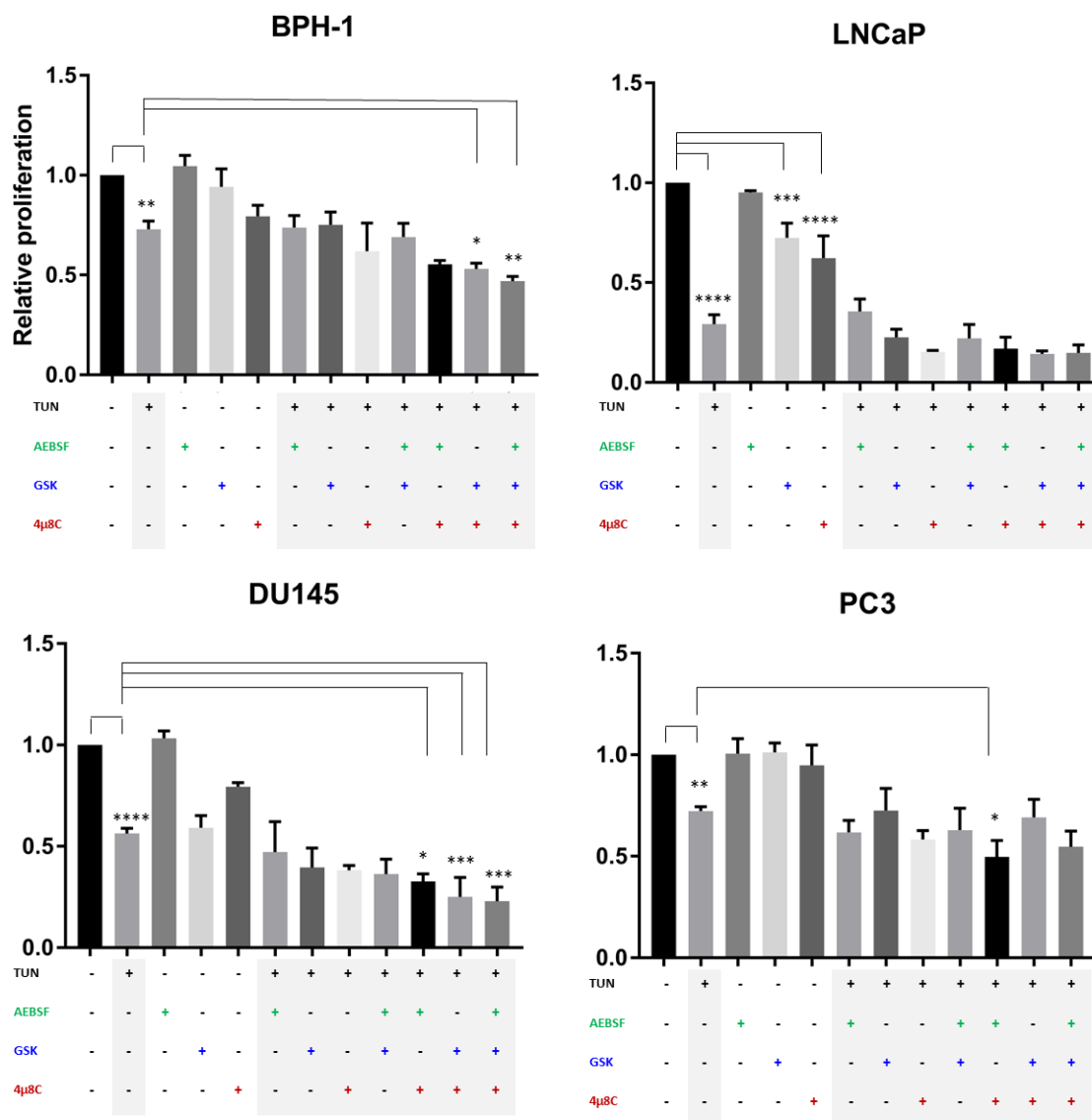


**Figure 3.6.2 Inhibition of UPR signalling further reduces proliferation during ER stress.**

BPH-1, LNCaP, DU145 and PC3 cells were treated with Tunicamycin (85nM, 600nM, 50nM, 50nM, respectively) and the inhibitors at 1μM (GSK) and 10 μM (AEBsf and 4μ8C) for 72h. DMSO was used as a control. Graphs are the mean of 3 individual repeats. One-way ANOVA tests were performed using GraphPAD Prism 7 software. \*p<0.05, \*\*p<0.005, \*\*\*p<0.0005.

The effect of UPR inhibitors upon UPR target gene expression was investigated across a panel of PCa cell lines (LNCaP, C42, 22RV1, DU145 and PC3) (Figures 3.4.3-7). The cells were grown in medium supplemented with 10% FBS and treated with 10  $\mu$ M UPR inhibitors for 24 h in the presence or absence of ER stress. As toyocamycin was used as a potent inhibitor of XBP1 splicing in the study conducted by (Sheng et al., 2015), this IRE1 $\alpha$  inhibitor was also included in these studies.

Inhibition of IRE1 $\alpha$  by 4 $\mu$ 8c significantly reduced the splicing of XBP1 in LNCaP and DU145 cells and resulted in an increase of ATF6 signalling (*HERPUD1*) in PC3 cells as well as the overexpression of *CHOP* in LNCaP and PC3 cells. Inhibition of PERK by GSK-2656157 was not able to significantly reduce the expression levels of *ATF4* in any of the cell lines, however, it resulted in the overexpression of *CHOP* in LNCaP cells and the ATF6 target gene *HERPUD1* in C42 cells. Moreover, splicing of XBP1 was also increased in LNCaP cells following PERK inhibition. Inhibition of ATF6 by AEBSF had no significant effect upon the expression of any of the UPR target genes studied in this experiment. It has also been observed that in all cell lines, toyocamycin was able to not only reduce the splicing of XBP1, but also to inhibit PERK and ATF6 signalling (*ATF4*, *HERPUD1*, *CHOP*).

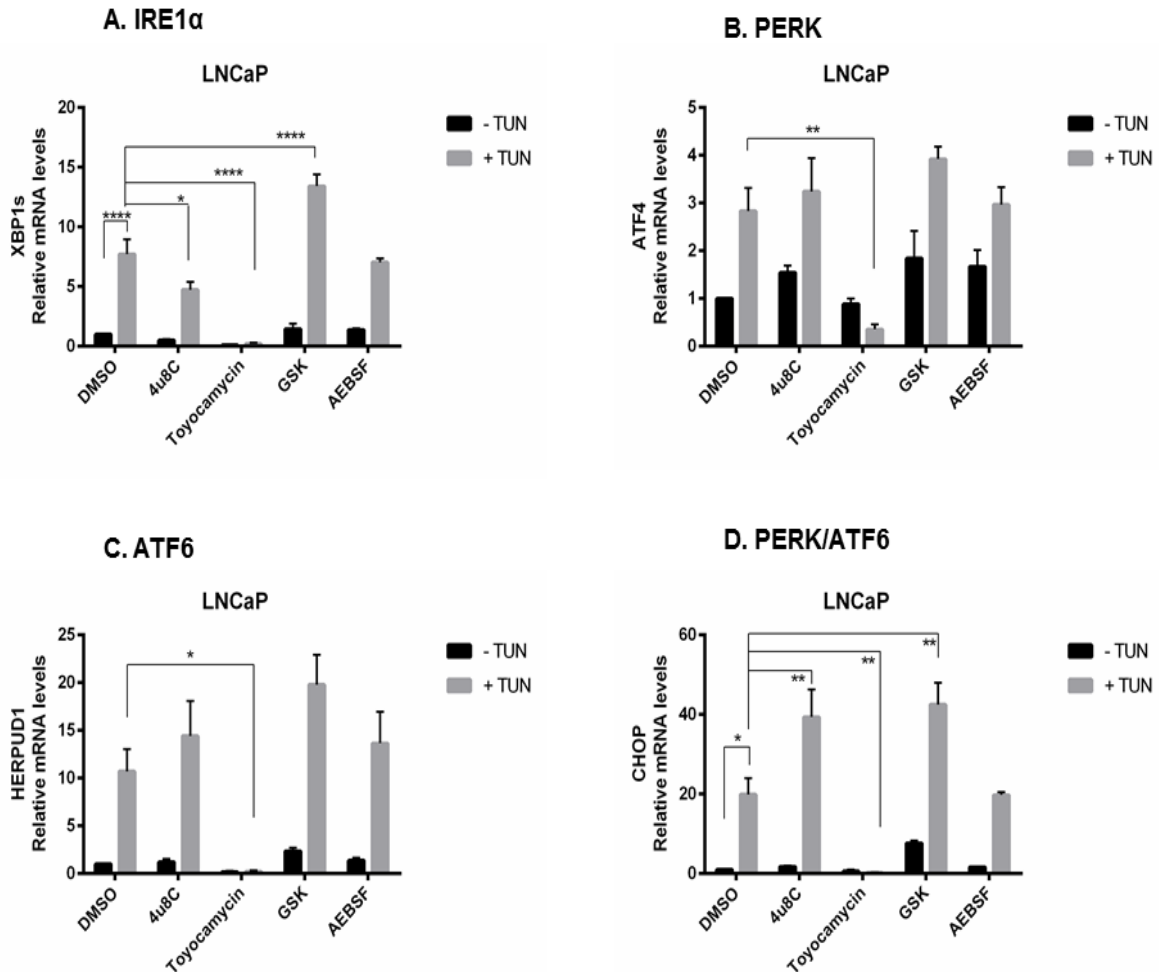


**Figure 3.6.3 Effects of UPR inhibitors upon UPR target gene expression in LNCaP cells.**

LNCaP cells were treated with 10  $\mu$ M Tunicamycin +/- 10  $\mu$ M UPR inhibitors for 24 hours and the activation of the UPR was assessed using q-PCR. **A.** IRE1 $\alpha$  activation. **B.** PERK activation. **C.** ATF6 activation. **D.** PERK/ATF6 activation. Graphs are the mean of 3 individual repeats. Two-way ANOVA tests were performed using GraphPAD Prism 7 software. \* $p < 0.05$ , \*\* $p < 0.005$ , \*\*\* $p < 0.0005$ .

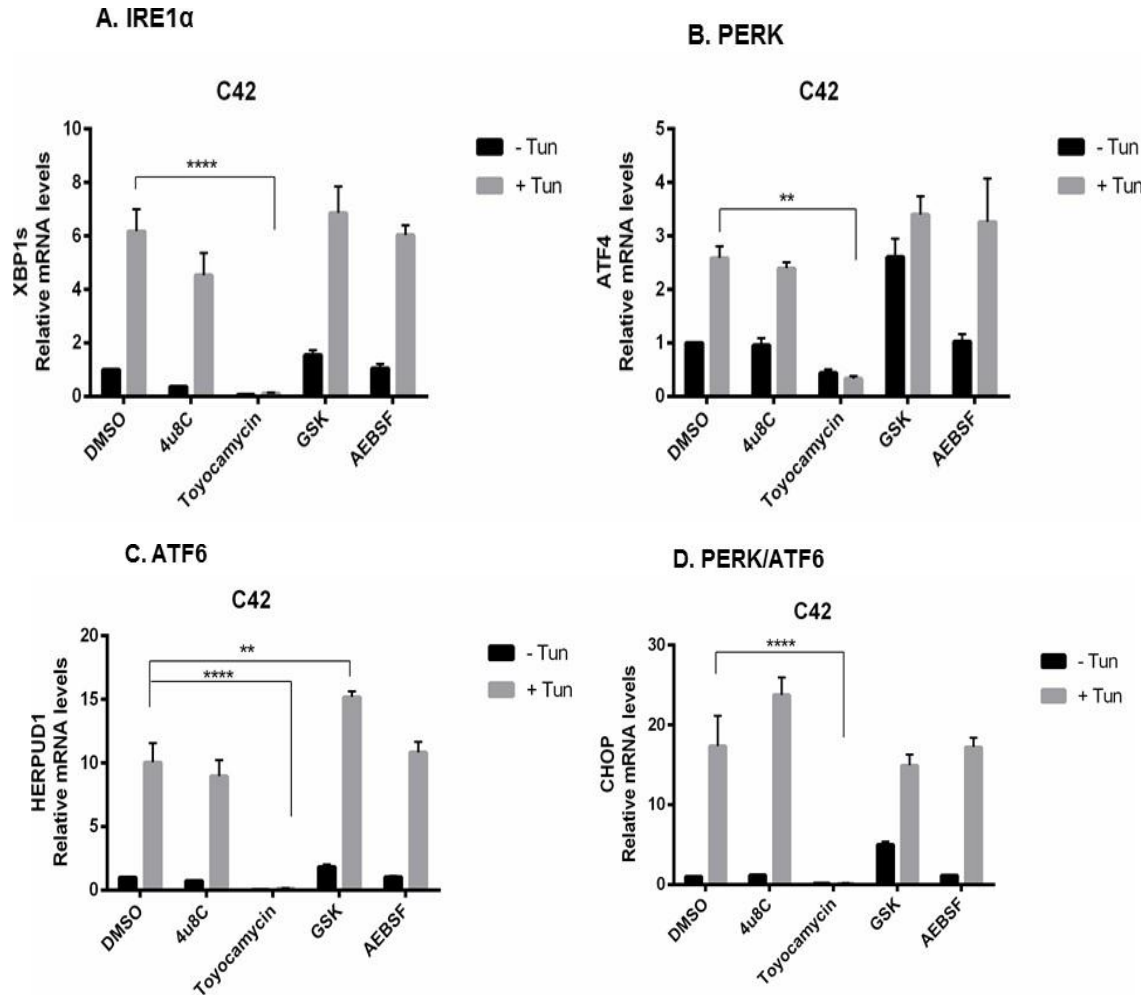


**Figure 3.6.4 Effects of UPR inhibitors upon UPR target gene expression in C42 cells.**

C42 cells were treated with 10  $\mu$ M Tunicamycin +/- 10  $\mu$ M UPR inhibitors for 24 hours and the activation of the UPR was assessed using q-PCR. **A.** IRE1 $\alpha$  activation. **B.** PERK activation. **C.** ATF6 activation. **D.** PERK/ATF6 activation. Graphs are the mean of 3 individual repeats. Two-way ANOVA tests were performed using GraphPAD Prism 7 software. \* $p < 0.05$ , \*\* $p < 0.005$ , \*\*\* $p < 0.0005$ .

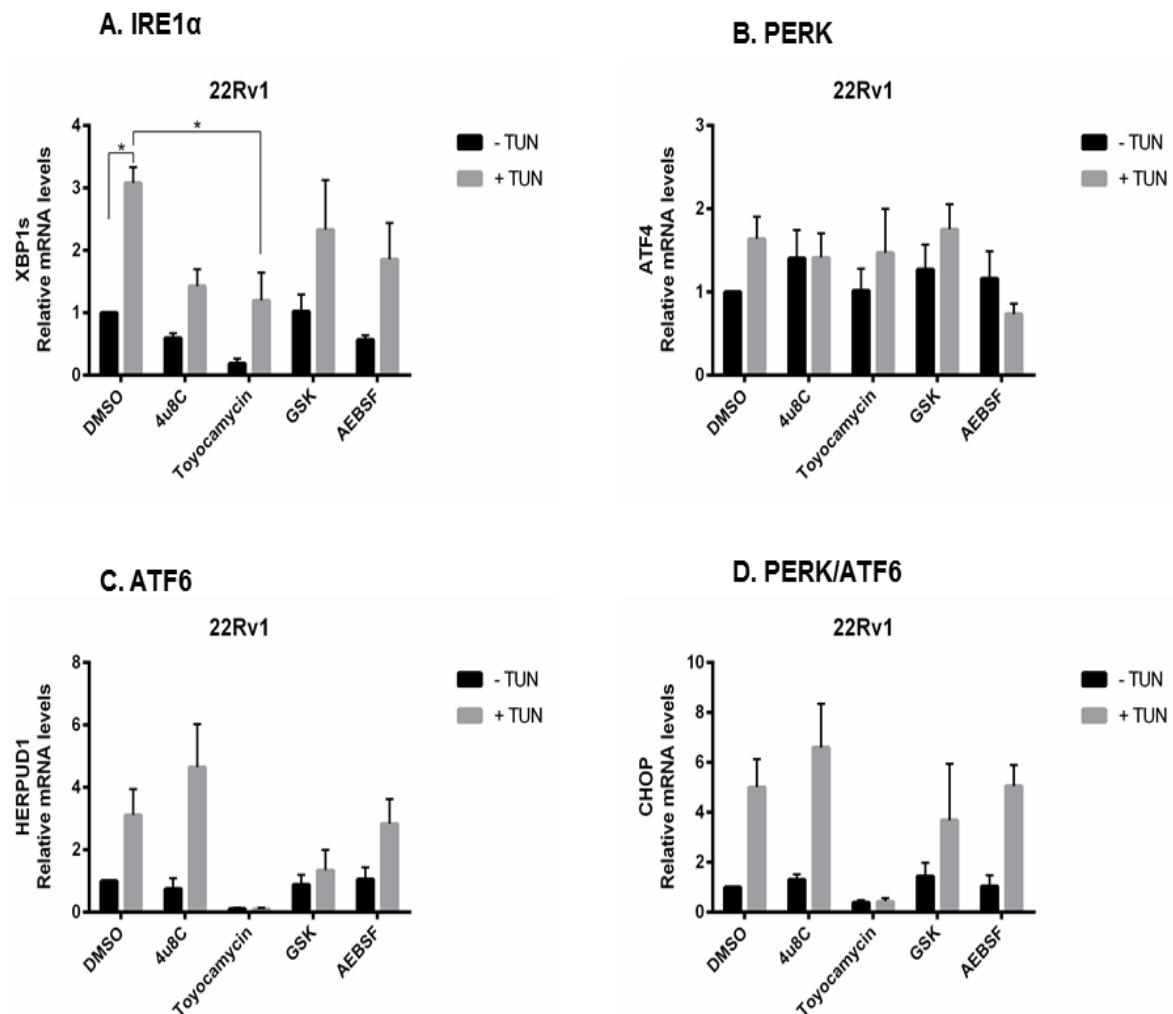


**Figure 3.6.5 Effects of UPR inhibitors upon UPR target gene expression in 22Rv1 cells.**

22Rv1 cells were treated with 10  $\mu$ M Tunicamycin +/- 10  $\mu$ M UPR inhibitors for 24 hours and the activation of the UPR was assessed using q-PCR. **A.** IRE1 $\alpha$  activation. **B.** PERK activation. **C.** ATF6 activation. **D.** PERK/ATF6 activation. Graphs are the mean of 3 individual repeats. Two-way ANOVA tests were performed using GraphPAD Prism 7 software. \* $p < 0.05$ , \*\* $p < 0.005$ , \*\*\* $p < 0.0005$ .

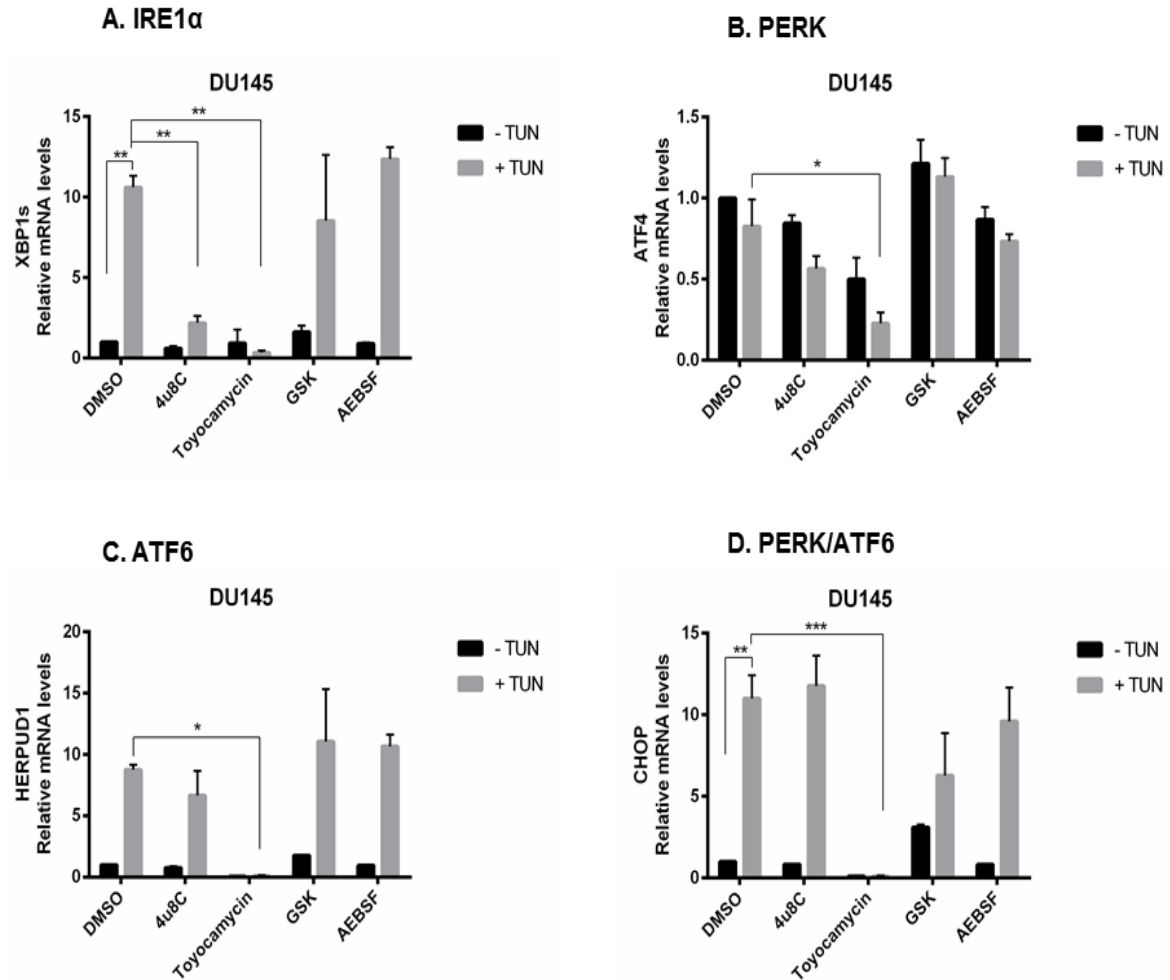


**Figure 3.6.6 Effects of UPR inhibitors upon UPR target gene expression in DU145 cells.**

DU145 cells were treated with 10  $\mu$ M Tunicamycin +/- 10  $\mu$ M UPR inhibitors for 24 hours and the activation of the UPR was assessed using q-PCR. **A.** IRE1 $\alpha$  activation. **B.** PERK activation. **C.** ATF6 activation. **D.** PERK/ATF6 activation. Graphs are the mean of 3 individual repeats. Two-way ANOVA tests were performed using GraphPAD Prism 7 software. \* $p < 0.05$ , \*\* $p < 0.005$ , \*\*\* $p < 0.0005$ .

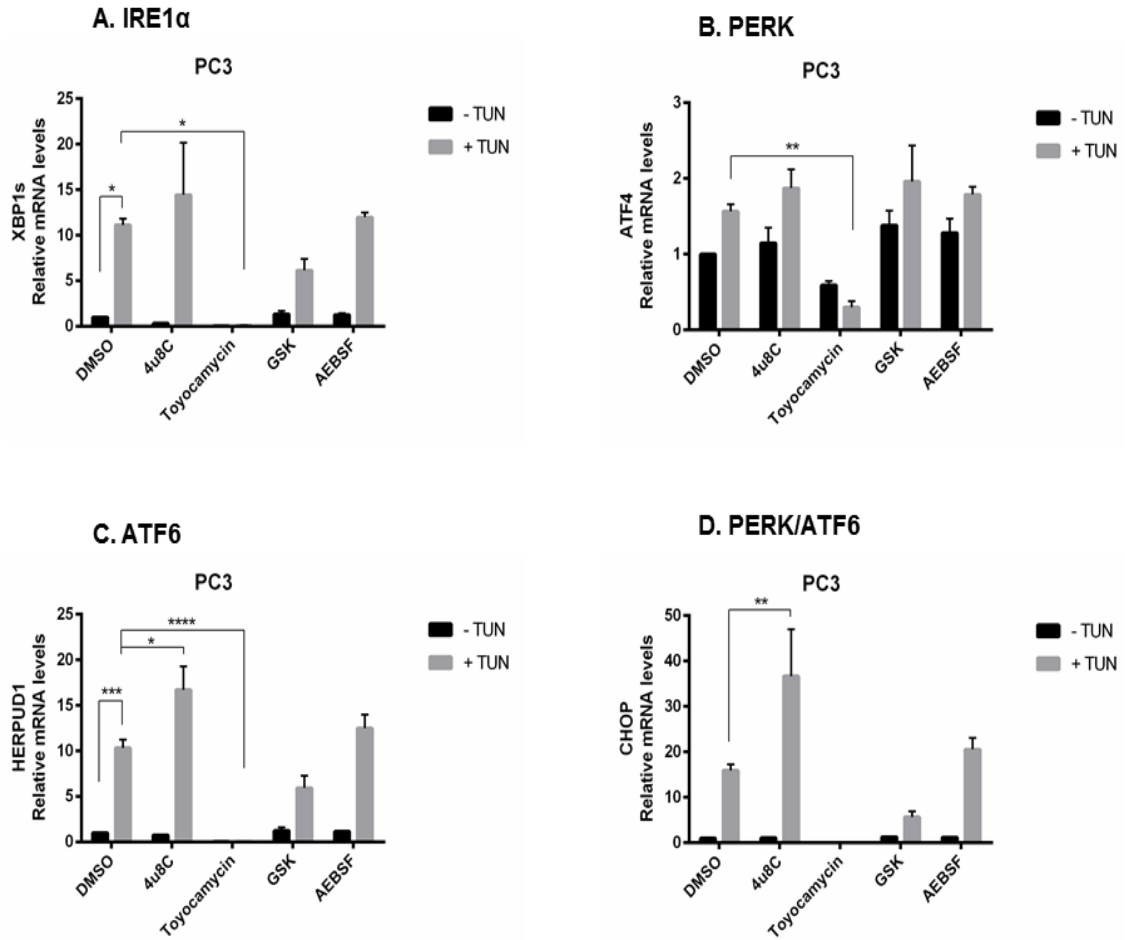


**Figure 3.6.7 Effects of UPR inhibitors upon UPR target gene expression in PC3 cells.**

PC3 cells were treated with 10  $\mu$ M Tunicamycin +/- 10  $\mu$ M UPR inhibitors for 24 hours and the activation of the UPR was assessed using q-PCR. **A.** IRE1 $\alpha$  activation. **B.** PERK activation. **C.** ATF6 activation. **D.** PERK/ATF6 activation. Graphs are the mean of 3 individual repeats. Two-way ANOVA tests were performed using GraphPAD Prism 7 software. \* $p < 0.05$ , \*\* $p < 0.005$ , \*\*\* $p < 0.0005$ .

### **3.7 Discussion**

In this chapter the effects of the tumour microenvironment upon the survival of PCa cells were characterised. In order to do this, tunicamycin was used to induce ER stress in a panel of PCa cell lines that represented different stages of the disease. Proliferation and flow cytometric assays were used to investigate the effects of stress upon PCa proliferation, cell cycle and cell death. qPCR assays were also performed to study the activation of UPR signalling in response to stress and to investigate the effects of targeting the three sensor proteins upon the expression of their target genes.

Four PCa cell lines were used in most experiments, and they were: (i) the BPH-1 cells – which are benign epithelial cells isolated from the prostate tissue of a patient with benign prostatic hyperplasia (Hayward et al., 1995) and were used as a control; (ii) the LNCaP cells – which are malignant epithelial cells that have been derived from a metastatic prostate adenocarcinoma tumour found in the lymph node of a 50-year-old patient; they express the AR and PSA at mRNA and protein level and are androgen responsive (Horoszewicz et al., 1983) therefore they have been used as a representative of the incipient stages of the disease; (iii) DU145 and PC3 which are malignant cells isolated from metastatic prostate tumours that had spread to the brain (Stone et al., 1978) and the vertebrae (Kaighn et al., 1979), respectively; they do not express the AR or PSA at mRNA or the protein level and are androgen independent (Namekawa et al., 2019, Cunningham and You, 2015); therefore they represent the metastatic, castrate resistant stage of PCa.

#### **3.7.1 UPR sensor proteins have high levels of expression in hormone sensitive models of Prostate Cancer**

The protein expression levels of the three UPR sensors were assessed in eight PCa cell lines (Figure 3.1) and it was observed that the levels of IRE1 $\alpha$  were low in

the normal and non-cancerous prostate cells as well as in the advanced metastatic stages of PCa. However, in the incipient stages of the disease, in the androgen responsive cell line LNCaP and its sublines C42 and C42B, IRE1 $\alpha$  was found to have high levels of expression. These results could suggest that IRE1 $\alpha$  has an important role during this hormone responsive stage of the disease, and they correlate with the findings of Sheng *et al.* who demonstrated that the expression of IRE1 $\alpha$  increased following androgen treatment and that this effect was regulated by the AR – which bound directly to the gene regulatory sites of IRE1 $\alpha$  and increased its expression (Sheng et al., 2015). Since AR signalling promotes PCa growth, the interaction between the AR and IRE1 $\alpha$  branch of the UPR could also promote cancer survival – an implication which has been recently confirmed by (Sheng et al., 2019). Therefore, the detection of IRE1 $\alpha$  in these cells, even in the absence of an ER-stressor, suggest that PCa utilises IRE1 $\alpha$  in the androgen-responsive stages of the disease and relies on its proliferative effects.

The expression of PERK was found to be relatively high and uniform across the normal, benign and androgen-responsive cells, however its expression was lower in the metastatic models. PERK has been found to be involved in various cancers where it has been shown to be differentially expressed and promoted tumour growth, autophagy, metastasis, the infiltration of immune cells in the tumour microenvironment and resistance to radiation (Wang et al., 2021). In PCa, PERK signalling has also been shown to promote metastatic progression of both hormone-sensitive and castrate resistant PCa through the phosphorylation of eIF2 $\alpha$  and the subsequent inhibition of global protein synthesis (Nguyen et al., 2018). However, the results presented here show that the basal levels of PERK in metastatic PCa cells are lower compared to the basal levels of PERK found in normal and androgen-sensitive cells.

Low levels of ATF6 were found in normal and benign prostate cells, with higher expression in androgen-responsive cells and highest in metastatic models. Although there is limited information available in the literature regarding the role of ATF6 in PCa, a recent study has shown that progression of PCa is associated with the activation of ATF6 (Pachikov et al., 2021). The S1P and S2P proteases, located in the Golgi, that cleave ATF6 are overexpressed during the progression of PCa, and the protein GCC185 that retains the two proteases in the Golgi apparatus is downregulated. Furthermore, Pachikov *et. al.* demonstrated that PCa promotes the fragmentation of the Golgi which leads to the translocation of S1P and S2P in the endoplasmic reticulum, where they cleave ATF6 directly. This accelerates the activation of ATF6 and its signalling, promoting the production of pro-metastatic metabolites. The authors also correlated the activation of ATF6 with AR signalling and disease stage (Pachikov et al., 2021). Our findings correlate with this study as ATF6 was expressed in both androgen responsive and metastatic models.

In summary, high levels of IRE1 $\alpha$ , PERK and ATF6 were recorded in the androgen responsive cell lines suggesting that the UPR is highly active during the hormone sensitive stage of the disease. However, in metastatic models, the sensor proteins had differential expression – with IRE1 $\alpha$  and PERK having low levels of expression and ATF6 having high levels of expression.

### **3.7.2 Androgen responsive cells attempt to delay cell death by entering into G1-phase arrest**

The effects of ER stress upon the proliferation, cell cycle and cell death of PCa were investigated using tunicamycin to induce ER stress in four cell lines. The effects of UPR stress upon PCa proliferation (Figure 3.2.1A), cell cycle (Figure 3.2.1B) and cell death (Figures 3.3.1-2) were subsequently assessed. Furthermore, inhibitors of

apoptosis, necrosis and ferroptosis were used in order to determine the type of cell death that is induced by ER stress (Figures 3.3.3-6).

It has been observed that the benign BPH-1 cells were least affected by ER stress – BPH1 proliferation was not greatly reduced by tunicamycin, it had no effect upon cell cycle and the cells were found to undergo significantly less apoptosis when compared to the other three lines. This would suggest that non-cancerous prostate cells have the capacity to deal with ER stress and, when linked with the previous western blot analysis, PERK signalling could play an important pro-survival role in these cells. Furthermore, the use of ferroptosis inhibitor Ferrostatin-1 (Zilka et al., 2017) was able to reduce the levels of PI inclusion in these cells. Ferroptosis is a type of cell death that is iron-dependent and is characterised by an accumulation of lipid hydroperoxides which results in plasma membrane damage. It is activated in response to stressful stimuli such as high or low temperatures, hypoxia, and radiation, and is regulated by a network of organelles such as the mitochondria, lysosomes, lipid droplets, peroxisomes, Golgi, the nucleus, and most importantly, the endoplasmic reticulum (Chen et al., 2021, Tang et al., 2021). The involvement of the UPR in the management of ferroptosis has been proven to be mainly through the PERK-eIF2 $\alpha$ -ATF4 axis (which can either promote ferroptosis or the resistance to this type of cell death), and through the CHOP-induced expression of the pro-apoptotic protein PUMA – which supports the crosstalk between ferroptosis and TRAIL-induced apoptosis (Lee et al., 2018, Chen et al., 2021). Taken together, these results suggest that continuous ER stress is able to induce apoptosis and perhaps ferroptosis in non-cancerous prostate cells.

When compared to the other three cell lines, the proliferation of the androgen-responsive LNCaP cells was the least affected by ER stress and this reduction in

proliferation was found to be caused by a G1-phase cell cycle arrest. Activation of PERK has been known to cause G1 phase arrest through the phosphorylation of eIF2 $\alpha$  and the subsequent inhibition of cyclin D1 synthesis (Brewer and Diehl, 2000); entering into G1 arrest allows the cells to initiate repair mechanisms (Murad et al., 2016), resolve the ER stress and delay apoptosis. Furthermore, although flow cytometric assays revealed that the cells were undergoing cell death, none of the cell death inhibitors could significantly reverse these effects and so it could not be confirmed the type of cell death, induced by ER stress, was present in this line. These results suggest that ER stress reduces the proliferation of LNCaP cells by causing a cell cycle arrest rather than by inducing cell death. Linked with the previous western blot analysis which showed that all UPR sensor proteins had high levels of expression in these cells, it may be said that during the hormone sensitive stages of the disease, PCa utilises all three UPR arms in order to promote cell survival.

The proliferation of the metastatic models DU145 and PC3 were greatly reduced by ER stress. Furthermore, the reduction in proliferation was not due to a cell cycle arrest, but because of ER stress-induced cell death. The use of flow cytometric assays and cell death inhibitors confirmed that DU145 and PC3 were undergoing apoptosis. Interestingly, the use of Ferrostatin-1 significantly increased the PI inclusion levels of PC3 cells. Ferroptosis is a type of programmed cell-death (Tang et al., 2019) and the inhibition of this mechanism of cell death may result in an increase of other uncontrolled cell death mechanisms, such as necrosis, that disrupt the plasma membrane and allow the entrance of PI in the cell, and the subsequent staining of DNA. The results from the previous western blot analysis showed that there were low levels of IRE1 $\alpha$  in these cells and, when compared to the hormone sensitive stages of the disease, these metastatic models also had lower levels of PERK. Because of this,

the cells might not have been able to efficiently resolve the stress and, as a result, their proliferation was reduced. Although ATF6 had high levels of expression in these cells and plays a mainly pro-survival role, it can also activate the expression of the pro-apoptotic gene *CHOP*, which could explain the high levels of apoptosis that were recorded in these lines.

To summarise, non-cancerous prostate cells are the most resistant to ER stress and they retain their ability to resolve the stress, mainly through a PERK-regulated mechanism. Androgen-responsive cells utilise all three UPR sensor proteins in order to restore homeostasis and attempt to delay cell death by entering into a G1 phase arrest. Finally, metastatic models are the most sensitive to ER stress, probably because they have lower levels of IRE1 $\alpha$  and PERK and so they might lose the ability to efficiently deal with the stress.

### **3.7.3 UPR-induced apoptosis is dependent on caspase 8 and its activating complex**

It has previously been demonstrated that one mechanism by which UPR signalling promotes cell death is through the upregulation of *CHOP* by ATF4, ATF6 and XBP1s, and its subsequent activation by the p38 MAPK (downstream of the IRE1 $\alpha$ -ASK1 axis) (Sano and Reed, 2013). The activated transcription factor CHOP induces the expression of apoptotic targets such as: GADD34 (which promotes the dephosphorylation of eIF2 $\alpha$  and restores protein synthesis and the translation of pro-apoptotic mRNAs), ER oxidoreductase 1 (ERo-1 $\alpha$ , which promotes the release of Ca<sup>2+</sup> from the ER via the IP<sub>3</sub> Receptor), and death receptor 5 (DR5, TRAIL Receptor-2) (Sano and Reed, 2013). DR5 is crucial for the caspase-8 mediated apoptosis and Lu *et. al.* demonstrated that the accumulation of DR5 in the endoplasmic reticulum and Golgi in response to ER stressors resulted in a ligand-independent activation of DR5

and the formation of a death-inducing signalling complex (DISC)-like platform which initiated apoptosis. The caspase 8-activating complex is composed of caspase 8, DR5 and caspase 8 adaptor Fas-associated death domain (FADD) (Lu et al., 2014). In order to assess whether this was the mechanism through which tunicamycin induced apoptosis in PCa cells, knock-out DU145 cell lines, that lacked the expression of FADD or caspase-8, were used (Figure 3.4). Indeed, the levels of apoptosis in the knock-out lines were significantly lower compared to the parental DU145 cells, suggesting that the UPR-induced apoptosis in PCa is dependent on caspase 8 and its activating complex. However, since the depletion of caspase 8 and FADD did not completely rescue the cells from apoptosis, other cell death mechanisms could be active in these cells. Further investigations should aim to identify these processes.

#### **3.7.4 Deficient UPR signalling in castrate-resistant models of Prostate Cancer**

Another aim of this study was to investigate the activation of the UPR sensor proteins in response to stress. To do so, tunicamycin was used to induce ER stress in BPH-1, LNCaP, DU145 and PC3 cells and the effect upon UPR target gene expression, after 6 and 24 hours of treatment, was investigated (Figure 3.5.1). It was observed that in benign prostate cells, IRE1 $\alpha$  and ATF6 signalling were activated after 6 h of stress and that ATF6 signalling was maintained throughout the 24 h of treatment. Activation of ATF6 was studied by measuring the mRNA levels of its target gene *HERPUD1*. The HERPUD1 protein resides in the ER and is involved in the ERAD process, where it transports ubiquitinated substrates to the proteasome for degradation (Ho and Chan, 2015). Furthermore, the mRNA levels of *CHOP* were not significantly increased in the 24 h period, suggesting that in the first 24 h of stress, UPR signalling is restoring homeostasis via IRE1 $\alpha$ /XBP1s axis and through the upregulation of ERAD pathways (ATF6/XBP1s).

In LNCaP cells, all three UPR arms were activated after 6 h of stress, and activation of IRE1 $\alpha$  was maintained throughout the 24 h period. These results correlate with the sensor protein expression levels found in these cells (Figure 3.1) and with the cell cycle analysis (Figure 3.2.1B) – LNCaP cells were the only cells to enter into G1 arrest and also the only cells that had the PERK arm active during stress. Furthermore, the mRNA levels of the pro-apoptotic *CHOP* were significantly upregulated after both 6 and 24 h of stress. Interestingly, there was a dramatic increase in the expression of *CHOP* after 6 h of treatment, which was then followed by a decline in its expression levels – observed at 24 h. Previous studies have demonstrated that CHOP induces the expression of pro-survival autophagy genes before activating the transcription of pro-apoptotic genes, playing an important role in switching between autophagy and apoptosis (Hu et al., 2018). Taken together with our previous findings, these results show once again that all three UPR are active during the hormone sensitive stage of disease and that IRE1 $\alpha$  signalling is maintained throughout the 24 h of stress. As the proliferation of these cells was also the least affected by stress due to a cell cycle arrest, these results suggest that the induction of *CHOP* in the first 6 h of stress resulted in the upregulation of autophagy-associated genes that promote survival and delay cell death. PERK signalling has also been found to reprogram autophagic gene expression in order to promote cancer survival (Bu and Diehl, 2016), however further investigations are needed in order to confirm these findings.

The metastatic models experienced a delay in the activation of UPR signalling, as none of the three arms were active in the first 6 h of stress. After 24 h, IRE1 $\alpha$  signalling was activated in DU145 cells and significantly increased levels of *CHOP* were found in PC3 cells. The decrease in proliferation and the high levels of apoptosis recorded in these cells may be due to the delayed activation of UPR signalling and the

selective upregulation of the pro-apoptotic transcription factor CHOP in PC3. Taken together with the proliferation and cell death assays, these results suggest that UPR signalling in metastatic models might be deficient, and further studies should aim to investigate the activity of UPR in metastatic, castrate resistant PCa.

### **3.7.5 Metastatic models of Prostate Cancer rely on ER-associated degradation (ERAD) pathway in order to survive**

Proliferation assays were used to assess whether inhibition of the UPR sensor proteins affects the growth of PCa. Initially, single agent treatments were performed to investigate whether the inhibition of UPR sensor proteins, in the absence of ER stress, affects the proliferation of PCa cells. Furthermore, the effects of combined treatments that inhibited one or more UPR arms in the presence of stress were also performed. It was observed that the proliferation of all four cell lines were reduced by the inhibition of PERK (Figure 3.6.1) suggesting that PERK is essential for cell survival.

Combined treatments performed in the benign prostate cells showed that inhibition of IRE1 $\alpha$  and PERK as well as inhibition of all three UPR arms, in the presence of ER stress, significantly reduced cell proliferation when compared to the cells that were only treated with tunicamycin. It was previously suggested that BPH-1 cells were able to maintain their ability to resolve ER stress mainly through a PERK-regulated mechanism (Section 3.5.2); moreover, IRE1 $\alpha$  and ATF6 signalling were both activated in response to stress (Section 3.5.4). As inhibition of these arms hindered the ability of the cells to deal with stress, these results suggest that BPH-1 cells are reliant upon the activity of all three UPR arms in order to survive.

Furthermore, inhibition of IRE1 $\alpha$  using 4 $\mu$ 8c (a compound that blocks the active site of IRE1 $\alpha$  and inhibits splicing of XBP1 and the RIDD process (Cross et al., 2012)) in the absence of stress, reduced the proliferation of LNCaP cells. These results

correlate with the findings of (Sheng et al., 2015, Sheng et al., 2019) where they demonstrated that inhibition of IRE1 $\alpha$  significantly reduces the proliferation of PCa *in vitro* and *in vivo*. I previously demonstrated that IRE1 $\alpha$  signalling was active throughout the 24 h of stress (Section 3.5.4) and that proliferation of LNCaP cells was the least affected by ER stress (Section 3.5.2). Therefore, the results so far show that IRE1 $\alpha$ /XBP1s signalling has proliferative effects in androgen responsive cells. Inhibition of PERK also reduced the proliferation of LNCaP cells and since previous experiments have shown that PERK signalling is active in these cells, this suggests that this signalling plays a pro-survival role in androgen responsive cells. Finally, combined treatments had no significant effect upon the proliferation of LNCaP cells.

In metastatic DU145 cells, inhibition of IRE1 $\alpha$  and ATF6, IRE1 $\alpha$  and PERK, as well as inhibition of all three UPR arms, in the presence of ER stress, further reduced proliferation. Since only IRE1 $\alpha$  signalling was active after 24 h of stress, and its sole inhibition did not further reduce cell proliferation, the results may suggest a crosstalk between IRE1 $\alpha$  and ATF6 and PERK signalling pathways that facilitates cell survival. PC3 cells responded similarly to DU145, where inhibition of IRE1 $\alpha$  and ATF6 in the presence of stress further reduced proliferation. Previous studies have demonstrated that activated ATF6 induces the expression and accumulation of *XBP1* mRNA which is then spliced by IRE1 $\alpha$  (Siwecka et al., 2021). Another crosstalk between IRE1 $\alpha$  and ATF6 signalling has been demonstrated by (Yamamoto et al., 2007) who showed that XBP1s and ATF6 dimerise in order to induce the expression of target genes that encode for ERAD components. They also suggested that the simultaneous activation of the two signalling pathways is necessary in order to activate ERAD. As the simultaneous inhibition of IRE1 $\alpha$  and ATF6 signalling reduced the proliferation of both DU145 and PC3 cells, it suggests that these metastatic cells rely on the ERAD process

in order to survive. Moreover, the PERK/ATF4 axis also supports IRE1 $\alpha$  signalling by upregulating the expression of *IRE1 $\alpha$*  mRNA which leads to an increase in XBP1 splicing (Siwecka et al., 2021).

### **3.7.6 IRE1 $\alpha$ signalling promotes survival of androgen responsive cells**

The crosstalk between the three UPR arms have been further investigated by looking into the expression of UPR target genes in response to stress and in response to inhibition of each of the UPR sensor proteins (Figures 3.6.3-7). The cells were treated with tunicamycin and the UPR inhibitors and the expression of target genes was assessed by q-PCR. In order to obtain a broader view of UPR signalling in PCa, these experiments were performed in LNCaP, C42, 22Rv1, DU145 and PC3 cells.

In LNCaP cells, IRE1 $\alpha$ /XBP1s signalling was found to be active throughout the 24 h of stress and the inhibition of this pathway decreased proliferation. The inhibition of IRE1 $\alpha$  also resulted in a significant increase in the mRNA levels of the pro-apoptotic gene *CHOP*. These results correlate with our previous findings and confirm once again that IRE1 $\alpha$  plays a pro-survival role in the androgen responsive cells. Moreover, inhibition of PERK increased the expression of *CHOP* and *XBP1s*. Crosstalk between IRE1 $\alpha$  and PERK could be suggested where the splicing of XBP1 increases as a result of PERK inhibition.

In C42 cells, a subline of LNCaP that represents the progression of PCa from androgen dependence to independence (Thalmann et al., 1994), inhibition of PERK increased the expression of the ATF6 target gene *HERPUD1*. PERK was found to support the progression of both hormone sensitive and castrate resistant models (Nguyen et al., 2018), therefore the activation of the ERAD component HERPUD1 in response to PERK inhibition could also promote PCa cell survival.

Finally, in PC3 cells, inhibition of IRE1 $\alpha$  increased the expression of *HERPUD1* and *CHOP*. It may be proposed that the lack of IRE1 $\alpha$  signalling further increased the stress levels, and as a result *HERPUD1* was activated to promote the degradation of misfolded proteins by ERAD. *CHOP* was also activated, and based on our previous findings, it may be proposed that its activation resulted in the activation of pro-apoptotic genes.

### **3.7.7 Conclusions**

This chapter demonstrated that UPR signalling is highly active during the hormone-sensitive stage of PCa, and that this activity supports cell survival by promoting G1 arrest, allowing the cells to resolve the ER stress and evade cell death. Castrate resistant models of PCa were the most sensitive to ER stress, however UPR signalling needs to be further characterised during this stage of the disease. Possible crosstalk between the three arms of the UPR may also play an important role in promoting cell survival.

## **Chapter 4: Characterising the effects of androgens and antiandrogens upon UPR signalling in prostate cancer**

In the previous chapter, I demonstrated that the UPR is highly active in the androgen dependent stages of PCa. The cells representing this stage of the disease were the most responsive to ER stress and entered G1 arrest in order to promote cell survival. As previously mentioned, the normal development of the prostate is regulated by androgens which act through the androgen receptor (AR). The AR activates genes which promote cell growth and survival and so it also plays a crucial role in the development and progression of prostate cancer (Pienta and Bradley, 2006). Tumours that have spread from the prostate are often treated with hormone therapy that block the AR signalling pathway and inhibit tumour growth (Brooke and Bevan, 2009). These therapies aim to prevent the binding of androgen to the AR (anti-androgens) or to lower the circulating levels of androgens (androgen depletion therapy). However, despite their initial success, these therapies cannot completely inhibit AR activity (Chen et al., 2009) and invariably fail. The tumours develop resistance and progress to the aggressive and difficult to treat castrate resistant stage, for which few therapeutic options exist (Katsogiannou et al., 2015).

Prostate cancer, like many other solid tumours, is characterised by uncontrolled proliferation of transformed cells, which grow in an environment that is known to compromise ER function and cause ER stress (Storm et al., 2016). The activation of the UPR enables PCa cells to survive, adapt to adverse environmental conditions and promote therapy resistance (Corazzari et al., 2017, Storm et al., 2016). Importantly, the UPR has also been shown to be directly regulated by the AR, linking the UPR to the key oncogenic driver of PCa. For instance, the AR was able to bind to gene regulatory sites and activate IRE1 $\alpha$  signalling whilst inhibiting PERK

signalling. Inhibition of the IRE1 $\alpha$  branch reduced PCa cell growth in both *in vitro* and *in vivo* models (Sheng et al., 2015, Sheng et al., 2019). Furthermore, XBP1s was found to have common genomic binding sites with the AR, and knockdown of XBP1s reduced the expression of AR and UPR target genes (Stelloo et al., 2020).

To further our understanding of the role of the AR in UPR signalling, the effects of androgens and antiandrogens upon the expression of UPR components in PCa was investigated. In addition, the effect of UPR targeting upon AR signalling was also characterised.

#### **4.1 Effects of androgen and anti-androgens upon expression of UPR components**

In order to assess whether androgen affects the expression of UPR components in PCa, four AR positive cells were grown in hormone depleted RPMI medium for 72h and then treated with the synthetic androgen mibolerone for 24h. The mRNA and protein levels of the UPR sensor proteins and of the ER chaperone BiP were assessed by qPCR and western blotting (Figure 4.1.1). It was observed that androgen increased the protein levels of IRE1 $\alpha$  in all cell lines, but surprisingly, this was only seen at the RNA level in LNCaP cells.

The mRNA levels of PERK were also increased in response to androgen treatment in C42 cells. At the protein level, PERK did not show a trend towards being regulated by androgen in LNCaP or C42 cells, but it does appear to be regulated in C42B cells in response to this treatment. Interestingly, the basal levels of PERK were lower in 22Rv1 cells compared to the other AR positive cells and its expression appears to be weakly regulated by androgen treatment.

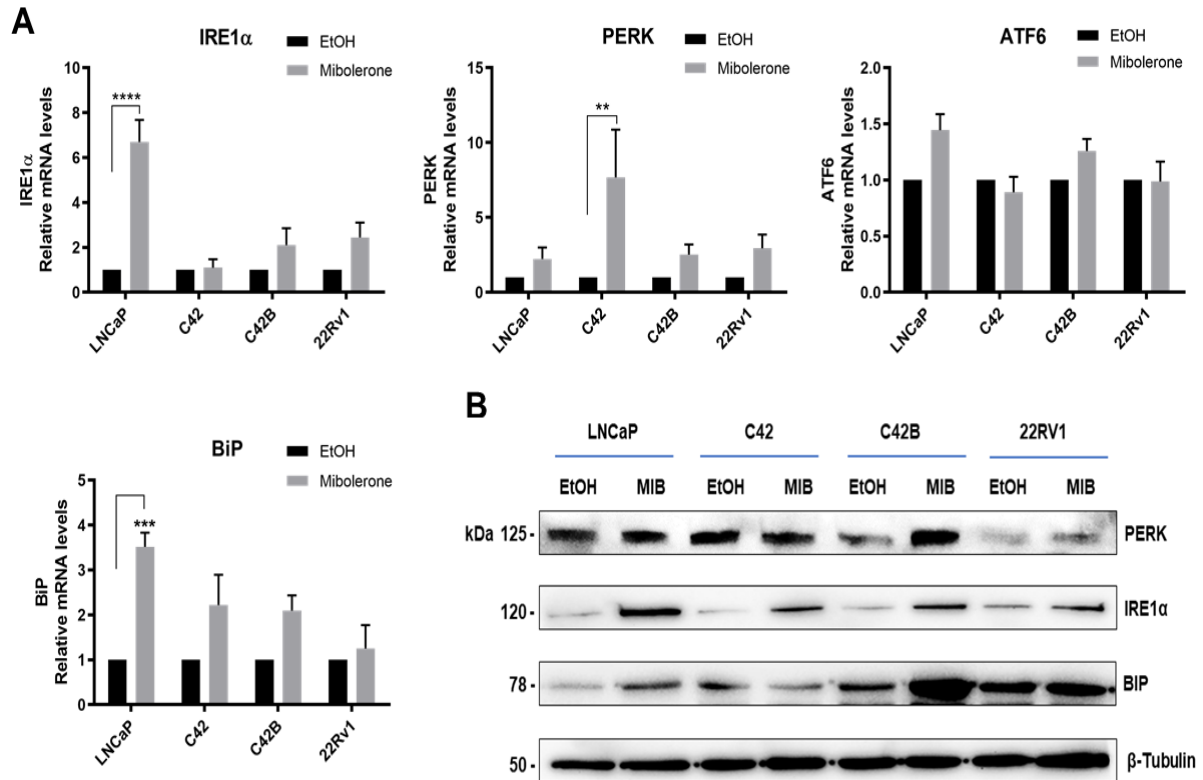


**Figure 4.1.1 Expression of UPR components in response to androgen.**

LNCaP, C42, C42B and 22Rv1 cells were kept at 37°C in RPMI 1640 containing 5% SFCS for 72h, then treated with 1nM Mibolerone for 24h. **A.** The mRNA expression levels of UPR components were assessed by q-PCR. Graphs are representative of 3 individual repeats. Two-way ANOVA tests were performed using GraphPAD Prism 8 software. **B.** Protein levels of UPR components. Samples were separated by SDS page and visualised by western blotting. 30 µg of protein were loaded into each lane and β-Tubulin was used as a loading control. \* $p < 0.05$ , \*\* $p < 0.005$ , \*\*\* $p < 0.0005$ .

Androgen treatment increased the mRNA levels of BiP in all cell lines, but this was only found to be significant in LNCaP cells. At the protein level, BiP expression was also found to be increased in response to androgen in LNCaP and C42B cells. However, no change was recorded in 22Rv1 cells and BiP expression appears to decrease slightly in response to androgen in C42 cells. Additionally, the basal levels of BiP were higher in 22Rv1 cells compared to the other cell lines.

Therefore, it was observed that androgen was able to affect the expression of multiple UPR components, but this regulation was cell line specific. It up-regulated the mRNA and protein levels of the UPR sensor proteins IRE1 $\alpha$  and PERK, as well as those of the ER chaperone BiP. Interestingly, in 22Rv1 cells, which represent a more advanced stage of the disease (Table 3.1), the basal protein levels of PERK and BiP were different compared to the cell lines that represented the androgen sensitive stages of PCa.

As a next step, I assessed the effects of androgen upon the expression of UPR target genes (Figures 4.1.2-3). The cells were grown in hormone depleted media for 72 h and then were treated with mibolerone for 24 h. After the RNA was harvested, the expression of UPR target genes were assessed by q-PCR. As a positive control, the effects of androgen and the antiandrogens were assessed upon the AR target gene *TMPRSS2*. As expected, the AR target gene (*TMPRSS2*) was upregulated in response to androgen and successfully inhibited by the antiandrogens. The splicing of *XBP1*, which is a result of IRE1 $\alpha$  activation, was also significantly increased by androgen treatment in both LNCaP and C42 cells and this was inhibited when cells were co-treated with the antiandrogens. Furthermore, the expression of *HERPUD1*, a target gene of ATF6, was also increased in the presence of androgen (LNCaP), whereas *CHOP*, a pro-apoptotic gene downstream of PERK

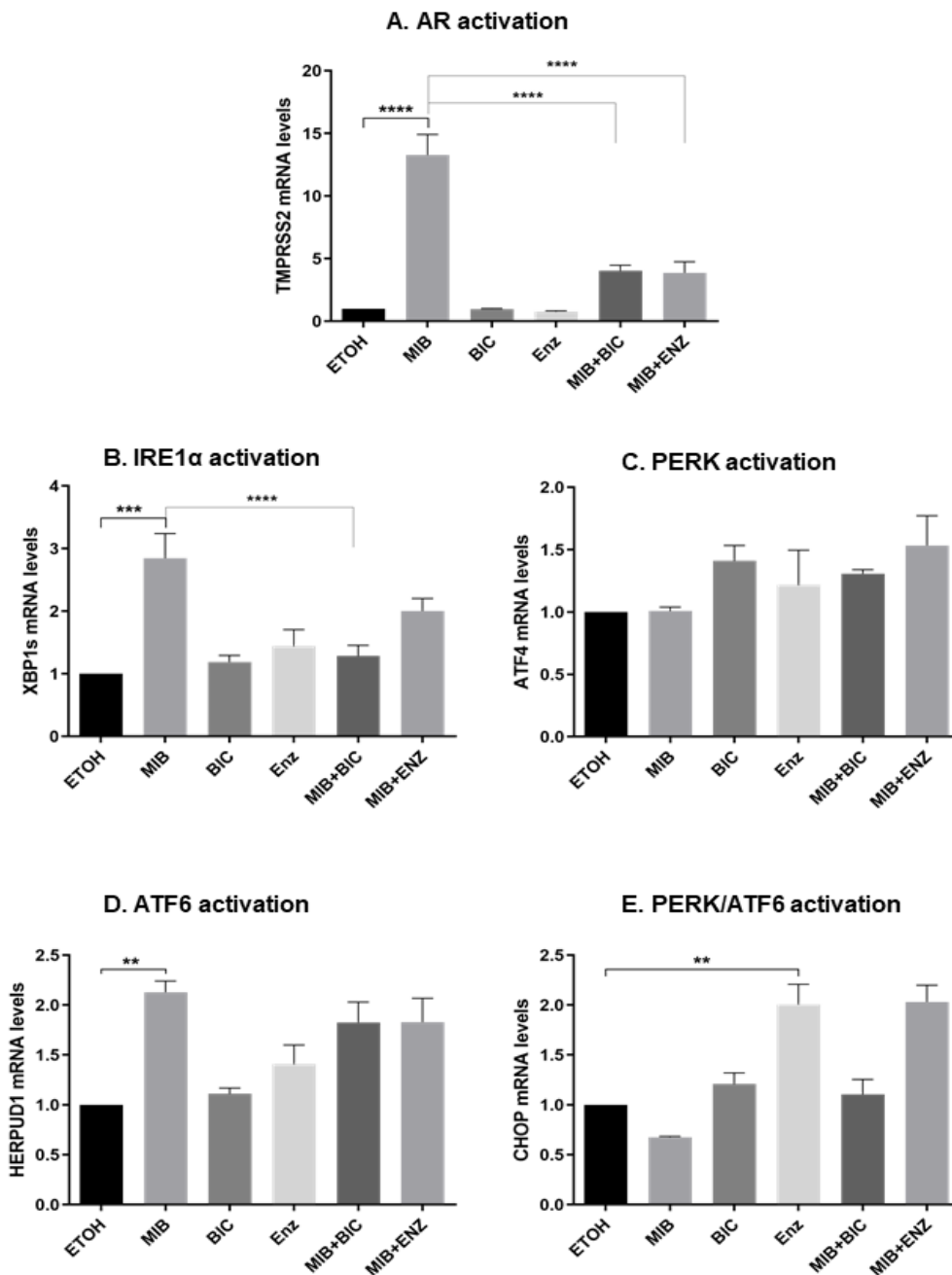


**Figure 4.1.2 UPR activation in response to androgen and antiandrogens.**

LNCaP cells were kept at 37°C in RPMI 1640 containing 5% SFCS for 72h, then treated with 1nM Mibolerone ± 10 nM Bicalutamide or 10 μM Enzalutamide for 24h. Gene expression of UPR target genes was assessed by q-PCR. Graphs are representative of 3 individual repeats. Two-way ANOVA tests were performed using GraphPAD Prism 7 software. \*p<0.05, \*\*p<0.005, \*\*\*p<0.0005.

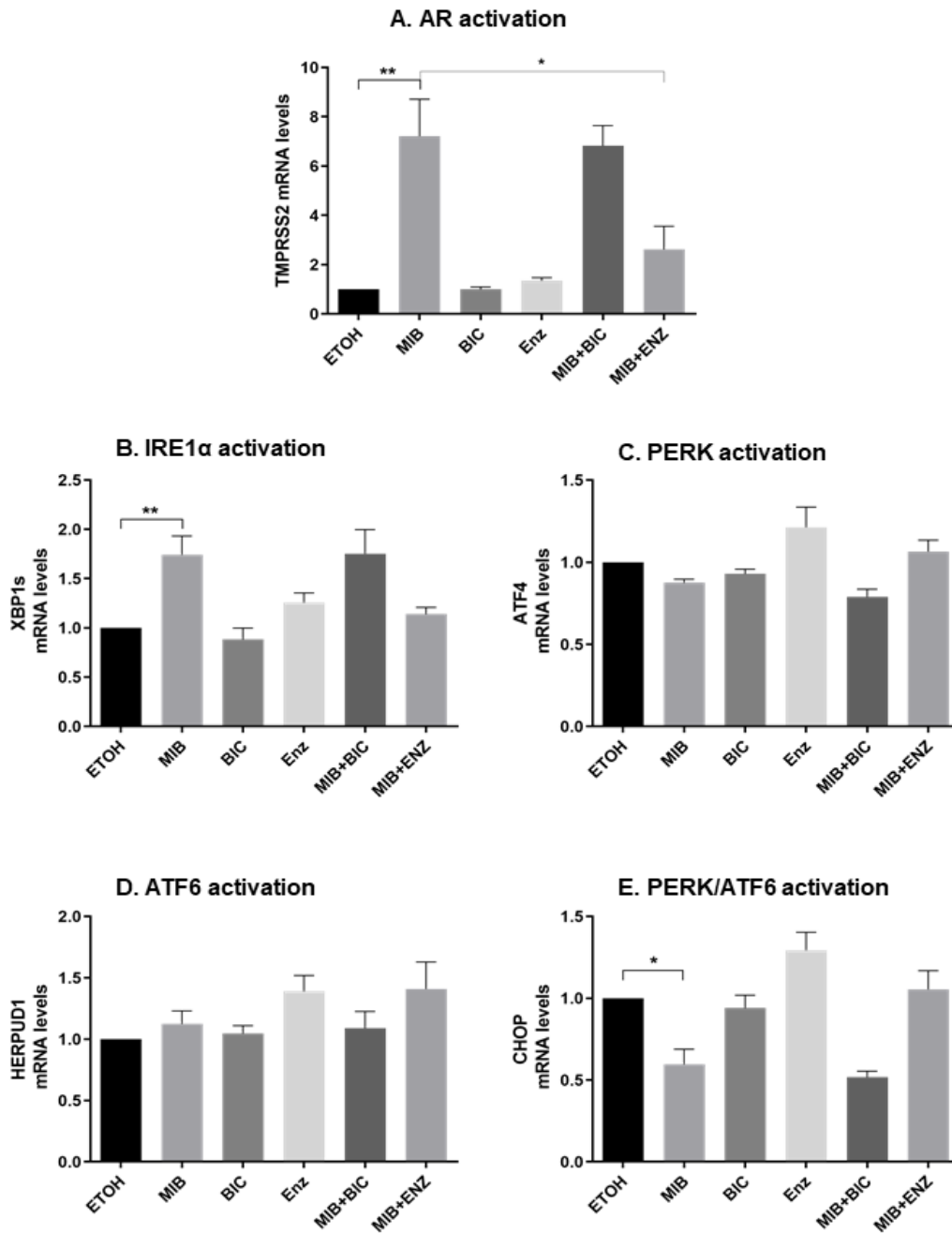


**Figure 4.1.3 UPR activation in response to androgen and antiandrogens.**

C42 cells were kept at 37°C in RPMI 1640 containing 5% SFCS for 72h, then treated with 1nM Mibolerone  $\pm$  10 nM Bicalutamide or 10  $\mu$ M Enzalutamide for 24h. Gene expression of UPR target genes was assessed by q-PCR. Graphs are representative of 3 individual repeats. Two-way ANOVA tests were performed using GraphPAD Prism 7 software. \* $p < 0.05$ , \*\* $p < 0.005$ , \*\*\* $p < 0.0005$ .

and ATF6 (Sano and Reed, 2013), was downregulated by androgen (C42). In contrast, the expression of *CHOP* was increased by Enzalutamide.

It has been observed that androgen is able to up-regulate the expression levels of the ER chaperone BiP and of the UPR sensor proteins. Moreover, the target genes of these sensor proteins were also up-regulated or down-regulated in response to androgen and anti-androgen treatment. Androgen seemed to activate the pro-survival response of the UPR through the upregulation of *XBP1s* and *HERPUD1* and downregulation of *CHOP*, whereas anti-androgens reversed that effect. These results suggest that there is a clear link between the androgen signalling and the UPR.

## **4.2 Effects of UPR inhibitors upon AR signalling**

### **4.2.1 Targeting BiP**

A previous study has shown that the activated AR promotes prostate cancer survival by promoting endoplasmic reticulum homeostasis (Bennett et al., 2010). In response to androgen treatment, the AR helps the cells to adapt to ER stress by upregulating the expression of the ER chaperone BiP. The upregulation of BiP by the AR occurs independently of the ER stress pathway and results in a delayed onset of autophagy and cell death (Bennett et al., 2010). To further characterise the role of BiP in PCa, the effects of BiP inhibition upon the proliferation of PCa cells and upon the activation of AR signalling were investigated.

Prostate cell lines (BPH-1, LNCaP, DU145 and PC3) were grown in medium supplemented with 10% FBS and treated with a dose range of the BiP inhibitor HA15 (Cerezo et al., 2016) for 72 h. The effects upon proliferation were measured using crystal violet assays (Figure 4.2.1A). It was observed that the proliferation of all of lines was reduced by the inhibitor, with the LNCaP and benign prostate cells BPH-1

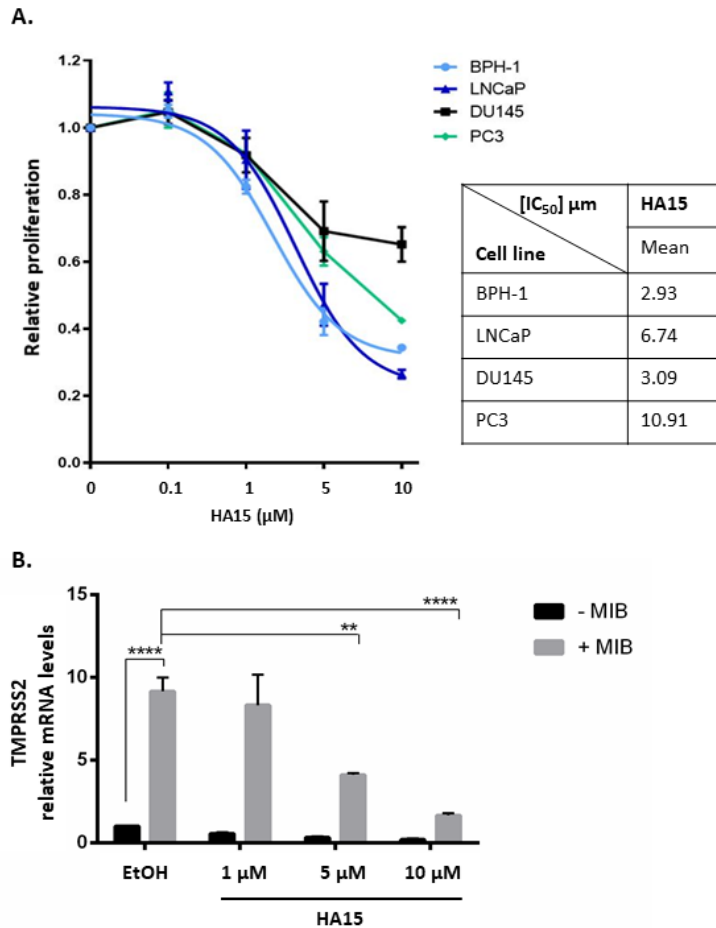


**Figure 4.2.1 The BiP inhibitor HA15 reduces PCa proliferation and the expression of the AR target gene *TMPRSS2*.**

**A.** Cells were grown in at 37°C in RPMI supplemented with 10% FBS and treated with a dose range of HA15 for 72 h. Proliferation was assessed using crystal violet assays. **B.** LNCaP cells were incubated at 37°C in RPMI 1640 containing 5% SFCS for 72h and treated with 1 nM mibolerone (MIB) ± a dose range of HA15 for 24 h. Graphs are representative of 3 individual repeats. Two-way ANOVA tests were performed using GraphPAD Prism 7 software. \* $p < 0.05$ , \*\* $p < 0.005$ , \*\*\* $p < 0.0005$

being the most sensitive and DU145 and PC3 the most resistant.

To investigate the effect of BiP inhibition upon AR activity, LNCaP cells were grown in hormone-depleted medium for 72 h and treated with a dose range of HA15 for 24 h in the presence and absence of mibolerone. The effects of BiP inhibition upon AR signalling were assessed by qPCR (Figure 4.2.1B). As expected, androgen treatment significantly increased the expression of the AR target gene *TMPRSS2*. HA15 inhibited the androgen-induced expression of *TMPRSS2* in a dose dependent manner suggesting that the activity of the AR is dependent on BiP.

#### **4.2.2 Targeting IRE1 $\alpha$ , PERK, and ATF6**

To see if inhibition of the UPR pathways has an effect upon androgen signalling, AR positive cell lines (LNCaP, C42, C42B, 22RV1) were grown in hormone depleted medium for 72 h and then with mibolerone and the UPR inhibitors for 24 h. The inhibitors blocked the activation of IRE1 $\alpha$  (4 $\mu$ 8C, Toyocamycin), PERK (GSK-2656157) and ATF6 (AEBSF) and were used in the presence or absence of androgen to investigate any changes in UPR and AR target gene expression, measured by qPCR (Figures 4.2.2.1-5).

*TMPRSS2* was upregulated in response to androgen in LNCaP, C42 and C42B cells. *TMPRSS2* inducibility in response to androgen was weaker in 22RV1; a possible effect of the constitutively active AR splice variants present in this line (Figure 4.2.2.1). Interestingly, AR activation was inhibited by toyocamycin (in all four cell lines) and by GSK-2656157 in C42B cells. Androgen treatment also increased XBP1s (downstream of IRE1 $\alpha$ ) in LNCaP and C42B, but this was not found to be significant (Figure 4.2.2.2). Treatment with the IRE1 $\alpha$  inhibitor 4 $\mu$ 8C reversed this androgen induction and toyocamycin reduced XBP1s below basal levels in all of the lines tested. Interestingly, GSK-2656157 treatment led to an increase in XBP1s in

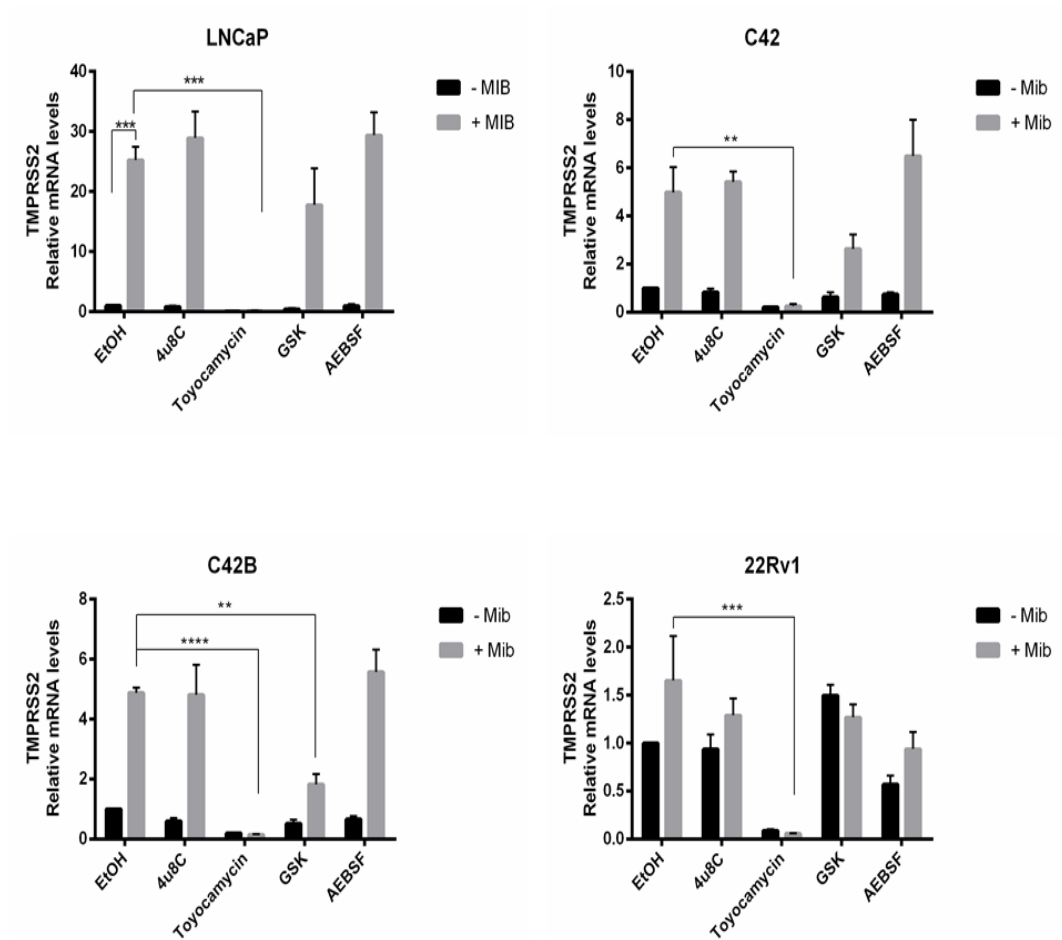


**Figure 4.2.2.1 Androgen Receptor activity in response to androgen and UPR inhibitors.**

Cells were kept at 37°C in RPMI 1640 containing 5% SFCS for 72h, treated with Miboleron 1 nM ± UPR inhibitors 10 μM for 24 hours. The activation of the UPR was assessed using q-PCR. Graphs are representative of 3 individual repeats. Two-way ANOVA tests were performed using GraphPAD Prism 7 software. \*p<0.05, \*\*p<0.005, \*\*\*p<0.0005.

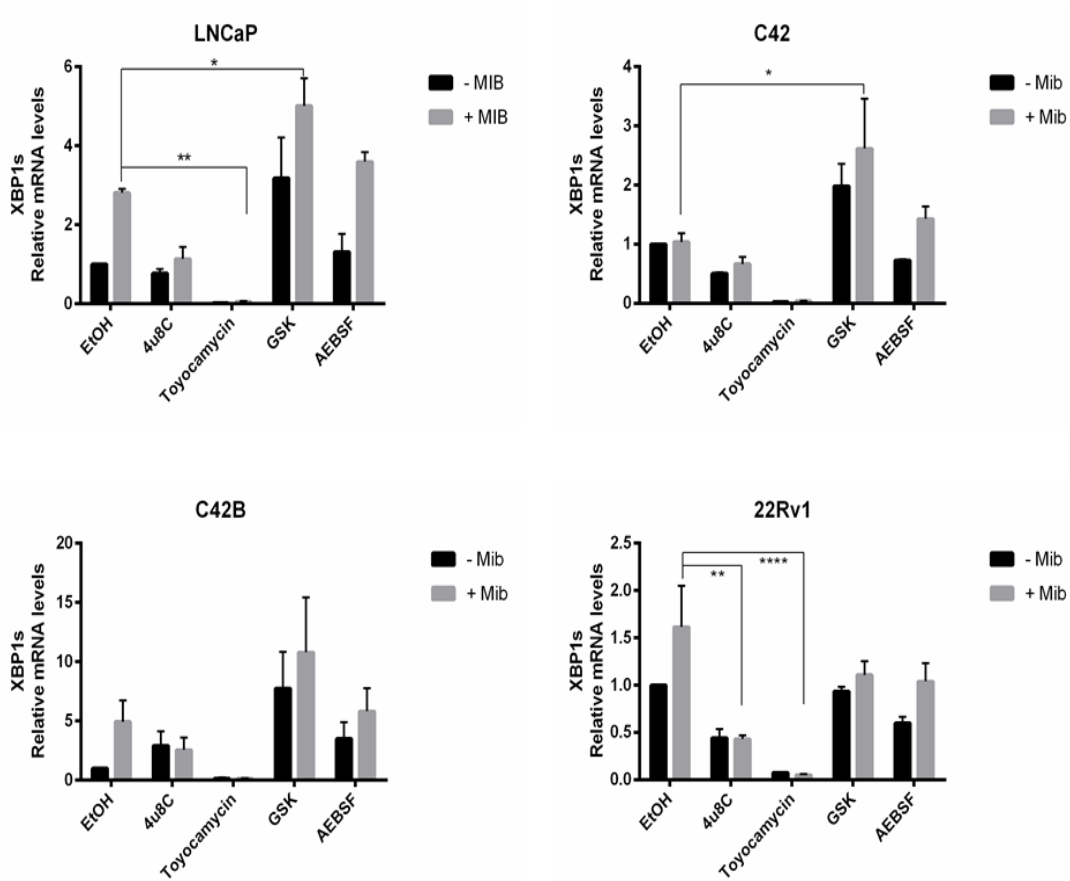


**Figure 4.2.2.2 IRE1 $\alpha$  activation in response to androgen and UPR inhibitors.**

Cells were kept at 37°C in RPMI 1640 containing 5% SFCS for 72h, treated with Miboleron 1 nM  $\pm$  UPR inhibitors 10  $\mu$ M for 24 hours. The activation of the UPR was assessed using q-PCR. Graphs are representative of 3 individual repeats. Two-way ANOVA tests were performed using GraphPAD Prism 7 software. \* $p$ <0.05, \*\* $p$ <0.005, \*\*\* $p$ <0.0005.

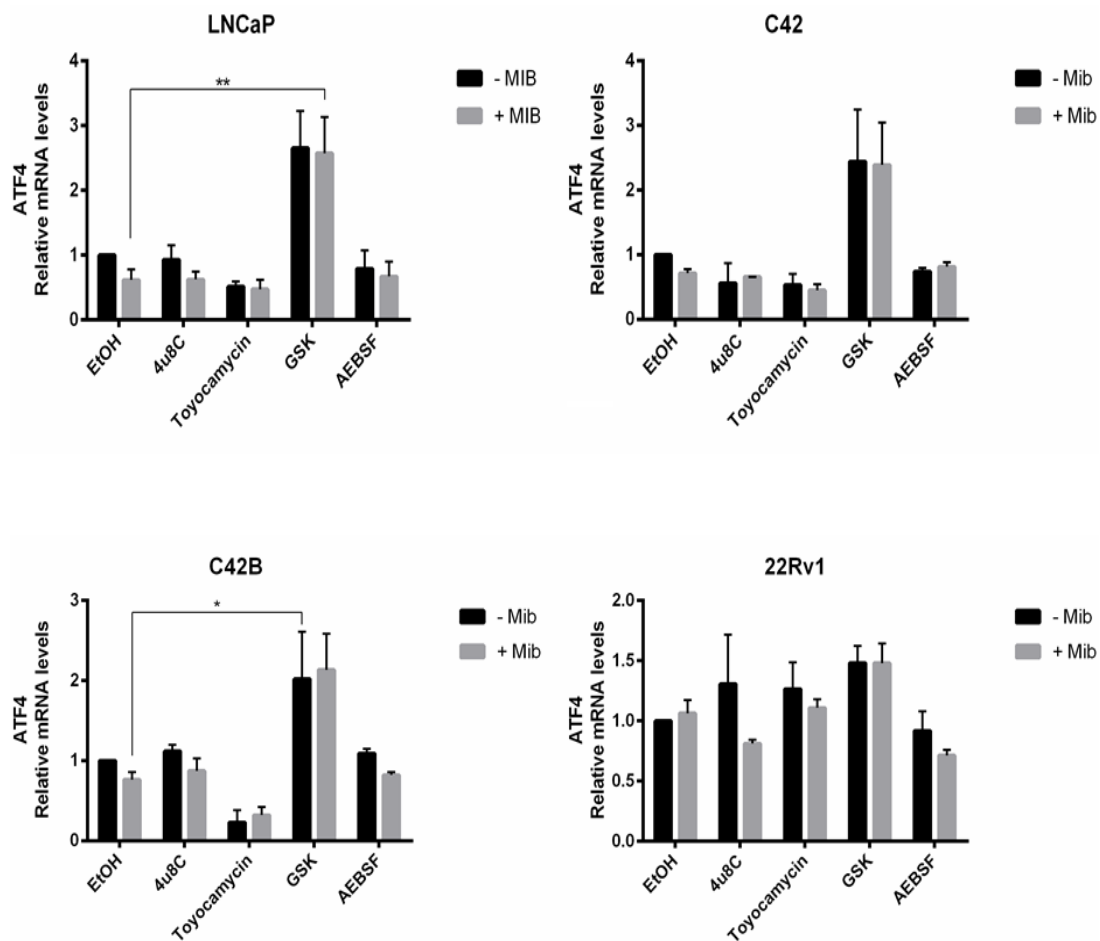


**Figure 4.2.2.3 PERK activation in response to androgen and UPR inhibitors.**

Cells were kept at 37°C in RPMI 1640 containing 5% SFCS for 72h, treated with Mibolerone 1 nM ± UPR inhibitors 10 μM for 24 hours. The activation of the UPR was assessed using q-PCR. Graphs are representative of 3 individual repeats. Two-way ANOVA tests were performed using GraphPAD Prism 7 software. \*p<0.05, \*\*p<0.005, \*\*\*p<0.0005.

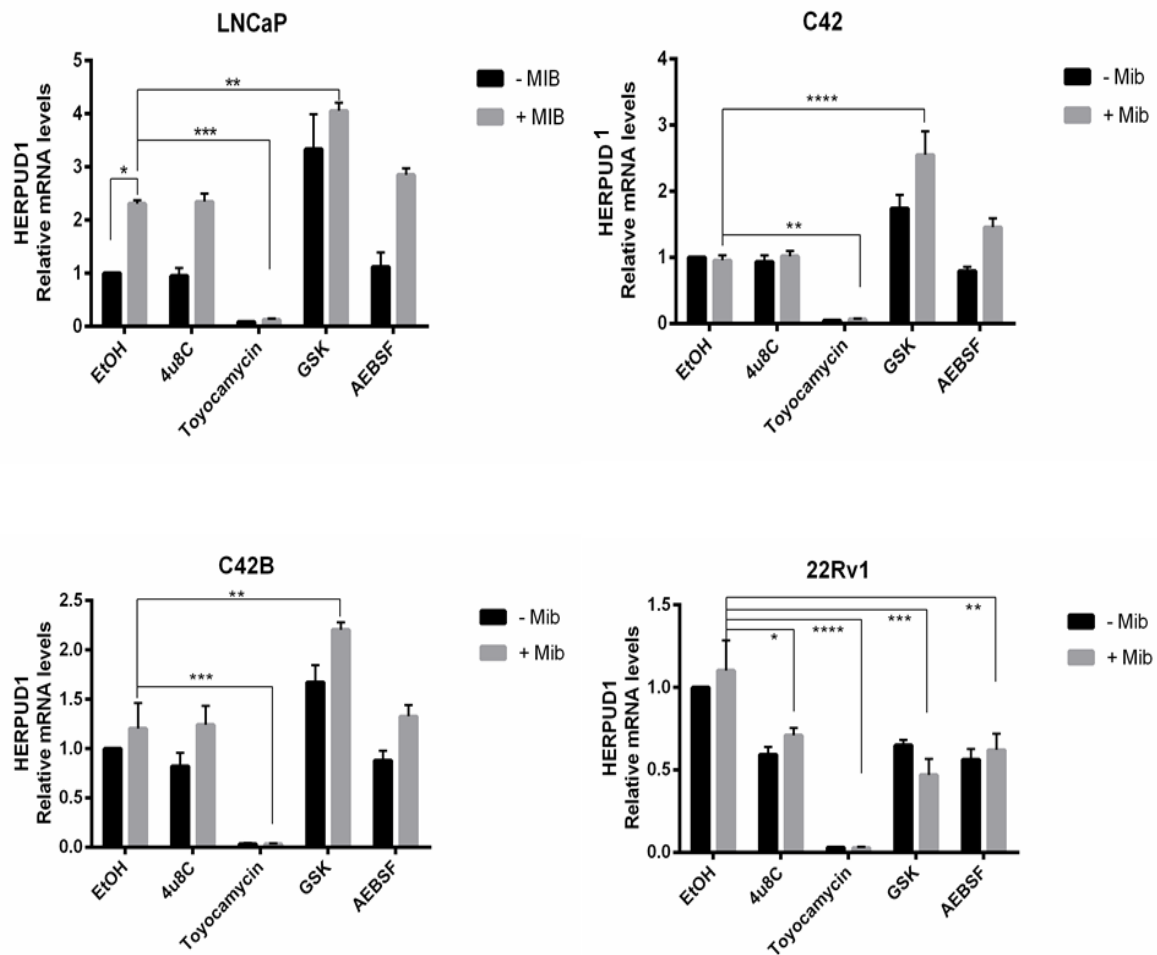


**Figure 4.2.2.4 ATF6 activation in response to androgen and UPR inhibitors.**

Cells were kept at 37°C in RPMI 1640 containing 5% SFCS for 72h, treated with Mibolerone 1 nM ± UPR inhibitors 10 μM for 24 hours. The activation of the UPR was assessed using q-PCR. Graphs are representative of 3 individual repeats. Two-way ANOVA tests were performed using GraphPAD Prism 7 software. \*p<0.05, \*\*p<0.005, \*\*\*p<0.0005.

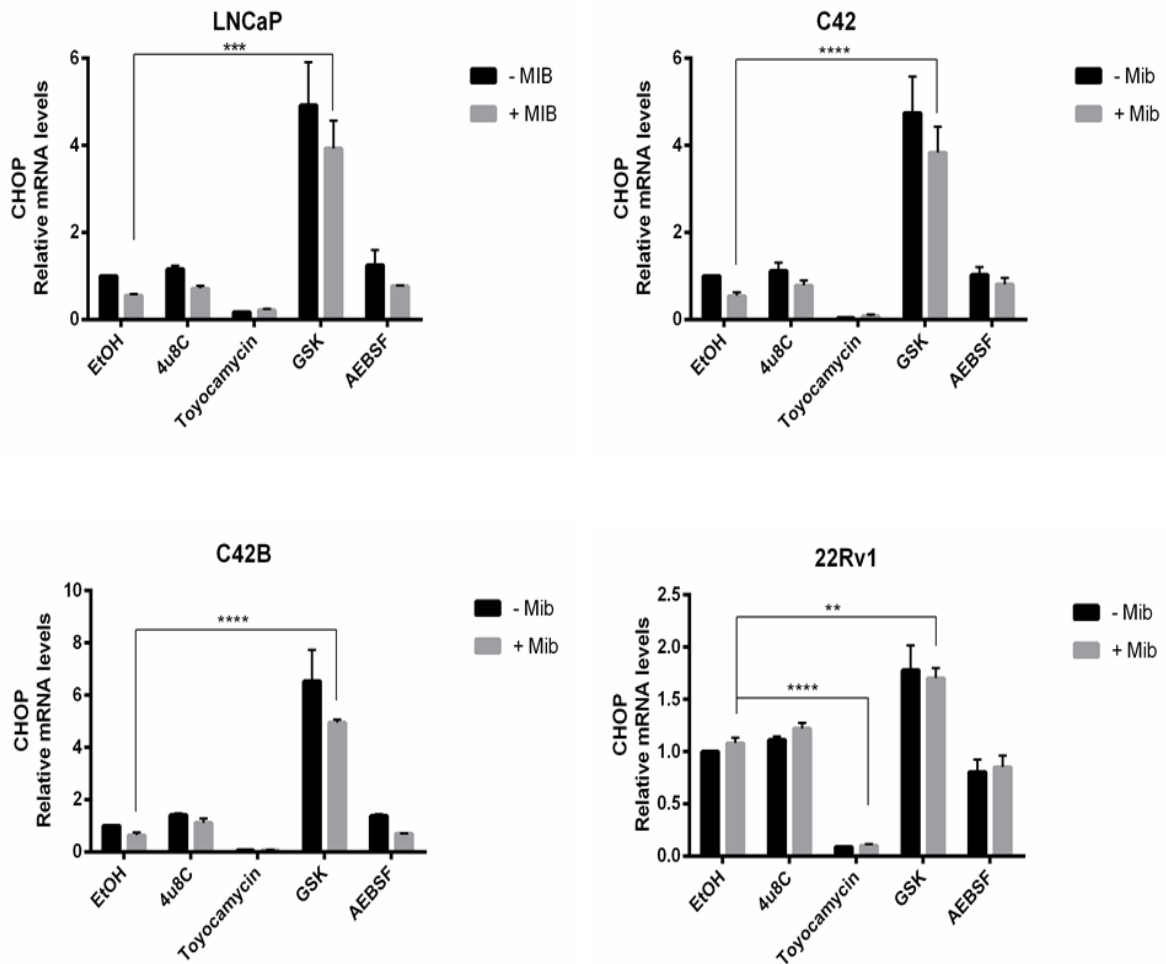


**Figure 4.2.2.5 PERK/ATF6 activation in response to androgen and UPR inhibitors.**

Cells were kept at 37°C in RPMI 1640 containing 5% SFCS for 72h, treated with Miboleron 1 nM ± UPR inhibitors 10 μM for 24 hours. The activation of the UPR was assessed using q-PCR. Graphs are representative of 3 individual repeats. Two-way ANOVA tests were performed using GraphPAD Prism 7 software. \*p<0.05, \*\*p<0.005, \*\*\*p<0.0005.

LNCaP, C42 and C42B.

To investigate if androgen regulates PERK signalling, *ATF4* expression was analysed. Unexpectedly, the PERK inhibitor GSK-2656157 did not decrease *ATF4* expression in any of the cell lines and surprisingly increased *ATF4* in LNCaP and C42B. Androgen and the other UPR inhibitors had no significant effect upon PERK activation in any of the cell lines (Figure 4.2.2.3).

To investigate if androgen regulates ATF6 signalling, the mRNA levels of *HERPUD1* was assessed. Androgen increased the expression of *HERPUD1* in LNCaP cells and inhibition of IRE1 $\alpha$  decreased the expression of *HERPUD1* in 22Rv1. Inhibition of PERK also decreased *HERPUD1* in 22Rv1 cells, but induced expression in LNCaP, C42 and C42B cells (Figure 4.2.2.4). Additionally, the mRNA levels of *CHOP* were increased by PERK inhibition in all cell lines tested (Figure 4.2.5).

In summary, AR signalling was reduced in response to the inhibition of PERK signalling in C42B. Furthermore, targeting of IRE1 $\alpha$  reduced the expression of the ATF6 target gene (22Rv1), whilst inhibition of PERK increased the expression of *HERPUD1*, *XBP1s* and *CHOP* genes. Inhibition of ATF6 had no significant effect upon AR signalling and upon the other UPR pathways.

### **4.3 Discussion**

In this chapter, the effect of androgen and anti-androgens upon UPR signalling in androgen dependent PCa was explored. For these experiments, four AR positive cells were used: LNCaP, C42, C42B, 22Rv1. The C42 and C42B lines were derived from LNCaP cells; both express the AR and PSA at the mRNA and protein levels and have been used in PCa research as a representative of PCa progression from androgen dependence to androgen independence (Cunningham and You, 2015,

Thalmann et al., 1994). 22Rv1 cells express the AR at both the mRNA and protein level and the mRNA of PSA. The cells also endogenously express two AR splice variants that are activated in a ligand-independent manner and so they represent a model of hormone refractory tumour progression (Cunningham and You, 2015). The effects of androgen and anti-androgen treatments upon the expression of UPR components were assessed by qPCR and western blotting.

It has been observed that IRE1 $\alpha$  was upregulated in response to androgen treatment at the RNA and protein level. There was also an increase in the splicing of XBP1, correlating with the findings of (Erzurumlu and Ballar, 2017, Sheng et al., 2015). Moreover, androgen treatment also increased the expression of *HERPUD1*, a component of the ERAD protein complex (Américo-Da-Silva et al., 2018), in LNCaP cells (Figure 4.1.2). XBP1s induces the expression of various genes that promote ER homeostasis, including those which encode for the ERAD components (He et al., 2010). Similar to my findings, a previous study showed that androgens upregulate the IRE1 $\alpha$  branch of the UPR in order to increase the activity of ERAD, one of the most effective ways of degrading misfolded proteins and restoring proteostasis, to promote tumour growth (Erzurumlu and Ballar, 2017). Therefore, my findings suggest that one of the mechanisms through which the AR promotes survival and adaptation of PCa cells to the adverse environmental conditions is through crosstalk with the UPR pathways. Interestingly, it was also observed that the upregulation of IRE1 $\alpha$  at the protein level was most evident in LNCaP cells and that this upregulation decreased in the models representing more advanced disease. Moreover, inhibition of IRE1 $\alpha$  with 4 $\mu$ 8c in 22Rv1 lead to an increase in ATF6 signalling, which was demonstrated by the upregulation of *HERPUD1* mRNA (Figure 4.2.2.4).

PERK had high levels of expression across LNCaP - C42B cells and lower

levels in 22Rv1. This correlates with my previous results where I found that PERK was highly expressed in androgen positive (LNCaP, C42, C42B) and non-cancerous prostate cells (BPH1) whilst the lowest expression was recorded in 22Rv1 cells (Figure 3.1). Androgen was able to significantly increase the mRNA levels of PERK only in C42 cells and its protein levels in the C42B line. On the other hand, androgen treatment had no significant effect upon the expression of its target gene ATF4. Sheng *et. al.* (2015) also showed that the mRNA levels of ATF4 were not affected by androgen treatment; they also demonstrated that androgen decreases the levels of phosphorylated eIF2 $\alpha$  in LNCaP and VCaP cells and so they proposed that androgens selectively inhibit the PERK signalling arm in these androgen responsive cells (Sheng et al., 2015). On the other hand, high levels of phosphorylated eIF2 $\alpha$  were found in a PDX model of advanced PCa which was derived from a patient with metastatic CRPC; the activation of PERK was found to promote metastatic growth (Nguyen et al., 2018).

Although these studies investigated the importance of PERK in primary and castrate resistant PCa, there is currently no data available to document the role of PERK during the progression of PCa from hormone naïve to the castrate resistant stage. In this section, I addressed this limitation and found that PERK is upregulated by androgens in C42 and C42B cells – mibolerone increased the expression levels of PERK mRNA in C42 and its protein levels in C42B cells. Furthermore, in C42B cells, inhibition of PERK signalling in the presence of androgen significantly reduced the expression levels of the AR target gene *TMPRSS2* (Figure 4.2.2.1). These results suggest that as the disease progresses to an androgen independent stage, PERK is needed to sustain the adaptive activity of the AR and that targeting this arm of the UPR could be a viable option to reduce therapy resistance. However, inhibition of

PERK in the presence of androgen increased the expression of the pro-survival genes *XBP1s* and *HERPUD1* in LNCaP, C42 and C42B cells. The mRNA levels of the pro-apoptotic *CHOP* were also elevated in response to PERK inhibition in all lines, and so it could not be determined whether PERK supports progression of PCa from androgen dependence to androgen independence. Further investigations are needed in order to fully characterise the role of PERK during this stage of the disease.

The effect of the anti-androgens bicalutamide and enzalutamide upon the expression of AR and UPR target genes was also investigated. In LNCaP cells, both anti-androgens were able to inhibit the activation of the AR. As previously mentioned, *XBP1s* expression was increased in response to androgen treatment and bicalutamide was able to reverse this effect. Treatment with enzalutamide increased the mRNA expression of the pro-apoptotic gene *CHOP*. C42 cells represent a more advanced stage of PCa and only enzalutamide was able to inhibit AR activation. Furthermore, neither bicalutamide nor enzalutamide had any significant effect upon the expression of UPR target genes.

It has been observed that androgen upregulated the mRNA (LNCaP) and protein expression of the cochaperone BiP in LNCaP and C42B cells. Similar to the findings presented here, another study showed that dihydrotestosterone (DHT) treatment increased the expression of BiP in LNCaP cells (Tan et al., 2011). Using tissue microarrays, the study also showed that the cytoplasmic and membranous expression of BiP was higher in castrate resistant PCa when compared to hormone naïve PCa. Similar to their findings, the protein expression levels of BiP in 22Rv1, which represent a more advanced stage of PCa, were higher than its expression in LNCaP and the activation of BiP by the AR was found to promote cell survival and resulted in a delayed onset of autophagy and cell death (Bennett et al., 2010).

Inhibition of BiP reduced the proliferation of benign prostate cells, LNCaP cells and of the castrate resistant models. The proliferation of LNCaP was the most affected by this treatment confirming the pro-survival activity of BiP and AR. Moreover, inhibition of BiP also reduced the activation of the AR in a dose dependent manner. This data therefore supports the mechanism proposed by (Bennett et al., 2010) through which the AR promotes the adaptation of PCa cells to their adverse environmental conditions by upregulating BiP. These findings also supplement their conclusions by showing that AR signalling is also dependent on the activity of the ER chaperone BiP.

### Conclusions

This chapter has further characterised the pro-survival role of the crosstalk between IRE1 $\alpha$  and AR in hormone naïve PCa. It also showed that depending on the stage of the disease, PERK plays different roles in PCa. Finally, it showed that AR signalling is dependent upon the proper functioning of the ER chaperone BiP, strengthening once again the link between the UPR and androgen signalling in PCa.

## **Chapter 5: Investigation of the ATF6 interactome using a modified mammalian expression system**

The endoplasmic reticulum (ER) is involved in many cellular processes, such as the regulation of calcium homeostasis, lipogenesis, gluconeogenesis, and organelle biogenesis; however, the main roles of the ER include the regulation of protein synthesis, folding and secretion (Hetz, 2012). As protein folding can only be performed under specific conditions, the ER provides an internal environment that allows the formation of disulphide bonds – such as oxidizing conditions and high calcium concentrations. The ER also contains protein chaperones and protein folding enzymes necessary in this process, in order to prevent the aggregation of the newly synthesized proteins during structural maturation (Hetz and Papa, 2018, Morreall et al., 2019). When misfolded proteins accumulate above a critical threshold, BiP, an ER chaperone, dissociates from the three sensor proteins - IRE1 $\alpha$ , PERK and ATF6 and binds to the unfolded proteins in the ER instead. This allows the sensor proteins to initiate the Unfolded Protein Response (Hetz, 2012).

Dysfunction of UPR signalling has been linked with the development and progression of many disorders including Type I and II diabetes mellitus, various neurodegenerative diseases, atherosclerosis and cancer (Ni et al., 2018, Bell et al., 2016, Tufanli et al., 2017, Lee et al., 2020). For example, increased levels of phosphorylated IRE1 $\alpha$  and overexpression of XBP1 were found to accelerate the progression of Huntington disease by supporting the aggregation of the mutated huntingtin protein and inducing neural death (Ni et al., 2018), whilst targeting IRE1 $\alpha$  in Alzheimer's Disease improved the cognitive and synaptic functions and reduced the formation of amyloid deposits and the activation of astrocytes (Duran-Aniotz et al., 2017). Additional studies demonstrated that targeting IRE1 $\alpha$  signalling was able

to prevent the development of Type I diabetes (Lee et al., 2020) and slow the progression of atherosclerosis (Tufanli et al., 2017). PERK signalling has also been associated with the development of chronic diseases and the progression of cancer, Alzheimer's disease and diabetes (Bell et al., 2016).

Recent studies have demonstrated the medical relevance of ATF6. For instance, its activation was found to be crucial to the outcome of brain and myocardial ischemia (Blackwood et al., 2019, Yu et al., 2017). Using an ATF6-KI mouse model, Yu *et al.* showed that the forced activation of ATF6 is able to reduce the infarct volume and improve the functional outcome after an ischaemic stroke. Further, pharmacological activation of ATF6 was also found to preserve the heart function after an acute myocardial infarction and ameliorate damage during reperfusion (Blackwood et al., 2019). Moreover, ATF6 was able to protect against retinal degeneration in a retinitis pigmentosa mouse model by clearing the P23H rhodopsin from the rod photoreceptors and ultimately retaining retinal homeostasis (Lee et al., 2021). Due to the role of ATF6 in protein homeostasis and cell survival in unfavourable conditions, the protein also plays various roles in cancer, particularly in tumour dormancy and resistance to treatments. For example, ATF6 was found to be constitutively active in dormant cells and overexpressed in metastatic and recurrent tumours (Urrea et al., 2016). Its overexpression correlated with poor prognosis of colon tumours and increased chemotherapy resistance in chronic myeloid leukaemia and quiescent squamous carcinoma cells (Lin et al., 2007, Higa et al., 2014, Schewe and Aguirre-Ghiso, 2008). It therefore represents a potential therapeutic target for multiple cancer types.

The crystal structure of IRE1 $\alpha$  and PERK have already been solved (Ali et al., 2011, Carrara et al., 2015a, Zhou et al., 2006), allowing the development of

therapeutic agents that target these UPR sensor proteins in several diseases. In contrast, the expression and purification of ATF6 has proved problematic. To further our understanding of ATF6 function, and to aid in the development of novel therapies, solving the structure of ATF6 remains a priority. Solving the structure of a membrane protein is a challenging process because membrane proteins have a partial hydrophobic surface, are flexible and lack stability. Therefore, many difficulties can be encountered during protein expression, solubilisation, purification, crystallisation, data collection and structure determination (Carpenter et al., 2008). Although membrane proteins can be expressed in bacteria or yeast, eukaryotic proteins, such as ATF6, require mammalian cell lines that provide the necessary machinery for post-translational modifications (Carpenter et al., 2008). However, this process results in the attachment of large, heterogeneous, and conformationally flexible glycans to the protein, which can become a significant issue during the process of protein structure determination (Chaudhary et al., 2012).

To address the technical issues associated with the production of membrane-bound proteins, I used a modified cell line to express ATF6. HEK293S GnTI(-) (Reeves et al., 2002) are human embryonic kidney cells that lack N-acetylglucosaminyltransferase I (GnTI) – an enzyme involved in the process of *N*-linked glycosylation. Without this enzyme, *N*-linked glycans cannot be synthesised and so, a homogenous Man<sub>5</sub>-GlcNac<sub>2</sub> structure is formed instead. This structure can be easily removed by endo- and exoglycosidases (Chaudhary et al., 2012, Reeves et al., 2002). It is hoped that the use of this modified expression system will provide an advantage in the process of expression, solubilisation, and structure determination of membrane proteins. In this chapter, I demonstrate that using this system ATF6 is expressed as a

functional protein that can be used in further experiments to advance our understanding of its function in normal and diseased cells.

### **5.1 Generation of stable HEK293S GnTI(-) cell lines for the tetracycline-induced ATF6 gene expression**

In order to avoid toxicity problems that are often encountered during the development of stable cell lines (Reeves et al., 2002), the 1D4-tagged ATF6 was cloned into the tetracycline-inducible vector pACMV-tetO. The construct was stably transfected into HEK293S GnTI(-) cells and multiple colonies were picked and expanded into 24-well plates. Once the cells were confluent, they were induced with tetracycline (1 µg/ml) and sodium butyrate (5 mM) for 72h. A dot blot was used to screen for the expression of the 1D4 tagged protein across the panel of stably transfected clones (Figure 5.1). It was observed that most of the clones successfully expressed the tagged protein when induced with tetracycline and sodium butyrate. Colonies p1.5 and p2.1 were selected for future experiments.

### **5.2 Optimisation of the induction conditions and confirmation of ATF6 expression**

In order to reduce the levels of stress that the cells undergo during induction, optimisation of the induction conditions is necessary. I aimed to determine whether sodium butyrate would enhance expression, as well as the lowest dose of tetracycline that is able to induce gene expression (Figure 5.2.1A). Once the optimal concentrations had been identified, a time course experiment was performed to establish the optimum length of induction (Figure 5.2.1B). The protein expression levels were assessed using western blotting. For these experiments, the blots were probed for the 1D4 epitope. In both clones, induction with tetracycline at a

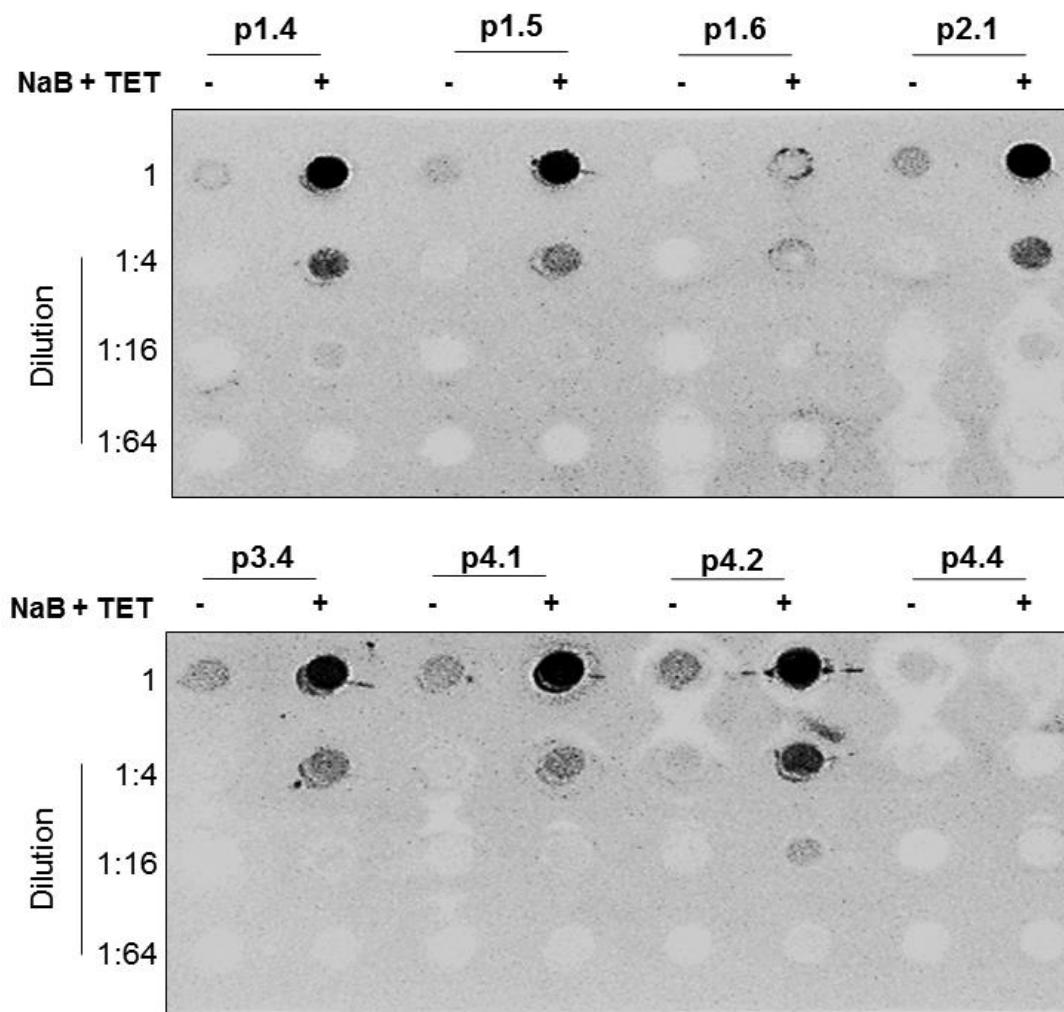


**Figure 5.1 Expression of the 1D4-tagged protein across a panel of stably transfected colonies.**

HEK293S GnTI(-) were stably transfected with pACMV-tetO 1D4-ATF6 and clones generated. Clones were induced with tetracycline (1 µg/ml) and sodium butyrate (5 mM) for 72h. Cells were harvested and crude cell lysates were loaded on the first row and serially diluted in the rows immediately below. The dot blot membrane was probed for the 1D4 epitope and protein expression visualised using ECL. NaB, sodium butyrate; TET, tetracycline.

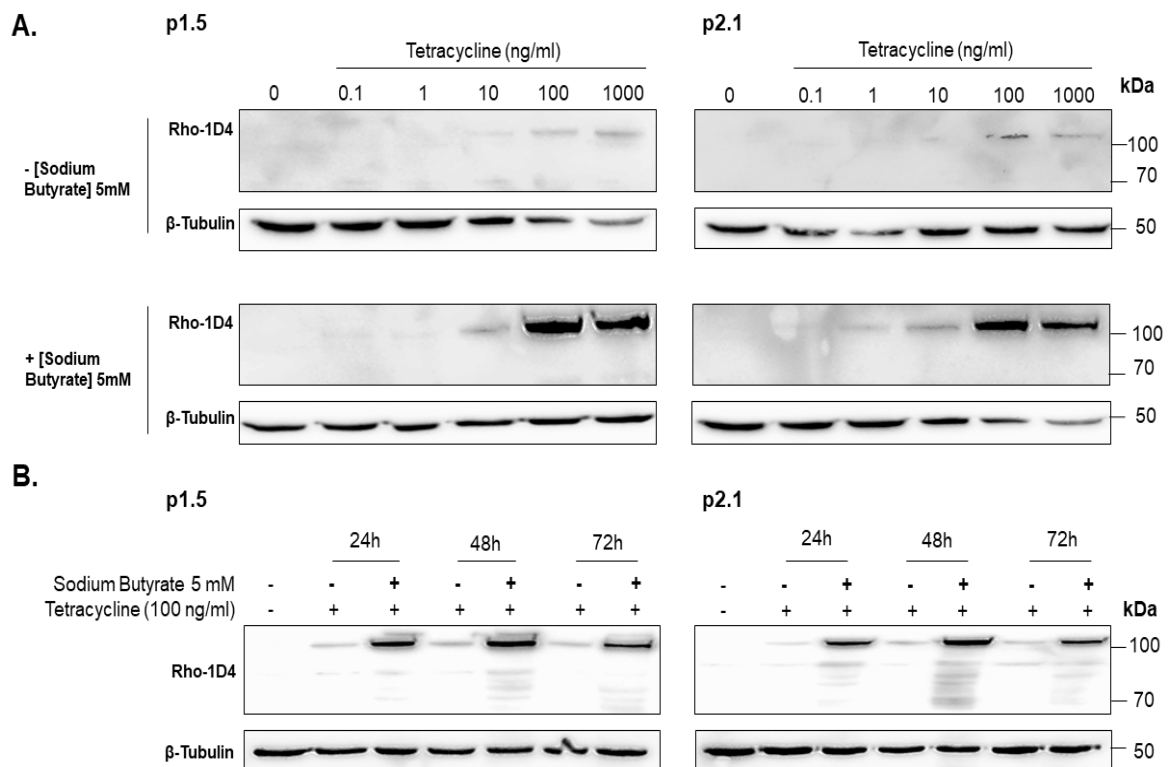


**Figure 5.2.1 Expression of the 1D4-tagged protein under different conditions.**

A. Clones (p1.5 and p2.1) were induced for 72 h using a dose range of tetracycline in the presence or absence of sodium butyrate (5 mM). B. Cells were induced with tetracycline (100 ng/ml) with or without sodium butyrate for 24, 48 and 72h. Samples were separated by SDS page and visualised using immunoblotting. 30 µg of protein were loaded into each lane and β-tubulin was used as a loading control.

concentration of 100 ng/ml and 1 µg/ml resulted in the expression of a ~110 kDa protein. Furthermore, the addition of sodium butyrate considerably increased the expression of this protein. Following this experiment, it was concluded that a tetracycline dose of 100 ng/ml together with sodium butyrate (5 mM) was optimal for ATF6 induction. Furthermore, as expression was maximal at 48 h, the length of induction was shortened from 72 h to 48 h.

The literature suggests that the full-length ATF6 is a 90 kDa protein and that the cleaved version of ATF6 is a 50 kDa protein (Haze et al., 1999a). Induction of our cells however, resulted in the expression of a 110 kDa protein. Western blot samples are usually heated before gel electrophoresis, to denature the proteins, however membrane proteins tend to aggregate during this process. In order to investigate whether heating of the samples prior to loading was affecting the size of the protein, another experiment was performed. The clones were induced for 48h, lysed with 1% DDM-PBS (w/v) instead of RIPA buffer, and not heated before loading (Figure 5.2.2). The heating step did not affect the migration of the protein on the gel, as the 110 kDa protein could still be observed in the induced samples.

### **5.3 Protein purification**

#### **5.3.1 Affinity purification**

Next, protein purification was performed in order to validate the expression of ATF6. The cells were induced for 48h and lysed with 1% DDM-PBS. Immunoprecipitation was then performed in three steps. First, the tagged proteins were separated from the lysate using Rho-1D4 beads. Then, during the washing step, any unwanted proteins were removed from the column. Finally, the tagged proteins were competitively eluted through the addition of the Rho-1DR peptide. The washes and eluates were subsequently visualised using Coomassie blue staining and immunoblotting

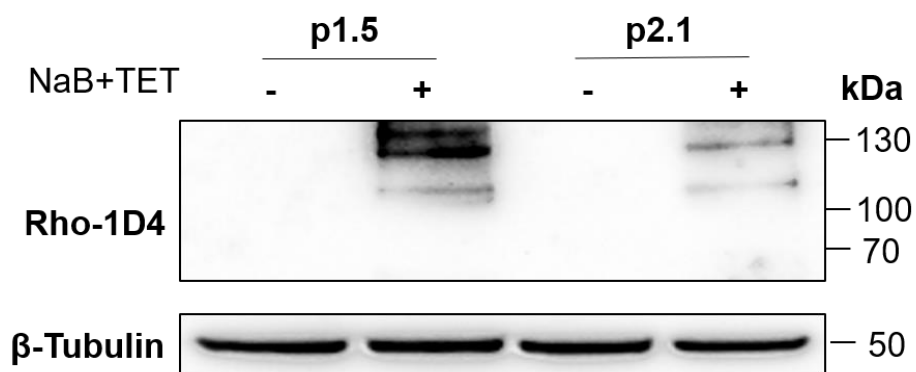


**Figure 5.2.2 The effect of not boiling the samples upon protein migration.**

The clones (p1.5 and p2.1) were induced with tetracycline (100 ng/ml) and 5 mM sodium butyrate for 48h, and then lysed with 1% DDM-PBS (w/v). Samples were separated by SDS page and visualised using immunoblotting. 30  $\mu$ g of protein were loaded into each lane and  $\beta$ -tubulin was used as a loading control. NaB, sodium butyrate; TET, tetracycline.

(Figure 5.3.1.1A). Using the Rho-1D4 antibody, three different sized bands were detected in the eluates: the 110 kDa protein as well as a 70 and 50 kDa protein. On the other hand, only a protein of 70 kDa was detected by Coomassie blue staining. To better visualise how pure the elution was, eluates 2, 3 and 4 were concentrated into one sample and then visualised using Coomassie Blue staining (Figure 5.3.1.1B). A faint band of 110 kDa as well as another two ~70 kDa bands were detected in the concentrated eluates. The 110 kDa, and the upper of the ~70 kDa bands, were excised and mass spectrometry performed. The 110 kDa protein was identified as ATF6 (Figure 5.3.1.2, 43% coverage) and the top 70 kDa band was identified as BiP (Figure 5.3.1.3, 56% coverage).

### **5.3.2 Cleavage of ATF6 in response to Endoplasmic Reticulum stress**

To investigate whether the expressed ATF6 is a functional protein, UPR stress was induced to investigate if the protein is cleaved. To do this, the cells were treated with a dose range of Tunicamycin for 24 h or induced for 24 h and then treated with Tunicamycin for a further 24 h. ATF6 cleavage was subsequently assessed using western blotting (Figure 5.3.2.1). Full-length ATF6 was detected in all of the induced samples. Fragments of 50 kDa were present at the low concentrations of Tunicamycin and in the control sample. On the other hand, a shift in size was observed under conditions of elevated ER stress, where smaller fragments of 40 kDa were identified; these fragments correspond to the published sizes of the cleaved ATF6 (Haze et al., 1999a).

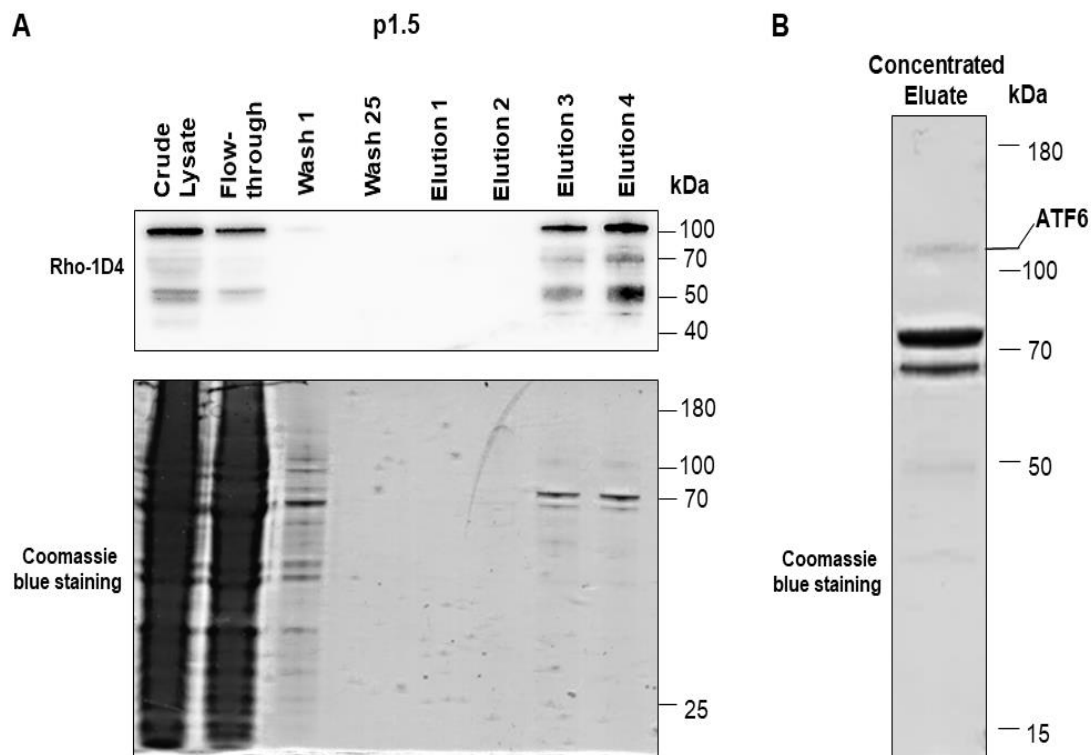


**Figure 5.3.1.1 Visualisation of the purified proteins by western blotting and Coomassie blue staining.**

Clone p1.5 was induced for 48 h and lysed with 1% DDM-PBS (w/v). Purification of the tagged protein was performed using the Rho-1D4 peptide. **A.** The samples were separated by SDS-PAGE and visualised using western blotting and Coomassie blue staining. **B.** Elutions 2, 3 and 4 were concentrated using a Amicon® Ultra – 0.5 Centrifugal Filter Devices kit. 10 µl of the concentrated sample was loaded and protein levels visualised using Coomassie blue staining.

A.

**cAMP-dependent transcription factor ATF6 alpha (P18850), 75.4 kDa**

**32 Unique Peptides, 73 PSMs, 43% coverage**

MGEFAGVAGTMESPFSPGLFHRLDEWDSDALFAELGYFTDTDELQLEAANETYENNFNLDLDFDLMLPWESDIWDINNQICT  
 VKDIKAEPQPLSPASSYSVSSPRSVDSYSSTQHVPEELDLSSSSQMSPLSLYGENSNLSLSSAEPLKEDKPVGTGPRNKTEENG  
 LTPKKKIQVNSKPSIQPKPLLLPAAPKPTQTNSSVPAKTIITQTVPTLMPLAKQPIISLQAPATKGGQTVLLSQPTVVQLQAP  
 GVLPSAQPVLA VAGGVTQLPNHVNVVVPAPSANSPVNGKLSVTKPVLQSTMRNVGSDIAVLRQQRMIKNRESACQSRKKKK  
 EYMLGLEARLKAALSENEQLKKENGT LK RQLDEVVSENQR LKVPSPKRRVVCVMIVLAFIILNYGPM SMLEQDSR RMNPSVS  
 PANQRHLLGFSAKEA QDTS DGI IQK NSYRYDHSVSN DKALMVLTEEPLLYIPPPCQPLINTTESLRNLNHELGRGWVHRHEV  
 ERTKSRRTNNQ QKTRILQGALEQGSNSQLMAVQY TET TSSISRNSGSELQVYYASPRSYQDFFEAIRR RGDTFYVVSFRRL  
 HLLL PATTHNK TTRPKMSIVLPAININENVINGQDYEVMMQIDCQVMDTRILHIKSSSVPPYLRDQQRNQTNTFFGSPPAAT  
 EATHVVSTIPESLQ

B.

A.		Protein score	# Unique	# PSMs	Coverage
Protein	UniProtKB	(SEQUEST HT)	Peptides		
ATF6	P18850	227.28	32	73	43%
B.		Sequence	# PSMs	Xcorr	(SEQUEST HT)
Peptide	ILQGALEQGSNSQLMAVQYTETTSSISR		5	6.94	
	DIKAEPQPLSPASSYSVSSPR		2	5.65	
	NSGSELQVYYASPR		3	4.5	
	LKAALSENEQLKK		4	4.39	
	RQLDEVVSENQR		2	4.29	
	RGDTFYVVSFR		5	3.71	
	QQPIISLQAPATK		3	3.67	
	AEPQPLSPASSYSVSSPR		2	3.58	
	TIIITVPTLMPLAK		3	3.49	
	SVDSYSSTQHVPEELDLSSSSQMSPLSLYGENSNLSLSSPEPLK		1	3.39	
	RDHLLL PATTHNK		1	3.33	
	TIIITVPTLMPLAK		3	3.19	
	IQVNSKPSIQPKPLLLPAAPK		2	3.13	
	DHLLL PATTHNK		1	3.07	
	QLDEVVSENQR		3	3.03	
	KEYMLGLEAR		1	2.99	
	LSVTKPVLQSTMR		1	2.96	
	HLLGFSAK		2	2.96	
	KEYMLGLEAR		1	2.94	
	AALSENEQLK		1	2.85	
	MNPSVSPANQR		2	2.84	
	RMNPSVSPANQR		1	2.77	
	SYQDFFEAIRR		1	2.68	
	EAQDTS DGI IQK		2	2.65	
	GDTFYVVSFR		1	2.58	
	NVGSDIAVLR		2	2.55	
	KKEYMLGLEAR		2	2.52	
	LSVTKPVLQSTMR		2	2.51	
	AALSENEQLKK		1	2.48	
	KKEYMLGLEAR		1	2.35	
	MNPSVSPANQR		2	2.35	
	SSSVPPYLR		3	2.28	
	SYQDFFEAIR		1	2.19	
	EYMLGLEAR		4	2.06	

**Figure 5.3.1.2 Mass Spectrometry data for ATF6.**

The cells were induced for 48 h and the protein was purified by immunoprecipitation. The eluates were separated by SDS-PAGE and the 110 kDa band was excised and sent for mass spectroscopy analysis. A. Sequence coverage. B. Details for each of the identified peptide. PSM, peptide spectrum match.

A.

**Endoplasmic Reticulum chaperone BiP\_Human (P11021), 72.3 kDa**

**40 Unique Peptides, 122 PSMs, 56% coverage**

MKLSLVAAMLLLLLSAARAEEDDKKEDVGTVVGIDLGTTYSVGVFKNGRVEIIANDQGNRITPSYVAFTPEGERLIGDAAK  
 NQLTSNPENTVFDACKLIGR~~TWNDPSVQQDIK~~FLPFKVVEK~~TKPFYIQVDIGGGQTKTFAPEEISAMVLT~~KMKETAEAYLG  
 KKVTHAVVTPAYFNDAQRQATK~~DAGTIAGLNVMRI~~INEPTAAAIAYGLDKR~~E~~GKKNILVFDLGGGTFDVSLLTIDNGVFE  
 VVATNGDTHLGGEDFDQR~~VMEHFIK~~LYKKKTGKDVKDNRAVQKLRREVEKAKRALSSQHQR~~IEIESFYEGEDFSETLTR~~  
 AKFEELNMDLFR~~STMKPVQKVL~~EDSDLK~~KSDIDEIVLVGGSTR~~IPKIQQLVK~~EFFNGKEPSR~~GINPDEAVAYGAAVQAGVL  
 SGGQDTGDLVLLDVCPLTLGIETVGGVMTKLI~~PRNTVVPTKKSQIFSTASDNQPTVTIKVYEGERPLTKDNHLLGTFDLTG~~  
~~I~~PPAPRGVPQIEVTFEIDVNGILRVTAEDKGTGNKN~~ITITNDQNR~~LTPEEIER~~MVNDAEKFAEEDKK~~LKERIDTR~~NELES~~  
 YAYS~~LKNQIGDKEKLGKK~~~~LSSEDKETMEK~~AVEEK~~IEWLESHQDADIEDFK~~AK~~KKELEEIVQPIISKLYGSAGPPPTGEEDT~~  
 AEKDEL

B.

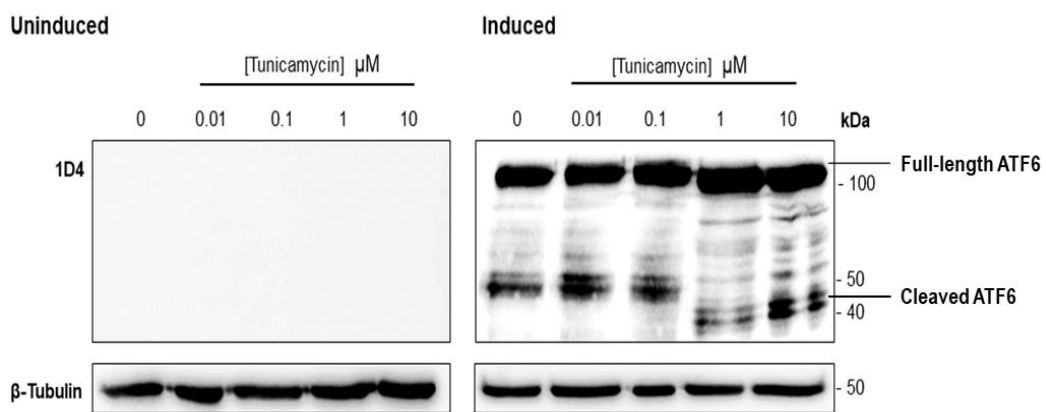
A.		Protein score	# Unique Peptides	# PSMs	Coverage
Protein	UniProtKB	(SEQUEST HT)			
BiP	P11021	320.19	40	122	56%

B.		Sequence	# PSMs	Xcorr (SEQUEST HT)
Peptide	LYGSAGPPPTGEEDTAEKDEL		3	5.02
	SQIFSTASDNQPTVTIK		2	4.4
	KVTHAVVTPAYFNDAQR		3	4.35
	KSDIDEIVLVGGSTR		7	4.16
	ITPSYVAFTPEGER		6	3.77
	KSQIFSTASDNQPTVTIK		2	3.76
	NQLTSNPENTVFDACK		10	3.76
	DNHLLGTFDLTGIPPAPR		5	3.74
	NGRVEIIANDQGNR		6	3.72
	KTKPYIQVDIGGGQTK		3	3.61
	VTHAVVTPAYFNDAQR		1	3.39
	IINEPTAAAIAYGLDKR		6	3.37
	NQLTSNPENTVFDACK		3	3.36
	VTHAVVTPAYFNDAQR		4	3.27
	KKELEEIVQPIISK		2	3.23
	MKETAEAYLGK		4	3.13
	NQLTSNPENTVFDACKR		3	3.1
	ELEEIVQPIISK		3	3.04
	MVNDAEKFAEEDKK		1	2.98
	SDIDEIVLVGGSTR		2	2.97
	MKETAEAYLGKK		2	2.94
	AKFEELNMDLFR		2	2.91
	KVTHAVVTPAYFNDAQR		1	2.81
	TWNDPSVQQDIK		6	2.81
	IEWLESHQDADIEDFK		1	2.78
	NQLTSNPENTVFDACKR		1	2.74
	LSSEDKETMEK		1	2.67
	AKFEELNMDLFR		3	2.63
	TFAPEEISAMVLT		3	2.63
	MVNDAEKFAEEDKK		1	2.53
	NGRVEIIANDQGNR		1	2.51
	VEIIANDQGNR		8	2.49
	IEIESFYEGEDFSETLTR		1	2.49
	TKPYIQVDIGGGQTK		1	2.45
	MKETAEAYLGK		1	2.45
	ITITNDQNR		1	2.42
	EFFNGKEPSR		1	2.35
	MVNDAEKFAEEDK		1	2.31
	VMEHFIK		2	2.29
	IINEPTAAAIAYGIDK		5	2.28
	EFFNGKEPSR		1	2.18
	LYGSAGPPPTGEEDTAEK		1	2.12
	ETAEAYLGK		1	2.12
	DAGTIAGLNVMR		1	2.09
	NELESYAYSLK		3	2.08
	DAGTIAGLNVMR		2	2.06
	VYEGERPLTK		1	1.98
	NTVVPTKK		1	1.92
	ITPEEIER		3	1.91
	ETAEAYLGKK		1	1.9

**Figure 5.3.1.3 Mass Spectrometry data for BiP.**

The cells were induced for 48 h and the protein was purified by immunoprecipitation. The eluates were separated by SDS-PAGE and the ~70 kDa band was excised and sent for mass spectroscopy analysis. A. Sequence coverage. B. Details for each of the identified peptide. PSM, peptide spectrum match.



**Figure 5.3.2.1 Cleavage of ATF6 in response to ER stress.**

The cells (p1.5 clone) were induced for 24h and then treated with a dose range of Tunicamycin for a further 24h. The samples were separated by SDS-PAGE and proteins visualised using immunoblotting. 30  $\mu\text{g}$  of protein were loaded into each lane and  $\beta$ -tubulin was used as a loading control. Images representative of 3 individual repeats.

## 5.4 Characterisation of the ATF6 interactome

Little is known about proteins that interact with ATF6 in the absence or presence of UPR stress. To investigate the interactome of ATF6, a pull-down assay was performed to identify the interaction partners of ATF6 under different conditions (control/no treatment; induced; induced and ER stress). The experiment was performed in triplicate, analyzed by mass spectroscopy and the proteins were visualized by western blotting and Coomassie blue staining. First, the presence of the full-length and cleaved ATF6, as well as of the ER chaperone BiP, was investigated and were confirmed to be present in the induced samples (Figure 5.4.1). To characterise the ATF6 interactome, the immunoprecipitated samples were subjected to quantitative mass spectroscopy analysis (performed by the Functional Genomics and Proteomics Laboratories, University of Birmingham). The interaction partners of ATF6 were identified by analyzing the mass spectrometric data sets using the Maxquant software. The spectral count values were used as a measure of protein abundance and G-tests were performed to assess the significance of the results. The statistically significant results are summarized in Figure 5.4.2 and Table 5.4.1.

The presence of ATF6 in the induced and stressed samples was confirmed by the mass spectroscopy analysis and although ATF6 appeared to be less abundant in the stressed samples, this difference was not found to be statistically significant ( $p > 0.6$ ). Sixty proteins have been identified as potential interaction partners of ATF6 and most of them were associated with the cytoskeleton – such as the spectrin beta chain non-erythrocytic 1 (Spectrin  $\beta$ -II), Ras GTPase-activating-like protein (p195), as well as several unconventional myosins and actin-like proteins. Other proteins include the Transitional Endoplasmic Reticulum ATPase (VCP/p97) - which was identified in the induced samples and plays multiple roles in the maintenance of ER homeostasis

(Kadowaki et al., 2015), and the DNA-dependent protein kinase catalytic subunit – which was identified both in the induced samples and in the presence of ER stress and has a role in the detection of DNA damage, especially during the G1 phase of the cell cycle (Hudson et al., 2005). Surprisingly, BiP has not been identified as an interaction partner in any of the samples.

In order to validate the results of the mass spectrometry data, two proteins were chosen to be analyzed by western blotting – the Ras GTPase-activating-like protein (p195), identified only in the presence of ER stress, and Spectrin  $\beta$ -II which was present in both treatments but was significantly more abundant in the stressed cells (Figure 5.4.2-3). As expected, Spectrin  $\beta$ -II was detected in the samples that were induced and treated with tunicamycin, but the protein not detectable by western blot in the induced and the control samples. The presence of the p195 protein was observed in all treatments, with lower levels of expression in the control and induced samples and highest level in the stressed cells. To assess whether the western blot results matched the mass spectrometric data, the spectral counts for Spectrin  $\beta$ -II and p195 from each sample were normalized to the spectral counts of ATF6 and then the average of the normalized spectral counts for each condition was calculated and plotted in a graph. The western blot results for Spectrin  $\beta$ -II matched the mass spectrometric analysis however a different trend was seen for p195. In the mass spectrometry data, p195 was found to be highest in the stressed cells and was not detected in the control or in the induced cells.

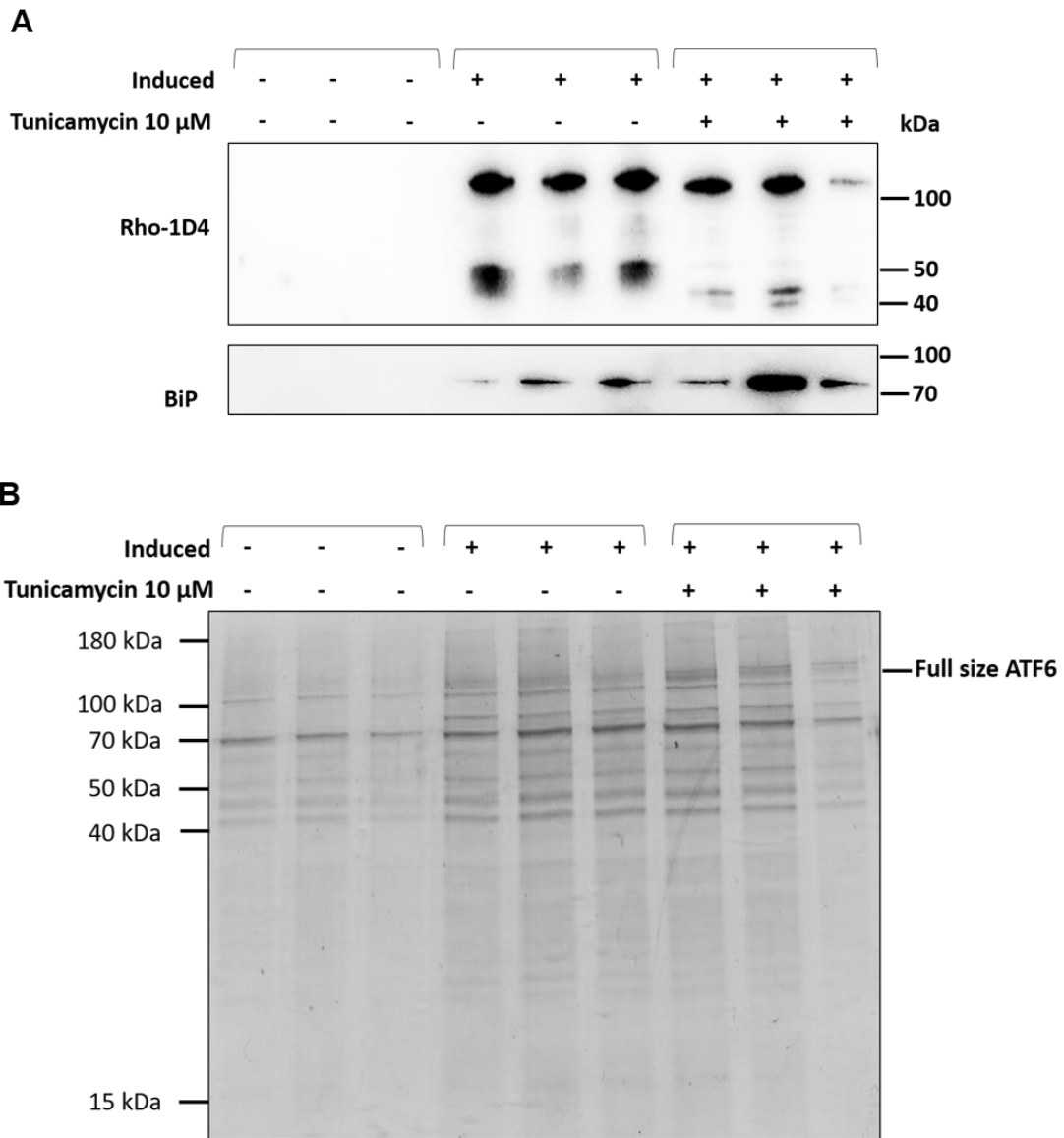


**Figure 5.4.1 ATF6 pull-down.**

The cells were treated as indicated and lysed with 1% DDM-PBS (w/v). Purification of the tagged protein was performed using the Rho-1D4 peptide. The samples were separated by SDS-PAGE and visualised using western blotting and Coomassie blue staining. A. Visualization of the purified proteins by western blotting. B. Visualization of the purified proteins by Coomassie blue staining.

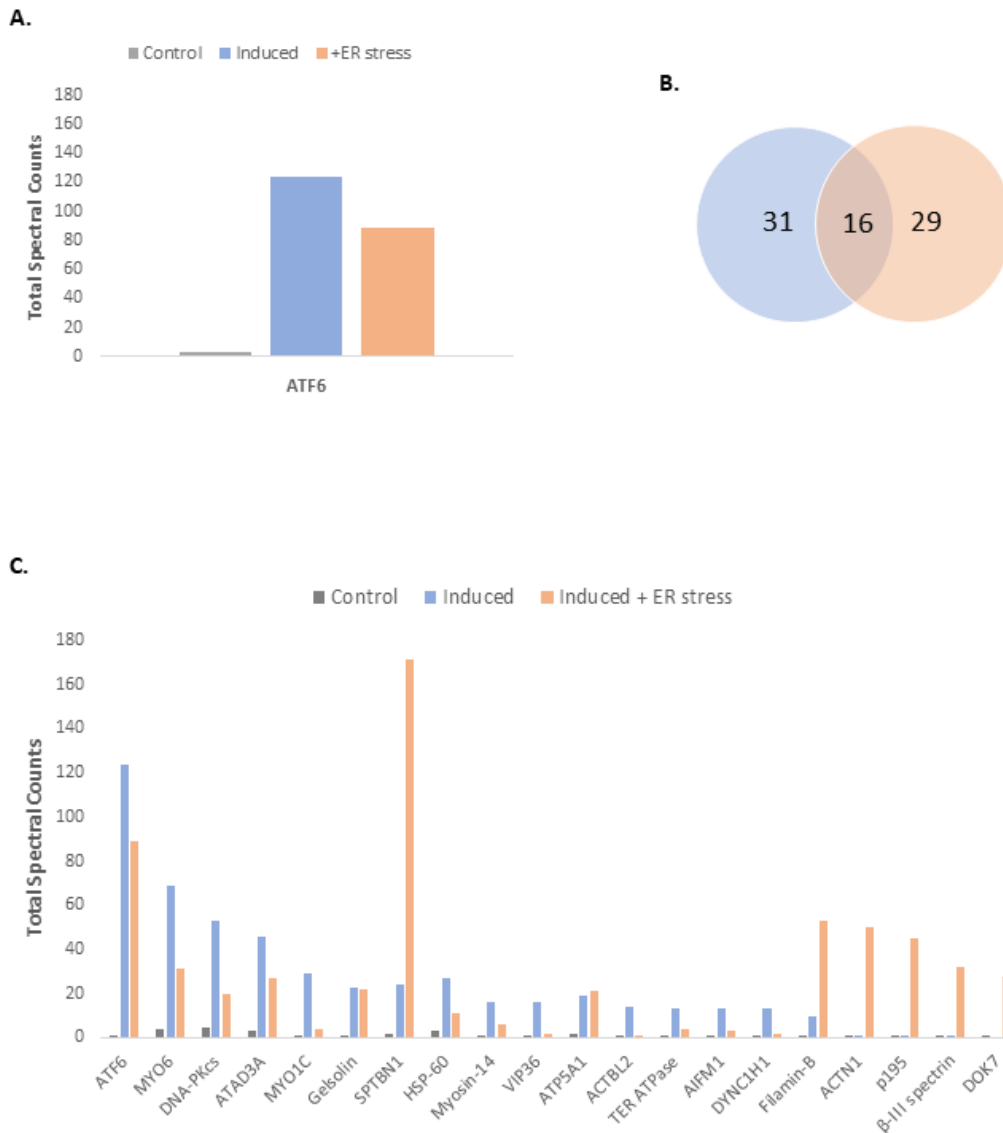


**Figure 5.4.2 Mass Spectrometry analysis of the pull-down samples.**

The data set was analysed using the Maxquant software and G-tests were performed to identify the significant results. A. Graph showing the total spectral counts of ATF6 identified in each condition. B. Venn diagram showing the number of interacting partners of ATF6 in the induced and stressed samples. C. Proteins identified in the uninduced, induced and stressed samples. Graphs show the first 20 significant proteins identified in the induced and stressed samples.

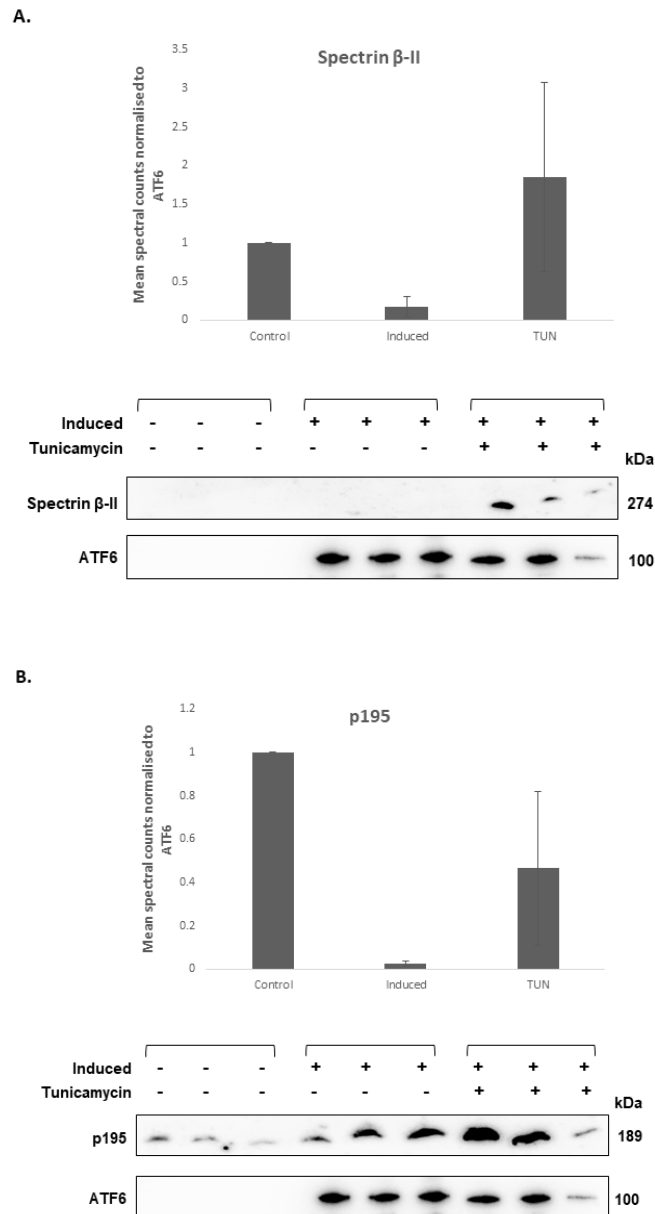


**Figure 5.4.3 Validation of mass spectrometry data via western blot.**

Graphs show the spectral counts for Spectrin  $\beta$ -II and p195 that were normalised to the spectral counts of ATF6. Values are the mean spectral counts for each condition  $\pm$  SD. Pull-down samples were separated by SDS page and the proteins were visualised using immunoblotting. A. Validation of Spectrin  $\beta$ -II. B. Validation of p195.

**Table 5.4.1 Table summarising all the interaction partners of ATF6 that were identified in the induced samples and in the presence of ER stress.**

PROTEIN NAME	PROTEIN ID (UniProtKB)	TOTAL SPECTRAL COUNTS			P-VALUE	
		Un-induced	Induced	ER stress	Induced	ER stress
Cyclic AMP-dependent transcription factor ATF-6 alpha (ATF6)	P18850	0	124	89	2.13E-33	7.8E-32
Unconventional myosin-VI (MYO6)	Q9UM54	4	69	31	5.73E-15	2.9E-08
DNA-dependent protein kinase catalytic subunit (DNA-PKcs)	P78527	5	53	20	3.32E-10	0.00022
ATPase family AAA domain-containing protein 3A (ATAD3A)	Q9NVI7	3	46	27	3.89E-10	9.8E-08
Unconventional myosin-Ic (MYO1C)	O00159	0	29	4	8.32E-08	0.09893
Gelsolin	P06396	0	23	22	3.14E-06	6.8E-08
Spectrin beta chain, non-erythrocytic 1 (SPTBN1)	Q01082	2	24	171	1.51E-05	4.38E-60
60 kDa heat shock protein, mitochondrial (HSP-60)	P10809	3	27	11	1.62E-05	0.00815
Myosin-14	Q7Z406	0	16	6	0.00021	0.02169
Vesicular integral-membrane protein (VIP36)	Q12907	0	16	2	0.00021	0.42968
ATP synthase subunit alpha, mitochondrial (ATP5A1)	P25705	2	19	21	0.00025	1.4E-06

Beta-actin-like protein 2 (ACTBL2)	Q562R1	0	14	0	0.00068	0.86518
Transitional endoplasmic reticulum ATPase (TER ATPase)	P55072	0	13	4	0.00124	0.09893
Apoptosis-inducing factor 1, mitochondrial (AIFM1)	O95831	0	13	3	0.00124	0.20792
Cytoplasmic dynein 1 heavy chain 1 (DYNC1H1)	Q14204	1	13	2	0.00124	0.42968
ATP synthase subunit beta, mitochondrial (ATP5F1B)	P06576	5	23	17	0.00162	0.00144
ATP-citrate synthase (ACL)	P53396	0	12	1	0.00223	0.86518
Voltage-dependent anion-selective channel protein 2 (VDAC2)	P45880	5	22	9	0.00255	0.12711
Nucleolar protein 56 (NOP56)	O00567	0	11	3	0.00401	0.20792
Unconventional myosin-1d (MYO1D)	O94832	0	11	1	0.00401	0.86518
Filamin-B	O75369	0	10	53	0.0072	7E-19
Unconventional myosin-XVIIIa (MYO18A)	Q92614	0	10	13	0.0072	9.1E-05
Tropomodulin-3 (TMOD3)	Q9NYL9	0	9	11	0.0129	0.00044
Heat shock 70 kDa protein 4L (HSPA4L)	O95757	0	9	1	0.0129	0.86518
ATPase family AAA domain-containing protein 3B (ATAD3B)	Q5T9A4	0	8	4	0.02301	0.09893

Tropomyosin alpha-4 chain; Tropomyosin beta chain	P67936; P07951	0	7	8	0.0409	0.00462
Dolichyl-diphosphooligosaccharide--protein glycosyltransferase subunit 1 (RPN1)	P04843	0	7	6	0.0409	0.02169
Very-long-chain (3R)-3-hydroxyacyl-CoA dehydratase 3 (HACD3)	Q9P035	0	7	2	0.0409	0.42968
Unconventional myosin-Ib (MYO1B)	O43795	0	7	0	0.0409	0.86518
DnaJ homolog subfamily B member 11 (DNAJB11)	Q9UBS4	0	7	0	0.0409	0.86518
Nucleolar protein 58 (NOP58)	Q9Y2X3	0	7	0	0.0409	0.86518
Alpha-actinin-1 (ACTN1)	P12814	0	3	50	0.38344	8.30E-18
Ras GTPase-activating-like protein IQGAP1 (p195)	P46940	0	1	45	0.91234	5.03E-16
Spectrin beta chain, non-erythrocytic 2 (Beta-III spectrin)	O15020	0	0	32	0.91234	2.06E-11
Dedicator of cytokinesis protein 7 (DOK7)	Q96N67	0	4	28	0.22199	5.29E-10
PDZ and LIM domain protein 1 (PDLIM1)	O00151	0	0	12	0.91234	0.0002
Coronin; Coronin-1C	Q9ULV4	0	1	11	0.91234	0.00044
Band 4.1-like protein 2 (EPB41L2)	O43491	0	0	8	0.91234	0.00462
Actin, alpha cardiac muscle 1 (ACTC1)	P68032	6	6	16	0.78729	0.0063
	Q02978	1	6	6	0.07235	0.02169

Mitochondrial 2-oxoglutarate/malate carrier protein  
(OGCP)

60S ribosomal protein L38 (RPL38)	P62899	1	6	6	0.07235	0.02169
Cofilin-1; Cofilin-2	P23528	2	4	7	0.52463	0.03857
Myosin light polypeptide 6 (MYL6)	P60660	5	11	11	0.22511	0.04579
60S ribosomal protein L30 (RPL30)	P62888	1	3	5	0.38344	0.04652
Glutamine--tRNA ligase (GlnRS)	P47897	1	3	5	0.38344	0.04652

## 5.5 Discussion

Here, I aimed to overcome some of the difficulties that are encountered during the process of expression and purification of membrane proteins, which has been a significant issue for groups that have tried to determine the crystal structure of ATF6. Stable HEK293S GnTI(-) cells were generated for the tetracycline-induced ATF6 gene expression. The induction of gene expression in these cells resulted in the expression of a 110 kDa protein which, upon mass spectrometry analysis, was confirmed to be ATF6. Further experiments demonstrated that the protein is cleaved in response to ER stress and aimed to further our understanding of ATF6 by determining its interaction partners.

Because there was a discrepancy between the published size of ATF6 and the size of the induced protein, there was uncertainty over whether the protein expressed was indeed ATF6. ATF6 is encoded by a gene located on chromosome 1 (locus 1q23.2) and consists of 670 amino acids. Its molecular weight has been reported as 74.6 kDa and 90 kDa (Haze et al., 1999a, Breuza et al., 2016). Several factors, such as post-translational modifications can affect the migration of a protein on a gel and this might explain the higher molecular weight that I observed for this protein. Similar to my findings, another study identified a 110 kDa protein as being the full length ER-localised ATF6 (Schindler and Schekman, 2009), indicating that we are overexpressing the correct protein. As heating of the western blot samples did not affect the migration of the protein on the gel (Figure 5.2.2), it can be concluded that the process of cell induction resulted in the expression of a 110 kDa protein and that it was not an artefact of the sample preparation. Mass spectrometry analysis confirmed successful expression of ATF6, with a coverage of 43% (Figure 5.3.1.2).

The next important step was to demonstrate that the protein is cleaved in response to tunicamycin-induced ER stress (Figure 5). ATF6 is embedded in the ER membrane and is held in an inactive state by BiP. Upon the dissociation of BiP from the luminal domain of ATF6, the Golgi localisation sequence is exposed allowing the protein to be translocated to the Golgi apparatus, where it is cleaved by Site-1 and Site-2 proteases (Taouji et al., 2013). Cleavage of ATF6 in response to ER stress results in the formation of two fragments – the cytoplasmic N-terminus domain of 50 kDa and the luminal C-terminus domain (40 kDa) (Haze et al., 1999a). The 1D4 epitope was cloned into the C-terminus of ATF6 and so, the expected size of the cleaved fragment was 40 kDa. Bands of 50 kDa were found at the lower doses of Tunicamycin as well as in the absence of the ER stress inducer. In conditions of elevated ER stress, at the highest concentrations of Tunicamycin, fragments of 40 kDa were identified, suggesting that ATF6 is correctly cleaved in response to ER stress. Similarly to tunicamycin, our modified expression system impairs the process of N-linked glycosylation (Reeves et al., 2002) and therefore the cells are already experiencing ER stress before the addition of tunicamycin. This could explain the presence of the 50 kDa fragments that were detected in the control samples and in the absence of the ER stress inducer.

To advance our understanding of ATF6, we aimed to identify novel interaction partners of the protein. One of the known interaction partners of ATF6 is XBP1, the downstream transcription factor of IRE1 $\alpha$  pathway. Yamamoto *et al.* (2007) demonstrated that ATF6 $\alpha$  heterodimerizes with XBP1 by performing sequential immunoprecipitation of ATF6 $\alpha$  and XBP1 from HeLa cells that were metabolically labelled with <sup>35</sup>S-methionine and <sup>35</sup>S-cysteine and continued to show that their heterodimerization is important for the induction of ER-associated degradation

(ERAD) components (Yamamoto et al., 2007). Another interaction partner of ATF6 is THBS4, a member of the Ca<sup>2+</sup>-binding glycoproteins called thrombospondins (Lynch et al., 2012). These proteins have various biological roles, and their expression is dramatically increased in response to stress and tissue damage or remodelling (Kazerounian et al., 2008). THBS4 resides within the ER and, through its interaction with the luminal domain of ATF6 $\alpha$ , it induces an adaptive stress response that protects the myocyte cells from ER-associated cell death (Lynch et al., 2012).

BiP also binds the luminal domain of ATF6, and through this interaction ATF6 is held in an inactive conformation. Investigations performed by Shen *et al.*, (2005) showed that BiP binds ATF6 in a stable manner and that dissociation of BiP from ATF6 is performed by actively restarting the BiP ATPase cycle. Their findings showed that the ATF6-BiP complex was not affected during the immunoprecipitation of ATF6 and moreover, that the amount of coprecipitated BiP was 5 to 10 times more than the amount of ATF6 (Shen et al., 2005). Our findings correlate to the ones of the previous study as we have also co-precipitated BiP during the purification of ATF6, and the abundance of this protein was higher than ATF6 (Figures 5.3.1.1, 5.3.1.3 and 5.4.1). However, mass spectrometric analysis of the pull-down assay could not identify BiP as a binding partner of ATF6, possibly as a result of the poor quality of the spectra. This mass spectrometry limitation can be caused by a number of reasons such as the presence of contaminants in the sample, or incomplete digestion or fragmentation (McHugh and Arthur, 2008).

Sixty novel interaction partners of ATF6 were identified by the mass spectrometric analysis of the pull-down samples (Figure 5.4.2 and Table 5.4.1), the majority of which were proteins associated with the cytoskeleton, such as Spectrin  $\beta$ -II and p195 which were validated by a western blot analysis (Figure 5.4.3). The roles

that Spectrin  $\beta$ -II plays in the cells have been reviewed by (Yang et al., 2021) - it is an important cytoskeletal protein involved in the maintenance of cell structure and has additional roles in regulating the processes of cell adhesion, cell spreading, as well as cell proliferation, cell cycle and apoptosis. Spectrin B-II is also important during the developmental stage of various organs and dysfunction of this protein has been associated with developmental disabilities and several diseases, including cancer (Yang et al., 2021). The p195 protein is involved in various cellular process including cell migration, regulation of actin,  $\beta$ -catenin-mediated transcription,  $\text{Ca}^{2+}$ /calmodulin signalling and microtubule function, with the main role of this protein being the regulation of cytoskeletal function (Li et al., 2005). p195 was also found to have a possible role in cell cycle regulation – the protein translocates into the nucleus during the G1/S phase of the cell cycle, associates with the DNA replication complex factors RPA32 and PCNA and stimulates cell cycle progression (Johnson et al., 2011). Among the other interacting partners identified by the analysis are several mitochondrial proteins and others such as DNAJB11, a co-chaperone of BiP that assists in protein folding, trafficking and degradation (Cornec-Le Gall et al., 2018).

Therefore, the stable tetracycline-inducible HEK293S GnTI(-) cell line has allowed me to express functional ATF6 that can be used in further experiments (e.g. structural studies). This expression system will provide an advantage in the process of expression, solubilisation and structure determination of ATF6 and of other membrane proteins. Furthermore, the characterisation of the interacting proteins will advance our understanding of how ATF6 regulates the cellular response to ER stress in normal and diseased cells.

## **Chapter 6: General Discussion and Concluding Remarks**

### **6.1 Characterising the UPR in Prostate Cancer**

Prostate cancer is the most common malignancy in men and the second most common form of cancer in the UK (Attard et al., 2016). It starts in the prostate, which is a secretory gland in the male reproductive system that helps in the production of semen (Moore et al., 2011). Its development and function is regulated by androgens, which act through the androgen receptor (AR) in order to maintain the functional state of the gland (Heinlein and Chang, 2004). The AR activates genes that promote cell growth and survival and so it also plays a crucial role in the development and progression of PCa (Chen et al., 2009). Tumours that have spread from the prostate, or have relapsed from prostatectomy, are mainly treated with androgen deprivation therapy (ADT) that blocks this signalling pathway in order to stop cancer growth (Rebello et al., 2021). Despite the initial success of these therapies, the disease often progresses to an incurable, castrate resistant stage (Brooke and Bevan, 2009, Huang et al., 2018) for which few therapeutic options exist (Leung et al., 2021). Metastatic, castrate-resistant prostate cancer is an important cause of cancer mortality (Amoroso et al., 2021) and modulation of the unfolded protein response, which was found to be involved in the pathology of many diseases, including cancer (Hetz et al., 2020, Oakes and Papa, 2015), may be a promising approach for the management of PCa and CRPC.

The prostate is a secretory gland and so it is reliant upon the proper functioning of the endoplasmic reticulum (Hetz, 2012), through which proteins fold and flow. Moreover, prostate cancer tumours represent a stressful environment which is characterized by a lack of oxygen and nutrients that impair the redox potential and the formation of disulphide bonds; these stressful conditions affect the process of protein

folding and lead to an accumulation of misfolded proteins in the ER (also termed ER stress) (Storm et al., 2016, Morreall et al., 2019). In response to stress, three sensor proteins – IRE1 $\alpha$ , PERK and ATF6, initiate several signal transduction pathways, collectively called the unfolded protein response (UPR) in order to restore homeostasis (Corazzari et al., 2017). The UPR pathways work together to maintain the function of the ER and the accuracy of protein folding by reducing the rate of global translation, increasing the folding capacity of the ER and by degrading the misfolded proteins via the ER-associated degradation (ERAD) and autophagy pathways. However, under conditions of chronic ER stress, the UPR switches to a pro-apoptotic response that initiates programmed cell death (Hetz et al., 2020). In PCa, the activation of the UPR has been shown to enable the cells to survive and adapt to their adverse environmental conditions (Storm et al., 2016). For example, the IRE1 $\alpha$ /XBP1 branch has been shown to support the proliferation of both hormone responsive PCa and CRPC (Sheng et al., 2015, Sheng et al., 2019), whilst PERK is highly active in advanced PCa where it promotes tumour progression (Nguyen et al., 2018). However, despite the medical relevance of this pathway, our understanding of the UPR in PCa is still limited.

Therefore, this study aimed to characterize the activity of UPR during all the stages of the disease - starting from benign prostate cells and up to castrate-resistant models of PCa.

### **6.1.1 Benign prostate cells (BPH-1)**

It has been shown that non-cancerous prostate cells (BPH-1) were the most resistant to ER stress and they relied upon the activity of all three UPR arms in order to survive. The cells retained their ability to resolve stress mainly through the IRE1 $\alpha$ /XBP1s axis and through the upregulation of ERAD pathways by ATF6 and

XBP1s. However, in conditions of prolonged ER stress, BPH-1 cells that have been irreparably damaged were found to undergo apoptosis. These results suggest that there was no dysregulation of the UPR signalling in the benign prostate cells.

### **6.1.2 Hormone responsive Prostate Cancer (LNCaP)**

In hormone responsive PCa, the AR has been shown to directly activate the IRE1 $\alpha$ /XBP1s pathway - which restored homeostasis and promoted cell survival (Sheng et al., 2015, Sheng et al., 2019) by increasing the activity of ERAD (Erzurumlu and Ballar, 2017). My results correlated with these studies and provided additional data to support the adaptive role of the crosstalk between IRE1 $\alpha$  and AR in hormone naïve PCa. I have also showed that, even in the absence of androgens, IRE1 $\alpha$ /XBP1s signalling is highly active in response to ER stress and its activation sustains LNCaP cell survival and proliferation.

This study has also furthered our understanding of the role of PERK in hormone responsive PCa. Sheng *et. al.* proposed that androgens selectively inhibit the PERK signalling arm during this stage of the diseases (Sheng et al., 2015). Here, I demonstrated that although androgen treatment does not affect the mRNA or protein levels of PERK, the activation of this protein in response to ER stress causes LNCaP cells to enter into G1 arrest, allowing the cells to initiate repair mechanisms (Murad et al., 2016), resolve the stress and delay apoptosis. These effects were confirmed by proliferation and flow cytometric assays. ATF6 has also been shown to be expressed at high levels during the hormone responsive stage of the disease, and it was activated in response to both ER stress and androgen treatment. Taken together, the results show that hormone responsive PCa utilizes all three UPR arms in order to promote ER homeostasis and cell survival.

In addition to the regulation of the three sensor proteins, it has been demonstrated that androgens, through the AR, are also able to upregulate the expression of BiP (Bennett et al., 2010, Tan et al., 2011). The upregulation of BiP by the AR was performed independently of the ER stress pathway and was shown to delay the onset of autophagy and cell death (Bennett et al., 2010). These findings led the authors to propose a novel mechanism through which the AR supports PCa survival, that is by promoting ER homeostasis (Bennett et al., 2010). My data supports the aforementioned mechanism and continues to show that AR signalling is also dependent on the activity of BiP. These results suggest that there might be a functional synergy between the two proteins, and this requires further investigation.

### **6.1.3 Progression of Prostate Cancer from androgen dependence to androgen independence (C42, C42B, 22Rv1)**

The present study showed that during the progression of PCa from hormone responsive to a castrate resistant stage, androgen treatment increased the mRNA and protein levels of PERK in C42 and C42B cells. Moreover, inhibition of PERK significantly reduced the mRNA levels of the AR target gene *TMPRSS2*, suggesting a crosstalk between PERK and AR during this stage of the disease. As previously mentioned, androgens upregulate the expression of BiP, but as the disease progresses to a castrate resistant stage, it has been observed that androgen treatment no longer affects the expression of BiP. Furthermore, the endogenous expression of BiP was also higher in 22Rv1 cells compared to LNCaP cells. A previous study has shown that the expression of BiP is higher in CRPC compared to hormone responsive PCa (Tan et al., 2011). Our findings correlate with this study and supplements our knowledge by showing that the upregulation of BiP remains constant during the

progression of PCa from androgen dependence to independence, and that it occurs independently of the androgen signalling pathway.

#### **6.1.4 Castrate resistant Prostate Cancer (DU145, PC3)**

The castrate resistant cell culture models of PCa were found to be the most sensitive to ER stress – their proliferation was greatly reduced in the presence of ER stress and the cells underwent high levels of apoptosis. It has also been observed that the activation of the UPR in response to stress was delayed in these metastatic models of PCa and that both DU145 and PC3 cells were dependent on the ERAD pathway in order to resolve the stress and survive. Although it has been shown that one mechanism through which androgens promote survival of androgen sensitive LNCaP cells is through the upregulation of ERAD activity (Erzurumlu and Ballar, 2017), little is known about the ERAD pathway in castrate resistant PCa. This study has found that this pathway is also active during the advanced stages of the disease, and further studies should determine the role of ERAD and UPR signalling in therapy resistant prostate cancer.

#### **6.2 Investigation of the ATF6 interactome using a modified mammalian expression system**

ATF6 is one of the three sensor proteins that initiates the UPR in response to accumulation of unfolded proteins in the endoplasmic reticulum (Hetz, 2012). In response to ER stress, ATF6 translocates to the Golgi apparatus where it is cleaved by S1P and S2P proteases. The cytoplasmic domain of ATF6 is then released from the Golgi apparatus and translocates to the nucleus where it acts as a transcription factor (Haze et al., 1999b). ATF6 restores homeostasis by activating the expression of genes that encode for ERAD components, increasing the folding capacity of the ER

(upregulation of ER chaperones) and inducing autophagy (Bommiasamy and Popko, 2011, Yu et al., 2017).

ATF6 plays a major role in regulating protein homeostasis and so it has been associated with various diseases, including retinitis pigmentosa (Lee et al., 2021), and brain and cardiac ischemia (Blackwood et al., 2019, Yu et al., 2017) where its activation protects the affected tissues. However, activation of ATF6 in multiple cancer types was found to promote tumour dormancy and resistance to treatments (Urrea et al., 2016). Moreover, ATF6 has been recently associated with the progression of PCa and its activation was correlated with AR signalling and disease stage (Pachikov et al., 2021).

In order to allow the development of novel therapeutic agents that target ATF6 in cancer, solving the structure of ATF6 remains a priority. Several groups have tried to determine the crystal structure of ATF6, however the expression and purification of ATF6 has proved problematic (personal communication).

As ATF6 is a membrane protein (Hetz, 2012), it needs to be expressed in a mammalian system that allows post-translational processes including N-linked glycosylation to take place, which facilitates its folding into a functional state (Andréll and Tate, 2013). However, in most mammalian expression systems this process results in the attachment of large, heterogenous and conformationally flexible N-glycans to the protein which can become a hurdle during the process of crystallization (Chaudhary et al., 2012). In this study, I addressed this limitation by using a modified human embryonic kidney cell line (HEK293S GnTI-) that does not allow the synthesis of complex N-glycans but supports the formation of a homogenous Man<sub>5</sub>-GlcNac<sub>2</sub> structure instead (Reeves et al., 2002). This homogenous structure is more structurally

silent and can be easily removed by endo- and exoglycosidases (Chaudhary et al., 2012, Reeves et al., 2002).

A stable tetracycline-inducible HEK293S GnTI- cell line that allows the expression of a functional ATF6 protein was generated and this was used in additional experiments in order to characterize the ATF6 interactome under different conditions (induced, induced and ER stress). Mass spectrometric analysis of the pull-down samples identified 60 novel interaction partners of ATF6 – 31 of which were identified in the induced samples, and 29 in the presence of ER stress. Most of the interaction partners of ATF6 were found to be associated with the cytoskeleton – such as the Spectrin  $\beta$ -II and the Ras GTPas-activating-like protein (p195). Spectrin  $\beta$ -II is an important cytoskeletal protein, and its dysfunction was associated with the pathogenesis of several diseases, including cancer (Yang et al., 2021), whilst p195 is involved in the regulation of cell cycle during the G1/S phase (Johnson et al., 2011). Other interaction partners include the Transitional Endoplasmic Reticulum ATPase (VCP) which maintains the ER homeostasis (Kadowaki et al., 2015), the DNA-dependent protein kinase catalytic subunit which detects DNA damage during G1 phase arrest (Hudson et al., 2005), DNAJB11 – a co-chaperone of BiP that is involved in protein folding and degradation (Cornec-Le Gall et al., 2018) as well as several mitochondrial proteins. Therefore, this study has identified novel interaction partners of ATF6, and their characterization will further our understanding of how ATF6 coordinates cellular responses in response to ER stress.

### **6.3 Concluding remarks**

In conclusion, this study has determined that UPR signalling is different depending on the stage of the disease. For example, it has been observed that the benign prostate cells (BPH-1) retained their ability to deal with ER stress and as a

result, their proliferation was not greatly reduced. However, the cells that could not resolve the stress were found to undergo apoptosis. Starting from the androgen responsive cells (LNCaP) that represented the incipient, hormone responsive stage of prostate cancer, a dysregulation of UPR signalling could be observed – as the cells attempted to evade ER stress-induced cell death by entering into a G1-phase arrest. The findings of this study have strengthened the link between the UPR and the survival of PCa during this stage of the disease and showed that the cells utilize all three UPR arms in order to resolve the stress; the results also suggested that there could be a functional synergy between the activity of BiP and the pro-survival signalling of the AR.

Interestingly, PERK might play an important role during the progression of PCa, as its mRNA and protein levels have been increased following androgen treatment, and its inhibition decreased the expression of the AR target gene *TMPRSS2*. However, future experiments should aim to investigate the activation of PERK during this stage of the disease by determining the expression levels of phosphorylated eIF2 $\alpha$  – a downstream effector of PERK (Liu et al., 2015). Furthermore, a delayed and deficient UPR signalling has been observed in castrate-resistant models of prostate cancer (DU145, PC3) and the cells were dependent on the ERAD pathway in order to resolve the stress. Taken together, these findings have helped us obtain a broader view of the UPR signalling in prostate cancer and furthered our understanding of how this cancer utilizes the UPR in order to survive.

A limitation of this study was the fact that it utilized RT-qPCR to assess differences in the expression of a limited number of UPR target genes in response to various treatments. A better approach would be the use of transcriptomic technologies that would allow the identification of gene expression changes across the whole

transcriptome (Lowe et al., 2017) – that would provide an in-depth look at UPR signalling across the different stages of the disease.

Finally, a stable tetracycline-inducible HEK293S GnTI(-) cell line has been generated and used for the expression of the UPR sensor protein ATF6 and the characterization of its interactome. Novel interaction partners have been identified and the characterization of these proteins will further our understanding of how ATF6 regulates cellular responses in response to ER stress. Further the line, the use of this modified expression system could also facilitate future studies to investigate the structure of this protein.

#### **6.4 Future work**

Further investigations should aim to identify a suitable target that can be modulated in order to block PCa tumour growth. For example, the role of PERK during the progression of PCa from hormone dependent to castrate resistant stage should be further characterized. It would also be useful to determine the importance of ERAD and UPR signalling during the castrate resistant stages of PCa and look into the role of ATF6 signalling in the progression of the disease; this could be done by performing an RNA-sequencing analysis. It would also be helpful to investigate the expression levels of phosphorylated PERK and those of the other UPR components in clinical samples by performing immunohistochemistry or tissue microarray on patient tumours. This may identify therapeutic vulnerabilities that can be exploited to prevent tumour progression.

Further investigations should also aim to verify the localisation of ATF6 in the recombinant HEK293S GnTI- cells and to determine whether the protein translocates to the Golgi apparatus and the nucleus whilst the cells are under ER stress. A pathway enrichment analysis and gene ontology enrichment analysis should also be performed

to validate the list of proteins that were identified as interaction partners of ATF6 and to gain insight into the roles of these interactions. As a next step, it would also be useful to verify whether ATF6 co-localises with its interaction partners and if they do, to identify the location of their co-localisation. Further studies should utilise the modified expression system used in this study and focus on determining the structure of ATF6 by x-ray crystallography or cryogenic-electron microscopy. With that data, drug discovery projects can be initiated to identify small molecule inhibitors with specificity for ATF6.

## Bibliography

- ACOSTA-ALVEAR, D., ZHOU, Y., BLAIS, A., TSIKITIS, M., LENTS, N. H., ARIAS, C., LENNON, C. J., KLUGER, Y. & DYNLACHT, B. D. 2007. XBP1 controls diverse cell type- and condition-specific transcriptional regulatory networks. *Mol Cell*, 27, 53-66.
- ADAMS, C. J., KOPP, M. C., LARBURU, N., NOWAK, P. R. & ALI, M. M. U. 2019. Structure and Molecular Mechanism of ER Stress Signaling by the Unfolded Protein Response Signal Activator IRE1. *Frontiers in Molecular Biosciences*, 6, 11.
- ALI, M. M., BAGRATUNI, T., DAVENPORT, E. L., NOWAK, P. R., SILVA-SANTISTEBAN, M. C., HARDCASTLE, A., MCANDREWS, C., ROWLANDS, M. G., MORGAN, G. J., AHERNE, W., COLLINS, I., DAVIES, F. E. & PEARL, L. H. 2011. Structure of the Ire1 autophosphorylation complex and implications for the unfolded protein response. *Embo j*, 30, 894-905.
- AMIN-WETZEL, N., NEIDHARDT, L., YAN, Y., MAYER, M. P. & RON, D. 2019. Unstructured regions in IRE1 $\alpha$  specify BiP-mediated destabilisation of the luminal domain dimer and repression of the UPR. *Elife*, 8.
- AMIN-WETZEL, N., SAUNDERS, R. A., KAMPHUIS, M. J., RATO, C., PREISLER, S., HARDING, H. P. & RON, D. 2017. A J-Protein Co-chaperone Recruits BiP to Monomerize IRE1 and Repress the Unfolded Protein Response. *Cell*, 171, 1625-1637.e13.
- AMOROSO, F., GLASS, K., SINGH, R., LIBERAL, F., STEELE, R. E., MAGUIRE, S., TARAPORE, R., ALLEN, J. E., VAN SCHAEYBROECK, S., BUTTERWORTH, K. T., PRISE, K., O'SULLIVAN, J. M., JAIN, S., WAUGH, D. J. & MILLS, I. G. 2021. Modulating the unfolded protein response with ONC201 to impact on radiation response in prostate cancer cells. *Sci Rep*, 11, 4252.
- AMÉRICO-DA-SILVA, L., DIAZ, J., BUSTAMANTE, M., MANCILLA, G., OYARZÚN, I., VERDEJO, H. E. & QUIROGA, C. 2018. A new role for HERPUD1 and ERAD activation in osteoblast differentiation and mineralization. *Faseb j*, 32, 4681-4695.
- ANDRÉLL, J. & TATE, C. G. 2013. Overexpression of membrane proteins in mammalian cells for structural studies. *Mol Membr Biol*, 30, 52-63.
- ARAP, M. A., LAHDENRANTA, J., MINTZ, P. J., HAJITOU, A., SARKIS, A. S., ARAP, W. & PASQUALINI, R. 2004. Cell surface expression of the stress response chaperone GRP78 enables tumor targeting by circulating ligands. *Cancer Cell*, 6, 275-84.
- ASADA, R., KANEMOTO, S., KONDO, S., SAITO, A. & IMAIZUMI, K. 2011. The signalling from endoplasmic reticulum-resident bZIP transcription factors involved in diverse cellular physiology. *J Biochem*, 149, 507-18.
- ATTARD, G., PARKER, C., EELES, R. A., SCHRÖDER, F., TOMLINS, S. A., TANNOCK, I., DRAKE, C. G. & DE BONO, J. S. 2016. Prostate cancer. *The Lancet*, 387, 70-82.
- AUMULLER, G. & SEITZ, J. 1990. Protein secretion and secretory processes in male accessory sex glands. *Int Rev Cytol*, 121, 127-231.
- BAGHBAN, R., ROSHANGAR, L., JAHANBAN-ESFAHLAN, R., SEIDI, K., EBRAHIMI-KALAN, A., JAYMAND, M., KOLAHIAN, S., JAVAHERI, T. & ZARE, P. 2020. Tumor microenvironment complexity and therapeutic implications at a glance. *Cell Communication and Signaling*, 18, 59.
- BAI, S., CAO, S., JIN, L., KOBELSKI, M., SCHOUEST, B., WANG, X., UNGERLEIDER, N., BADDOO, M., ZHANG, W., COREY, E., VESSELLA, R. L., DONG, X., ZHANG, K., YU, X., FLEMINGTON, E. K. & DONG, Y. 2019. A positive role of c-Myc in regulating androgen receptor and its splice variants in prostate cancer. *Oncogene*, 38, 4977-4989.

- BARLOWE, C. 2002. COPII-dependent transport from the endoplasmic reticulum. *Curr Opin Cell Biol*, 14, 417-22.
- BELL, M. C., MEIER, S. E., INGRAM, A. L. & ABISAMBRA, J. F. 2016. PERK-opathies: An Endoplasmic Reticulum Stress Mechanism Underlying Neurodegeneration. *Current Alzheimer research*, 13, 150-163.
- BENNETT, H. L., FLEMING, J. T., O'PREY, J., RYAN, K. M. & LEUNG, H. Y. 2010. Androgens modulate autophagy and cell death via regulation of the endoplasmic reticulum chaperone glucose-regulated protein 78/BiP in prostate cancer cells. *Cell Death Dis*, 1, e72.
- BERTOLOTTI, A., ZHANG, Y., HENDERSHOT, L. M., HARDING, H. P. & RON, D. 2000. Dynamic interaction of BiP and ER stress transducers in the unfolded-protein response. *Nature Cell Biology*, 2, 326-332.
- BLACKWOOD, E. A., AZIZI, K., THUERAUF, D. J., PAXMAN, R. J., PLATE, L., KELLY, J. W., WISEMAN, R. L. & GLEMBOTSKI, C. C. 2019. Pharmacologic ATF6 activation confers global protection in widespread disease models by reprogramming cellular proteostasis. *Nature Communications*, 10, 187.
- BOMMIASAMY, H. & POPKO, B. 2011. Chapter Six - Animal Models in the Study of the Unfolded Protein Response. In: CONN, P. M. (ed.) *Methods in Enzymology*. Academic Press.
- BREUZA, L., POUX, S., ESTREICHER, A., FAMIGLIETTI, M. L., MAGRANE, M., TOGNOLLI, M., BRIDGE, A., BARATIN, D., REDASCHI, N. & UNIPROT, C. 2016. The UniProtKB guide to the human proteome. *Database : the journal of biological databases and curation*, 2016, bav120.
- BREWER, J. W. & DIEHL, J. A. 2000. PERK mediates cell-cycle exit during the mammalian unfolded protein response. *Proc Natl Acad Sci U S A*, 97, 12625-30.
- BREWER, J. W., HENDERSHOT, L. M., SHERR, C. J. & DIEHL, J. A. 1999. Mammalian unfolded protein response inhibits cyclin D1 translation and cell-cycle progression. *Proc Natl Acad Sci U S A*, 96, 8505-10.
- BROOKE, G. N. & BEVAN, C. L. 2009. The role of androgen receptor mutations in prostate cancer progression. *Curr Genomics*, 10, 18-25.
- BROOKE, G. N., CULLEY, R. L., DART, D. A., MANN, D. J., GAUGHAN, L., MCCRACKEN, S. R., ROBSON, C. N., SPENCER-DENE, B., GAMBLE, S. C., POWELL, S. M., WAIT, R., WAXMAN, J., WALKER, M. M. & BEVAN, C. L. 2011. FUS/TLS is a novel mediator of androgen-dependent cell-cycle progression and prostate cancer growth. *Cancer Res*, 71, 914-24.
- BROOKE, G. N., PARKER, M. G. & BEVAN, C. L. 2008. Mechanisms of androgen receptor activation in advanced prostate cancer: differential co-activator recruitment and gene expression. *Oncogene*, 27, 2941-50.
- BROWN, C. J., GOSS, S. J., LUBAHN, D. B., JOSEPH, D. R., WILSON, E. M., FRENCH, F. S. & WILLARD, H. F. 1989. Androgen receptor locus on the human X chromosome: regional localization to Xq11-12 and description of a DNA polymorphism. *Am J Hum Genet*, 44, 264-9.
- BU, Y. & DIEHL, J. A. 2016. PERK Integrates Oncogenic Signaling and Cell Survival During Cancer Development. *J Cell Physiol*, 231, 2088-96.
- BURIKHANOV, R., ZHAO, Y., GOSWAMI, A., QIU, S., SCHWARZE, S. R. & RANGNEKAR, V. M. 2009. The tumor suppressor Par-4 activates an extrinsic pathway for apoptosis. *Cell*, 138, 377-88.

- CARLESSO, A., CHINTHA, C., GORMAN, A. M., SAMALI, A. & ERIKSSON, L. A. 2019. Effect of Kinase Inhibiting RNase Attenuator (KIRA) Compounds on the Formation of Face-to-Face Dimers of Inositol-Requiring Enzyme 1: Insights from Computational Modeling. *Int J Mol Sci*, 20.
- CARPENTER, E. P., BEIS, K., CAMERON, A. D. & IWATA, S. 2008. Overcoming the challenges of membrane protein crystallography. *Curr Opin Struct Biol*, 18, 581-6.
- CARRARA, M., PRISCHI, F., NOWAK, P. R. & ALI, M. M. 2015a. Crystal structures reveal transient PERK luminal domain tetramerization in endoplasmic reticulum stress signaling. *Embo j*, 34, 1589-600.
- CARRARA, M., PRISCHI, F., NOWAK, P. R., KOPP, M. C. & ALI, M. M. 2015b. Noncanonical binding of BiP ATPase domain to Ire1 and Perk is dissociated by unfolded protein CH1 to initiate ER stress signaling. *Elife*, 4.
- CARRASCO, S. & MEYER, T. 2011. STIM proteins and the endoplasmic reticulum-plasma membrane junctions. *Annu Rev Biochem*, 80, 973-1000.
- CEREZO, M., LEHRAIKI, A., MILLET, A., ROUAUD, F., PLAISANT, M., JAUNE, E., BOTTON, T., RONCO, C., ABBE, P., AMDOUNI, H., PASSERON, T., HOFMAN, V., MOGRABI, B., DABERT-GAY, A. S., DEBAYLE, D., ALCOR, D., RABHI, N., ANNICOTTE, J. S., HÉLIOT, L., GONZALEZ-PISFIL, M., ROBERT, C., MORÉRA, S., VIGOUROUX, A., GUAL, P., ALI, M. M. U., BERTOLOTTO, C., HOFMAN, P., BALLOTTI, R., BENHIDA, R. & ROCCHI, S. 2016. Compounds Triggering ER Stress Exert Anti-Melanoma Effects and Overcome BRAF Inhibitor Resistance. *Cancer Cell*, 29, 805-819.
- CHAUDHARY, S., PAK, J. E., GRUSWITZ, F., SHARMA, V. & STROUD, R. M. 2012. Overexpressing human membrane proteins in stably transfected and clonal human embryonic kidney 293S cells. *Nat Protoc*, 7, 453-66.
- CHEN, G. Y. & NUNEZ, G. 2010. Sterile inflammation: sensing and reacting to damage. *Nat Rev Immunol*, 10, 826-37.
- CHEN, X., ILIOPOULOS, D., ZHANG, Q., TANG, Q., GREENBLATT, M. B., HATZIAPOSTOULOU, M., LIM, E., TAM, W. L., NI, M., CHEN, Y., MAI, J., SHEN, H., HU, D. Z., ADORO, S., HU, B., SONG, M., TAN, C., LANDIS, M. D., FERRARI, M., SHIN, S. J., BROWN, M., CHANG, J. C., LIU, X. S. & GLIMCHER, L. H. 2014. XBP1 promotes triple-negative breast cancer by controlling the HIF1alpha pathway. *Nature*, 508, 103-107.
- CHEN, X., KANG, R., KROEMER, G. & TANG, D. 2021. Organelle-specific regulation of ferroptosis. *Cell Death & Differentiation*.
- CHEN, Y. & BRANDIZZI, F. 2013. IRE1: ER stress sensor and cell fate executor. *Trends Cell Biol*, 23, 547-55.
- CHEN, Y., CLEGG, N. J. & SCHER, H. I. 2009. Anti-androgens and androgen-depleting therapies in prostate cancer: new agents for an established target. *Lancet Oncol*, 10, 981-91.
- CLAESSENS, F., DENAYER, S., VAN TILBORGH, N., KERKHOF, S., HELSEN, C. & HAELENS, A. 2008. Diverse roles of androgen receptor (AR) domains in AR-mediated signaling. *Nucl Recept Signal*, 6, e008.
- CLARKE, H. J., CHAMBERS, J. E., LINIKER, E. & MARCINIAK, S. J. 2014. Endoplasmic reticulum stress in malignancy. *Cancer Cell*, 25, 563-73.
- CORAZZARI, M., GAGLIARDI, M., FIMIA, G. M. & PIACENTINI, M. 2017. Endoplasmic Reticulum Stress, Unfolded Protein Response, and Cancer Cell Fate. *Front Oncol*, 7, 78.
- CORNEC-LE GALL, E., OLSON, R. J., BESSE, W., HEYER, C. M., GAINULLIN, V. G., SMITH, J. M., AUDRÉZET, M. P., HOPP, K., PORATH, B., SHI, B., BAHETI, S., SENUM, S. R., ARROYO, J., MADSEN, C. D., FÉREC, C., JOLY, D., JOURET, F., FIKRI-BENBRAHIM, O., CHARASSE, C.,

- COULIBALY, J. M., YU, A. S., KHALILI, K., PEI, Y., SOMLO, S., LE MEUR, Y., TORRES, V. E. & HARRIS, P. C. 2018. Monoallelic Mutations to DNAJB11 Cause Atypical Autosomal-Dominant Polycystic Kidney Disease. *Am J Hum Genet*, 102, 832-844.
- CROFT, A., TAY, K. H., BOYD, S. C., GUO, S. T., JIANG, C. C., LAI, F., TSENG, H. Y., JIN, L., RIZOS, H., HERSEY, P. & ZHANG, X. D. 2014. Oncogenic activation of MEK/ERK primes melanoma cells for adaptation to endoplasmic reticulum stress. *J Invest Dermatol*, 134, 488-497.
- CROSS, B. C. S., BOND, P. J., SADOWSKI, P. G., JHA, B. K., ZAK, J., GOODMAN, J. M., SILVERMAN, R. H., NEUBERT, T. A., BAXENDALE, I. R., RON, D. & HARDING, H. P. 2012. The molecular basis for selective inhibition of unconventional mRNA splicing by an IRE1-binding small molecule. *Proceedings of the National Academy of Sciences*, 109, E869.
- CRUK. 2014. *Prostate Cancer Statistics* [Online]. Available: <http://www.cancerresearchuk.org/health-professional/cancer-statistics/statistics-by-cancer-type/prostate-cancer#heading-Three> [Accessed 10/01/2018].
- CRUK. 2015. *Prostate Cancer - Risks and Causes* [Online]. Available: <http://www.cancerresearchuk.org/about-cancer/prostate-cancer/risks-causes> [Accessed 10/01/2018].
- CRUK. 2016a. *Prostate Cancer - Screening* [Online]. Available: <http://www.cancerresearchuk.org/about-cancer/prostate-cancer/getting-diagnosed/screening> [Accessed 10/01/2018].
- CRUK. 2016b. *Prostate Cancer - Types and grades* [Online]. Available: <http://www.cancerresearchuk.org/about-cancer/prostate-cancer/types-grades> [Accessed 10/01/2018].
- CUNNINGHAM, D. & YOU, Z. 2015. In vitro and in vivo model systems used in prostate cancer research. *J Biol Methods*, 2.
- CUTRESS, M. L., WHITAKER, H. C., MILLS, I. G., STEWART, M. & NEAL, D. E. 2008. Structural basis for the nuclear import of the human androgen receptor. *J Cell Sci*, 121, 957-68.
- DART, D. A., WAXMAN, J., ABOAGYE, E. O. & BEVAN, C. L. 2013. Visualising androgen receptor activity in male and female mice. *PLoS One*, 8, e71694.
- DAVIES, P., WATT, K., KELLY, S. M., CLARK, C., PRICE, N. C. & MCEWAN, I. J. 2008. Consequences of poly-glutamine repeat length for the conformation and folding of the androgen receptor amino-terminal domain. *J Mol Endocrinol*, 41, 301-14.
- DE LECEA, L., KILDUFF, T. S., PEYRON, C., GAO, X., FOYE, P. E., DANIELSON, P. E., FUKUHARA, C., BATTENBERG, E. L., GAUTVIK, V. T., BARTLETT, F. S., 2ND, FRANKEL, W. N., VAN DEN POL, A. N., BLOOM, F. E., GAUTVIK, K. M. & SUTCLIFFE, J. G. 1998. The hypocretins: hypothalamus-specific peptides with neuroexcitatory activity. *Proc Natl Acad Sci U S A*, 95, 322-7.
- DENMEADE, S. R. & ISAACS, J. T. 2002. A history of prostate cancer treatment. *Nature Reviews Cancer*, 2, 389.
- DURAN-ANIOTZ, C., CORNEJO, V. H., ESPINOZA, S., ARDILES Á, O., MEDINAS, D. B., SALAZAR, C., FOLEY, A., GAJARDO, I., THIELEN, P., IWAWAKI, T., SCHEPER, W., SOTO, C., PALACIOS, A. G., HOOZEMANS, J. J. M. & HETZ, C. 2017. IRE1 signaling exacerbates Alzheimer's disease pathogenesis. *Acta Neuropathol*, 134, 489-506.
- ENGLISH, A. R. & VOELTZ, G. K. 2013. Endoplasmic reticulum structure and interconnections with other organelles. *Cold Spring Harb Perspect Biol*, 5, a013227.

- ERZURUMLU, Y. & BALLAR, P. 2017. Androgen Mediated Regulation of Endoplasmic Reticulum-Associated Degradation and its Effects on Prostate Cancer. *Scientific Reports*, 7, 40719.
- EVANS, R. M. 1988. The steroid and thyroid hormone receptor superfamily. *Science*, 240, 889-95.
- FELDMAN, B. J. & FELDMAN, D. 2001. The development of androgen-independent prostate cancer. *Nat Rev Cancer*, 1, 34-45.
- FRIEDMAN, J. R. & VOELTZ, G. K. 2011. The ER in 3D: a multifunctional dynamic membrane network. *Trends in Cell Biology*, 21, 709-717.
- GALLUZZI, L., MAIURI, M. C., VITALE, I., ZISCHKA, H., CASTEDO, M., ZITVOGEL, L. & KROEMER, G. 2007. Cell death modalities: classification and pathophysiological implications. *Cell Death & Differentiation*, 14, 1237-1243.
- GELMANN, E. P. 2002. Molecular biology of the androgen receptor. *J Clin Oncol*, 20, 3001-15.
- GREENLEE, R. T., HILL-HARMON, M. B., MURRAY, T. & THUN, M. 2001. Cancer statistics, 2001. *CA Cancer J Clin*, 51, 15-36.
- GUILLEMETTE, T., RAM, A. F. J., CARVALHO, N. D. S. P., JOUBERT, A., SIMONEAU, P. & ARCHER, D. B. 2011. Chapter One - Methods for Investigating the UPR in Filamentous Fungi. In: CONN, P. M. (ed.) *Methods in Enzymology*. Academic Press.
- H LEE, C., AKIN-OLUGBADE, O. & KIRSCHENBAUM, A. 2011. *Overview of Prostate Anatomy, Histology, and Pathology*.
- HAILE, S. & SADAR, M. D. 2011. Androgen receptor and its splice variants in prostate cancer. *Cell Mol Life Sci*, 68, 3971-81.
- HAN, D., LERNER, A. G., VANDE WALLE, L., UPTON, J. P., XU, W., HAGEN, A., BACKES, B. J., OAKES, S. A. & PAPA, F. R. 2009. IRE1 $\alpha$  kinase activation modes control alternate endoribonuclease outputs to determine divergent cell fates. *Cell*, 138, 562-75.
- HARDING, H. P., ZHANG, Y. & RON, D. 1999. Protein translation and folding are coupled by an endoplasmic-reticulum-resident kinase. *Nature*, 397, 271-4.
- HART, L. S., CUNNINGHAM, J. T., DATTA, T., DEY, S., TAMEIRE, F., LEHMAN, S. L., QIU, B., ZHANG, H., CERNIGLIA, G., BI, M., LI, Y., GAO, Y., LIU, H., LI, C., MAITY, A., THOMAS-TIKHONENKO, A., PERL, A. E., KOONG, A., FUCHS, S. Y., DIEHL, J. A., MILLS, I. G., RUGGERO, D. & KOUMENIS, C. 2012. ER stress-mediated autophagy promotes Myc-dependent transformation and tumor growth. *J Clin Invest*, 122, 4621-34.
- HAWKSWORTH, D., RAVINDRANATH, L., CHEN, Y., FURUSATO, B., SESTERHENN, I. A., MCLEOD, D. G., SRIVASTAVA, S. & PETROVICS, G. 2010. Overexpression of C-MYC oncogene in prostate cancer predicts biochemical recurrence. *Prostate Cancer Prostatic Dis*, 13, 311-5.
- HAYAT, M. A. 2015. Chapter 1 - Introduction to Autophagy: Cancer, Other Pathologies, Inflammation, Immunity, Infection, and Aging, Volume 7. In: HAYAT, M. A. (ed.) *Autophagy: Cancer, Other Pathologies, Inflammation, Immunity, Infection, and Aging*. Amsterdam: Academic Press.
- HAYWARD, S. W., DAHIYA, R., CUNHA, G. R., BARTEK, J., DESHPANDE, N. & NARAYAN, P. 1995. Establishment and characterization of an immortalized but non-transformed human prostate epithelial cell line: BPH-1. *In Vitro Cell Dev Biol Anim*, 31, 14-24.
- HAZE, K., YOSHIDA, H., YANAGI, H., YURA, T. & MORI, K. 1999a. Mammalian Transcription Factor ATF6 Is Synthesized as a Transmembrane Protein and Activated by Proteolysis in Response to Endoplasmic Reticulum Stress. 10, 3787-3799.

- HAZE, K., YOSHIDA, H., YANAGI, H., YURA, T. & MORI, K. 1999b. Mammalian transcription factor ATF6 is synthesized as a transmembrane protein and activated by proteolysis in response to endoplasmic reticulum stress. *Mol Biol Cell*, 10, 3787-99.
- HE, B., KEMPPAINEN, J. A., VOEGEL, J. J., GRONEMEYER, H. & WILSON, E. M. 1999. Activation function 2 in the human androgen receptor ligand binding domain mediates interdomain communication with the NH(2)-terminal domain. *J Biol Chem*, 274, 37219-25.
- HE, Y., SUN, S., SHA, H., LIU, Z., YANG, L., XUE, Z., CHEN, H. & QI, L. 2010. Emerging roles for XBP1, a sUPeR transcription factor. *Gene expression*, 15, 13-25.
- HEBERT, D. N., FOELLMER, B. & HELENIUS, A. 1995. Glucose trimming and reglucosylation determine glycoprotein association with calnexin in the endoplasmic reticulum. *Cell*, 81, 425-33.
- HEINLEIN, C. A. & CHANG, C. 2004. Androgen receptor in prostate cancer. *Endocr Rev*, 25, 276-308.
- HENTTU, P. & VIHKO, P. 1994. Prostate-specific antigen and human glandular kallikrein: two kallikreins of the human prostate. *Ann Med*, 26, 157-64.
- HETZ, C. 2012. The unfolded protein response: controlling cell fate decisions under ER stress and beyond. *Nat Rev Mol Cell Biol*, 13, 89-102.
- HETZ, C. & PAPA, F. R. 2017. The Unfolded Protein Response and Cell Fate Control. *Molecular Cell*.
- HETZ, C. & PAPA, F. R. 2018. The Unfolded Protein Response and Cell Fate Control. *Mol Cell*, 69, 169-181.
- HETZ, C., ZHANG, K. & KAUFMAN, R. J. 2020. Mechanisms, regulation and functions of the unfolded protein response. *Nature Reviews Molecular Cell Biology*, 21, 421-438.
- HIGA, A., TAOUI, S., LHOMOND, S., JENSEN, D., FERNANDEZ-ZAPICO, M. E., SIMPSON, J. C., PASQUET, J. M., SCHEKMAN, R. & CHEVET, E. 2014. Endoplasmic reticulum stress-activated transcription factor ATF6alpha requires the disulfide isomerase PDIA5 to modulate chemoresistance. *Mol Cell Biol*, 34, 1839-49.
- HO, D. V. & CHAN, J. Y. 2015. Induction of Herpud1 expression by ER stress is regulated by Nrf1. *FEBS Lett*, 589, 615-20.
- HOLLIEN, J. & WEISSMAN, J. S. 2006. Decay of endoplasmic reticulum-localized mRNAs during the unfolded protein response. *Science*, 313, 104-7.
- HOROSZEWICZ, J. S., LEONG, S. S., KAWINSKI, E., KARR, J. P., ROSENTHAL, H., CHU, T. M., MIRAND, E. A. & MURPHY, G. P. 1983. LNCaP model of human prostatic carcinoma. *Cancer Res*, 43, 1809-18.
- HU, H., TIAN, M., DING, C. & YU, S. 2018. The C/EBP Homologous Protein (CHOP) Transcription Factor Functions in Endoplasmic Reticulum Stress-Induced Apoptosis and Microbial Infection. *Front Immunol*, 9, 3083.
- HUANG, Y., JIANG, X., LIANG, X. & JIANG, G. 2018. Molecular and cellular mechanisms of castration resistant prostate cancer. *Oncol Lett*, 15, 6063-6076.
- HUBER, A. L., LEBEAU, J., GUILLAUMOT, P., PETRILLI, V., MALEK, M., CHILLOUX, J., FAUVET, F., PAYEN, L., KFOURY, A., RENNO, T., CHEVET, E. & MANIE, S. N. 2013. p58(IPK)-mediated attenuation of the proapoptotic PERK-CHOP pathway allows malignant progression upon low glucose. *Mol Cell*, 49, 1049-59.
- HUDSON, J. J., HSU, D. W., GUO, K., ZHUKOVSKAYA, N., LIU, P. H., WILLIAMS, J. G., PEARS, C. J. & LAKIN, N. D. 2005. DNA-PKcs-dependent signaling of DNA damage in Dictyostelium discoideum. *Curr Biol*, 15, 1880-5.

- HUMPHREY, P. A. 2004. Gleason grading and prognostic factors in carcinoma of the prostate. *Modern Pathology*, 17, 292-306.
- HWANG, J. & QI, L. 2018. Quality Control in the Endoplasmic Reticulum: Crosstalk between ERAD and UPR pathways. *Trends Biochem Sci*, 43, 593-605.
- JENSTER, G., VAN DER KORPUT, J. A., TRAPMAN, J. & BRINKMANN, A. O. 1992. Functional domains of the human androgen receptor. *J Steroid Biochem Mol Biol*, 41, 671-5.
- JHENG, J. R., LAU, K. S., LAN, Y. W. & HORNG, J. T. 2018. A novel role of ER stress signal transducer ATF6 in regulating enterovirus A71 viral protein stability. *J Biomed Sci*, 25, 9.
- JING, X., YANG, F., SHAO, C., WEI, K., XIE, M., SHEN, H. & SHU, Y. 2019. Role of hypoxia in cancer therapy by regulating the tumor microenvironment. *Molecular Cancer*, 18, 157.
- JOHNSON, M., SHARMA, M., BROCARDO, M. G. & HENDERSON, B. R. 2011. IQGAP1 translocates to the nucleus in early S-phase and contributes to cell cycle progression after DNA replication arrest. *Int J Biochem Cell Biol*, 43, 65-73.
- KADOWAKI, H., NAGAI, A., MARUYAMA, T., TAKAMI, Y., SATRIMAFITRAH, P., KATO, H., HONDA, A., HATTA, T., NATSUME, T., SATO, T., KAI, H., ICHIJO, H. & NISHITOH, H. 2015. Pre-emptive Quality Control Protects the ER from Protein Overload via the Proximity of ERAD Components and SRP. *Cell Rep*, 13, 944-56.
- KAIGHN, M. E., NARAYAN, K. S., OHNUKI, Y., LECHNER, J. F. & JONES, L. W. 1979. Establishment and characterization of a human prostatic carcinoma cell line (PC-3). *Invest Urol*, 17, 16-23.
- KATSOGIANNOU, M., ZIOUZIYOU, H., KARAKI, S., ANDRIEU, C., HENRY DE VILLENEUVE, M. & ROCCHI, P. 2015. The hallmarks of castration-resistant prostate cancers. *Cancer Treat Rev*, 41, 588-97.
- KAZEROUNIAN, S., YEE, K. O. & LAWLER, J. 2008. Thrombospondins in cancer. *Cell Mol Life Sci*, 65, 700-12.
- KHARABI MASOULEH, B., GENG, H., HURTZ, C., CHAN, L. N., LOGAN, A. C., CHANG, M. S., HUANG, C., SWAMINATHAN, S., SUN, H., PAIETTA, E., MELNICK, A. M., KOEFFLER, P. & MUSCHEN, M. 2014. Mechanistic rationale for targeting the unfolded protein response in pre-B acute lymphoblastic leukemia. *Proc Natl Acad Sci U S A*, 111, E2219-28.
- KOIVISTO, P., KONONEN, J., PALMBERG, C., TAMMELA, T., HYYTINEN, E., ISOLA, J., TRAPMAN, J., CLEUTJENS, K., NOORDZIJ, A., VISAKORPI, T. & KALLIONIEMI, O. P. 1997. Androgen receptor gene amplification: a possible molecular mechanism for androgen deprivation therapy failure in prostate cancer. *Cancer Res*, 57, 314-9.
- KOPP, M. C., NOWAK, P. R., LARBURU, N., ADAMS, C. J. & ALI, M. M. 2018. In vitro FRET analysis of IRE1 and BiP association and dissociation upon endoplasmic reticulum stress. *Elife*, 7.
- KUMARI, D. & BRODSKY, J. L. 2021. The Targeting of Native Proteins to the Endoplasmic Reticulum-Associated Degradation (ERAD) Pathway: An Expanding Repertoire of Regulated Substrates. *Biomolecules*, 11.
- LABRIE, C., CUSAN, L., PLANTE, M., LAPOINTE, S. & LABRIE, F. 1987. Analysis of the androgenic activity of synthetic "progestins" currently used for the treatment of prostate cancer. *J Steroid Biochem*, 28, 379-84.
- LABRIE, F., DUPONT, A., BELANGER, A., LACOURSIERE, Y., RAYNAUD, J. P., HUSSON, J. M., GAREAU, J., FAZEKAS, A. T., SANDOW, J., MONFETTE, G. & ET AL. 1983. New approach

- in the treatment of prostate cancer: complete instead of partial withdrawal of androgens. *Prostate*, 4, 579-94.
- LEE, A. H., CHU, G. C., IWAKOSHI, N. N. & GLIMCHER, L. H. 2005. XBP-1 is required for biogenesis of cellular secretory machinery of exocrine glands. *Embo j*, 24, 4368-80.
- LEE, E. J., CHAN, P., CHEA, L., KIM, K., KAUFMAN, R. J. & LIN, J. H. 2021. ATF6 is required for efficient rhodopsin clearance and retinal homeostasis in the P23H rho retinitis pigmentosa mouse model. *Sci Rep*, 11, 16356.
- LEE, H., LEE, Y.-S., HAREDA, Q., PIETRZAK, S., OKTAY, H. Z., SCHREIBER, S., LIAO, Y., SONTHALIA, S., CIECKO, A. E., CHEN, Y.-G., KELES, S., SRIDHARAN, R. & ENGIN, F. 2020. Beta Cell Dedifferentiation Induced by IRE1 $\alpha$  Deletion Prevents Type 1 Diabetes. *Cell Metabolism*, 31, 822-836.e5.
- LEE, K. P., DEY, M., NECULAI, D., CAO, C., DEVER, T. E. & SICHERI, F. 2008. Structure of the dual enzyme Ire1 reveals the basis for catalysis and regulation in nonconventional RNA splicing. *Cell*, 132, 89-100.
- LEE, Y. S., LEE, D. H., CHOUDRY, H. A., BARTLETT, D. L. & LEE, Y. J. 2018. Ferroptosis-Induced Endoplasmic Reticulum Stress: Cross-talk between Ferroptosis and Apoptosis. *Mol Cancer Res*, 16, 1073-1076.
- LERNER, A. G., UPTON, J. P., PRAVEEN, P. V., GHOSH, R., NAKAGAWA, Y., IGBARIA, A., SHEN, S., NGUYEN, V., BACKES, B. J., HEIMAN, M., HEINTZ, N., GREENGARD, P., HUI, S., TANG, Q., TRUSINA, A., OAKES, S. A. & PAPA, F. R. 2012. IRE1 $\alpha$  induces thioredoxin-interacting protein to activate the NLRP3 inflammasome and promote programmed cell death under irremediable ER stress. *Cell Metab*, 16, 250-64.
- LEUNG, D. K., CHIU, P. K., NG, C. F. & TEOH, J. Y. 2021. Novel Strategies for Treating Castration-Resistant Prostate Cancer. *Biomedicines*, 9.
- LI, Z., MCNULTY, D. E., MARLER, K. J., LIM, L., HALL, C., ANNAN, R. S. & SACKS, D. B. 2005. IQGAP1 promotes neurite outgrowth in a phosphorylation-dependent manner. *J Biol Chem*, 280, 13871-8.
- LILJA, H. 1985. A kallikrein-like serine protease in prostatic fluid cleaves the predominant seminal vesicle protein. *J Clin Invest*, 76, 1899-903.
- LILJA, H., ULMERT, D. & VICKERS, A. J. 2008. Prostate-specific antigen and prostate cancer: prediction, detection and monitoring. *Nature Reviews Cancer*, 8, 268.
- LIN, Y. H., FRIEDERICHS, J., BLACK, M. A., MAGES, J., ROSENBERG, R., GUILFORD, P. J., PHILLIPS, V., THOMPSON-FAWCETT, M., KASABOV, N., TORO, T., MERRIE, A. E., VAN RIJ, A., YOON, H. S., MCCALL, J. L., SIEWERT, J. R., HOLZMANN, B. & REEVE, A. E. 2007. Multiple gene expression classifiers from different array platforms predict poor prognosis of colorectal cancer. *Clin Cancer Res*, 13, 498-507.
- LIU, J., XIAO, M., LI, J., WANG, D., HE, Y., HE, J., GAO, F., MAI, L., LI, Y., LIANG, Y., LIU, Y. & ZHONG, X. 2017. Activation of UPR Signaling Pathway is Associated With the Malignant Progression and Poor Prognosis in Prostate Cancer. *Prostate*, 77, 274-281.
- LIU, Z., LV, Y., ZHAO, N., GUAN, G. & WANG, J. 2015. Protein kinase R-like ER kinase and its role in endoplasmic reticulum stress-decided cell fate. *Cell Death & Disease*, 6, e1822-e1822.
- LOPEZ-CRUZAN, M., SHARMA, R., TIWARI, M., KARBACH, S., HOLSTEIN, D., MARTIN, C. R., LECHLEITER, J. D. & HERMAN, B. 2016. Caspase-2 resides in the mitochondria and mediates apoptosis directly from the mitochondrial compartment. *Cell Death Discovery*, 2, 16005.

- LOWE, R., SHIRLEY, N., BLEACKLEY, M., DOLAN, S. & SHAFEE, T. 2017. Transcriptomics technologies. *PLoS Comput Biol*, 13, e1005457.
- LU, M., LAWRENCE, D. A., MARSTERS, S., ACOSTA-ALVEAR, D., KIMMIG, P., MENDEZ, A. S., PATON, A. W., PATON, J. C., WALTER, P. & ASHKENAZI, A. 2014. Opposing unfolded-protein-response signals converge on death receptor 5 to control apoptosis. *Science*, 345, 98-101.
- LYNCH, J. M., MAILLET, M., VANHOUTTE, D., SCHLOEMER, A., SARGENT, M. A., BLAIR, N. S., LYNCH, K. A., OKADA, T., ARONOW, B. J., OSINSKA, H., PRYWES, R., LORENZ, J. N., MORI, K., LAWLER, J., ROBBINS, J. & MOLKENTIN, J. D. 2012. A thrombospondin-dependent pathway for a protective ER stress response. *Cell*, 149, 1257-68.
- MA, Y. & HENDERSHOT, L. M. 2004a. ER chaperone functions during normal and stress conditions. *J Chem Neuroanat*, 28, 51-65.
- MA, Y. & HENDERSHOT, L. M. 2004b. The role of the unfolded protein response in tumour development: friend or foe? *Nat Rev Cancer*, 4, 966-77.
- MADDEN, E., LOGUE, S. E., HEALY, S. J., MANIE, S. & SAMALI, A. 2019. The role of the unfolded protein response in cancer progression: From oncogenesis to chemoresistance. *Biol Cell*, 111, 1-17.
- MANDELIN, J., CARDO-VILA, M., DRIESSEN, W. H., MATHEW, P., NAVONE, N. M., LIN, S. H., LOGOTHETIS, C. J., RIETZ, A. C., DOBROFF, A. S., PRONETH, B., SIDMAN, R. L., PASQUALINI, R. & ARAP, W. 2015. Selection and identification of ligand peptides targeting a model of castrate-resistant osteogenic prostate cancer and their receptors. *Proc Natl Acad Sci U S A*, 112, 3776-81.
- MATHIEU, K., JAVED, W., VALLET, S., LESTERLIN, C., CANDUSSO, M.-P., DING, F., XU, X. N., EBEL, C., JAULT, J.-M. & ORELLE, C. 2019. Functionality of membrane proteins overexpressed and purified from E. coli is highly dependent upon the strain. *Scientific Reports*, 9, 2654.
- MAUREL, M., CHEVET, E., TAVERNIER, J. & GERLO, S. 2014. Getting RIDD of RNA: IRE1 in cell fate regulation. *Trends Biochem Sci*, 39, 245-54.
- MCHUGH, L. & ARTHUR, J. W. 2008. Computational methods for protein identification from mass spectrometry data. *PLoS Comput Biol*, 4, e12.
- MCNEAL, J. E. 1981. The zonal anatomy of the prostate. *Prostate*, 2, 35-49.
- MONTGOMERY, R. B., MOSTAGHEL, E. A., VESSELLA, R., HESS, D. L., KALHORN, T. F., HIGANO, C. S., TRUE, L. D. & NELSON, P. S. 2008. Maintenance of intratumoral androgens in metastatic prostate cancer: a mechanism for castration-resistant tumor growth. *Cancer Res*, 68, 4447-54.
- MOORE, K. L., AGUR, A. M. R. & DALLEY, A. F. 2011. *Essential Clinical Anatomy*, Lippincott Williams & Wilkins.
- MORAES, I., EVANS, G., SANCHEZ-WEATHERBY, J., NEWSTEAD, S. & STEWART, P. D. 2014. Membrane protein structure determination - the next generation. *Biochim Biophys Acta*, 1838, 78-87.
- MORI, K., MA, W., GETHING, M. J. & SAMBROOK, J. 1993. A transmembrane protein with a cdc2+/CDC28-related kinase activity is required for signaling from the ER to the nucleus. *Cell*, 74, 743-56.
- MORREALL, J., HONG, F. & LI, Z. 2019. The Regulation of the Unfolded Protein Response and Its Roles in Tumorigenesis and Cancer Therapy. In: CLARKE, R. (ed.) *The Unfolded Protein Response in Cancer*. Cham: Springer International Publishing.

- MURAD, H., HAWAT, M., EKHTIAR, A., ALJAPAWA, A., ABBAS, A., DARWISH, H., SBENATI, O. & GHANNAM, A. 2016. Induction of G1-phase cell cycle arrest and apoptosis pathway in MDA-MB-231 human breast cancer cells by sulfated polysaccharide extracted from *Laurencia papillosa*. *Cancer Cell Int*, 16, 39.
- MUZ, B., DE LA PUENTE, P., AZAB, F. & AZAB, A. K. 2015. The role of hypoxia in cancer progression, angiogenesis, metastasis, and resistance to therapy. *Hypoxia (Auckl)*, 3, 83-92.
- NAMBA, T., CHU, K., KODAMA, R., BYUN, S., YOON, K. W., HIRAKI, M., MANDINOVA, A. & LEE, S. W. 2015. Loss of p53 enhances the function of the endoplasmic reticulum through activation of the IRE1 $\alpha$ /XBP1 pathway. *Oncotarget*, 6, 19990-20001.
- NAMEKAWA, T., IKEDA, K., HORIE-INOUE, K. & INOUE, S. 2019. Application of Prostate Cancer Models for Preclinical Study: Advantages and Limitations of Cell Lines, Patient-Derived Xenografts, and Three-Dimensional Culture of Patient-Derived Cells. *Cells*, 8.
- NCBI. 2019. *ATF6 activating transcription factor 6 [Homo sapiens (human)]* [Online]. Available: <https://www.ncbi.nlm.nih.gov/gene/22926> [Accessed 03/06/2019].
- NGUYEN, H. G., CONN, C. S., KYE, Y., XUE, L., FORESTER, C. M., COWAN, J. E., HSIEH, A. C., CUNNINGHAM, J. T., TRUILLET, C., TAMEIRE, F., EVANS, M. J., EVANS, C. P., YANG, J. C., HANN, B., KOUMENIS, C., WALTER, P., CARROLL, P. R. & RUGGERO, D. 2018. Development of a stress response therapy targeting aggressive prostate cancer. *Sci Transl Med*, 10.
- NI, H., RUI, Q., LI, D., GAO, R. & CHEN, G. 2018. The Role of IRE1 Signaling in the Central Nervous System Diseases. *Current neuropharmacology*, 16, 1340-1347.
- NICKEL, J. C. 2003. Classification and diagnosis of prostatitis: a gold standard? *Andrologia*, 35, 160-7.
- NICOLETTI, I., MIGLIORATI, G., PAGLIACCI, M. C., GRIGNANI, F. & RICCARDI, C. 1991. A rapid and simple method for measuring thymocyte apoptosis by propidium iodide staining and flow cytometry. *J Immunol Methods*, 139, 271-9.
- NØRGAARD, M., JENSEN, A., JACOBSEN, J. B., CETIN, K., FRYZEK, J. P. & SØRENSEN, H. T. 2010. Skeletal related events, bone metastasis and survival of prostate cancer: a population based cohort study in Denmark (1999 to 2007). *J Urol*, 184, 162-7.
- OAKES, S. A. & PAPA, F. R. 2015. The role of endoplasmic reticulum stress in human pathology. *Annu Rev Pathol*, 10, 173-94.
- PACHIKOV, A. N., GOUGH, R. R., CHRISTY, C. E., MORRIS, M. E., CASEY, C. A., LAGRANGE, C. A., BHAT, G., KUBYSHKIN, A. V., FOMOCHKINA, I. I., ZYABLITSKAYA, E. Y., MAKALISH, T. P., GOLUBINSKAYA, E. P., DAVYDENKO, K. A., EREMENKO, S. N., RIETHOVEN, J.-J. M., MAROLI, A. S., PAYNE, T. S., POWERS, R., LUSHNIKOV, A. Y., MACKE, A. J. & PETROSYAN, A. 2021. The non-canonical mechanism of ER stress-mediated progression of prostate cancer. *Journal of Experimental & Clinical Cancer Research*, 40, 289.
- PAEZ, D., LABONTE, M. J., BOHANES, P., ZHANG, W., BENHANIM, L., NING, Y., WAKATSUKI, T., LOUPAKIS, F. & LENZ, H. J. 2012. Cancer dormancy: a model of early dissemination and late cancer recurrence. *Clin Cancer Res*, 18, 645-53.
- PARK, H. R., OH, R., WAGNER, P., PANGANIBAN, R. & LU, Q. 2017. Chapter Two - New Insights Into Cellular Stress Responses to Environmental Metal Toxicants. In: GALLUZZI, L. (ed.) *International Review of Cell and Molecular Biology*. Academic Press.
- PARKER, J. L. & NEWSTEAD, S. 2016. Membrane Protein Crystallisation: Current Trends and Future Perspectives. *Adv Exp Med Biol*, 922, 61-72.

- PEARSE, B. R. & HEBERT, D. N. 2010. Lectin chaperones help direct the maturation of glycoproteins in the endoplasmic reticulum. *Biochim Biophys Acta*, 1803, 684-93.
- PETROVA, V., ANNICCHIARICO-PETRUZZELLI, M., MELINO, G. & AMELIO, I. 2018. The hypoxic tumour microenvironment. *Oncogenesis*, 7, 10.
- PIENTA, K. J. & BRADLEY, D. 2006. Mechanisms Underlying the Development of Androgen-Independent Prostate Cancer. *Clinical Cancer Research*, 12, 1665.
- PIZZORNO, J. 2014. Glutathione! *Integr Med (Encinitas)*, 13, 8-12.
- PLUQUET, O., DEJEANS, N., BOUCHECAREILH, M., LHOMOND, S., PINEAU, R., HIGA, A., DELUGIN, M., COMBE, C., LORIOT, S., CUBEL, G., DUGOT-SENANT, N., VITAL, A., LOISEAU, H., GOSLINE, S. J., TAOUJI, S., HALLETT, M., SARKARIA, J. N., ANDERSON, K., WU, W., RODRIGUEZ, F. J., ROSENBAUM, J., SALTEL, F., FERNANDEZ-ZAPICO, M. E. & CHEVET, E. 2013. Posttranscriptional regulation of PER1 underlies the oncogenic function of IREalpha. *Cancer Res*, 73, 4732-43.
- POBRE, K. F. R., POET, G. J. & HENDERSHOT, L. M. 2019. The endoplasmic reticulum (ER) chaperone BiP is a master regulator of ER functions: Getting by with a little help from ERdj friends. *J Biol Chem*, 294, 2098-2108.
- POOTRAKUL, L., DATAR, R. H., SHI, S. R., CAI, J., HAWES, D., GROSHEN, S. G., LEE, A. S. & COTE, R. J. 2006. Expression of stress response protein Grp78 is associated with the development of castration-resistant prostate cancer. *Clin Cancer Res*, 12, 5987-93.
- PÄLLMANN, N., LIVGÅRD, M., TESIKOVA, M., ZEYNEP NENSETH, H., AKKUS, E., SIKKELAND, J., JIN, Y., KOC, D., KUZU, O. F., PRADHAN, M., DANIELSEN, H. E., KAHRAMAN, N., MOKHLIS, H. M., OZPOLAT, B., BANERJEE, P. P., UREN, A., FAZLI, L., RENNIE, P. S. & SAATCIOGLU, F. 2019. Regulation of the unfolded protein response through ATF4 and FAM129A in prostate cancer. *Oncogene*, 38, 6301-6318.
- QI, L., TSAI, B. & ARVAN, P. 2017. New Insights into the Physiological Role of Endoplasmic Reticulum-Associated Degradation. *Trends Cell Biol*, 27, 430-440.
- RAMASWAMY, S., TAMAYO, P., RIFKIN, R., MUKHERJEE, S., YEANG, C. H., ANGELO, M., LADD, C., REICH, M., LATULIPPE, E., MESIROV, J. P., POGGIO, T., GERALD, W., LODA, M., LANDER, E. S. & GOLUB, T. R. 2001. Multiclass cancer diagnosis using tumor gene expression signatures. *Proc Natl Acad Sci U S A*, 98, 15149-54.
- RAPOPORT, T. A. 2007. Protein translocation across the eukaryotic endoplasmic reticulum and bacterial plasma membranes. *Nature*, 450, 663-669.
- REBELLO, R. J., OING, C., KNUDSEN, K. E., LOEB, S., JOHNSON, D. C., REITER, R. E., GILLESSEN, S., VAN DER KWAST, T. & BRISTOW, R. G. 2021. Prostate cancer. *Nature Reviews Disease Primers*, 7, 9.
- REEVES, P. J., CALLEWAERT, N., CONTRERAS, R. & KHORANA, H. G. 2002. Structure and function in rhodopsin: high-level expression of rhodopsin with restricted and homogeneous N-glycosylation by a tetracycline-inducible N-acetylglucosaminyltransferase I-negative HEK293S stable mammalian cell line. *Proc Natl Acad Sci U S A*, 99, 13419-24.
- ROBERTS, R. O., LIEBER, M. M., BOSTWICK, D. G. & JACOBSEN, S. J. 1997. A review of clinical and pathological prostatitis syndromes. *Urology*, 49, 809-21.
- ROBINSON-RECHAVI, M., ESCRIVA GARCIA, H. & LAUDET, V. 2003. The nuclear receptor superfamily. *J Cell Sci*, 116, 585-6.
- RONG, R., MONTALBANO, J., JIN, W., ZHANG, J., GARLING, M., SHEIKH, M. S. & HUANG, Y. 2005. Oncogenic Ras-mediated downregulation of Gadd153/CHOP is required for Ras-induced cellular transformation. *Oncogene*, 24, 4867-4872.

- ROSENBERG, M., AZEVEDO, N. F. & IVASK, A. 2019. Propidium iodide staining underestimates viability of adherent bacterial cells. *Scientific Reports*, 9, 6483.
- ROUSCHOP, K. M., VAN DEN BEUCKEN, T., DUBOIS, L., NIESEN, H., BUSSINK, J., SAVELKOULS, K., KEULERS, T., MUJIC, H., LANDUYT, W., VONCKEN, J. W., LAMBIN, P., VAN DER KOGEL, A. J., KORITZINSKY, M. & WOUTERS, B. G. 2010. The unfolded protein response protects human tumor cells during hypoxia through regulation of the autophagy genes MAP1LC3B and ATG5. *J Clin Invest*, 120, 127-41.
- RUTKOWSKI, D. T. & HEGDE, R. S. 2010. Regulation of basal cellular physiology by the homeostatic unfolded protein response. *J Cell Biol*, 189, 783-94.
- SANDBERG, A. A. 1980. Endocrine control and physiology of the prostate. *Prostate*, 1, 169-84.
- SANO, R. & REED, J. C. 2013. ER stress-induced cell death mechanisms. *Biochim Biophys Acta*, 1833, 3460-3470.
- SARAON, P., JARVI, K. & DIAMANDIS, E. P. 2011. Molecular alterations during progression of prostate cancer to androgen independence. *Clin Chem*, 57, 1366-75.
- SATO, K. & NAKANO, A. 2007. Mechanisms of COPII vesicle formation and protein sorting. *FEBS Lett*, 581, 2076-82.
- SCHEWE, D. M. & AGUIRRE-GHISO, J. A. 2008. ATF6 $\alpha$ -Rheb-mTOR signaling promotes survival of dormant tumor cells in vivo. *Proc Natl Acad Sci U S A*, 105, 10519-24.
- SCHINDLER, A. J. & SCHEKMAN, R. 2009. In vitro reconstitution of ER-stress induced ATF6 transport in COPII vesicles. *Proceedings of the National Academy of Sciences*, 106, 17775.
- SCHWARZ, D. S. & BLOWER, M. D. 2016. The endoplasmic reticulum: structure, function and response to cellular signaling. *Cell Mol Life Sci*, 73, 79-94.
- SHEN, J., CHEN, X., HENDERSHOT, L. & PRYWES, R. 2002. ER stress regulation of ATF6 localization by dissociation of BiP/GRP78 binding and unmasking of Golgi localization signals. *Dev Cell*, 3, 99-111.
- SHEN, J., SNAPP, E. L., LIPPINCOTT-SCHWARTZ, J. & PRYWES, R. 2005. Stable binding of ATF6 to BiP in the endoplasmic reticulum stress response. *Mol Cell Biol*, 25, 921-32.
- SHENG, X., ARNOLDUSSEN, Y. J., STORM, M., TESIKOVA, M., NENSETH, H. Z., ZHAO, S., FAZLI, L., RENNIE, P., RISBERG, B., WAEHRE, H., DANIELSEN, H., MILLS, I. G., JIN, Y., HOTAMISLIGIL, G. & SAATCIOGLU, F. 2015. Divergent androgen regulation of unfolded protein response pathways drives prostate cancer. *EMBO Mol Med*, 7, 788-801.
- SHENG, X., NENSETH, H. Z., QU, S., KUZU, O. F., FRAHNOW, T., SIMON, L., GREENE, S., ZENG, Q., FAZLI, L., RENNIE, P. S., MILLS, I. G., DANIELSEN, H., THEIS, F., PATTERSON, J. B., JIN, Y. & SAATCIOGLU, F. 2019. IRE1 $\alpha$ -XBP1s pathway promotes prostate cancer by activating c-MYC signaling. *Nature Communications*, 10, 323.
- SIWECKA, N., ROZPĘDEK-KAMIŃSKA, W., WAWRZYNKIEWICZ, A., PYTEL, D., DIEHL, J. A. & MAJSTEREK, I. 2021. The Structure, Activation and Signaling of IRE1 and Its Role in Determining Cell Fate. *Biomedicines*, 9.
- STELLOO, S., LINDER, S., NEVEDOMSKAYA, E., VALLE-ENCINAS, E., DE RINK, I., WESSELS, L. F. A., VAN DER POEL, H., BERGMAN, A. M. & ZWART, W. 2020. Androgen modulation of XBP1 is functionally driving part of the AR transcriptional program. *Endocr Relat Cancer*, 27, 67-79.
- STONE, K. R., MICKEY, D. D., WUNDERLI, H., MICKEY, G. H. & PAULSON, D. F. 1978. Isolation of a human prostate carcinoma cell line (DU 145). *Int J Cancer*, 21, 274-81.
- STORM, M., SHENG, X., ARNOLDUSSEN, Y. J. & SAATCIOGLU, F. 2016. Prostate cancer and the unfolded protein response. *Oncotarget*, 7, 54051-54066.

- SZUL, T. & SZTUL, E. 2011. COPII and COPI traffic at the ER-Golgi interface. *Physiology (Bethesda)*, 26, 348-64.
- TAN, M. H. E., LI, J., XU, H. E., MELCHER, K. & YONG, E.-L. 2015. Androgen receptor: structure, role in prostate cancer and drug discovery. *Acta Pharmacol Sin*, 36, 3-23.
- TAN, S. S., AHMAD, I., BENNETT, H. L., SINGH, L., NIXON, C., SEYWRIGHT, M., BARNETSON, R. J., EDWARDS, J. & LEUNG, H. Y. 2011. GRP78 up-regulation is associated with androgen receptor status, Hsp70–Hsp90 client proteins and castrate-resistant prostate cancer. *The Journal of Pathology*, 223, 81-87.
- TANG, D., CHEN, X., KANG, R. & KROEMER, G. 2021. Ferroptosis: molecular mechanisms and health implications. *Cell Research*, 31, 107-125.
- TANG, D., KANG, R., BERGHE, T. V., VANDENABEELE, P. & KROEMER, G. 2019. The molecular machinery of regulated cell death. *Cell Research*, 29, 347-364.
- TAOUJI, S., WOLF, S. & CHEVET, E. 2013. Chapter Seventeen - Oligomerization in Endoplasmic Reticulum Stress Signaling. In: GIRALDO, J. & CIRUELA, F. (eds.) *Progress in Molecular Biology and Translational Science*. Academic Press.
- TAPLIN, M. E. & BALK, S. P. 2004. Androgen receptor: a key molecule in the progression of prostate cancer to hormone independence. *J Cell Biochem*, 91, 483-90.
- THALMANN, G. N., ANEZINIS, P. E., CHANG, S.-M., ZHAU, H. E., KIM, E. E., HOPWOOD, V. L., PATHAK, S., VON ESCHENBACH, A. C. & CHUNG, L. W. K. 1994. Androgen-independent Cancer Progression and Bone Metastasis in the LNCaP Model of Human Prostate Cancer. *Cancer Research*, 54, 2577.
- THOMAS, C., BÖGEMANN, M., KÖNIG, F., MACHTENS, S., SCHOSTAK, M., STEUBER, T. & HEIDENREICH, A. 2016. [Advanced Prostate Cancer Consensus Conference (APCCC) 2015 in St. Gallen : Critical review of the recommendations on diagnosis and therapy of metastatic prostate cancer by a German expert panel]. *Urologe A*, 55, 772-82.
- THORPE, A. & NEAL, D. 2003. Benign prostatic hyperplasia. *The Lancet*, 361, 1359-1367.
- TROMBETTA, E. S. & HELENIUS, A. 1998. Lectins as chaperones in glycoprotein folding. *Curr Opin Struct Biol*, 8, 587-92.
- TUFANLI, O., TELKOPARAN AKILLILAR, P., ACOSTA-ALVEAR, D., KOCATURK, B., ONAT, U. I., HAMID, S. M., ÇIMEN, I., WALTER, P., WEBER, C. & ERBAY, E. 2017. Targeting IRE1 with small molecules counteracts progression of atherosclerosis. *Proceedings of the National Academy of Sciences*, 114, E1395.
- URRA, H., DUFÉY, E., AVRIL, T., CHEVET, E. & HETZ, C. 2016. Endoplasmic Reticulum Stress and the Hallmarks of Cancer. *Trends Cancer*, 2, 252-262.
- URRA, H., DUFÉY, E., LISBONA, F., ROJAS-RIVERA, D. & HETZ, C. 2013. When ER stress reaches a dead end. *Biochim Biophys Acta*, 1833, 3507-3517.
- VEMBAR, S. S. & BRODSKY, J. L. 2008. One step at a time: endoplasmic reticulum-associated degradation. *Nature Reviews Molecular Cell Biology*, 9, 944-957.
- VERZE, P., CAI, T. & LORENZETTI, S. 2016. The role of the prostate in male fertility, health and disease. *Nature Reviews Urology*, 13, 379.
- WAGENLEHNER, F., PILATZ, A., LINN, T., DIEMER, T., SCHUPPE, H. C., SCHAGDARSURENGIN, U., HOSSAIN, H., MEINHARDT, A., ELLEM, S., RISBRIDGER, G. & WEIDNER, W. 2013. Prostatitis and andrological implications. *Minerva Urol Nefrol*, 65, 117-23.
- WALTER, P. & RON, D. 2011. The unfolded protein response: from stress pathway to homeostatic regulation. *Science*, 334, 1081-6.

- WANG, P., HAN, L., YU, M., CAO, Z., LI, X., SHAO, Y. & ZHU, G. 2021. The Prognostic Value of PERK in Cancer and Its Relationship With Immune Cell Infiltration. *Front Mol Biosci*, 8, 648752.
- WILDING, G. 1995. Endocrine control of prostate cancer. *Cancer Surv*, 23, 43-62.
- WILLIAMS, D. B. 2006. Beyond lectins: the calnexin/calreticulin chaperone system of the endoplasmic reticulum. *J Cell Sci*, 119, 615-23.
- WU, H. C., HSIEH, J. T., GLEAVE, M. E., BROWN, N. M., PATHAK, S. & CHUNG, L. W. 1994. Derivation of androgen-independent human LNCaP prostatic cancer cell sublines: role of bone stromal cells. *Int J Cancer*, 57, 406-12.
- WU, M. J., CHEN, C. J., LIN, T. Y., LIU, Y. Y., TSENG, L. L., CHENG, M. L., CHUU, C. P., TSAI, H. K., KUO, W. L., KUNG, H. J. & WANG, W. C. 2021. Targeting KDM4B that coactivates c-Myc-regulated metabolism to suppress tumor growth in castration-resistant prostate cancer. *Theranostics*, 11, 7779-7796.
- YAMAMOTO, K., SATO, T., MATSUI, T., SATO, M., OKADA, T., YOSHIDA, H., HARADA, A. & MORI, K. 2007. Transcriptional induction of mammalian ER quality control proteins is mediated by single or combined action of ATF6alpha and XBP1. *Dev Cell*, 13, 365-76.
- YANG, P., YANG, Y., SUN, P., TIAN, Y., GAO, F., WANG, C., ZONG, T., LI, M., ZHANG, Y., YU, T. & JIANG, Z. 2021.  $\beta$ II spectrin (SPTBN1): biological function and clinical potential in cancer and other diseases. *Int J Biol Sci*, 17, 32-49.
- YOSHIDA, H., MATSUI, T., YAMAMOTO, A., OKADA, T. & MORI, K. 2001. XBP1 mRNA is induced by ATF6 and spliced by IRE1 in response to ER stress to produce a highly active transcription factor. *Cell*, 107, 881-91.
- YOSHIDA, H., OKU, M., SUZUKI, M. & MORI, K. 2006. pXBP1(U) encoded in XBP1 pre-mRNA negatively regulates unfolded protein response activator pXBP1(S) in mammalian ER stress response. *J Cell Biol*, 172, 565-75.
- YU, Z., SHENG, H., LIU, S., ZHAO, S., GLEMBOTSKI, C. C., WARNER, D. S., PASCHEN, W. & YANG, W. 2017. Activation of the ATF6 branch of the unfolded protein response in neurons improves stroke outcome. *J Cereb Blood Flow Metab*, 37, 1069-1079.
- ZHANG, T., LI, N., SUN, C., JIN, Y. & SHENG, X. 2020. MYC and the unfolded protein response in cancer: synthetic lethal partners in crime? *EMBO Mol Med*, 12, e11845.
- ZHANG, Y., TSENG, C. C., TSAI, Y. L., FU, X., SCHIFF, R. & LEE, A. S. 2013. Cancer cells resistant to therapy promote cell surface relocalization of GRP78 which complexes with PI3K and enhances PI(3,4,5)P3 production. *PLoS One*, 8, e80071.
- ZHOU, J., LIU, C. Y., BACK, S. H., CLARK, R. L., PEISACH, D., XU, Z. & KAUFMAN, R. J. 2006. The crystal structure of human IRE1 luminal domain reveals a conserved dimerization interface required for activation of the unfolded protein response. *Proc Natl Acad Sci U S A*, 103, 14343-8.
- ZILKA, O., SHAH, R., LI, B., FRIEDMANN ANGELI, J. P., GRIESSER, M., CONRAD, M. & PRATT, D. A. 2017. On the Mechanism of Cytoprotection by Ferrostatin-1 and Liproxstatin-1 and the Role of Lipid Peroxidation in Ferroptotic Cell Death. *ACS Cent Sci*, 3, 232-243.
- ZINSZNER, H., KURODA, M., WANG, X., BATCHVAROVA, N., LIGHTFOOT, R. T., REMOTTI, H., STEVENS, J. L. & RON, D. 1998. CHOP is implicated in programmed cell death in response to impaired function of the endoplasmic reticulum. *Genes Dev*, 12, 982-95.